2011

Oceanic Light Absorption Properties: Assessment and Characterization in the Southeastern Bering Sea Using Field and Satellite Observations

Puneeta Suresh Naik
Louisiana State University and Agricultural and Mechanical College

OCEANIC LIGHT ABSORPTION PROPERTIES: ASSESSMENT AND CHARACTERIZATION IN THE SOUTHEASTERN BERING SEA USING FIELD AND SATELLITE OBSERVATIONS

A Dissertation

Submitted to the Graduate Faculty of the
Louisiana State University and
Agricultural and Mechanical College
in partial fulfillment of the
requirements for the degree of
Doctor of Philosophy

in
The Department of Oceanography and Coastal Sciences

by
Puneeta Suresh Naik
B.S., Goa University, 2003
M.S., Goa University, 2005
December 2011

DEDICATION

To my parents, Sunanda and Suresh Gangadhar Naik, for their encouragement and endless support.

ACKNOWLEDGEMENTS

I would like to express my gratitude to my major professor, Dr. Eurico J. D'Sa, for his support, patience, and encouragement throughout my graduate studies. I have been fortunate to have an advisor who gave me the liberty to explore on my own and at the same time the supervision to recover when my steps faltered. He has been, and will continue to be an important mentor to me. I would also like to express my sincere appreciation to my committee members, Dr. Mark C. Benfield, Dr. Bin Li, Dr. R. Eugene Turner, Dr. Nan D. Walker, and the dean's representative Dr. Michael E. Hellberg for their time, support and insightful comments throughout this effort. Though this dissertation is an individual work, it would not be possible without the assistance and efforts of a lot of people. I would like to give special thanks to the scientists (co-authors on the individual papers in this dissertation) who contributed much time and effort to this study. I would like to thank the National Aeronautics and Space Administration (NASA) for funding this project to Dr. Eurico J. D'Sa, Louisiana State University. During the summer of my first year in graduate school at Louisiana State University, I attended a five week summer course in Optical Oceanography at the University of Maine. I am extremely grateful to the organizers and teachers of this course for giving me an understanding on the basics of marine optics.

I am forever grateful to my parents for encouraging and being there for me always in everything that I do. My parents have been beyond supportive of everything I have ever wanted to do and I am appreciative they let me grow as an individual in places far away from home. I would like to thank my sisters for cheering me up during the difficult times of this research. Thank you to my friends and colleagues, especially Shatrughan Singh, for their positive attitude, understanding and support.

TABLE OF CONTENTS

LIST OF TABLES

LIST OF FIGURES

ABSTRACT

In recent decades the Bering Sea has been subjected to large climatic variability with cascading consequences on its productive marine ecosystem. Long-term as well as short-term monitoring is essential if we are to maintain its capability to supply the resources on which the national and local economy depend. Remote sensing together with in-situ and laboratory measurements of physical, biological and optical properties have considerable potential for monitoring and measuring the effects of climate-driven changes on this ecosystem. A major shortcoming to obtain accurate estimates of optically active components (such as colored dissolved organic matter, non-algal particulate matter, and phytoplankton) from ocean color remote sensors has been the lack of in-situ bio-optical data in the Bering Sea. To address this issue, the central part of this dissertation was to i) assess phytoplankton absorption of culture and seawater samples using spectrophotometric and pigment reconstruction methods and ii) obtain a suite of in-water measurements for characterization and parameterization of light absorption properties in the southeastern Bering Sea. One of the main objectives was to assess the bio-optical models and parameterizations currently used in satellite algorithms for the southeastern Bering Sea, which were found to be inapplicable in these waters due to the dominant contribution by CDOM absorption. The CDOM absorption accounted for greater than 50% of the diffuse light attenuation coefficient and caused the remote sensing reflectance to be lower, more in the blue than the green region of the visible spectrum, causing the blue to green reflectance ratios to decrease by a factor of ~2. The lower specific absorption relative to lower and middle latitudes indicated significant pigment packaging and/or change in pigment composition which was consistent with variability in phytoplankton community structure. These results suggested the need for developing regional algorithms and parameterizations; regional empirical algorithms

were developed using relationships between remotely sensed reflectances and properties of optically active components in the study region. The results from this dissertation will enhance our ability to achieve greater accuracy in deriving remotely measured optical parameters of sub-arctic regions required for an improved understanding of biological responses to climatic forcing.

CHAPTER 1: INTRODUCTION

Background

The Bering Sea has long been considered among the most productive marine ecosystems in the world [*Walsh and McRoy*, 1986] that supports nearly half of the U.S fishery catch [*NRC*, 1996; *Overland and Stabeno*, 2004]. Physical processes and seasonal sea-ice advance and retreat in the Bering Sea play a major role in controlling water mass properties and shaping the character of pelagic and benthic ecosystems found on the shelf. Chlorophyll distributions and primary productivity studies illustrate that the Bering Sea is a highly productive region, with elevated primary productivity ranging from 175–275 g C m^{-2} yr^{-1} near the shelf break [*Springer et al.*, 1996] and abundance of benthic biomass [*Grebmeier et al.*, 1995]. However, over the last few decades the Bering Sea has been subjected to large climatic fluctuations and is among the most rapidly changing marine ecosystem [*Grebmeier et al.*, 2006; *Hunt et al.*, 2002; *Overland and Stabeno*, 2004; *Springer*, 1999]. Cold-water, Arctic species have been replaced by organisms more indicative of temperate zones and reduced sea-ice cover has been proposed to favor a 'pelagic' dominated ecosystem over the more typical 'benthic' dominated ecosystem indicative of Arctic Ocean shelves including the Northern Bering Sea shelf [*Piepenburg*, 2005]. Extensive jellyfish populations have reoccurred [*Napp et al.*, 2002], and the usual prominent coccolithophorid blooms of the southeastern Bering Sea [*Merico et al.*, 2006; *Stockwell et al.*, 2001] have been absent over the last few years. While most of these changes have been observed on the southeastern shelf, there is some evidence of change on the northern shelf as well [*Grebmeier et al.*, 2006; *Overland and Stabeno*, 2004]. Many of these changes have been attributed to global climate change and recent fluctuations in sea ice extent [*Hunt et al.*, 2002; *Rho and Whitledge*, 2007]. In recent years many studies have focused on this region due to its

biological diversity, economic impact and rapid changes. A great deal of research has centered on changing sea ice extent and its effect on the biological environment. In addition to impacting the distribution and abundance of higher trophic levels, climate change could be affecting pelagic phytoplankton primary production (PP) and food web dynamics [*Hunt and Stabeno*, 2002; *Hunt et al.*, 2002], the extent of which is uncertain. In contrast to continued sea-ice loss observed in the Arctic, cold conditions have persisted in the Bering Sea during winter/spring in recent years (2007-2011 with 2009-2010 being the coldest) following the warm 2001-2005 years [*Napp*, 2011], suggesting a decoupling between the two environments. The effect of rising temperatures and loss of sea ice on PP is also uncertain [*Grebmeier et al.*, 2010], with some studies indicating a decrease in PP based on benthic biomass and oxygen utilization [*Grebmeier et al.*, 2006], while others predicting an increase in PP owing to the longer growing season [*Loeng et al.*, 2005].

As the Bering Sea ecosystem responds to variations in climate, its capability to supply the resources on which the national and local economy depends will possibly change [*Grebmeier et al.*, 2006]. The implication of these changes on the physical environment and biota is difficult to forecast, owing both to the complexity of the interrelationships and to the limited duration and spatial coverage of observations made in the Bering Sea. A need for both short- and long- term monitoring is thus needed to identify the mechanisms linking short- and long-term physical changes to ecosystem variability, with longer term monitoring being critical for understanding and predicting changes in this ecosystem [*Sigler et al.*, 2010]. To accomplish this goal we require a combination of in-situ and laboratory measurements to determine the in-water physical, biological, optical properties within the region, as well as validated remote sensing observations to extend in-situ measurements. Remote sensing in combination with in-situ and laboratory

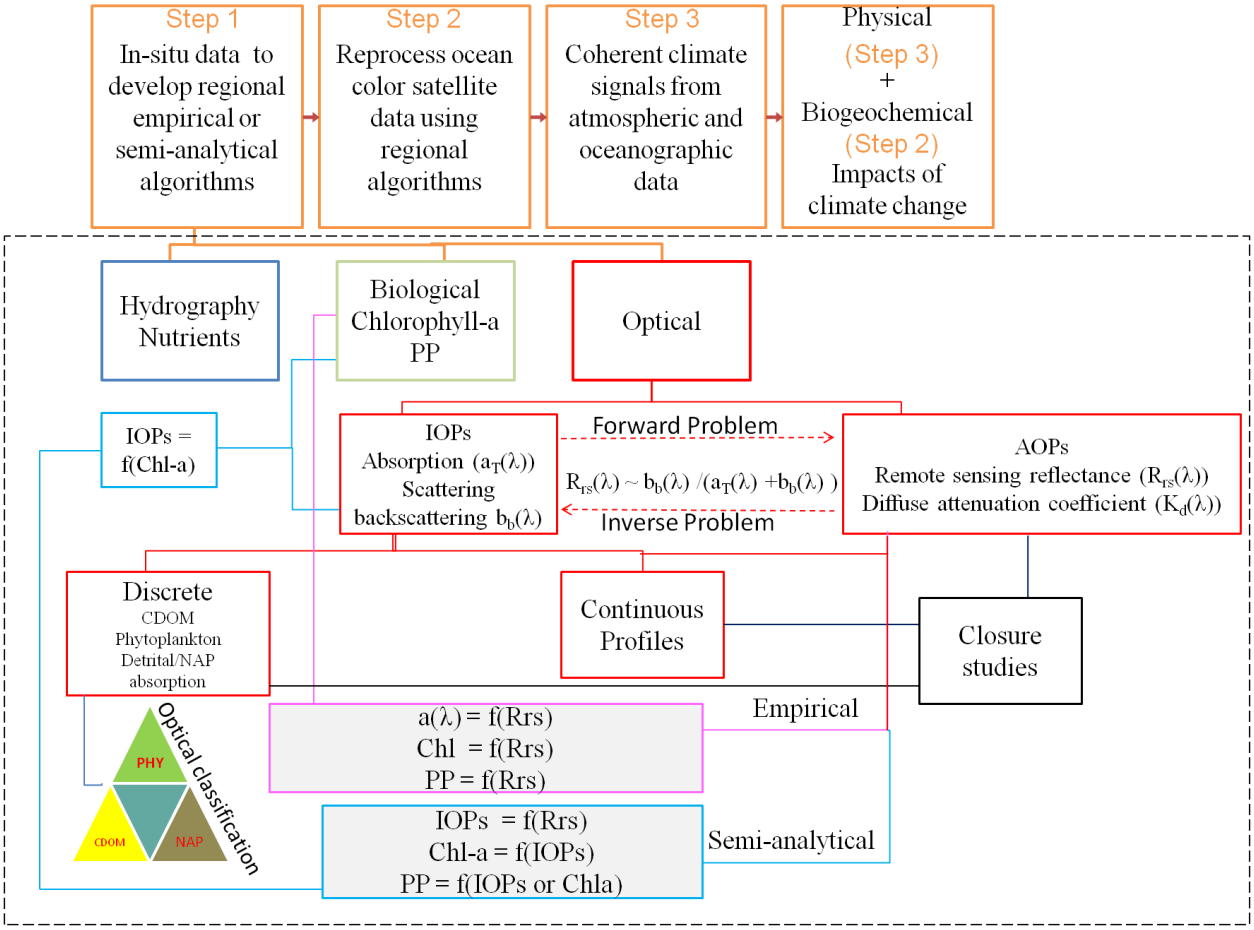

Figure 1.1. Simple schematic diagram of main goals of the NASA project (orange boxes)) and outline (indicated by the black dashed box) of the role of this dissertation in the framework of the NASA project.

measurements of physical biological and optical properties have considerable potential for monitoring and measuring the effects of such climate-driven changes on this ecosystem. Ocean color remote sensing is an important tool in conjunction with in-situ observations that can be used to understand both long and short-term variability with improved spatial and temporal resolution in the Bering Sea ecosystem. Ocean color has been extensively used at lower latitudes with success, but is hindered by a lack of baseline data on bio-optical properties that affect ocean color at higher latitudes such as in the Arctic and Bering Sea. While, a few studies on bio-optical properties have been documented for the Arctic Ocean, this is the first extensive study on bio-

optical properties in the Bering Sea. The research described in this dissertation is an attempt to combine in-situ and laboratory measurements of light absorption properties with modeling of underwater radiation fields and satellite remote sensing observations of ocean color for the southeastern Bering Sea. Most of the data used in this dissertation were collected as a part of the NASA funded project "Spatial and temporal variability in chlorophyll, primary production and carbon export in the Bering Sea linked to climate change." The main goals of this project are to "investigate the likely impacts of environmental anomalies in the Bering Sea on phytoplankton biodiversity, biomass distribution and productivity, and to understand the potential consequences of these on carbon export." A simple schematic diagram describing the main steps in reaching these goals and outlining my area of research are shown in Figure 1.1. Within the overall NASA project, specific objectives of this dissertation were:

- Determine the relation of absorption properties with respect to hydrographic and biogeochemical characteristics in each domain during the in-situ data collection.
- Compare specific phytoplankton absorption in southeastern Bering Sea waters relative to lower and middle latitudes waters.
- Parameterize and model phytoplankton and non-algal particulate (NAP) plus colored dissolved organic matter (CDOM) absorption spectra through spectral relationships.
- Identify the constituent (phytoplankton, NAP, or CDOM) that dominates light absorption in the southeastern Bering Sea waters and its influence on above water/under water light field and chlorophyll-a estimates from ocean color algorithms.
- Develop empirical algorithms and assess the standard semi-empirical Quasi Analytical Algorithm (QAA) for retrieval of absorption coefficients (phytoplankton and NAP plus CDOM) using MERIS and MODIS ocean color satellite data.

Study Region

The Bering Sea is a semi-enclosed sub-arctic sea linking the Pacific Ocean to the Arctic Ocean, with a deep ocean basin to the west and broad continental shelf on the east. The eastern Bering Sea shelf can be classified in to three domains, coastal (<50 m depth), middle (50-100 m), and outer (100-200 m) shelf domains based on oceanographic fronts (Figure 1.2) [*Coachman*, 1986]. Each of these domains has distinctive physical [*Coachman*, 1986], chemical [*Mathis et al.*, 2010], and biological environments [*Cooney and Coyle*, 1982]. The coastal domain which extends from the coast to 50 m isobath has a well-mixed water column due to wind and tidal currents. The inner front located approximately at the 50 m isobath separates the inner and the middle domains, while the central front generally follows the 100 m isobath representing a slow shift from the middle domain to the outer domain. The middle domain is well stratified with a two layer system, a wind mixed surface layer over denser tidally mixed bottom layer. The outer domain is similar in structure to the middle domain except the wind mixed surface layer is separated from the bottom layer by a transitional layer [*Kachel et al.*, 2002].

An important feature of the Bering Sea is the significant interannual variability in sea-ice cover [*Hunt et al.*, 2002; *Stabeno et al.*, 2001] that is related to large scale climatological patterns such as El Niño/Southern Oscillation (ENSO) and the Pacific-North American pattern (PNA) through atmospheric teleconnections and the Aleutian Low pressure system [*Niebauer*, 1988; *Stabeno et al.*, 2001; *Stabeno et al.*, 1999]. The Aleutian Low is a statistical feature resulting from the passage of storms across the Aleutian Island chain [*Stabeno et al.*, 1999], which are perturbed by the teleconnections. The intensification and southeastward displacement from the normal of the Aleutian low during an El Niño event is related to anomalous warming in the Bering Sea, while during La Nina events the weakening and westward displacement from the

normal of the Aleutian low is related to anomalous cooling in the Bering Sea [*Niebauer*, 1988]. The Aleutian low is typically weak during the summer, while during the winter Siberian high dominates Asia and the Aleutian low is strong. The juxtaposition of these features results in strong pressure gradients with an order of magnitude weaker wind torque in summer than in winter [*Stabeno et al.*, 1999]. The strong frigid winds from the northeast result in sea-ice formation during winter that has been described by a "conveyor belt" analogy [*Muench and Ahlnas*, 1976; *Overland and Pease*, 1982]. Sea ice that is produced in the northern Bering Sea is advected southward by winds where it comes in contact with warmer waters in the southern shelf thus cooling the water column [*Stabeno et al.*, 2007]. The leading edge of the ice is continuously melting, introducing cold, relatively fresh water into the water column which facilitates the further ice advance along the shelf [*Niebauer et al.*, 1999]. The ingression of the cold fresh water throughout the water column generates a lower layer of cold water. This cold layer gets isolated as the surface water warms up during the spring-summer season forming a feature known as the cold pool which is 40-50 m thick with temperatures below 2°C [*Kachel et al.*, 2002]. The southern edge of this cold pool represents an ecotone between arctic and subarctic communities and is considered to be shifting northwards in response to loss of sea ice, with the simultaneous migration of the arctic–subarctic species in the southeastern Bering Sea shelf [*Mueter and Litzow*, 2008]. During summer, the magnitude of solar radiation and wind speed at the sea surface are the most important atmospheric forcing that control the heating of the upper ocean during summer [*Stabeno et al.*, 2001]. The general circulation in the Bering Sea is part of the North Pacific sub-arctic gyre with advection of Pacific water from the Aleutian Stream through the various passes along the Aleutian Islands with net outflow into the Arctic through the Bering Strait (Figure 1.2) [*Schumacher and Stabeno*, 1998]. In the Bering Sea basin, circulation is in

the form of a cyclonic gyre, with the northward flowing Bering Slope current (BSC) forming the eastern current and the southward flowing Kamchatka current forming the western current and the Aleutian North Slope Current (ANSC) connecting the inflow through Amukta Pass and Amchitka Pass with the Bering Slope Current [*Schumacher and Stabeno*, 1998]. The circulation on the eastern Bering Sea is generally northwestward. While the northward transport through the Bering Strait is important to the Arctic Ocean, its effect on the circulation in the Bering Sea basin is negligible although influential in determining the circulation of the northern shelf [*Stabeno et al.*, 1999]. Although tidal energy governs most of the shelf circulation, some along-shelf flow along the bathymetry to the northwest is apparent in the coastal and outer domains [*Coachman*, 1986; *Overland and Roach*, 1987; *Stabeno et al.*, 1999]. On-shelf flow supplies nutrients to the shelf [*Stabeno et al.*, 1999; *Stabeno et al.*, 2006], whereas tidal mixing transports coastally

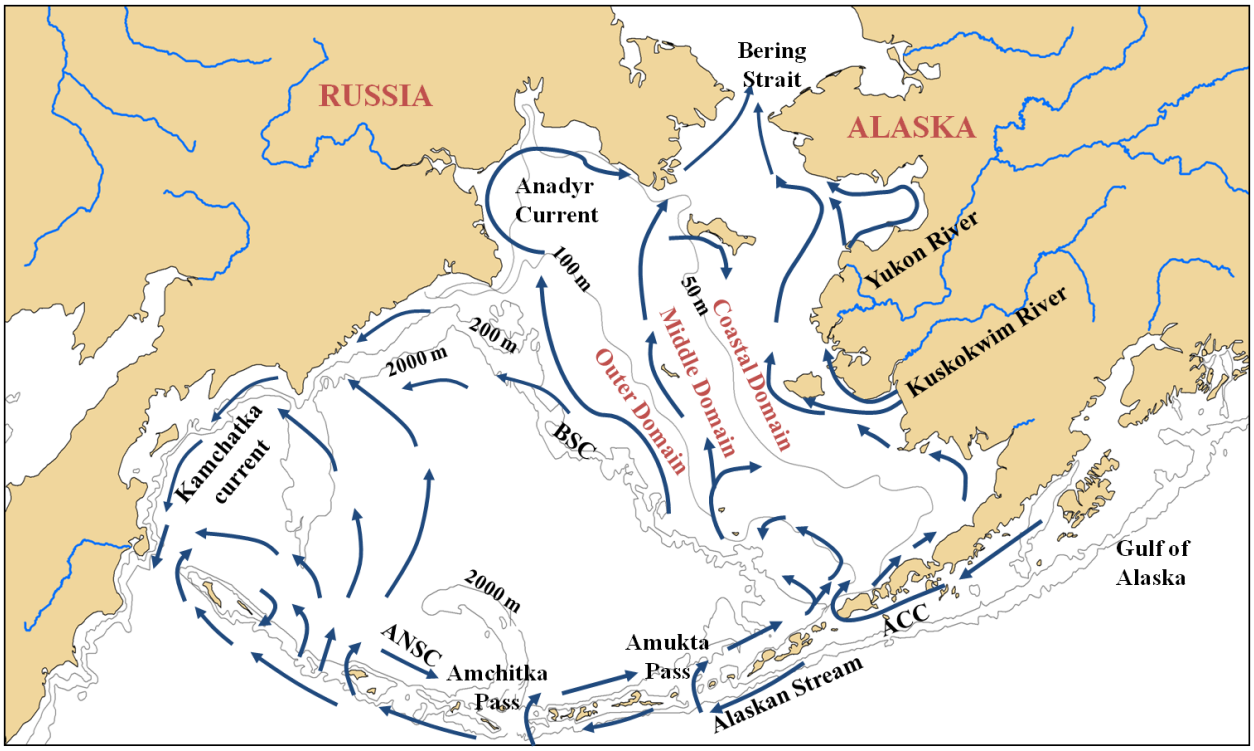

Figure 1.2. Study area showing the hydrographic domains and general circulation (arrows).

derived iron offshore towards the deep Bering Sea basin [*Aguilar-Islas et al.*, 2008]. The highest concentrations of iron and macronutrients tend to coincide at the Central Front. To the north, this productive water upwells as nutrient-rich Anadyr Water (AW), which makes its way into the Arctic Ocean via the western Bering Strait. Apart from ice melt, the Bering shelf receives a large volume of freshwater input from the Yukon and Kuskokwim rivers. The Yukon River has the fifth largest drainage basin in North America and delivers an annual average discharge of ~200 km^3 freshwater to the northern Bering shelf [*Stabeno et al.*, 2006] while Kuskokwim has a much smaller drainage basin delivering ~34 km^3 of freshwater to the southern and eastern parts of the Bering Sea [*Feely et al.*, 1981]. Although the maximum influence of river runoff is in the coastal domain, its influence is significant on the vertical structure of the coastal domain where it combines with shelf waters forming the low salinity water mass known as the Alaskan Coastal waters (ACW) [*Coachman*, 1986] which advects slowly northward to the narrow (90 km) and shallow (<50 m) Bering Strait, where it enters the Arctic Ocean [*Stabeno et al.*, 1999]. The ACW constitutes approximately one third of the flow into the Arctic Ocean with the AW making up the remaining. The AW is the primary source of dissolved nutrients to the western Arctic Ocean [*Codispoti et al.*, 2005], supporting high biomass in the southern Chukchi Sea [*Springer and McRoy*, 1993].

In the southeastern Bering Sea, PP occurs in two phases which is dependent on the timing of sea ice retreat. During early spring decreased wind mixing and melting of sea ice results in a stratified water column at the ice edge zone, which promotes an intense bloom at the ice edge. The PP is limited by the density stratification caused by retreating ice forming fresh melt water layer which cannot be overcome by wind mixing [*Niebauer et al.*, 1995]. The duration of this bloom is determined by the availability of shallow nutrients and represents the bulk of annual PP

on the eastern shelf [*Springer*, 1999; *Walsh and McRoy*, 1986]. The second phase of PP occurs when the solar radiation increases and stabilizes the water column to sustain an open water bloom. In the coastal domain PP is limited by the lack of continuous supply of macronutrients, as the frontal systems prohibit the high levels of nutrients from the middle and outer domain. Early in the season, nutrient concentrations are limited while iron concentrations are high in the coastal domain that allow for swift maximization of production rates; however extended periods of PP are limited by nutrient depletion [*Bond and Overland*, 2005; *Rho et al.*, 2005]. In the middle domain, the confluence of waters rich in iron derived from mixing of sediments of middle and coastal domains in the water column by tidal currents and the nutrient rich basin waters causes a significant buildup of biomass during summer. The intersection of the inverse gradients of nutrients overlap in the region of the central front where a highly productive region known as the "Green Belt" covers parts of both the Middle and Outer domains and the slope [*Okkonen et al.*, 2004; *Sambrotto et al.*, 2008; *Springer et al.*, 1996]. In this region PP is sustained throughout summer by the replenishment of nutrients by energetic eddies shed from the sharp front accompanying the northward-flowing Bering Slope Current [*Mizobata and Saitoh*, 2004]. The extent of sea-ice and timing of the sea-ice retreat is critical to PP. When sea-ice retreats later during the season, solar radiation is strong enough for PP to occur, with minimal grazing pressure and an increase in the carbon export to the benthos. When sea ice retreat occurs early during the season, light levels are not sufficient for production and the bloom is delayed. During the time between sea ice retreat and the increase in light levels sufficient enough for bloom formation, the solar radiation increases and heats up the water column, providing favorable condition for zooplankton growth. Once the bloom develops the zooplankton biomass is high, with the likely decrease in export of carbon to the benthos [*Saitoh et al.*, 2002].

The Role of Ocean Color Remote Sensing, the Problem and Conceptual Framework

Remote sensing is dependent on measurements of the spectral composition of light (ocean color) that emerges from the ocean surface and is influenced by the optical properties of the water and its constituents. By using appropriate bio-optical models and previous knowledge on how various substances influence the ocean color, remote sensing measurements can provide information on the water composition, the chlorophyll content and the PP in the upper ocean. However, existing uncertainties in our knowledge of bio-optical properties and modeling of underwater light fields point to the need for additional research, especially in the more complex Arctic regions. Although great progress has been made recently on ocean color observations using satellite sensors (SeaWiFS and MODIS), only a limited number of studies have been published on the interpretation and validation of satellite imagery for the Arctic; in fact, there has been no study on bio-optical properties in the Bering Sea. Previous studies using ocean color in the Arctic have shown that the annual PP in the Arctic has increased yearly by an average of 27.5 Tg C yr^{-1} since 2003 and by 35 Tg C yr^{-1} between 2006 and 2007. 30% of this increase has been attributed to decreased minimum summer ice extent and 70% to a longer phytoplankton growing season [*Arrigo et al.*, 2008]. While, in the Bering Sea synoptic spatial patterns of chlorophyll in conjunction with physical variables (e.g. SST, wind speeds) using ocean color data and multi-sensor satellite data have been analyzed [*Naik and D'Sa*, 2010; *Saitoh et al.*, 2002] (see Appendix B). The accuracy of these estimates is dependent on bio-optical models as well as the inputs to these models. In most satellite based PP models, chlorophyll-a is one of the most important input variable [*Behrenfeld and Falkowski*, 1997; *Campbell et al.*, 2002; *Carr et al.*, 2006; *Platt and Sathyendranath*, 1988]. Numerous studies have shown that there are large discrepancies between remote sensing reflectance ratio-derived and in-situ measured

chlorophyll-a concentrations in various regions within the Arctic Ocean [*Cota et al.*, 2004; *Matsuoka et al.*, 2007; *Mitchell*, 1992; *Stramska et al.*, 2006]. Previous studies suggest that pigment concentrations derived for the Bering Sea using global ocean color algorithms are lower than in-situ estimates [*Maynard and Clark*, 1987]. More recently, Schallenberg et al., (2008), demonstrated that chlorophyll-a was overestimated by the SeaWiFS OC2 algorithm in the Bering Sea. These discrepancies in the Arctic have been attributed to the unique bio-optical properties (lower specific phytoplankton absorption and high CDOM) in these regions relative to lower latitudes as well as limited data for the development of ocean color algorithms [*Cota et al.*, 2003; *Matsuoka et al.*, 2007; *Stramska et al.*, 2006; *Wang et al.*, 2005]. To address this concern, one achievable approach is to use semi-analytical models, which are inherently more flexible for retrieving phytoplankton biomass compared to purely empirical algorithms [*Carder et al.*, 1999; *Lee et al.*, 2002]. The retrieval accuracy of semi-analytical algorithms is often better than that of empirical algorithms [*Bukata et al.*, 1995; *Sathyendranath*, 2000]. However, the performance of these algorithms relies on accurate parameterization in the spectral models for the absorption coefficients of phytoplankton pigments and other light absorbing constituents. The spectral models for phytoplankton absorption are subject to spatial and temporal variation due to changing pigment composition and package effect. Therefore, regional in situ studies on the variability of phytoplankton absorption properties are fundamental to parameterizing the spectral models used in remote sensing algorithm.

Optical Properties of Natural Waters

The objective of this section is to provide the reader with the basic theoretical foundations for understanding the optical properties of water focusing on those used in this dissertation. The amount of light that penetrates to a given depth depends primarily on the properties of the air-

water interface and the optical properties of the constituents in the water column, such as the absorption, scattering, and scattering phase function. The optical properties of water can be divided into two mutually exclusive classes - Inherent optical properties (IOPs) and Apparent optical properties (AOPs) [*Preisendorfer*, 1976]. IOPs depend solely upon the medium and hence are independent of the ambient light field within the medium. IOPs include absorption, scattering and attenuation coefficients, refractive index and volume scattering function. The absorption coefficient explains how the medium absorbs light, and the volume scattering function describes how a medium scatters light; these are the two fundamental IOPs, based on which other IOP's can be derived. AOPs depend on both the medium (hence IOPs) and geometrical distribution of the light field. AOPs include scalar and vector irradiances, reflectance's average cosines, and diffuse attenuation coefficients [*Kirk*, 1994].

Natural waters are complex mixture consisting living or non-living, organic or inorganic, dissolved or particulate matter which are divided based on the operational definition that dissolved material is everything that passes through a filter whose pore size is ~ 0.2 -0.7 μm. These solutes and particles are both optically significant and highly variable in type and concentration. Therefore, the optical properties of natural waters show large temporal and spatial variability. Particulate matter and dissolved substances together with pure sea water determine the optical characteristics of natural water bodies and affect the amount of light that can penetrate through the water column.

When light penetrates the ocean, photons are either absorbed or scattered. While absorption removes the photons permanently from the path, scattering redirects the angle of the photon path. The absorption and scattering together determine the attenuation of underwater light field. The magnitude and spectral shape of absorption depends upon the concentration and composition of

the particulate and dissolved components as well as pure water (Figure 1.3). The IOPs are conservative and therefore the magnitude of the absorption coefficient varies linearly with the concentration of the absorbing constituent. The total absorption coefficient of seawater can be expressed as the sum of the absorption coefficients of each component (measured in m^{-1}) within the water column:

$$a_T(\lambda) = a_W(\lambda) + a_{CDOM}(\lambda) + a_{PHY}(\lambda) + a_{NAP}(\lambda) \quad \text{(Eq. 1)}$$

$$a_P(\lambda) = a_{PHY}(\lambda) + a_{NAP}(\lambda) \quad \text{(Eq. 2)}$$

$$a_{DG}(\lambda) = a_{CDOM}(\lambda) + a_{NAP}(\lambda) \quad \text{(Eq. 3)}$$

where $a_W(\lambda)$, $a_{CDOM}(\lambda)$, $a_{PHY}(\lambda)$, $a_{NAP}(\lambda)$, $a_P(\lambda)$ and $a_{DG}(\lambda)$ are absorption coefficients due to water, colored dissolved organic matter (CDOM), phytoplankton, non-algal matter (NAP), total particulate matter and dissolved plus detrital matter, respectively. The CDOM and NAP have similar spectral shape with strongest absorption in the blue and decreasing absorption with increasing wavelength, but CDOM has a steeper spectral slope [*Kirk*, 1994]. Absorption by water is weak in the blue and strong in the red (Figure 1.3) and varies with temperature and salinity. The particulate absorption is separated into phytoplankton and NAP by extraction in methanol as suggested by Kishino et al., 1985 [*Kishino et al.*, 1985]. The most spectral variability among the absorption coefficients is shown by phytoplankton absorption (Figure 1.3 and 1.4) due to absorption by various pigments but in general show two prominent peaks in blue and region due to the presence of chlorophyll-a. Pigments have unique absorption spectra which give a range of colors to phytoplankton and a range of spectral shapes to the respective absorption coefficients (Figure 1.3 and Figure 1.4). The major groups of pigments are the chlorophylls, the carotenoids

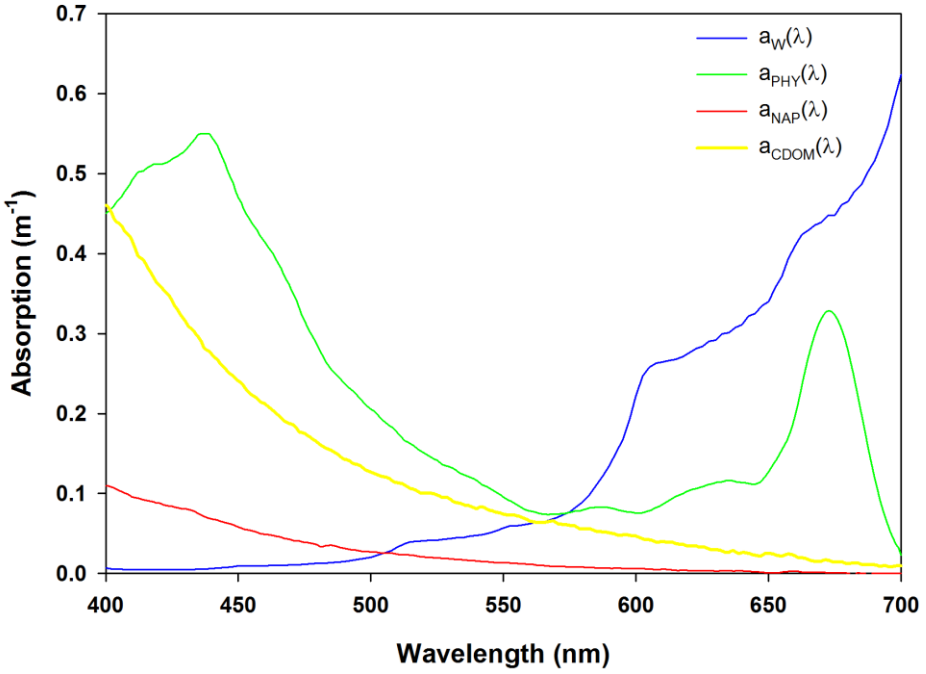

Figure 1.3. An example of absorption spectra of CDOM, NAP, phytoplankton and pure water.

and the phycobiliproteins. The chlorophyll specific absorption coefficient of phytoplankton, $a^*_{PHY}(\lambda)$, is defined as the $a_{PHY}(\lambda)$ per unit concentration of chlorophyll-a [*Morel and Bricaud*, 1981] and is important for estimating the amount of light absorbed by the phytoplankton. The value of $a^*_{PHY}(\lambda)$ was formerly considered to be relatively constant, averaging approximately 0.016 m^2 (mg chl-a)$^{-1}$ [*Bannister*, 1974], and most bio-optical models for estimating PP have frequently considered $a^*_{PHY}(\lambda)$ as constant, using mean value determined by Bannister, (1974). However, it is currently documented that the magnitude and the spectral shape of $a^*_{PHY}(\lambda)$ vary significantly [*Bricaud et al.*, 1995] (Figure 1.4). The variability in the magnitude and spectral shape of $a^*_{PHY}(\lambda)$ can be primarily be attributed to two factors: (1) package effect; i.e. pigments packed into chloroplasts are less efficient in absorbing light per unit pigment mass, than when in solution [*Kirk*, 1994], and/or (2) pigment composition of phytoplankton cells [*Bidigare et al.*, 1990; *Hoepffner and Sathyendranath*, 1991].

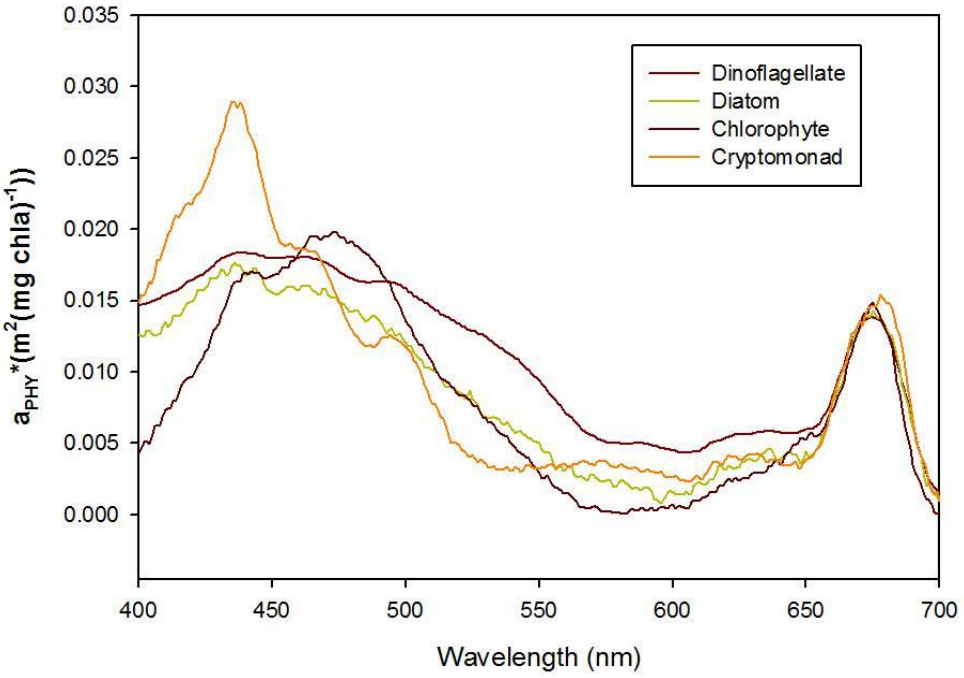

Figure 1. 4. Variability in specific phytoplankton absorption for different taxonomic groups.

Absorption of light in a fluid medium is commonly defined in the context of a collimated beam of light passing through a sample of known thickness, with loss of the incident light beam being attributable only to absorption [*Kirk*, 1994]. This dimensionless term and is usually the data returned by commercial spectrophotometers. Absorbance of a substance, also known as optical density (abbreviated as Abs(λ) or OD(λ)), is defined as the base 10 logarithm of the quotient of the intensity of the light passing through a sample and the intensity of the light passing through a blank [*Kirk*, 1994]. Absorption coefficient is defined in terms of the natural logarithm, so it is related to absorbance (optical density) as follows:

$$a(\lambda) = \frac{2.303\,[\mathrm{Abs}(\lambda)]}{l} \qquad \text{(Eq. 4)}$$

where l is the pathlength of the cuvette (usually 1 cm or 10 cm), λ is the wavelength, and the factor 2.303 converts the base 10 logarithm to the natural logarithm.

For $a_P(\lambda)$ measurements the pathelength is determined by dividing the volume filtered by the filter paper clearance area. However a pathlength amplification correction factor (β) has to be applied owing to multiple scattering within the filter paper [*Mitchell and Kiefer*, 1988]. The β factor is defined as the ratio of optical to geometric pathlength which is the ratio of volume filtered to the filter paper clearance area [*Butler*, 1964; *Duntley*, 1942]. In measurements of $a_P(\lambda)$ this is the largest source of error [*Mitchell et al.*, 2003] and hence in total light absorption. Quantitative corrections for pathlength amplifications have been determined empirically, by measuring Abs(λ) of particles in suspensions and relating it to Abs(λ) of particles measured on the filters [*Shibata*, 1958]. The eq. 4 for particulate absorption can then be expressed as:

$$Abs_s(\lambda) = a\,[Abs_f(\lambda)] + b\,[Abs_f(\lambda)]^2 \qquad \text{(Eq. 5)}$$

$$ap(\lambda) = \frac{2.303\,\lfloor Abs_s(\lambda)\rfloor}{(V/A)} \qquad \text{(Eq. 6)}$$

The coefficients a and b are determined empirically by applying a quadratic relation between Abs(λ) of particles in suspensions ($Abs_s(\lambda)$) and Abs(λ) of particles on the filters ($Abs_f(\lambda)$) and are dependent on the spectrophotometer configuration as well as phytoplankton species. $a_P(\lambda)$ (m^{-1}) is the total particulate absorption. The coefficient 2.303 is a factor for converting from base e to base 10 logarithm, V (m^3) is the volume filtered, and A (m^2) the filter paper clearance area.

Scattering intensifies attenuation mainly by increasing the pathlength a photon must traverse as well as by redirecting light into the backscattered direction and eventually out of the water.

The total scattering coefficient, $b(\lambda)$, and the backscattering coefficient, $b_b(\lambda)$, (measured in m^{-1}) are defined as:

$$b(\lambda) = 2\pi \int_0^{\pi} \beta(\theta)\sin(\theta)\,d\theta \qquad \text{(Eq. 7)}$$

$$b_b(\lambda) = 2\pi \int_{\pi/2}^{\pi} \beta(\theta)\sin(\theta)\,d\theta \qquad \text{(Eq. 8)}$$

where λ is the wavelength, θ is the scattering angle and $\beta(\theta,\lambda)$ is the volume scattering function (VSF) that describes the angular distribution of scattered radiation [*Preisendorfer*, 1976]. Like absorption, total scattering includes contribution from particulate and pure water except that scattering by CDOM is taken to be negligible [*Dall'Olmo et al.*, 2009].

The processes of scattering and absorption by dissolved and particulate matter in the ocean affect the spectrum and radiance distribution of the light emerging from the ocean, the so called water-leaving radiance. Water leaving radiances, reflectances and diffuses attenuation coefficients are the most commonly used AOPs. More specifically remote sensing reflectance ($R_{rs}(\lambda)$) is the AOP of choice for remote sensing of oceans [*O'Reilly et al.*, 1998].

The spectral irradiance reflectance ($R(\lambda)$) (no units) is defined as the ratio of upwelling to downwelling plane irradiances.

$$R(z,\lambda) = \left[\frac{E_u(z,\lambda)}{E_d(z,\lambda)}\right] \qquad \text{(Eq. 9)}$$

While the $R_{rs}(\lambda)$ (sr^{-1}) is defined as:

$$R_{rs}(0^+,\lambda) = \left[\frac{L_w(0^+,\lambda)}{E_d(0^+,\lambda)}\right] \qquad \text{(Eq. 10)}$$

where $E_u(z,\lambda)$ and $E_d(z,\lambda)$ are the upwelling and downwelling irradiances (W m^{-2} nm^{-1}) at depth 'z'. $L_w(0^+,\lambda)$ is the water leaving radiance (W m^{-2} nm^{-1} sr^{-1}) just above the sea surface (0^+).

The various radiances and irradiances all decrease approximately exponentially with depth in homogeneous water column which can be expressed as:

$$E_d(z,\lambda) = E_d(0,\lambda)\ \exp\left[-\int_0^z K_d(z,\lambda)dz\right] \qquad \text{(Eq. 11)}$$

where $K_d(z,\lambda)$ is the diffuse attenuation coefficient for spectral downwelling irradiance, which can be obtained by solving the above equation:

$$K_d(z,\lambda) = -\frac{1}{Ed(z,\lambda)}\left[\frac{d\left(Ed(z,\lambda)\right)}{dz}\right] \qquad \text{(Eq. 12)}$$

Similar expressions can be obtained for other diffuse attenuation coefficients [*Kirk*, 1994].

The primary goal of ocean color remote sensing is to describe the radiant flux that emerges from the ocean, and then by analysis of that flux, to derive information on the constituents existing in the water (e.g. phytoplankton, CDOM, and suspended sediments), this is so called 'inverse problem' [*Kirk*, 1994]. While, the forward radiative transfer problem is to predict the spectral distribution of $L_w(0^+,\lambda)$ based on a quantitative description of IOPs in the ocean. Both problems require the treatment of the radiative transfer equation to retrieve accurate or approximate numerical solutions. Models based on numerical simulations of the complex radiative transfer have been developed to obtain simplified relationships between AOPs such as $R_{rs}(\lambda)$ and $K_d(\lambda)$ to $a(\lambda)$, and $b_b(\lambda)$, of the medium through approximations:

$$R_{rs}(\lambda) = 0.54\,(f/Q)\left[\frac{b_b(\lambda)}{a_T(\lambda)+b_b(\lambda)}\right] \qquad \text{(Eq. 13)}$$

where the value of 0.54 accounts for the Fresnel reflectivity at the sea surface, f/Q ratio was set equal to 0.094 [*Gordon et al.,* 1988]; and

$$K_d(\lambda) = \frac{1}{\mu_0}\left[a_T(\lambda)^2 + (g_1\mu_0 - g_2)a_T(\lambda)b_b(\lambda)\right]^{1/2} \qquad \text{(Eq. 14)}$$

μ_0 is the cosine of the solar zenith angle (calculated from date and time of station location), g_1 and g_2 are constants taken equal to 0.425 and 0.19 respectively [*Kirk,* 1994]. Backscattering will have a larger influence on $R_{rs}(\lambda)$ compared to $K_d(\lambda)$, while more absorbing the water the lesser will be $R_{rs}(\lambda)$ and greater will be $K_d(\lambda)$.

Most ocean color algorithms utilize the blue to green $R_{rs}(\lambda)$ ratios for estimation of optically active constituents (e.g. chlorophyll-a) [*O'Reilly et al.,* 1998]. As the AOPs (e.g. $R_{rs}(\lambda)$) are dependent on the IOPs, variability in IOPs would consequently cause variations in $R_{rs}(\lambda)$. For e.g. higher CDOM absorption would result in lower blue to green $R_{rs}(\lambda)$ ratios and hence overestimation of chlorophyll-a, while lower $a^*_{PHY}(\lambda)$ would result in higher blue to green $R_{rs}(\lambda)$ ratios and hence underestimation of chlorophyll-a. The optical characteristics of natural waters are highly variable in different water bodies depending on biogeochemical processes. Natural waters having similar bio-optical character can be described by similar bio-optical models, hence natural waters can be classified based on their optical characteristics and the way they affect the spectral characteristics and magnitude of light penetrating through the water column. Classification of natural waters based on their optical properties into different types was introduced several decades ago [*Jerlov,* 1977; *Smith and Baker,* 1978]. A number of classifications have been proposed in order to describe the optical complexity of natural waters, the first being the use of Secchi disk invented in 1865 [*Arnone et al.,* 2004].

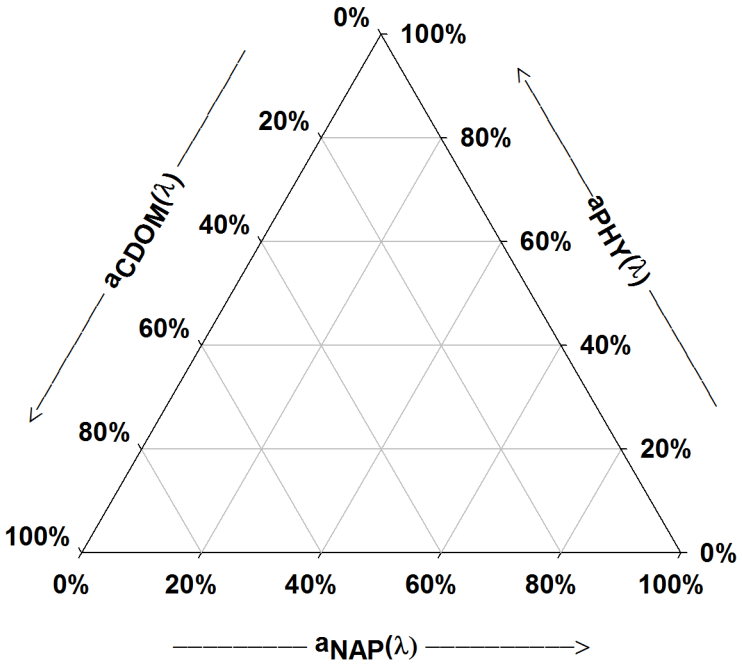

Figure 1.5. A schematic of ternary plot for optical classification of waters based on absorption coefficients of CDOM, phytoplankton and NAP.

The most common classification scheme is the classification of natural waters into Case 1 or Case 2 waters which was introduced by Morel and Prieur (1977) [*Morel and Prieur*, 1977], and developed later by Gordon and Morel (1983) [*Gordon and Morel*, 1983]. According to this classification, Case 1 waters are those waters in which phytoplankton and its associated materials are the primary components responsible for variations in optical properties of the water. While Case 2 waters are influenced not just by phytoplankton and related materials, but also by other substances, that vary independently of phytoplankton, particularly inorganic particles in suspension and CDOM. This classification scheme is qualitative; the means of going from a qualitative classification scheme to a more quantitative one is obtained by calculating an absorption budget and representing it on ternary diagrams as illustrated in Figure 1.5 [*Sathyendranath*, 2000]. However this method is not strictly quantitative [see [*Sathyendranath*, 2000]]. Ternary diagrams are used to distinguish water masses optically by assigning a point in a

triangle based on the relative contribution of $a_{CDOM}(\lambda)$, $a_{PHY}(\lambda)$, and $a_{NAP}(\lambda)$ to the total absorption minus that of water ($a_{T\text{-}W}(\lambda)$) at a specific wavelength. A point at the apex of triangle indicates waters where absorption is dominated by a single constituent whereas a point at the center of the triangle indicates waters where there is an equal contribution to absorption by all the constituents. Classification schemes as represented by Figure 1.5 have important outcomes from the perspective of modeling and interpretation of optical data.

The measurement of ocean color using space-based radiometers such as the Sea-viewing Wide Field-of-view Sensor (SeaWiFS), the Moderate Resolution Imaging Spectroradiometer (MODIS), and the Medium-Resolution Imaging Spectrometer (MERIS) allows us to examine changes in the Arctic ecosystem. This dissertation is focused on the characterization of the light absorption properties of the southeastern Bering Sea waters, and how these properties affect the underwater light field as well as the net amount of light radiating from the upper ocean (water leaving radiance ($L_w(\lambda)$)), as this is the variable measured using remote sensors. Concurrently, the inverse problem is how $L_w(\lambda)$ could be used to obtain optically active constituents (such as phytoplankton, CDOM and NAP) in these waters. I also focus on the classification of the southeastern Bering Sea waters based on the light absorption budget using ternary diagrams.

Specific questions addressed in the framework of this dissertation were:

(i) How are the absorption coefficients of phytoplankton, CDOM and NAP in the southeastern Bering Sea waters distributed with respect to hydrographic and biogeochemical characteristics of the shelf and can these be parameterized using spectral relationships?

(ii) How does the specific phytoplankton absorption in the southeastern Bering Sea compare relative to lower and middle latitudes waters?

(iii) What is the contribution of phytoplankton, CDOM and NAP to the total light absorption in Bering Sea waters (optical classification through absorption budget) and how do they affect the light field?

(iv) How is the "optical closure" between measured IOPs and modeled AOPs based on simplified radiative transfer modeling?

(v) How well do satellite estimates of remote sensing reflectance and surface absorption coefficients in the southeastern Bering Sea waters compare to in-situ measurements and are the bio-optical models or empirical relationships currently used in satellite algorithms applicable to the southeastern Bering Sea waters?

The approach towards this dissertation is comprised of two-parts, the first part is to develop effectual methodological techniques and the second part is the applications of these techniques to the study region. **Chapters 2** and **3** of this dissertation pertain to the general methodology. As the primary source of error in measurements of particulate absorption (and hence total absorption) are due to pathlength amplification, a set of laboratory experiments were carried out to determine the pathlength amplification factor using phytoplankton cultures grown in the laboratory and natural water samples for two different spectrophotometer configurations used in this study (**Chapter 2**). At the same time comparisons were made between the two instruments to test the performance of the instruments to measure phytoplankton absorption. The basic methodological techniques for understanding the optical variability in absorption properties were developed and applied to the Atchafalaya shelf region which are optically complex waters (case 2 waters with high non-covarying CDOM and NAP absorption) (**Chapter 3**). This study showed the potential utility of these techniques to decipher intermingling optically active constituents and its subsequent effect on ocean color retrievals. Similar techniques were applied to the

southeastern Bering Sea, which are also case 2 waters (high non-covarying CDOM absorption). The **Chapter 3** has been published as a journal paper in the International Journal of Remote Sensing.

In **Chapter 4** the light absorption properties are described with respect to hydrographic and biogeochemical characteristics in each domain to show their spatial variability and parameterization of the absorption coefficients using simple spectral relationships are presented. The bio-optical properties of polar regions have been shown to be significantly different from lower latitudes particularly due to lower specific phytoplankton absorption [Mitchell and Holm-Hansen, 1991; Mitchell, 1992; Fenton et al., 1994; Dierssen and Smith]. **Chapter 4** discusses these differences in relation to chlorophyll-a concentration. The relative contribution of the absorption coefficients to the total non-water absorption in the form of ternary plots at specific wavelengths of the visible domain are presented and explained in **Chapter 4**. The validation of remote sensing observations from satellite instruments with in-situ measurements and underwater light modeling using IOPs allow ocean color data to be used to examine the concentration and composition of optical constituents in surface waters over larger temporal and spatial scales. It is important to analyze the main concerns that effect the agreement between satellite and in-situ measurements. To evaluate the above issues, in-situ measurements of in-water optical properties and radiation fields were conducted and laboratory measurements of absorption coefficients were analyzed (**Chapter 4 and Chapter 5**). The combination of detailed measurements conducted allowed for an "optical closure" study, as measured IOPs can be used to model AOPs (Rrs(λ) and Kd(λ)), while measured Rrs(λ) and Kd(λ)) can be compared to the model's results. Such closure studies serves dual purposes, first it provides confidence on the accuracy of individual measurements and second it helps to understand the uncertainties in ocean

color algorithms (**Chapter 4**). The in-situ analyses of absorption properties were also applied to the interpretation and validation of satellite observations (**Chapter 5**). The **Chapter 5** has been published as a journal paper in the Journal of Applied Remote Sensing. Most of the satellite algorithms used to obtain estimates of chlorophyll concentration and light absorption in the water are based on "global" parameterizations and bio-optical models, whether these methods are applicable for southeastern Bering Sea waters are shown in **Chapters 4 and 5.** Finally, in **Chapter 6** of this dissertation, I summarize my results and propose areas for future work.

References

Aguilar-Islas, A. M., R. D. Rember, C. W. Mordy, and J. Wu (2008), Sea ice derived dissolved iron and its potential influence on the spring algal bloom in the Bering Sea, Geophysical Research Letters, 35(24).

Arnone, R. A., A. M. Wood, and R. W. Gould (2004), The evolution of optical water mass classification, Oceanography, 17, 14–15.

Arrigo, K., G. van Dijken, and S. Pabi (2008), Impact of a shrinking Arctic ice cover on marine primary production, Geophysical Research Letters, 35(19).

Bannister, T. (1974), Production equations in terms of chlorophyll concentration, quantum yield, and upper limit to production, Limnology and Oceanography, 19(1), 1-12.

Behrenfeld, M., and P. Falkowski (1997), Photosynthetic rates derived from satellite-based chlorophyll concentration, Limnology and Oceanography, 42(1), 1-20.

Bond, N., and J. Overland (2005), The importance of episodic weather events to the ecosystem of the Bering Sea shelf, Fisheries Oceanography, 14(2), 97-111.

Bricaud, A., M. Babin, A. Morel, and H. Claustre (1995), Variability in the chlorophyll-specific absorption-coefficients of natural phytoplankton - analysis and parameterization, Journal of Geophysical Research-Oceans, 100(C7), 13321-13332.

Bukata, R., J. Jerome, K. Kondratyev, and D. Pozdnyakov (1995), Optical properties and remote sensing of inland and coastal waters, CRC Press, Boca Raton, Fla.

Butler, W. L. (1964), Absorption spectroscopy in vivo - theory and application, Annual Review of Plant Physiology, 15, 451-460.

Campbell, J., et al. (2002), Comparison of algorithms for estimating ocean primary production from surface chlorophyll, temperature, and irradiance, Global Biogeochemical Cycles, 16(3).

Carder, K. L., F. Chen, Z. Lee, S. Hawes, and D. Kamykowski (1999), Semianalytic Moderate-Resolution Imaging Spectrometer algorithms for chlorophyll a and absorption with bio-optical domains based on nitrate-depletion temperatures, Journal of Geophysical Research-Oceans, 104(C3), 5403.

Carr, M., et al. (2006), A comparison of global estimates of marine primary production from ocean color, Deep Sea Research Part II-Topical Studies in Oceanography, 53(5-7), 741-770.

Coachman, L. K. (1986), Circulation, water masses, and fluxes on the southeastern Bering Sea shelf, Continental Shelf Research, 5(1-2), 23-108.

Codispoti, L., C. Flagg, V. Kelly, and J. Swift (2005), Hydrographic conditions during the 2002 SBI process experiments, Deep Sea Research Part II-Topical Studies in Oceanography, 52(24-26), 3199-3226.

Cooney, R. T., and K. O. Coyle (1982), Trophic implications of cross-shelf copepod distributions in the southeastern Bering Sea, Marine Biology, 70(2), 187-196.

Cota, G. F., H. Wang, and J. C. Comiso (2004), Transformation of global satellite chlorophyll retrievals with a regionally tuned algorithm, Remote Sensing of Environment, 90(3), 373-377.

Cota, G. F., W. G. Harrison, T. Platt, S. Sathyendranath, and V. Stuart (2003), Bio-optical properties of the Labrador Sea, Journal of Geophysical Research-Oceans, 108(C7).

Dall'Olmo, G., T. K. Westberry, M. J. Behrenfeld, E. Boss, and W. H. Slade (2009), Significant contribution of large particles to optical backscattering in the open ocean, Biogeosciences, 6(6), 947-967.

Duntley, S. (1942), The optical properties of diffusing materials, Journal of the Optical Society of America, 32(2), 61-70.

Feely, R. A., G. J. Massoth, and A. J. Paulson (1981), The distribution and elemental composition of suspended particulate matter in Norton Sound and the northeastern Bering Sea shelf: implications for Mn and Zn recycling in coastal waters, The Eastern Bering Sea Shelf: Oceanography and Resources, 1, 321-337.

Gordon, H. R., and A. Morel (1983), Remote Assessment of Ocean Color for Interpretation of Satellite Visible Imagery, Springer-Verlag, New York, USA.

Gordon, H. R., O. B. Brown, R. H. Evans, J. W. Brown, R. C. Smith, K. S. Baker, and D. K. Clark (1988), A semianalytic radiance model of ocean color, Journal of Geophysical Research-Atmospheres, 93(D9), 10909-10924.

Grebmeier, J. M., W. O. Smith Jr., and R. J. Conover (1995), Biological processes on Arctic continental shelves: ice-ocean-biotic interactions, in Arctic Oceanography: Marginal Ice Zones and Continental Shelves., edited by W. O. Smith Jr and J. M. Grebmeier, AGU, Washington DC, USA.

Grebmeier, J. M., S. E. Moore, J. E. Overland, K. E. Frey, and R. Gradinger (2010), Biological response to recent Pacific Arctic sea ice retreats, EOS Transactions, 91, 161-168.

Grebmeier, J. M., J. E. Overland, S. E. Moore, E. V. Farley, E. C. Carmack, L. W. Cooper, K. E. Frey, J. H. Helle, F. A. McLaughlin, and S. L. McNutt (2006), A major ecosystem shift in the northern Bering Sea, Science, 311(5766), 1461-1464.

Hunt, G., and P. Stabeno (2002), Climate change and the control of energy flow in the southeastern Bering Sea, Progress in Oceanography, 55(1-2), 5-22.

Hunt, G., P. Stabeno, G. Walters, E. Sinclair, R. Brodeur, J. Napp, and N. Bond (2002), Climate change and control of the southeastern Bering Sea pelagic ecosystem, Deep Sea Research Part II-Topical Studies in Oceanography, 49(26), 5821-5853.

Jerlov, N. G. (1977), Classification of sea-water in terms of quanta irradiance, Journal Du Conseil, 37(3), 281-287.

Kachel, N., G. Hunt, S. Salo, J. Schumacher, P. Stabeno, and T. Whitledge (2002), Characteristics and variability of the inner front of the southeastern Bering Sea, Deep Sea Research Part II-Topical Studies in Oceanography, 49(26), 5889-5909.

Kirk, J. T. O. (1994), Light and Photosynthesis in Aquatic Ecosystems, 2 ed., Cambridge University Press, New York.

Kishino, M., M. Takahashi, N. Okami, and S. Ichimura (1985), Estimation of the spectral absorption-coefficients of phytoplankton in the sea, Bulletin of Marine Science, 37(2), 634-642.

Lee, Z., K. Carder, and R. Arnone (2002), Deriving inherent optical properties from water color: a multiband quasi-analytical algorithm for optically deep waters, Applied Optics, 41(27), 5755-5772.

Loeng, H., K. Brander, E. Carmack, S. Denisenko, K. Drinkwater, B. Hansen, K. Kovacs, P. Livingston, F. McLaughlin, and E. Sakshaug (2005), Marine systems Rep., 453-538 pp, Cambrindge Univ. Press, Cambridge, U. K.

Mathis, J., J. Cross, N. Bates, S. Moran, M. Lomas, C. Mordy, and P. Stabeno (2010), Seasonal distribution of dissolved inorganic carbon and net community production on the Bering Sea shelf, Biogeosciences, 7(5), 1769-1787.

Matsuoka, A., Y. Huot, K. Shimada, S. I. Saitoh, and M. Babin (2007), Bio-optical characteristics of the western Arctic Ocean: implications for ocean color algorithms, Canadian Journal of Remote Sensing, 33(6), 503-518.

Maynard, N. G., and D. K. Clark (1987), Satellite color observations of spring blooming in Bering Sea shelf waters during the ice edge retreat in 1980, Journal of Geophysical Research, 92(C7), 7127-7139.

Merico, A., T. Tyrrell, and T. Cokacar (2006), Is there any relationship between phytoplankton seasonal dynamics and the carbonate system?, Journal of Marine Systems, 59(1-2), 120-142.

Mitchell, B. G. (1992), Predictive biooptical relationships for polar oceans and marginal ice zones, Journal of Marine Systems, 3(1-2), 91-105.

Mitchell, B. G., and D. A. Kiefer (1988), Chlorophyll-a specific absorption and fluorescence excitation spectra for light-limited phytoplankton, Deep Sea Research Part I-Oceanographic Research Papers, 35(5), 639-663.

Mitchell, B. G., M. Kahru, J. Wieland, and M. Stramska (2003), Determination of spectral absorption coefficients of particles, dissolved materials and phytoplankton for discrete water samples, in Ocean Optics Protocols For Satellite Ocean Color Sensor Validation, Revision 4, Volume 4: Inherent optical properties: instruments, characterization, field measurements and data analysis protocols, edited by J. L. Mueller, G. S. Fargion and C. R. McClain, pp. 39-64, NASA Tech. Rep., Greenbelt, Maryland.

Mizobata, K., and S. Saitoh (2004), Variability of Bering Sea eddies and primary productivity along the shelf edge during 1998-2000 using satellite multisensor remote sensing, Journal of Marine Systems, 50(1-2), 101-111.

Morel, A., and L. Prieur (1977), Analysis of variations in ocean color, Limnology and Oceanography, 22(4), 709-722.

Morel, A., and A. Bricaud (1981), Theoretical results concerning light absorption in a discrete medium, and application to specific absorption of phytoplankton, Deep Sea Research Part I-Oceanographic Research Papers, 28(11), 1375-1393.

Muench, R. D., and K. Ahlnas (1976), Ice movement and distribution in Bering Sea from March to June 1974, Journal of Geophysical Research-Oceans and Atmospheres, 81(24), 4467-4476.

Mueter, F., and M. Litzow (2008), Sea ice retreat alters the biogeography of the Bering Sea continental shelf, Ecological Applications, 18(2), 309-320.

Naik, P., and E. J. D'Sa (2010), Empirical Orthogonal Function (EOF) analysis of sea-surface temperature and chlorophyll in the eastern Bering Sea, paper presented at Remote Sensing of the Ocean, Sea Ice, and Large Water Regions 2010, SPIE, Toulouse, France.

Napp, J. (2011), The Bering Sea: Current Status and Recent Events Rep., PICES Press.

Napp, J., C. Baier, R. Brodeur, K. Coyle, N. Shiga, and K. Mier (2002), Interannual and decadal variability in zooplankton communities of the southeast Bering Sea shelf, Deep Sea Research Part II-Topical Studies in Oceanography, 49(26), 5991-6008.

Niebauer, H. J. (1988), Effect of El Nino Southern Oscillation and north pacific weather patterns on interannual variability in the subarctic Bering Sea, Journal of Geophysical Research-Oceans, 93(C5), 5051-5068.

Niebauer, H. J., V. Alexander, and S. M. Henrichs (1995), A time-series study of the spring bloom at the Bering Sea-ice edge .1. Physical processes, chlorophyll and nutrient chemistry, Continental Shelf Research, 15(15), 1859-1877.

Niebauer, H. J., N. A. Bond, L. P. Yakunin, and V. V. Plotnikov (1999), An update on the climatology and sea ice of the Bering Sea, University of Alaska Sea Grant, Fairbanks, AK.

NRC (1996), The Bering Sea EcosystemRep., National Academy Press, Washington, D. C.

O'Reilly, J., S. Maritorena, B. Mitchell, D. Siegel, K. Carder, S. Garver, M. Kahru, and C. McClain (1998), Ocean color chlorophyll algorithms for SeaWiFS, Journal of Geophysical Research-Oceans, 103(C11), 24937-24953.

Okkonen, S., G. Schmidt, E. Cokelet, and P. Stabeno (2004), Satellite and hydrographic observations of the Bering Sea 'Green Belt', Deep Sea Research Part II-Topical Studies in Oceanography, 51(10-11), 1033-1051.

Overland, J. E., and C. H. Pease (1982), Cyclone climatology of the Bering Sea and its relation to sea ice extent, Monthly Weather Review, 110(1), 5-13.

Overland, J. E., and A. T. Roach (1987), Northward flow in the Bering and Chukchi Seas, Journal of Geophysical Research-Oceans, 92(C7), 7097-7105.

Overland, J. E., and P. J. Stabeno (2004), Is the climate of the Bering Sea warming and affecting the ecosystem?, EOS Transsations AGU, 85(33), 309-316.

Piepenburg, D. (2005), Recent research on Arctic benthos: common notions need to be revised, Polar Biology, 28(10), 733-755.

Platt, T., and S. Sathyendranath (1988), Oceanic primary production - estimation by remote-sensing at local and regional scales, Science, 241(4873), 1613-1620.

Preisendorfer, R. W. (1976), Hydrologic optics, 1757 pp., U.S. Dept. of Commerce, National Oceanic and Atmospheric Administration, Environmental Research Laboratories, Pacific Marine Environmental Laboratory, Honolulu.

Rho, T., and T. Whitledge (2007), Characteristics of seasonal and spatial variations of primary production over the southeastern Bering Sea shelf, Continental Shelf Research, 27(20), 2556-2569.

Rho, T., T. Whitledge, and J. Goering (2005), Interannual variations of nutrients and primary production over the southeastern Bering Sea shelf during the spring of 1997, 1998, and 1999, Oceanology, 45(3), 376-390.

Saitoh, S., T. Iida, and K. Sasaoka (2002), A description of temporal and spatial variability in the Bering Sea spring phytoplankton blooms (1997-1999) using satelite multi-sensor remote sensing, Progress in Oceanography, 55(1-2), 131-146.

Sambrotto, R., C. Mordy, S. Zeeman, P. Stabeno, and S. Macklin (2008), Physical forcing and nutrient conditions associated with patterns of Chl a and phytoplankton productivity in the southeastern Bering Sea during summer, Deep Sea Research Part II-Topical Studies in Oceanography, 55(16-17), 1745-1760.

Sathyendranath, S. (2000), Remote Sensing of Ocean Colour in Coastal, and Other Optically-Complex, WatersRep., IOCCG, Dartmouth, Canada.

Schallenberg, C., M. Lewis, D. Kelley, and J. Cullen (2008), Inferred influence of nutrient availability on the relationship between Sun-induced chlorophyll fluorescence and incident irradiance in the Bering Sea, Journal of Geophysical Research-Oceans, 113(C7).

Schumacher, J. D., and P. J. Stabeno (1998), The continental shelf of the Bering Sea, John Wiley and Sons, Inc., New York, NY.

Shibata, K. (1958), Spectrophotometry of intact biological materials - absolute and relative measurements of their transmission, reflection and absorption spectra, Journal of Biochemistry, 45(8), 599-623.

Sigler, M. F., H. R. Harvey, C. J. Ashjian, M. W. Lomas, J. M. Napp, P. J. Stabeno, and T. I. Van Pelt (2010), How Does Climate Change Affect the Bering Sea Ecosystem?, EOS Transactions, 91(48).

Smith, R. C., and K. S. Baker (1978), Optical classification of natural-waters, Limnology and Oceanography, 23(2), 260-267.

Springer, A., C. McRoy, and M. Flint (1996), The Bering Sea Green Belt: Shelf-edge processes and ecosystem production, Fisheries Oceanography, 5(3-4), 205-223.

Springer, A. M. (1999), Summary, conclusions, and recommendations, University of Alaska Sea Grant, Fairbanks, AK.

Springer, A. M., and C. P. McRoy (1993), The paradox of pelagic food webs in the northern Bering Sea .3. Patterns of primary production, Continental Shelf Research, 13(5-6), 575-599.

Stabeno, P., N. Bond, and S. Salo (2007), On the recent warming of the southeastern Bering Sea shelf, Deep Sea Research Part II-Topical Studies in Oceanography, 54(23-26), 2599-2618.

Stabeno, P., N. Bond, N. Kachel, S. Salo, and J. Schumacher (2001), On the temporal variability of the physical environment over the south-eastern Bering Sea, Fisheries Oceanography, 10(1), 81-98.

Stabeno, P. J., J. D. Schumacher, and K. Ohtani (1999), The physical oceanography of the Bering Sea, University of Alaska Sea Grant, Fairbanks, AK.

Stabeno, P. J., G. L. Hunt, J. M. Napp, and J. D. Schumacher (2006), Physical forcing of ecosystem dynamics on the Bering Sea shelf, John Wiley, New York, USA.

Stockwell, D., T. Whitledge, S. Zeeman, K. Coyle, J. Napp, R. Brodeur, A. Pinchuk, and G. Hunt (2001), Anomalous conditions in the south-eastern Bering Sea, 1997: nutrients, phytoplankton and zooplankton, Fisheries Oceanography, 10(1), 99-116.

Stramska, M., D. Stramski, S. Kaczmarek, D. B. Allison, and J. Schwarz (2006), Seasonal and regional differentiation of bio-optical properties within the north polar Atlantic, Journal of Geophysical Research-Oceans, 111(C8).

Walsh, J. J., and C. P. McRoy (1986), Ecosystem analysis in the southeastern Bering Sea, Continental Shelf Research, 5(1-2), 259-288.

Wang, J., G. F. Cota, and D. A. Ruble (2005), Absorption and backscattering in the Beaufort and Chukchi Seas, Journal of Geophysical Research-Oceans, 110(C4).

CHAPTER 2: PHYTOPLANKTON LIGHT ABSORPTION: ASSESSING SPECTROPHOTOMETRY AND SPECTRAL RECONSTRUCTION METHODS

Introduction

Estimation of light absorption by phytoplankton is important in determination of phytoplankton productivity from bio-optical models [*Behrenfeld and Falkowski*, 1997; *Sathyendranath et al.*, 1995] and for obtaining estimates of biological variables from remote sensing. It has been also used to provide information on taxonomic composition, and to analyze community structure [*Johnsen et al.*, 1994]. However, accurate estimates of phytoplankton absorption by conventional spectrophotometers are difficult due to relatively dilute concentrations of particulate matter in natural waters which are below the detection limits of laboratory spectrophotometers when measured on standard 1- or 10 cm cuvettes. A solution to this was first suggested by Yentsch, (1962), and later modified by Truper and Yentsch, (1967), where the latter concentrated bacterial cultures on a glass-fiber filters (GF/F) and measured the absorption directly on the wet filter. This technique known as the Quantitative filter technique (QFT) [*Mitchell*, 1990] is being used widely since then for measurement of light absorption of natural phytoplankton population [*Bricaud and Stramski*, 1990; *Kishino et al.*, 1985; *Mitchell and Kiefer*, 1988; *Yentsch and Phinney*, 1989]. The particulate absorption obtained from the QFT can be separated into absorption by phytoplankton and non-algal particulate matter (NAP) [*Kishino et al.*, 1985]. However, several sources of error have been identified in the QFT method that include, variations with saturation of filter paper and differential filter paper loading [*Mitchell*, 1990; *Roesler*, 1998], loses due to scattering (especially backscattering) [*Tassan and Ferrari*, 1995] and correction for baseline fluctuations and null corrections [*Mitchell et al.*, 2003]. The errors due to scattering can be reduced by using an integrating sphere attachment in conjunction with a

double beam spectrophotometer [*Nelson and Prezelin*, 1993]. But the issue of principal concern is pathlength amplification factor (β) that occurs due to multiple scattering within the filter paper. The β factor is defined as the ratio of optical to geometric pathlength which is the ratio of volume filtered to the filter paper clearance area [*Butler*, 1962; *Duntley*, 1942] and is the prime source of uncertainty in estimation of particulate absorption using the QFT method [*Roesler*, 1998]. The β factor is instrument (spectrophotometer configuration) as well as phytoplankton species and size dependent. Both theoretical [e.g. [*Lohrenz*, 2000; *Roesler*, 1998]] and empirical corrections [e.g. [*Arbones et al.*, 1996; *Bricaud and Stramski*, 1990; *Cleveland and Weidemann*, 1993; *Finkel and Irwin*, 2001; *Kiefer and SooHoo*, 1982; *Mitchell*, 1990; *Mitchell and Kiefer*, 1988]] for path amplification factor have been proposed. Most empirical corrections for β factor have been determined by measuring OD(λ) of phytoplankton suspensions and relating it to OD(λ) measured on the filters. The correction factor thus derived is then applied to field samples. Some consistency has been reported among the various empirical corrections for β factor [*Arbones et al.*, 1996; *Cleveland and Weidemann*, 1993; *Mitchell*, 1990; *Tassan and Ferrari*, 1995], but several studies have shown large deviations [*Finkel and Irwin*, 2001; *Moore et al.*, 1995]. There is significant uncertainty at present concerning the influence of phytoplankton/particle species/type, size, and refractive index on the β factor. The chief unresolved issues in the determination of β factor are the divergence in the β factor at high optical densities and the 'hysteresis effect' (several values of β for the same value of OD(λ)) leading to a wavelength dependency of the β factor [*Bricaud and Stramski*, 1990].

Taking into consideration the errors in measurement of particles concentrated on filter paper another alternative of enhancing spectroscopic sensitivity is to increase the sample cell pathlength by means of long-path cells [*Bricaud et al.*, 1981; *Peacock et al.*, 1994] or capillary

optical waveguide cells [*Belz et al.*, 1999; *D'Sa et al.*, 1999; *D'Sa and Steward*, 2001]. The reflective tube measurements have allowed in-situ measurements of absorption coefficients, regardless of difficulties with effects of bubbles and correction for scattering loses [*Zaneveld et al.*, 1990]. Using a similar principle as the reflective tube, various types of long-pathlength liquid core waveguides have been developed [*Fujiwara and Fuwa*, 1985] and introduced commercially by World Precision Instruments (Ultrapath™, WPI) (Figure 2.1). In such arrangements, light is guided in the liquid core, enters and passes through the capillary tubing and is reflected back into the liquid core at the glass/air or a low refractive index coating interface with optical fiber transporting light to and from the sample cell [*D'Sa et al.*, 1999; *D'Sa and Steward*, 2001]. These systems can be used for high-sensitivity UV-visible absorbance measurements and provide optical pathlengths up to tens of meters. Advantages in using a capillary waveguide include small sample volume (e.g., 100 μL to 10 mL) and higher sensitivity due to increased effective pathlength [*Miller et al.*, 2002]. Further, in conventional spectrophotometers with 1- and 10-cm cuvettes, a large amount of the scattered light will be lost, while in liquid core waveguides most of the scattered light will be trapped within the sample cell due to the waveguide action and eventually reach the detector. The liquid core waveguide systems have primarily been used to measure colored dissolved organic matter (CDOM) [*D'Sa et al.*, 1999] and rarely to measure particulate matter in suspension [*Belz et al.*, 2006; *D'Sa et al.*, 1998]. These studies have shown the potential for measurement of particulate matter in suspension on the waveguide. The Ultrapath waveguide can be used to measure particles concentrated on filter paper as well, by using a portable fiber optic based GF/F filter holder (Figure 2.1) [*Belz et al.*, 2006]. This set-up is much more portable allowing convenient absorption measurements of large number of samples

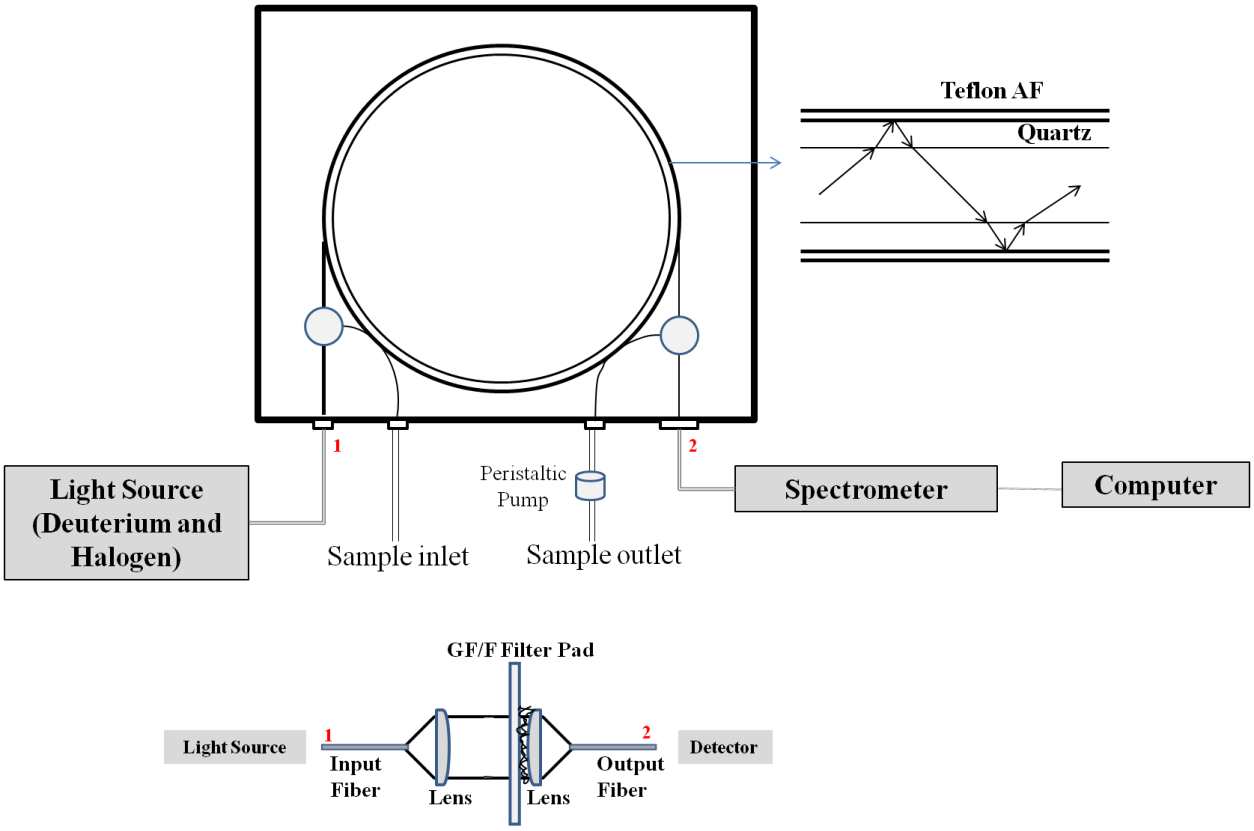

Figure 2.1. Schematic diagram of the Ultrapath waveguide system adapted from D'Sa et al., 1999 [*D'Sa et al.*, 1999], and the GF/F filter holder which is connected between points 1 and 2 (shown in red) adapted from Belz et al., 2006 [*Belz et al.*, 2006].

quickly in the field and is relatively less expensive than commercial spectrophotometers. There has been no study on measurements of particulates concentrated on filter paper on the Ultrapath waveguide.

Apart from purely spectrophotometric methods discussed earlier, the phytoplankton absorption spectra can also be determined by the approach suggested by Bidigare et al., 1990 using HPLC determined phytoplankton pigments. In this method phytoplankton absorption spectra is mathematically reconstructed by summation of the product of individual pigments concentration and their weight specific absorption coefficients [*Bidigare et al.*, 1990]. The major advantage of this method over the conventional spectrophotometric methods is that it can separate the total absorption into photosynthetically active and non-photosynthetically active

components [*Bidigare et al.*, 1989]. Unlike the spectrophotometric determination of phytoplankton absorption, the spectral reconstruction method is not influenced by the methanol treatment of particulate matter to obtain non-algal particulate matter absorption. However few disadvantages exist for the spectral reconstruction technique e.g. the reconstructed absorption spectra is affected by inefficient extraction of pigments and incorrect in-vivo specific absorption coefficients as well as the package effect (the absorption of pigments within cell structures is lower than when they are extracted in a solvent). Each of the above factors has a significant consequence on the reconstructed spectra, the package effect and inefficient extraction of pigments would cause overestimation and underestimation, respectively, of absorption spectra by the reconstructed spectra. The reconstruction method has been shown to perform reasonably well for open ocean waters [*Bidigare et al.*, 1990] but not as well for cultures and coastal waters for samples with significant package effect [*Nelson et al.*, 1993; *Sosik and Mitchell*, 1991].

In this study, a relationship between the $OD(\lambda)$ of samples in suspension ($OD_s(\lambda)$) and the optical density of the same sample on a GF/F filter ($OD_f(\lambda)$) are developed in order to determine our own β factor correction algorithm for the two different spectrophotometer configurations. The validity of the β factor is then tested by applying it to cultures and natural water samples. In order to test the potential of the Ultrapath waveguide to measure $OD(\lambda)$ and understand the variability in the relationship between $OD_s(\lambda)$ and $OD_f(\lambda)$ measured on the waveguide, a comparison of waveguide measurements to a double beam spectrophotometer equipped with an integrating sphere (Lambda 850) were evaluated. The differences in $OD(\lambda)$ observed between the two spectrophotometers are discussed in terms of scattering and pigment concentration of samples. Finally, we look determine phytoplankton absorption using the HPLC pigment

reconstruction approach of Bidigare et al., (1990) and compare to results obtained using the spectrophotometers.

Methods

Nine cultures were obtained from the Provasoli-Guillard Center for Culture of Marine Phytoplankton (CCMP) (Table 2.1) and grown in f/2 enriched sterile seawater medium [*Guillard and Ryther*, 1962] illumination of approximately 100 μmol photons m^{-2} s^{-1} under a 12:12 dark: light cycle . They were chosen to cover wide variations in the shape and size of the cells, pigment composition, structure of the cell wall, and intracellular pigment concentration. Before the spectrophotometric analysis, cultures were diluted with filtered culture media to provide a range of optical densities (OD(λ)).

Natural water samples were obtained from various estuarine, coastal and open ocean regions. Since phytoplankton cells are in low density in natural samples, they were concentrated so that measurements could be made on a 1cm cuvette. The samples were filtered on 0.22 μm Nucleopore membrane filters and resuspended in a small volume of the filtrate [*Bricaud and Stramski*, 1990].

Measurements of optical density of suspensions ($OD_s(\lambda)$) were made with a dual grating double beam Perkin Elmer Lambda 850 spectrophotometer equipped with an integrating sphere (referred to as lambda 850 hereafter) on a 1cm quartz cuvette and WPI Ultrapath™ hyperspectral waveguide capillary system (Ultrapath, WPI Inc., Sarasota, FL, USA) (referred to as waveguide hereafter) at 2 nm interval. The Ultrapath is a spectrophotometer together with a waveguide and has a user-selectable pathlength (2, 10, 50 and 200 cm) through a fiber optic cable (Figure 2.1) (D'Sa *et al.*, 1998). A peristaltic pump is used to inject water samples from a beaker containing the suspension into the sample cell at low rate. The incident light is provided by Deuterium and

Halogen light sources that is coupled to the sample cell via a fiber optic cable. The light travels by internal reflection within the waveguide and after exiting the waveguide is collected by a fiber optic cable connected to a photodiode array fiber optic spectrometer. The spectrophotometer is specified to have a dynamic range of 0.002 – 231 m^{-1}, with a maximum deviation in replicate spectra < 0.001 OD units [*Miller et al.*, 2002]. The sample cell was cleaned between measurements using successive rinses of Methanol, 10% HCL and Milli-Q water. $OD_s(\lambda)$ were measured on the waveguide by setting the pathlength to 2 cm and using culture filtrate as the blank. The $OD_s(\lambda)$ for the lambda 850 spectrophotometer was determined by placing phytoplankton culture in a 1cm quartz cuvette with the same volume of culture filtrate serving as a blank. For concentrated natural samples, the measurements were similar to those mentioned above except that filtrates of concentrated natural samples were used as blanks.

To measure the particles optical density of particle on filter paper ($OD_f(\lambda)$), samples were filtered onto 25 mm GF/F filters under low vacuum. Culture and natural samples volumes were chosen so that the geometric pathlength of the filtered samples matched the pathlength in the cuvette [*Cleveland and Weidemann*, 1993; *Finkel and Irwin*, 2001]. For measurements of particles on filters, the Ultrapath waveguide had an attachment for mounting filter papers which connected the light source and detector by fiber optic cables [*Belz et al.*, 2006] (Figure 2.1).A collimated light beam incident perpendicular to the GF/F filter is transmitted or scattered through the GF/F filter and collected by a second collimating lens behind the filter and coupled into an exit fiber [*Belz et al.*, 2006]. Similarly, the lambda 850 had a special filter holder which was placed at the entrance of the integrating sphere. The blank was obtained from the same volume of filtrate, filtered under low pressure onto a second filter. During the analyses saturation was maintained between the sample and blank filter [*Mitchell*, 1990]. The filters were placed in the

spectrophotometer on the special filter holders immediately after the filtration step. All measured OD(λ) were shifted to zero near the infrared region.

The pathlength amplification factor (β) can be determined by comparing $OD_s(\lambda)$ and $OD_f(\lambda)$. The relationships between $OD_s(\lambda)$ and $OD_f(\lambda)$ were fitted to a quadratic equation between 400 – 700 nm at 2 nm interval, as done in previous studies [*Arbones et al.*, 1996; *Cleveland and Weidemann*, 1993; *Mitchell*, 1990].

$$OD_s(\lambda) = a\,[OD_f(\lambda)] + b\,[OD_f(\lambda)]^2 \qquad \text{(Eq. 1)}$$

The coefficients a and b were determined for each of the nine cultures at different dilutions and all the cultures taken together.

Phytoplankton absorption spectra were obtained by using the Quantitative filter technique (QFT) [*Mitchell*, 1990] and corrected for pathlength amplification developed in this study, for comparison of with those reconstructed from HPLC [*Bidigare et al.*, 1990]. To separate the phytoplankton pigments within the particulate matter from non-algal material (NAP), methanol extraction was done [*Kishino et al.*, 1985]. OD(λ) measurements of total particulate matter ($OD_P(\lambda)$) were obtained by scanning the sample filter paper first, then the filter paper was scanned again after methanol extraction to obtain NAP optical density ($OD_{NAP}(\lambda)$). The $OD_p(\lambda)$ (corrected for pathlength amplification using eq. 1) was converted to absorption coefficients by using the equation:

$$ap(\lambda) = \frac{2.303\,[ODp(\lambda)]}{(V/A)} \qquad \text{(Eq. 2)}$$

where $a_P(\lambda)$ (m^{-1}) is the total particulate absorption. The coefficient 2.303 is a factor for converting from base e to base 10 logarithm, V (m^3) is the volume filtered, and A (m^2) the filter paper clearance area. $OD_{NAP}(\lambda)$ (corrected for pathlength amplification using eq.1) was converted to $a_{NAP}(\lambda)$ using the equation shown above. The phytoplankton absorption ($a_{PHY}(\lambda)$ (m^-

[1])) spectra were obtained by subtracting the $a_{NAP}(\lambda)$ (m^{-1}) from $a_P(\lambda)$ using the relation shown below:

$$a_{PHY}(\lambda) = a_P(\lambda) - a_{NAP}(\lambda) \quad \text{(Eq. 3)}$$

The LISST-100X (Laser In Situ Scattering and Transmissometry (LISST); Sequoia Scientific, Inc.) is an instrument that measures light scattering of a particle suspension at small forward angles, and inverts this information to estimate the particle size distribution (PSD) [*Agrawal and Pottsmith*, 2000]. A collimated laser beam (wavelength 670 nm) illuminates particles and the light scattered is sensed by a 32-ring detector (angle of acceptance equals 0.027°). Each ring measures the scattering intensity over a range of small forward angles for 32 different size classes logarithmically spaced from 2.5 to 500 μm. The instrument has been shown to provide reasonable results for laboratory phytoplankton cultures [*Karp-Boss et al.*, 2007; *Reynolds et al.*, 2010], and natural particles in coastal waters [*Ahn and Grant*, 2007]. For measurements of particles in suspension from cultures and natural samples, a manufacture supplied sample chamber was inserted into the optical head of the instrument. The samples were slowly poured into the sample chamber to avoid bubble formation, after cleaning of the optical windows with lens paper. Prior to sample analysis a background scan was measured using filtered seawater corresponding to samples. For each sample more than100 scans were collected. With the software provided by the manufacturers, the scattering intensities measured by the detector were mathematically inverted to obtain the PSD assuming that particles are spherical. The volume scattering function (VSF) (m^{-1} sr^{-1}) for the LISST 100X was obtained according to the method described by Agrawal, (2005). Normalized VSF (sr^{-1}) was obtained by dividing VSF by the beam attenuation coefficient (c (λ)) (m^{-1}).

For High-performance liquid chromatography (HPLC) determination, samples were filtered onto 25 mm GF/F paper and stored in liquid nitrogen until analysis. HPLC was used to determine pigments in the samples. Reconstructed absorption spectra of phytoplankton assemblages were calculated according to Bidigare et al. (1990). Reconstructed phytoplankton absorption ($a_{PHY}'(\lambda)$) at 2 nm intervals from 400 to 700 nm was calculated as the product of the concentration of phytoplankton and the specific absorption spectra of individual pigment groups, as follows:

$$a_{PHY}'(\lambda) = \sum_{i=1}^{n} c_i a_i^*(\lambda) \qquad \text{(Eq. 4)}$$

where c_i is the HPLC volume based concentration of pigment (mg m^{-3}); and $a_i^*(\lambda)$ is the specific absorption coefficient at wavelength λ (m^2 mg^{-1}). The pigment-specific absorption spectra were derived from absorption measurements of pure standards and were wavelength-shifted to match in-vivo absorption maxima [*Bidigare et al.*, 1990]. Pigment absorption spectra used represented chlorophylls (chlorophyll-a, chlorophyll-b, chlorophyll-$c_1 + c_2$), photosynthetic carotenoids (as the sum of peridinin, fucoxanthin, 19'-hexanoyloxyfucoxanthin, 19'-butanoyloxyfucoxanthin and prasinoxanthin) and photoprotective carotenoids (zeaxanthin, alloxanthin, diadinoxanthin and diatoxanthin). Extracted pigments are known to have higher absorption relative to the same pigments in intact cells due to the package effect [*Morel and Bricaud*, 1981]. To correct for the package effect, the Nelson et al., (1993) approach was used, as discussed next.

The fractional reduction in pigment absorption due to package effect ($Q_a^*(\lambda)$), defined as the ratio of the actual absorption coefficient, $a_{PHY}(\lambda)$, to the absorption coefficient of the same material in solution, $a_{PHY}'(\lambda)$ can be calculated as [*Morel and Bricaud*, 1981]:

$$Q_a^*(\lambda) = \frac{3}{2}\frac{Q_a(\lambda)}{\rho'(\lambda)} \qquad \text{(Eq. 5)}$$

where ρ' the dimensionless product of the absorption coefficient of the cell material ($a_{cm}(\lambda)$) and the cell diameter (d), represents the optical thickness of particles along its diameter [*Morel and Bricaud*, 1981] and $Q_a(\lambda)$ is the absorption efficiency given by van de Hulst, (1958):

$$Q_a(\lambda) = 1 + \frac{2^{-\rho'(\lambda)}}{\rho'(\lambda)} + 2\frac{e^{-\rho'(\lambda)} - 1}{\rho'(\lambda)^2} \quad \text{(Eq. 6)}$$

The chlorophyll-specific reconstructed spectrum ($a^*_{PHY}'(\lambda)$) is given by:

$$a^*_{PHY}{}'(\lambda) = \frac{a_{cm}(\lambda)}{C_i} \quad \text{(Eq. 7)}$$

where C_i is the intracellular chlorophyll-a concentration per unit cell volume (mg m^{-3}). Using the above equation ρ'(λ) can be written as:

$$\rho'(\lambda) = a_{cm}(\lambda)d = a^*_{PHY}{}'(\lambda)C_i d \quad \text{(Eq. 8)}$$

$Q_a^*(\lambda)$ can also be estimated as [*Morel and Bricaud*, 1981]:

$$Q_a{}^*(\lambda) = \frac{a^*_{PHY}(\lambda)}{a_{PHY}{}'(\lambda)} \quad \text{(Eq. 9)}$$

If $Q_a^*(\lambda)$ can be estimated, then the reconstructed spectra corrected for package effect can be calculated as the product of $a_{PHY}'(\lambda)$ and $Q_a^*(\lambda)$ [*Nelson et al.*, 1993]. Using eq. 9, $Q_a^*(\lambda)$ can be calculated at a single wavelength (676 nm in our study as at this wavelength chlorophyll-a is the dominant pigment). This value of $Q_a^*(\lambda)$ can be used in eq. 5 and solved simultaneously with eq. 6 to get ρ'(λ) which allows the estimation of wavelength independent product of C_i and d using eq. 8. The product of Ci and d can then be used to calculate $Q_a^*(\lambda)$ at all other wavelengths. Finally, the reconstructed spectra corrected for package effect can be calculated as the product of $Q_a^*(\lambda)$ and $a_{PHY}'(\lambda)$ [*Nelson et al.*, 1993].

Results and Discussion

Pathlength Amplification Factor for Lambda 850 and Ultrapath Waveguide

Following Mitchell, 1990 pathlength amplification were determined by fitting a quadratic equation to each pair of $OD_s(\lambda)$ and $OD_f(\lambda)$ between 400 nm to 700 nm at 2 nm interval for both lambda 850 and waveguide measurements. Values of $OD_s(\lambda)$ were restricted to <0.4 to reduce the influence of multiple scattering on the $OD_s(\lambda)$ and $OD_f(\lambda)$ relationship and as field data usually do not exceed this value [*Cleveland and Weidemann*, 1993; *Mitchell*, 1990]. In some samples $OD_s(\lambda)$ and $OD_f(\lambda)$ relation showed the 'hysteresis effect', where for the same value of $OD_f(\lambda)$ multiple values of $OD_s(\lambda)$ were observed depending on the wavelength [*Arbones et al.*, 1996; *Bricaud and Stramski*, 1990; *Roesler*, 1998]. The hysteresis did not show any species dependence but was rather dependent on the concentration of the samples, mainly occurring at low absorbing regions of the spectra (~ 540 nm – 590 nm – range is depended on the species) and was more severe at lower culture concentration (Figure 2.2a and Figure 2.3a). The hysteresis effect was much higher in waveguide measurements and was almost negligible for majority of the lambda 850 measurements (Figure 2.2a and Figure 2.3a). To avoid the biasing of our results due to this effect we either removed the regions of low absorption from the spectra where the hysteresis was present [*Nelson and Robertson*, 1993] or excluded spectra with very large hysteresis loops from the analysis. The above exclusions were mainly applicable to the waveguide measurements and not as much for the lambda 850 measurements (5 samples only).

The results of fitting a quadratic equation for all pairs of $OD_s(\lambda)$ and $OD_f(\lambda)$ for lambda 850 are shown in Figure 2.2b and Table 2.1. The variation of coefficients from species to species and

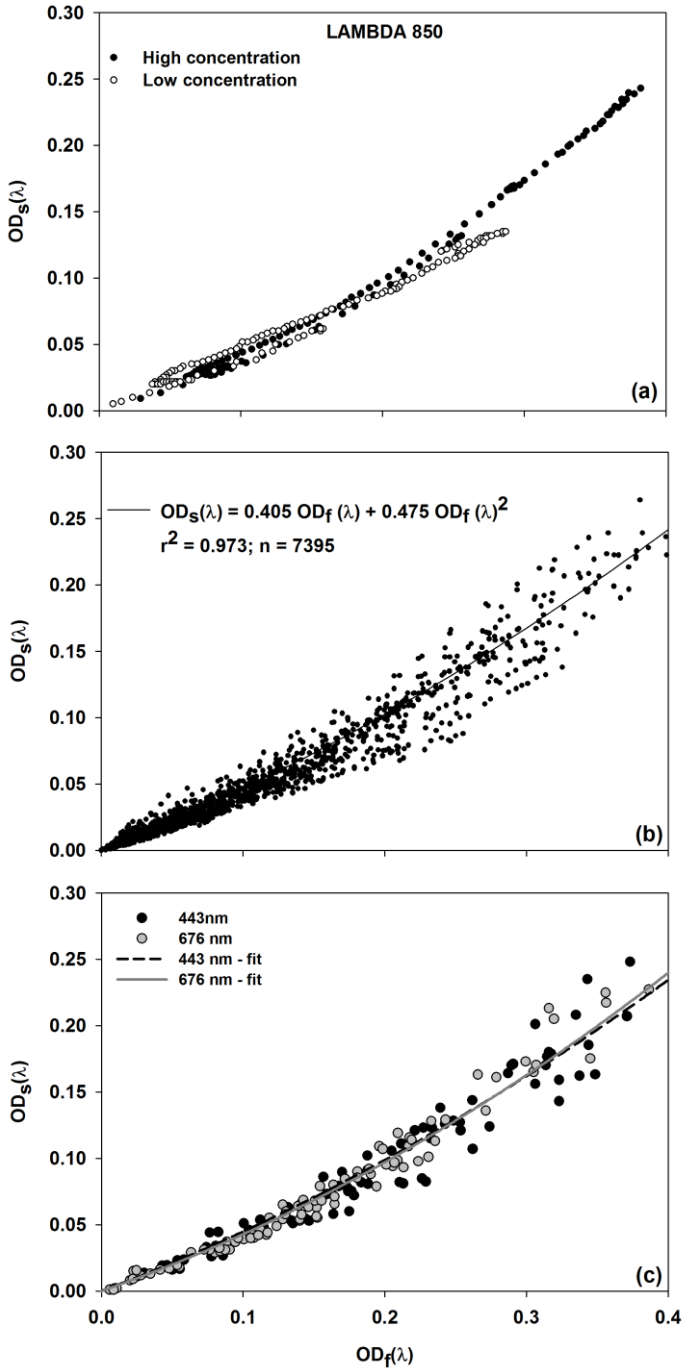

Figure 2.2. Relationship between (a) optical density of particles in suspension ($OD_s(\lambda)$) and optical density of particles on filter paper ($OD_f(\lambda)$) for lambda 850. The black solid line is the quadratic fit to the data, (b) $OD_s(\lambda)$ and $OD_f(\lambda)$ for lambda 850 at 443 nm (solid black circles) and 676 nm (solid gray circles). The black and gray dashed lines represent the quadratic fit for 443 nm and 676 nm, respectively.

Table 2.1. List of phytoplankton cultures and their coefficients (a and b) obtained by applying a quadratic fit (see eq. 1) between optical density of phytoplankton in suspension ($OD_s(\lambda)$) and optical density of phytoplankton on filter paper ($OD_f(\lambda)$). S.E. is represents the standard error.

Phytoplankton Species	**Taxonomic Class**	**Shape**	**a**	**S. E**	**b**	**S. E**	**r^2**
Thalassiosira nordenskioeldii	Coscinodiscophyceae	Forms chains	0.445	0.010	0.531	0.064	0.993
Chaetoceros atlanticus	Coscinodiscophyceae	Forms chains	0.378	0.007	0.503	0.021	0.991
Coscinodiscus radiatus	Coscinodiscophyceae	Centric	0.475	0.005	0.167	0.010	0.985
Skeletonema costatum	Coscinodiscophyceae	Forms chains	0.475	0.003	0.790	0.040	0.993
Phaeocystis antarctica	Prymnesiophyceae	Forms colonies	0.487	0.006	0.205	0.051	0.989
Myrionecta rubra	Ciliatea	Obovoid	0.495	0.009	0.225	0.060	0.989
Heterocapsa arctica	Dinophyceae	Oval armored	0.424	0.006	0.648	0.091	0.996
Pyramimonas parkeae	Prasinophyceae	Oval	0.468	0.003	0.726	0.061	0.992
Emiliania huxleyi	Prymnesiophyceae	Spherical	0.457	0.008	0.751	0.055	0.997

for all data pooled together is similar to that observed by other studies on β factor [*Arbones et al.*, 1996; *Cleveland and Weidemann*, 1993; *Mitchell*, 1990; *Nelson and Robertson*, 1993]. The fit for all data pooled together was robust with no effect of removal or addition of certain species data. Significant differences were found between the β corrections of individual species (F-test, $p<0.001$) consistent with other studies [*Arbones et al.*, 1996; *Finkel and Irwin*, 2001; *Moore et al.*, 1995]. Within the species the coefficient 'a' was less variable relative to coefficient 'b' (Table 2.1). The coefficient 'a' was not significantly different for species, but the coefficient 'b' was significantly different (F-test, $p<0.001$). Further the coefficient 'b' was inversely correlated to the HPLC chlorophyll-a concentration ($r^2 = 0.65$; $p<0.001$) and to average particle size estimated from LISST ($r^2 = 0.55$; $p<0.001$) (data not shown). So, much of the variations in the β

correction arise from the concentration of phytoplankton pigments and their size. The variability in phytoplankton species and size influence β by mostly influencing the $OD_s(\lambda)$ measurements, as stronger scattering due smaller cell sizes and cell shape or material would be overshadowed by the scattering of the filter, but would significantly affect the cuvette measurements. Especially for smaller particle size the VSF will have relatively more scattering at larger angles which is not collected by the detector optics even an integrating sphere. Similar to previous studies [e.g. [*Arbones et al.*, 1996; *Finkel and Irwin*, 2001; *Moore et al.*, 1995]], the significance of cell size and species composition on the β correction is corroborated by this study. Although these studies are consistent in terms of differences observed in species composition and β correction, the exact reason for these differences is still under debate. For e.g. inconsistency exists in the coefficient 'b', Moore et al., 1995 found 'b' coefficients are low for small sized cells (*Synechococcus sp*. and *Prochlorococcus marinus*), while in this and Finkel & Irwin, (2001) study the 'b' coefficients were lower for larger sized cells (Table 2.1). The reasons for these contradictions are not clear at present and warrant further research.

The β correction strongly depended on the range of OD(λ), with steeper relationships when higher OD(λ) were ignored and flatter relationship when higher OD(λ) were included similar to that observed by Mitchell et al., (1990). The sensitivity of β correction to the ranges in OD(λ) becomes more apparent while testing the wavelength dependency of β correction algorithm [*Cleveland and Weidemann*, 1993]. To check if there is a wavelength dependency of the β correction we applied the quadratic fit to wavelengths between 400-700 nm at every 10 nm. The coefficient 'a' showed little variation and was within 95% confidence intervals, but coefficient 'b' varied depending on the OD(λ) within the spectra, with wavelengths between 400-490 nm and 650-680 nm showing similar relationships. Results at two specific wavelengths (443 nm and

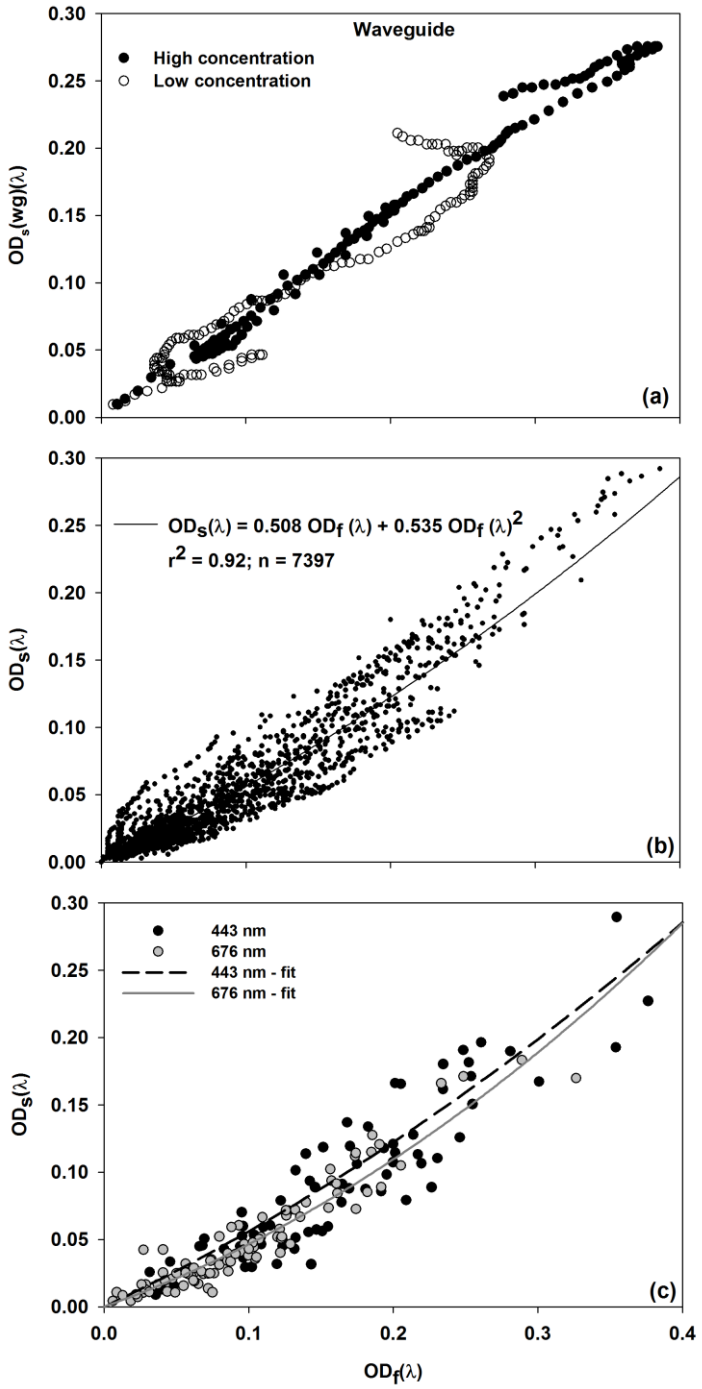

Figure 2.3. Relationship between (a) optical density of particles in suspension ($OD_s(\lambda)$) and optical density of particles on filter paper ($OD_f(\lambda)$) for waveguide. The black solid line is the quadratic fit to the data, (b) $OD_s(\lambda)$ and $OD_f(\lambda)$ for waveguide at 443 nm (solid black circles) and 676 nm (solid gray circles). The black and gray dashes lines represent the quadratic fit for 443 nm and 676 nm, respectively.

676 nm) are shown in Figure 2.2c. The fits for these two wavelengths are almost identical emphasizing that for similar ranges of OD(λ) the β was identical with no apparent wavelength dependency.

Obtaining a relationship between $OD_s(\lambda)$ and $OD_f(\lambda)$ for waveguide measurements is more complex, as the measurement of $OD_s(\lambda)$ in the waveguide is different from conventional spectrophotometers (Figure 2.1). Large hysteresis loops observed in this relationship, hindered the ability to determine accurate β for the waveguide (Figure 2.3a). Further, β correction differences between species were more noticeable in waveguide with differences present within species for different dilutions. However a statistically significant quadratic fit could be obtained albeit with large scatter for almost the whole range of $OD_s(\lambda)$ (Figure 2.3b). This relationship showed significant wavelength dependency (Figure 2.3c), with flatter relationship at 443 nm and steeper relationship at 676 nm. The relationship was sensitive to addition and removal of certain spectra, such a relationship is not applicable for β correction of particulate absorption. An insight into the variability of $OD_s(\lambda)$ and $OD_f(\lambda)$ measured on the waveguide can be obtained by comparisons with lambda 850 measurements (see next section). Such an analysis would serve dual purpose, firstly it would assist in obtaining an accurate pathlength amplification correction factor for the waveguide and secondly the potential of the waveguide to measure $OD_s(\lambda)$ and $OD_f(\lambda)$ could be tested relative to lambda 850.

Lambda 850 and Waveguide Comparisons

Previous studies have shown that the absorption measured using a spectrophotometer in conjunction with an integrating sphere (similar to lambda 850 in this study) is very close to the true absorption [*Morel and Bricaud*, 1981], hence the performance of the waveguide is tested by making comparisons between the waveguide and lambda 850 measurements. Comparisons of

$OD_f(\lambda)$ and $OD_s(\lambda)$ were made between the lambda 850 and waveguide for cultures as well as natural samples. Representative $OD_f(\lambda)$ for culture samples measured on the waveguide with a filter holder and lambda 850 are shown in Figure 2.4a. A very good agreement was observed between the two, with locations of primary absorption bands of chlorophyll-a at 443 nm and 676 nm as well as the other absorption bands between 450 - 500 nm corresponding to accessory pigments evident in both the spectra. However, the waveguide values showed an underestimation at the chlorophyll-a absorbance bands (443 nm and 676 nm) for all the species. The underestimation was greater at the red wavelengths relative to the blue wavelengths (Figure 2.4). Although the $OD_f(\lambda)$ was underestimated by the waveguide relative to the lambda 850, it was relatively small being on average 5% and never exceeded 10% (about 15 samples) for all the samples and at all wavelengths analyzed. Further, a strong linear relationship was observed between $OD_f(\lambda)$ from waveguide and lambda 850 at 676 nm and 443 nm for all dilutions of cultures (Figure 2.4b). The good agreement between the waveguide and lambda 850 $OD_f(\lambda)$ was not just restricted to culture samples, this was also observed in natural samples (Figure 2.4c). The natural samples were from diverse regions, collected from estuarine, coastal as well as open ocean waters from surface as well as depths corresponding to chlorophyll-a fluorescence maximum. The linear relationship did not show any regional trends, indicating that this relationship is valid for most environments and showed underestimations similar to culture samples. The strong linear relationship was observed at the 443 nm and 676 nm (Figure 2.4c) and also over the entire visible domain from 400 - 700 nm at 2 nm interval (data not shown). These results provide confidence on estimations of particulate absorption measurements using a waveguide with fiber optic filter holder.

Representative $OD_s(\lambda)$ for culture samples measured on the capillary waveguide and lambda

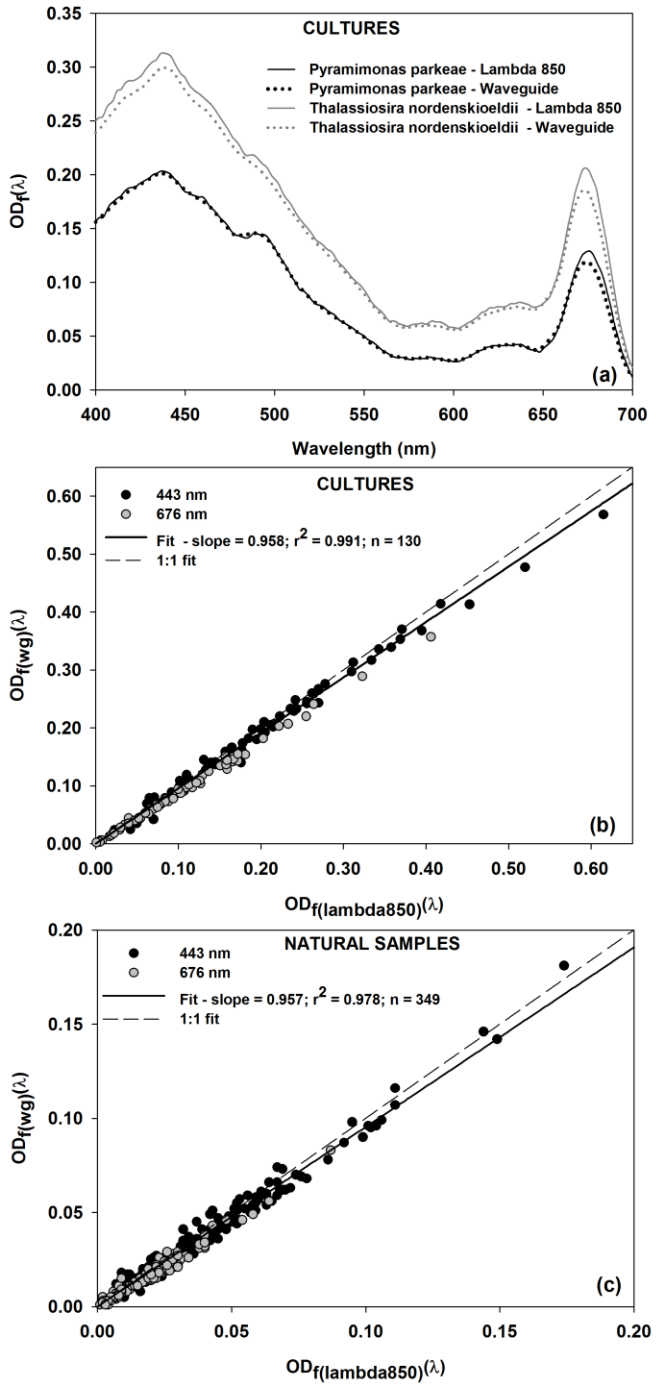

Figure 2.4. Comparison of (a) spectral shape of optical density of particles on filter paper ($OD_f(\lambda)$) for lambda 850 (solid lines) and waveguide (dotted lines) for two different cultures (b) $OD_f(\lambda)$ for lambda 850 and waveguide at two wavelengths 443 nm (solid black circles) and 676 nm (solid gray circles) for all cultures, and (c) $OD_f(\lambda)$ for lambda 850 and waveguide at two wavelengths 443 nm (solid black circles) and 676 nm (solid gray circles) for all natural samples. The black solid line is the best fit line and the black dashed line is the 1:1 fit for our data.

850 are shown in Figure 2.5a. The spectral shapes of $OD_s(\lambda)$ were similar to $OD_f(\lambda)$ showing the chlorophyll-a absorbance bands as well as bands corresponding to accessory pigments. However, the waveguide underestimated $OD_s(\lambda)$ in vicinity of the absorption peaks (Figure 2.5a). The underestimation in waveguide values relative to lambda 850 values were more pronounced for $OD_s(\lambda)$ compared to $OD_f(\lambda)$ measurements. The average percent difference between the waveguide and lambda 850 $OD_s(\lambda)$ was 15% and below 25% for all the samples. Despite the differences in magnitude of $OD_s(\lambda)$, a strong linear relationship was observed between waveguide and lambda 850 for cultures as well as natural samples (Figure 2.5b, c). A point to be noted here is that not all $OD_s(\lambda)$ were underestimated by the waveguide, while $OD_s(\lambda)$ around 676 nm was underestimated for all samples, some samples showed a slight overestimation between 400-580 nm. Since the differences in spectral shape between waveguide and lambda can be attributed to effects of scattering [*Belz et al.*, 2006; *D'Sa et al.*, 1998], the above observation indicate a differential effect of scattering across the visible domain. A better understanding of differences in magnitude at the absorption peaks of $OD_s(\lambda)$ and $OD_f(\lambda)$ can be comprehended by understanding the variable effects of scattering and absorption on light losses in waveguide measurements. The effect of scattering loses is accounted for in the waveguide and lambda 850 by subtracting absorbance values near the infra-red region, under the assumption that there is negligible absorption from particulate matter at these wavelengths and scattering loss is wavelength independent [*D'Sa et al.*, 1998; *Mitchell et al.*, 2003]. More refined scattering correction methods involve estimating the spectral shape of the scattering coefficient from the PSD and Mie theory [*Bricaud et al.*, 1983]. As the $OD_f(\lambda)$ spectra from waveguide and the lambda 850 matched for all the samples and wavelengths other than around the chlorophyll-a absorbance peaks, it suggests that major part of scattering is taken care of at most wavelengths.

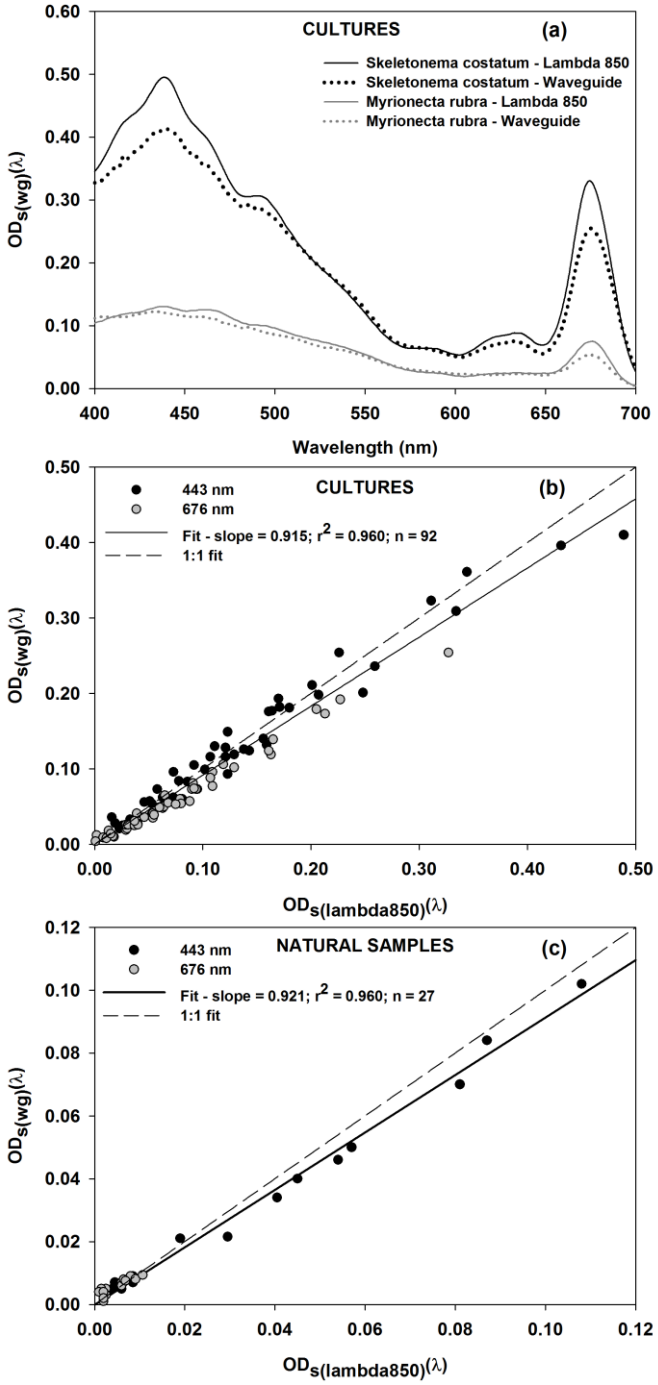

Figure 2.5. Comparison of (a) spectral shape of optical density of particles in suspension ($OD_s(\lambda)$) for lambda 850 (solid lines) and waveguide (dotted lines) for two different cultures (b) $OD_s(\lambda)$ for lambda 850 and waveguide at two wavelengths 443 nm (solid black circles) and 676 nm (solid gray circles) for all cultures, and (c) $OD_s(\lambda)$ for lambda 850 and waveguide at two wavelengths 443 nm (solid black circles) and 676 nm (solid gray circles) for all natural samples. The black solid line is the best fit line and the black dashed line is the 1:1 fit for our data.

The same cannot be said about the $OD_s(\lambda)$ measurements from waveguide. Some of these differences arise due to the fact, that transmission of light in a waveguide is limited by its acceptance angle, (θ_{WG} =20°), in contrast to an ideal integrating sphere. The better agreement of $OD_f(\lambda)$ values compared to $OD_s(\lambda)$ values can be understood by examining the optical characteristics of particles on filter paper relative to that of particles in suspension. For particles in suspension, scattering is dependent on suspended particles as well as the medium, while GF/F filter papers are inherently strong scatterers making the light field diffuse as such scattering is dependent more on filter paper than the particles on the filter paper [*Roesler,* 1998]. Addition of more particles in suspensions would result in significant scattering effect, while little effect of scattering would be seen on addition of particles to filter papers.

The effect of scattering in the two instruments was evaluated by making measurements of pigment extract and Maalox (aluminum hydroxide, magnesium hydroxide and simethicone) suspensions at 5 dilutions. Pigment extracts were obtained by extracting pigments from leaves in 100 ml of methanol (100%) and diluting it serially to get 10%, 25%, 50%, and 75%. While Maalox dilutions were prepared by diluting 1 ml of Maalox in 100 ml of water to obtain 100% dilution which was then diluted serially to obtain 10%, 25%, 50%, and 75%. Both the spectrophotometers showed a linear response for different dilutions of pigment extract and were in good agreement with each other for different wavelengths (Figure 2.6a). The effect of scattering on these results was evaluated by addition of known concentrations of Maalox to the pigment extract. The influence of scattering is apparent on $OD_s(\lambda)$ from the responses of the two instruments (Figure 2.6b). While the lambda 850 showed a very small increase, the waveguide showed a much greater increase with increasing concentration (Figure 2.6b). An inverse relationship was observed between difference in $OD_s(\lambda)$ from lambda 850 and waveguide, and

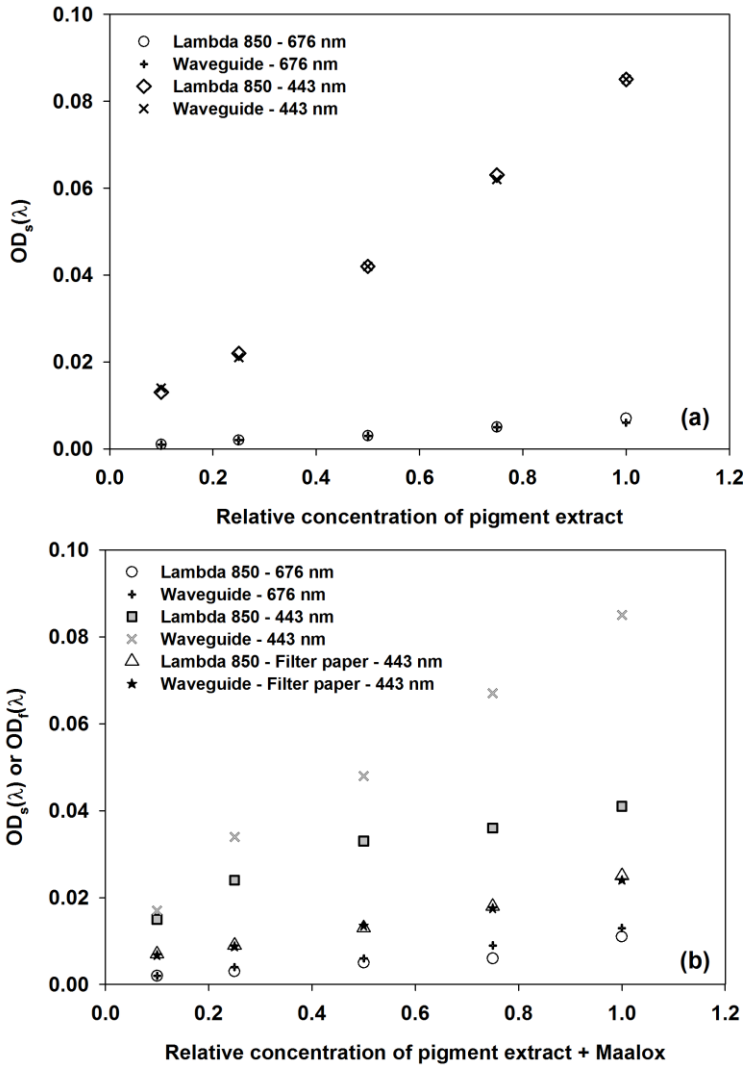

Figure 2.6. (a) Linear response of optical density of suspension ($OD_s(\lambda)$) for different concentration of pigment extracts measured on lambda 850 (circle and diamond) and waveguide (plus and cross) at 676 nm and 443 nm, respectively, (b) response of $OD_s(\lambda)$ for different concentrations of pigment extract plus Maalox measured on lambda 850 (circle and grey square) and waveguide (black plus and gray cross) at 676 nm and 443 nm, respectively, and response of optical density of particles on filter paper ($OD_f(\lambda)$) measured on lambda 850 (triangle) and waveguide (black star) at 443 nm is shown for comparison.

wavelength i.e. larger differences between the spectrophotometers were observed at shorter wavelengths (Figure 2.6b), indicating a wavelength dependent effect of scattering. This wavelength dependent effect of scattering in the waveguide measurements cannot be corrected by using a single wavelength from the near-infrared. In contrast to measurements of suspension

no difference between the two instruments or wavelength dependency was observed for the filter paper measurements (Figure 2.6b). These experimental results confirm the inherent differences between absorption measurements of particulate in suspensions and particulates on filter papers mentioned earlier.

Some of the differences in $OD_s(\lambda)$ can be also associated with the difficulty in measurement of the $OD(\lambda)$ of a suspension of scattering and absorbing particles as cells can settle within the samples holders in both the lambda 850 and waveguide. Also, species with stronger scattering due to cell wall shape and/or material (e.g. calcium carbonate in coccoliths) would produce a higher $OD(\lambda)$. In measurements of $OD(\lambda)$ by spectrophotometer (even with an integrating sphere) the backscattered and part of the side and forward scattered light will not be captured by the detector and will account for loss due to absorption. For measurement of $OD_s(\lambda)$ in the capillary waveguide light scattered by the cell suspension at angles greater than the numerical aperture of the waveguide are lost and are a function of the VSF [*Zaneveld et al.*, 1994]. The scattering corrections will vary from sample to sample depending upon the particles concentration, size distribution, and scattering efficiency. We will discuss some of these factors in relation to differences in $OD_s(\lambda)$ measured on the waveguide and lambda 850 in the next section.

Particles Size Distribution and VSF Measured Using LISST in Relation to Differences between Lambda 850 and Waveguide Capillary Flow Cell Measured $OD_s(\lambda)$

Light scattering by particles depends on the particle's size, index of refraction, composition, and shape [*van de Hulst*, 1958]. PSD measurements are included in this study to understand the scattering across the visible spectrum which depends on the shape of the PSD [*Stramski and Piskozub*, 2003]. PSD from LISST has been shown to be in good agreement with measurements from Coulter counter in laboratory studies [*Reynolds et al.*, 2010].

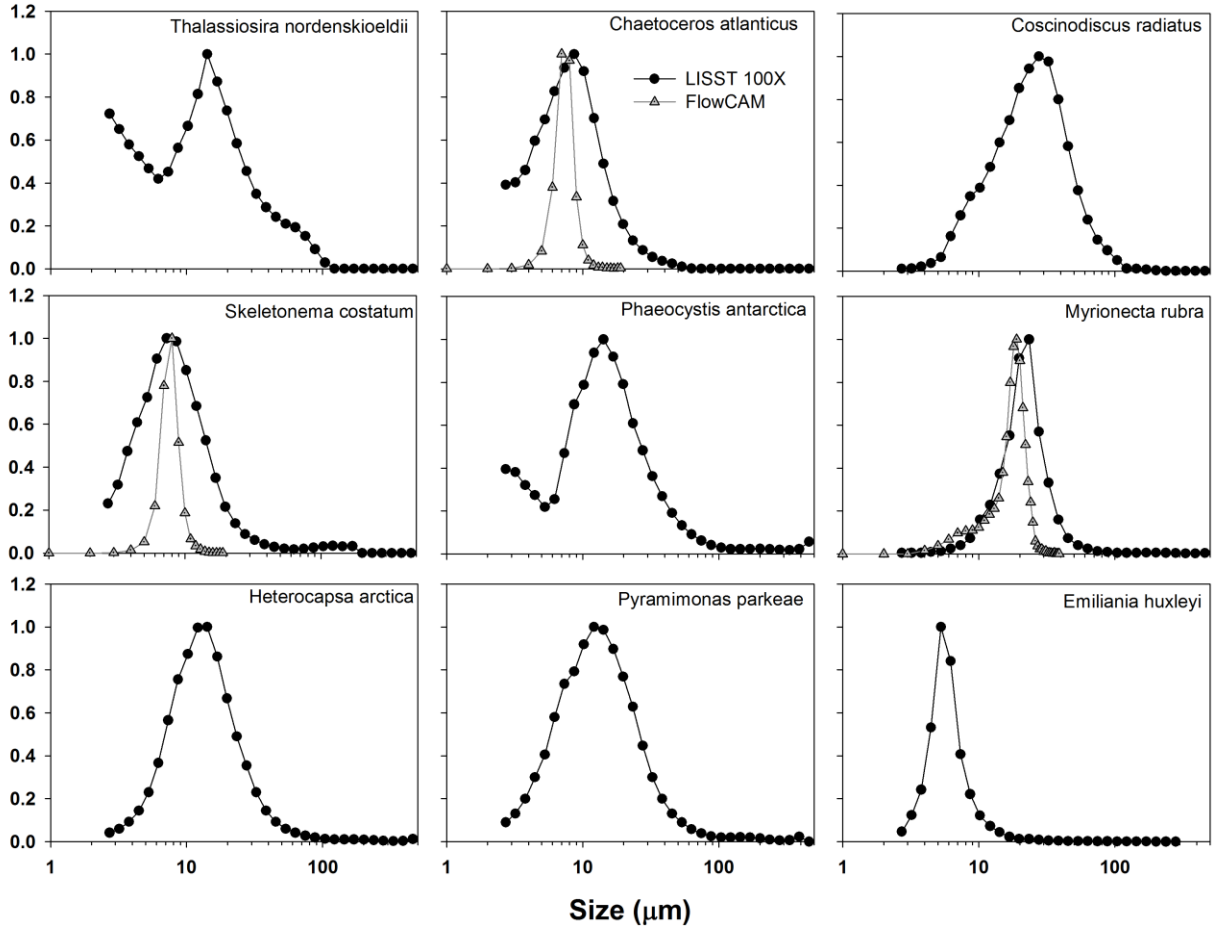

Figure 2.7. Particle size distribution (PSD) obtained using LISST 100X for nine cultures (black solid circles and solid line). The results from FlowCAM done for few samples are shown for comparison (gray solid triangles and solid line). The PSD was normalized to the modal peak to facilitate comparisons.

Figure 2.7 shows the PSD of 9 culture samples. As we were interested in looking at the shape of PSD we normalized the PSD to the modal peak. Comparisons between LISST and FlowCAM® (Fluid Imaging Technologies) PSD measurements done for a few samples were in good agreement, though the FlowCAM PSD were narrower than the LISST PSD. Features below a size range of ~3 μm (lower range of the detection limit of LISST) are not necessarily due to the sample, but can be artifacts due to the inversion process [*Agrawal et al.*, 2008]. Most PSD's showed a peaked distribution with mean diameter ranging from about 4-30μm.

Figure 2.8 shows the normalized VSFs computed from LISST measurements for 9 culture samples, and natural samples from estuarine and coastal regions. For cultures, the increasing particle size lead to a steeper VSF, with a narrower forward scattering lobe (Figure 2.7, Figure 2.8a). Scattering intensity as a function of angle varied by 4 orders of magnitude for these suspensions (Figure 2.8b). The general magnitude of the measured VSFs for natural samples is consistent with the Petzold curve obtained from a turbid harbor [*Petzold*, 1972]. However, significant variability in the shape of the VSFs measured with the LISST is observed. Note that the normalized VSFs were obtained as ratio of VSF and beam attenuation, so our normalized VSF's are underestimated with respect to those normalized using the scattering coefficient (scattering phase function).

In measurements of scattering suspensions in the capillary waveguide, measurements greater than the true absorption $a(\lambda)$ have been observed [*D'Sa et al.*, 1998]. If ε is the fraction of the scattering coefficient, $b(\lambda)$, that is lost, then

$$a_{WG}(\lambda) = a(\lambda) + \varepsilon\, b(\lambda)$$

Values of ε range from 0-1, for a perfect absorption meter ε should be close to zero.

In waveguide absorption measurements, we assume $\varepsilon\, b(\lambda) = a_{WG}(750)$, so subtracting this value from $a_{WG}(\lambda)$ at all wavelengths gives the corrected absorption,

$$a(\lambda) = a_{WG}(\lambda) - a_{WG}(750)$$

From measurements of VSF and the acceptance angle of the capillary waveguide, $\theta_{WG} = 20°$ the fraction of scattered light $(1-\varepsilon)$ collected by the capillary waveguide can be calculated as [*Belz et al.*, 2006; *D'Sa et al.*, 1998],

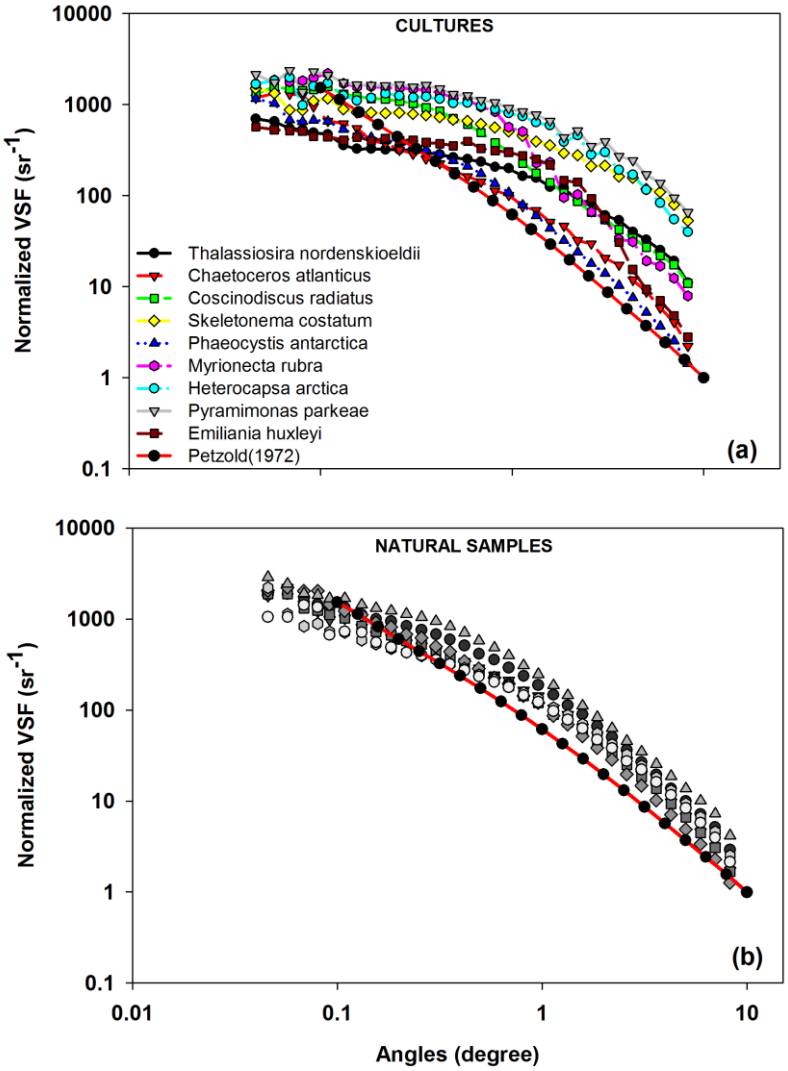

Figure 2.8. Normalized volume scattering function (VSF) (ratio of VSF to the beam attenuation coefficient) for (a) cultures, and (b) natural samples. The Petzold, (1972) data (solid black and solid red line) for turbid harbor is shown for comparison.

$$(1-\varepsilon) = 2\,\pi \int \beta(\theta)\,\sin\theta\;\, d\theta$$

where $\beta(\theta)$ is the normalized VSF. Using the VSF computed from LISST measurements and solving the above equation we found that the fraction of scattered light '1-ε' varied between 0.92-0.65. Ideally, this value should be one, however for the waveguide geometry this value was

found to be variable depending on the sample, implying that the measured $a_{WG}(\lambda)$ is significantly different from true $a(\lambda)$ for some samples.

Assuming that the lambda 850 $OD_s(\lambda)$ is accurate (true absorption), the difference between lambda 850 and waveguide $OD_s(\lambda)$ measurements reflect the error in the waveguide measurements. The VSF in small forward angles was directly correlated to the difference between lambda 850 and waveguide $OD_s(\lambda)$ measurements at 676 nm for cultures as well as natural samples ($r^2 = 0.62$; $p<0.001$) (data not shown). Further, the VSF and difference between the lambda 850 and waveguide $OD_s(\lambda)$ measurements at 676 nm were positively correlated to chlorophyll-a concentration measurements from HPLC ($r^2 = 0.85$; $p<0.001$ and $r^2 = 0.65$; $p<0.001$ respectively) (data not shown). The difference between the lambda 850 and waveguide $OD_s(\lambda)$ measurements at 676 nm was also inversely correlated to the product C_i*d (see eq. 8) from HPLC, indicating that smaller the size and intracellular chlorophyll-a product the larger the difference. The above results indicated that the difference in magnitude of $OD_s(\lambda)$ between waveguide and lambda 850 $OD_s(\lambda)$ measurements depended on both the pigmentation of the cells as well as scattering characteristics of the samples. Taking all these results together shows that larger differences between waveguide and lambda 850 are associated with stronger scattering and smaller cells with lower pigmentation, while smaller differences between the waveguide and lambda 850 are associated with weaker scattering and larger cells with higher pigmentation. These results are consistent with Morel, (1987) study, which showed that for diverse phytoplankton cultures and natural samples the specific backscattering coefficient is low for large and highly pigmented cells and the absorption coefficient was only slightly greater than the true absorption coefficient, while the specific backscattering coefficient was high for small

cells with low pigmentation and the absorption coefficient was 40% greater than the true absorption.

Apart from scattering effects on $OD_s(\lambda)$ from waveguide measurement, the refractive indices of particles is also important, especially in view of the difference in magnitude seen at the absorbance peaks (Figure 2.4a). Oceanic particles span a large range of indexes of refraction which are strongly related to the composition of the particles. Phytoplankton, mainly due to their high water fraction have low indices of refraction relative to water (1.02–1.07) [*Carder et al.*, 1972], while the indices of refraction change spectrally in the visible, these changes are small, except near strong absorption bands [*Aas*, 1996].

Applications of Pathlength Amplification Factor

From the earlier section we observed a good linear correlation between $OD_f(\lambda)$ (Figure 2.4a,b), while differences were found between $OD_s(\lambda)$ of cultures (Figure 2.5a,b) measured on waveguide and lambda 850. A good robust relationship was obtained between $OD_s(\lambda)$ and $OD_f(\lambda)$ measured on the lambda 850 for the β correction algorithm development (Figure 2.2b), a similar relationship could not be obtained for waveguide measurements (Figure 2.3b). As $OD_f(\lambda)$ was similar for both the spectrophotometers (Figure 2.4b), so most of the variability in the relationship between $OD_s(\lambda)$ and $OD_f(\lambda)$ for the waveguide (Figure 2.3a) can be attributed to the variability in $OD_s(\lambda)$ measured on the waveguide. To get the $OD_s(\lambda)$ between the lambda 850 and waveguide to match, accurate corrections for scattering loses have to be applied to the waveguide measurements. This scattering loss in waveguide is a function of the VSF (previous section) and wavelength dependent. Accurate corrections of $OD_s(\lambda)$ measured on the waveguide would require measurements of VSF and scattering (or attenuation) coefficients in addition to measurements of absorption coefficient. At present there is no accessory to measure $OD_s(\lambda)$ on

the waveguide other than the capillary waveguide system used in this study. Taking into account this fact and the above results, it is impractical to determine a β for the waveguide system in its present configuration and without complete set of the all measurements (VSF, b(λ) or c(λ), a(λ)). So, we suggest the use of β corrections algorithms determined for spectrophotometer with integrating sphere attachment (like lambda 850 in this study) to be applied to $OD_f(\lambda)$ measurements of waveguide, in view of strong linear relationship in $OD_f(\lambda)$ measurements between lambda 850 and waveguide.

The β correction algorithm for lambda 850 obtained for our study was similar to that obtained by Cleveland and Weidemann, (1993) and Arbones et al., (1996) and lower than that obtained by Mitchell, 1990 and higher than that obtained by Bricaud and Stramski, (1990). All the β correction algorithms are similar at lower values and diverge at higher values of OD(λ). The validity of the β amplification developed for lambda 850 was tested by appliying the β factor to cultures, a mixture of 2 or more cultures, as well as natural samples from different environments. In natural samples the density of phytoplankton is low; hence natural samples were first concentrated and then resuspended in a small volume of filtered seawater.

Figure 2.9 shows representative results of comparisons of $OD_s(\lambda)$ for culture and natural samples. Despite the significant difference in β correction between the species, reasonable agreement was found between cuvette measured and β corrected $OD_s(\lambda)$. The average percent difference for cultures (also mixture of cultures) was 9% and was always below 15%. The largest differences were seen in low green-yellow absorption regions and smallest differences were in the red region of the spectrum. Similarly for natural samples the average percent difference was 15% and always below 20% for all samples analyzed from different environments. The lowest

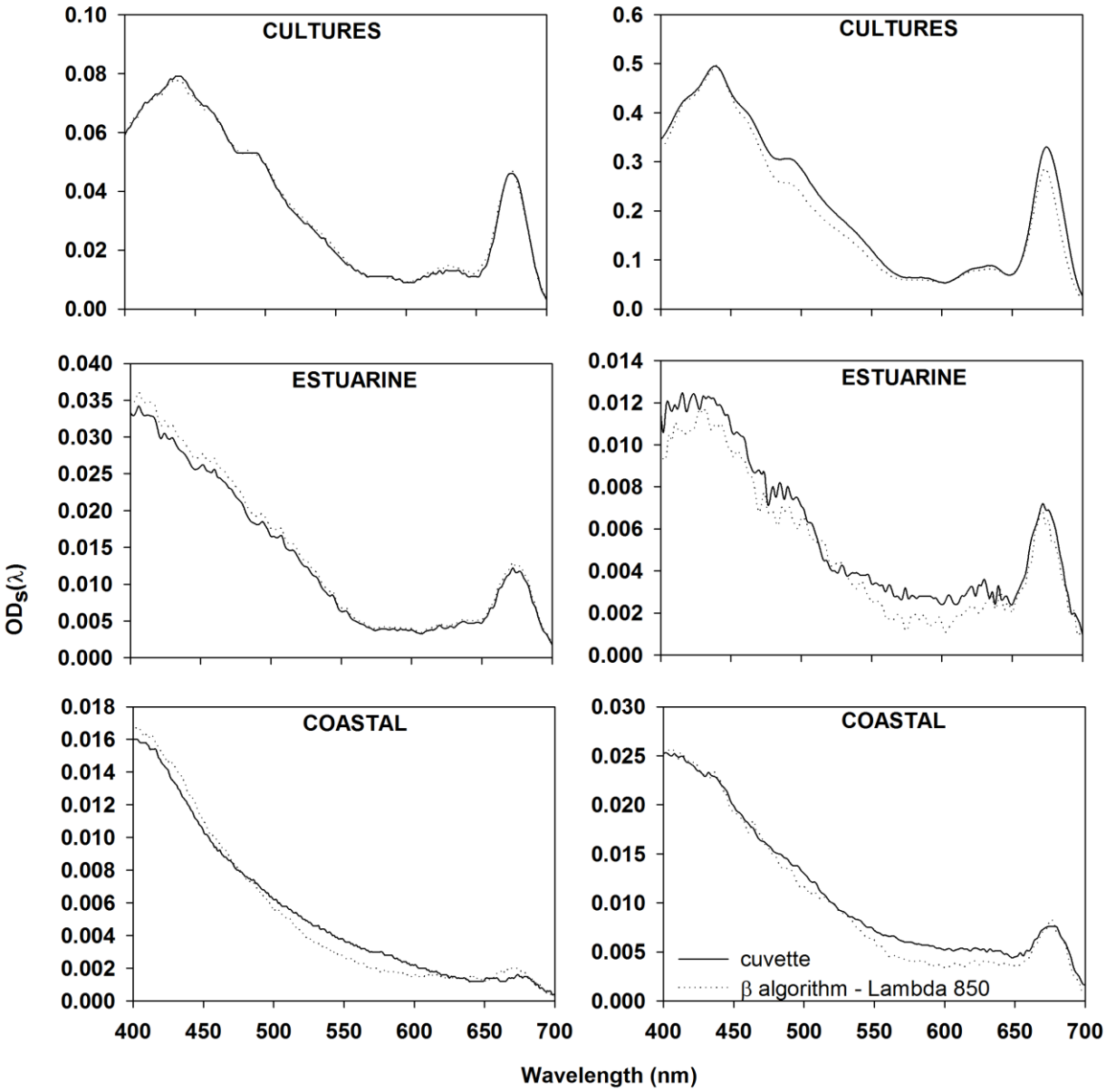

Figure 2.9. Spectral values of optical density of suspension ($OD_s(\lambda)$) measured in a cuvette on lambda 850 (solid black line) and obtained by using beta algorithm (dotted black line) developed in this study for lambda 850 for cultures and natural samples.

differences for natural samples were in the blue and red region and highest differences were seen in the green-yellow region.

These results are encouraging for the use of the filter pad method as a means of estimating particulate spectral absorption from both waveguide and lambda 850 taking into consideration that the study covered a wide variety of sample types and spanned a wide range of OD(λ).

Pigment Reconstruction of Phytoplankton Absorption Spectra

A comparison was made between the phytoplankton absorption spectra coefficients measured by QFT method corrected for the pathlength amplification factor from this study and the HPLC reconstructed phytoplankton absorption spectra [*Bidigare et al.,* 1990] to further examine and compare the phytoplankton absorption methods using our samples. Spectral reconstruction was done for cultures and natural water samples that were collected from diverse waters (estuarine and coastal) along the Louisiana Coast from the surface, the chlorophyll maximum florescence depth and the 1% light level depth.

The reconstructed spectra showed consistent overestimation relative to the measured absorption spectra for cultures and estuarine water samples. Figure 2.10 shows representative illustrations of this result, $a_{PHY}(\lambda)$ measured on both lambda 850 and waveguide for filter paper are shown for comparison. Only few culture samples showed reasonable agreement with the reconstructed spectra (Figure 2.10b). While for natural samples, the coastal samples showed a much better agreement relative to the estuarine samples. The average percent difference between the measured and reconstructed spectra was greater than 50% for the culture and estuarine samples while it was less than 40% for coastal samples. The reconstructed absorption spectra showed closer agreement at 676 nm rather than 443 nm (Figure 2.10). Differences between measured and reconstructed phytoplankton absorption spectra can be ascribed to 2 distinct factors; one is the package effect, and the other due to inconsistencies in the HPLC spectral reconstruction method (e.g. inaccurate specific pigment absorption spectra and missing

pigments). If we assume that errors in reconstructed absorption spectra were not due to errors in HPLC pigment determination or specific absorption coefficients of phytoplankton pigment, than the differences between the two spectra can be attributed to pigment package effect. This is a safe assumption to make at the red wavelengths but not in the blue-green wavelengths, as in the red wavelengths chlorophylls are the dominant pigments while in the blue green wavelengths a variety of pigments influence the phytoplankton absorption along with the chlorophylls [*Bricaud et al.*, 2004] (Figure 2.10e). The $a^*_{PHY}(676)$, where only absorption due to chlorophyll-a can be considered to be dominant, can be used to estimate the package effect. A comparison of measured and reconstructed $a^*_{PHY}(676)$ showed significant differences between most samples indicating package effect. The pigment package effect at 676 nm ($Q_a^*(676)$) can be calculated as the ratio of $a^*_{PHY}(676)$ to $a^*_{PHY}'(676)$ (see eq. 9), these values ranged from 0.9 to as low as 0.5. The package effect can also be calculated according to eq. 5. There was no significant difference between $Q_a^*(676)$ determined using eq. 5 or eq. 9. Figure 2.11 presents the variations of $Q_a(\lambda)$ and $Q_a^*(\lambda)$ at 443 nm and 676 nm as functions of ρ'. Q_a^* is always < 1 and tends toward 1 when ρ' is small (i.e. the particles are small, or $a_{cm}(\lambda)$ is small). The package effect was much stronger at the blue wavelengths compared to the red wavelengths (Figure 2.11) and was found to be greater in some culture samples compared to natural samples. Within the natural samples the coastal samples showed the least package effect in most of the samples, with few samples showing significant package effect consistent with Nelson et al., 1993 study (Figure 2.10e and f). The $Q_a^*(676)$ and $a^*_{PHY}(676)$ for the coastal samples did not show a significant trend for the surface, chlorophyll-a maximum depth and 1% light level depths, however slightly lower values were seen at the chlorophyll maximum depth.

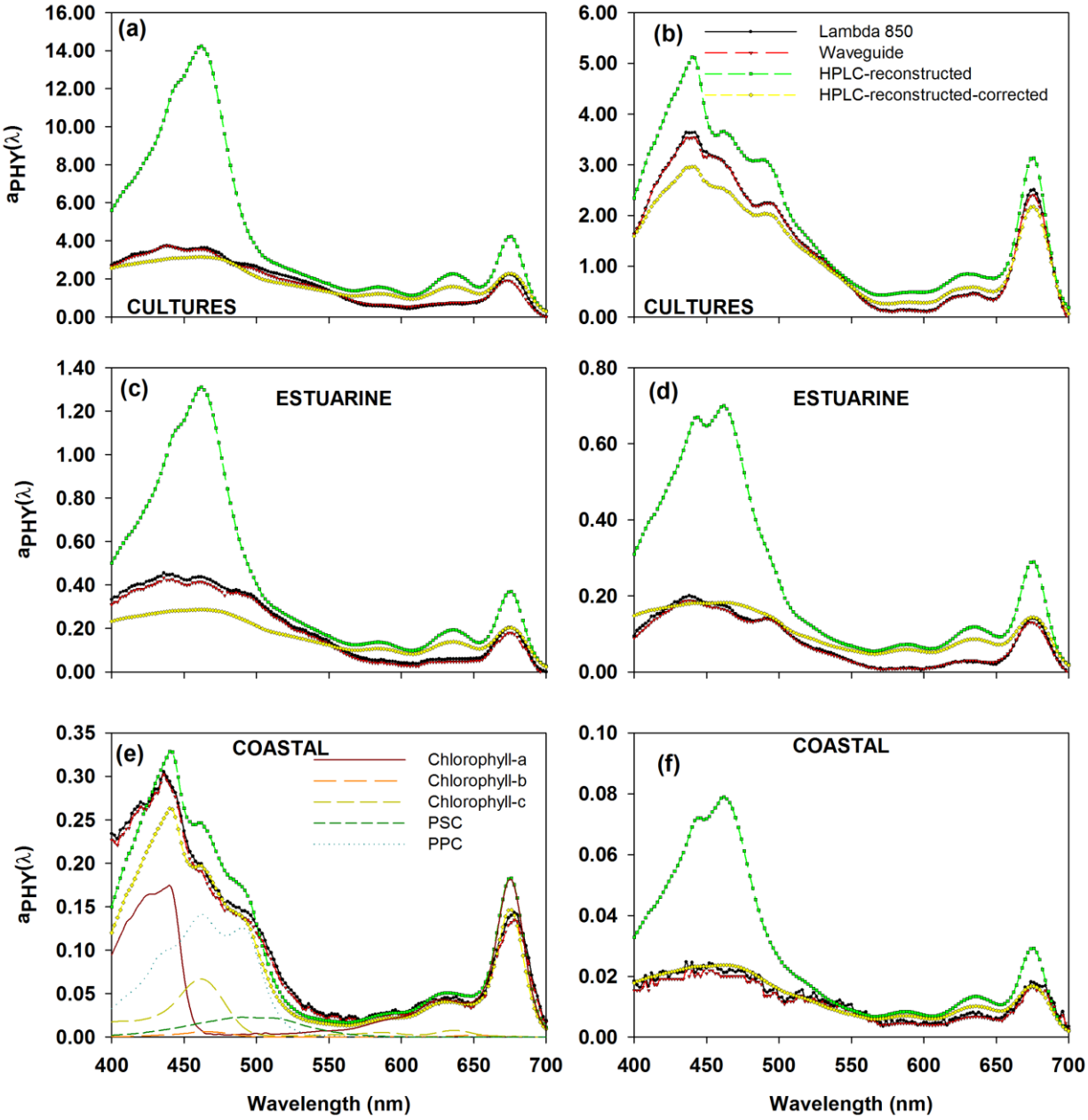

Figure 2.10. Phytoplankton absorption coefficient ($a_{PHY}(\lambda)$) of (a-b) cultures (c-d) estuarine samples, and (e-f) coastal samples, measured on lambda 850 (solid black circles), and waveguide (red triangles), reconstructed from HPLC pigment data (green squares), and reconstructed with correction for package effect (yellow diamonds). Contribution of each pigments (chlorophyll-a, chlorophyll-b, chlorophyll-c, photosynthetic carotenoids (PSC), and photoprotective carotenoids (PPC)) to reconstructed spectra is shown for one coastal water sample (e).

As the package effect was significant in most samples, correction for package effect must be included before the spectral reconstruction method can provide realistic estimates. Application of correction for package effect significantly reduced the overestimation between the reconstructed and measured absorption spectra for the culture, estuarine samples and for coastal samples with significant package effect (Figure 2.10). The reconstructed absorption spectra corrected for package effect underestimated and overestimated the measured absorption spectra below 550 nm and between 550-650 nm respectively. The reconstructed spectra corrected for package effect closely matched the measured absorption between 650 -700 nm, signified that the correction for package effect worked well. If we consider that by applying the package effect correction, the reconstructed spectra accounts for it then several reasons can be put forward for the underestimation and overestimation of $a_{PHY}(\lambda)$. The underestimations between 400-550 nm can be attributed to missing carotenoids and phycobilliproteins, or that phaeopigments could be erroneously included in the measured $a_{PHY}(\lambda)$ instead of $a_{NAP}(\lambda)$ as they are extractable by methanol. The overestimations between 550- 650 nm could be due to inaccurate in-vivo specific absorption coefficients in eq.4 especially chlorophyll-b and chlorophylly-$c_{1,2}$ as these are the pigments that mostly influence this region of the spectrum. Some of these differences after correction of reconstructed spectra for package effect could also be ascribed to estimation of package effect being derived assuming homogenous spherical particles [*Morel and Bricaud*, 1981]. The better agreement of cultures with near spherical shape relative to chain forming supports the above argument. But the good agreement for the coastal water samples where cells with varied shapes coexists indicates otherwise. Studies on spectral reconstruction [e.g. [*Nelson et al.*, 1993; *Sosik and Mitchell*, 1991]] have shown that the $a_{PHY}(\lambda)$ determined

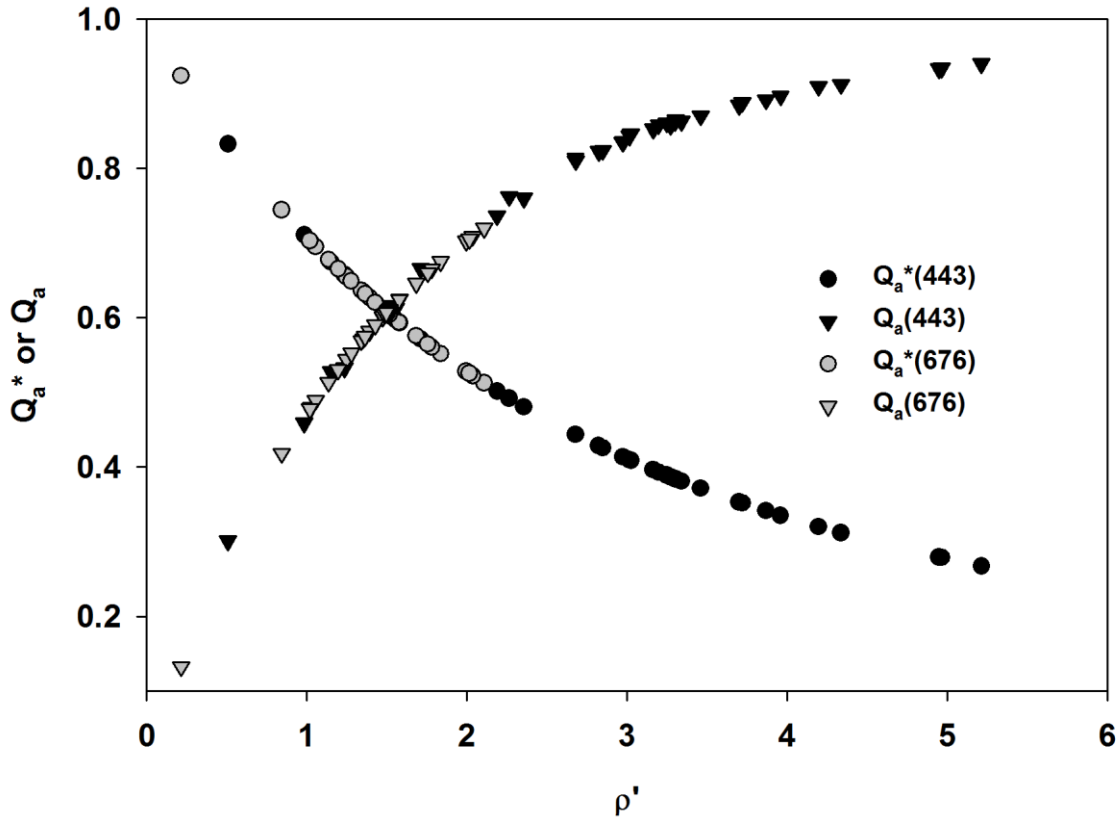

Figure 2.11. Optical absorption efficiency Qa (black and gray triangles) and the packaging parameter Qa* (black and gray circles) as a function of cellular optical thickness (product of intracellular chlorophyll concentration and cell diameter) at 443 nm and 676 nm, respectively.

spectrophotometrically using methanol treatment is indicative of total light absorption of the phytoplankton, while the $a_{PHY}(\lambda)$ determined by spectral reconstruction is more indicative of photosynthetic light absorption ability of the cells. Similar conclusions can be made from our study for coastal samples, which can be observed from the results of the coastal water samples where the reconstructed spectra is lower than the measured absorption spectra between for 400-425 nm and 500-550 nm (Figure 2.10e).

For the coastal water samples the package effect was small for most samples, so the application of the package effect correction had little effect on the reconstructed spectra. The average percent difference between the measured absorption spectra and reconstructed spectra

corrected for package effect from 400-700 nm was between 20-70% for cultures and estuarine samples and 7-38% for coastal water samples. The average percent difference was higher for cultures as compared to natural samples. According to results obtained here, the reconstructed phytoplankton absorption spectra provided reasonable estimates of phytoplankton absorption for samples with low package effect. While for samples with high package effect the reconstructed phytoplankton absorption spectra even after application of correction for package effect, does not provide accurate estimates of phytoplankton absorption.

Summary and Conclusions

The pathlength amplification factor (β) due to multiple scattering within the filter paper is the largest source of uncertainty in the measurements of particulate absorption which needs to be taken into account for its accurate measurements. For this purpose we developed a pathlength amplification correction algorithm for Ultrapath waveguide and Perkin Elmer lambda 850 using nine cultures at various dilutions. While the lambda 850 β algorithm was robust, the algorithm developed for waveguide was not as robust which was attributed to the differences seen in measurements of suspensions. The lambda 850 algorithm did not show any wavelength dependence but the problem of differences among phytoplankton species remains an issue for the algorithm. One approach to reduce this error is by making certain it is representative of the sample to which it is being applied. As it is difficult to correct the scattering losses in the waveguide without ancillary measurements and given the good agreement between filter paper measurements of waveguide and lambda 850, we suggest the use of pathlength amplification correction algorithms developed for spectrophotometers with integrating sphere (e.g. lambda 850 in our study) for corrections of particulate absorption measured on the waveguide with the GF/F

filter holder. The lambda 850 algorithm showed reasonable results when applied to cultures and natural water samples.

In order to understand the variability in β factor for the waveguide and test the potential of the waveguide to accurately measure particulate suspensions and filter paper measurements, comparisons were made between the waveguide and lambda 850 equipped with an integrating sphere. The comparison of optical density of phytoplankton/particles concentrated on filter paper ($OD_f(\lambda)$) measured in the waveguide and lambda 850 were in excellent agreement for cultures as well as natural samples at all wavelengths except the primary absorbance bands of chlorophyll-a, while the agreement between the two spectrophotometers was not as good for optical density of phytoplankton/particles in suspension ($OD_s(\lambda)$). Factors such as volume scattering function and acceptance angle of the waveguide detector were found to be important in measurements made on waveguide especially for particles in suspension. The $OD_s(\lambda)$ measured on the waveguide would have to be corrected for the wavelength dependent scattering which is not possible without simultaneous measurements of scattering (or attenuation) coefficients and VSF along with the absorption measurements.

The measured absorption spectra were compared to reconstructed absorption spectra determined using HPLC pigments and in-vivo specific absorption coefficients. The accuracy of the reconstructed spectra to determine phytoplankton absorption is primarily dependent on the extent of package effect in the sample. The package effect was found to be significant in culture and estuarine samples, and some coastal water samples. The coastal water samples showed the least package effect and hence the reconstructed absorption spectra for the coastal samples showed the best agreement with measured absorption spectra. The package effect was corrected by application of a package effect correction algorithm determined using the Nelson et al.,

(1993) approach. The reconstructed phytoplankton absorption spectra after application of the package effect correction algorithm showed a better agreement with measured phytoplankton absorption; however underestimations and overestimations were still evident between the measured and reconstructed spectra. The average percent difference between reconstructed phytoplankton absorption spectra corrected for package effect and measured absorption was highest for the cultures and estuarine samples and least for coastal samples. Overall the reconstructed phytoplankton absorption spectra provides good estimate for samples with low package effect.

The good performance of waveguide for at least the filter paper measurements and to a certain extent suspensions is encouraging as it has simplified optics, longer pathlength, high sensitivity, is very portable and easy to use. The study conducted here is intended to improve our ability to use and interpret measurements of particulate spectral absorption.

References

Aas, E. (1996), Refractive index of phytoplankton derived from its metabolite composition, Journal of Plankton Research, 18(12), 2223-2249.

Agrawal, Y. (2005), The optical volume scattering function: Temporal and vertical variability in the water column off the New Jersey coast, Limnology and Oceanography, 50(6), 1787-1794.

Agrawal, Y., and H. Pottsmith (2000), Instruments for particle size and settling velocity observations in sediment transport, Marine Geology, 168(1-4), 89-114.

Agrawal, Y., A. Whitmire, O. Mikkelsen, and H. Pottsmith (2008), Light scattering by random shaped particles and consequences on measuring suspended sediments by laser diffraction, Journal of Geophysical Research-Oceans, 113(C4), C04023.

Ahn, J., and S. Grant (2007), Size distribution, sources, and seasonality of suspended particles in southern California marine bathing waters, Environmental Science & Technology, 41(3), 695-702.

Arbones, B., F. Figueiras, and M. Zapata (1996), Determination of phytoplankton absorption coefficient in natural seawater samples: Evidence of a unique equation to correct the pathlength amplification on glass fiber filters, Marine Ecology Progress Series, 137(1-3), 293-304.

Behrenfeld, M., and P. Falkowski (1997), Photosynthetic rates derived from satellite-based chlorophyll concentration, Limnology and Oceanography, 42(1), 1-20.

Belz, M., K. Larsen, and K. Klein (2006), Fiber optic sample cells for polychromatic detection of dissolved and particulate matter in natural waters, in Advanced Environmental, Chemical, and Biological Sensing Technologies IV, edited, SPIE, Boston, MA, USA

Belz, M., P. Dress, A. Sukhitskiy, and S. Liu (1999), Linearity and effective optical pathlength of liquid waveguide capillary cells, in Internal Standardization and Calibration Architectures for Chemical Sensors, edited, pp. 271-281, SPIE, Boston, MA, USA

Bidigare, R., M. Ondrusek, J. Morrow, and D. Kiefer (1990), In-vivo absorption properties of algal pigments, in Ocean Optics X, edited by R. W. Spinrad, pp. 290-302, SPIE, Orlando, FL, USA

Bidigare, R. R., O. Schofield, and B. B. Prézelin (1989), Influence of zeaxanthin on quantum yield of photosynthesis of Synechococcus clone WH 7803(DC 2), Marine Ecology Progress Series., 56(1), 177-188.

Bricaud, A., and D. Stramski (1990), Spectral absorption-coefficients of living phytoplankton and non-algal biogenous matter - a comparison between the Peru upwelling area and the Sargasso Sea, Limnology and Oceanography, 35(3), 562-582.

Bricaud, A., A. Morel, and L. Prieur (1981), Absorption by dissolved organic-matter of the sea (yellow substance) in the UV and visible domains, Limnology and Oceanography, 26(1), 43-53.

Bricaud, A., A. Morel, and L. Prieur (1983), Optical-efficiency factors of some phytoplankters, Limnology and Oceanography, 28(5), 816-832.

Bricaud, A., H. Claustre, J. Ras, and K. Oubelkheir (2004), Natural variability of phytoplanktonic absorption in oceanic waters: Influence of the size structure of algal populations, Journal of Geophysical Research-Oceans, 109, C11010.

Butler, W. (1962), Absorption of light by turbid materials, Journal of the Optical Society of America, 52(3), 292-299.

Carder, K., R. Tomlinson, and G. Beardsley Jr (1972), A technique for the estimation of indices of refraction of marine phytoplankters, Limnology and Oceanography, 17, 833 - 839.

Cleveland, J., and A. Weidemann (1993), Quantifying absorption by aquatic particles - a multiple-scattering correction for glass-fiber filters, Limnology and Oceanography, 38(6), 1321-1327.

D'Sa, E., S. Lohrenz, C. Carroll, and H. Fein (1998), Liquid waveguide capillary flow cell for determining absorption of scattering suspensions: Comparison with an integrating sphere, in Ocean Optics XIV, edited, SPIE, Kailua-Kona, Hawaii, USA.

D'Sa, E., R. Steward, A. Vodacek, N. Blough, and D. Phinney (1999), Determining optical absorption of colored dissolved organic matter in seawater with a liquid capillary waveguide, Limnology and Oceanography, 44(4), 1142-1148.

D'Sa, E. J., and R. G. Steward (2001), Liquid capillary waveguide application in absorbance spectroscopy (reply to the comment by Byrne and Kaltenbacher), Limnology and Oceanography, 46(3), 742-745.

Duntley, S. (1942), The optical properties of diffusing materials, Journal of the Optical Society of America, 32(2), 61-70.

Finkel, Z., and A. Irwin (2001), Light absorption by phytoplankton and the filter amplification correction: cell size and species effects, Journal of Experimental Marine Biology and Ecology, 259(1), 51-61.

Fujiwara, K., and K. Fuwa (1985), Liquid core optical fiber total reflection cell as a colorimetric detector for flow-injection analysis, Analytical Chemistry, 57(6), 1012-1016.

Guillard, R., and J. Ryther (1962), Studies of marine planktonic diatoms. I. Cyclotella nana Hustedt, and Detonula confervacea (cleve) Gran, Canadian Journal of Microbiology, 8(2), 229-239.

Johnsen, G., O. Samset, L. Granskog, and E. Sakshaug (1994), In-vivo absorption characteristics in 10 classes of bloom-forming phytoplankton - taxonomic characteristics and responses to photoadaptation by means of discriminant and HPLC analysis, Marine Ecology Progress Series, 105(1-2), 149-157.

Karp-Boss, L., L. Azevedo, and E. Boss (2007), LISST-100 measurements of phytoplankton size distribution: evaluation of the effects of cell shape, Limnology and Oceanography-Methods, 5, 396-406.

Kiefer, D. A., and J. B. SooHoo (1982), Spectral absorption by marine particles of coastal waters of Baja California, Limnology and Oceanography, 27(3), 492-499.

Kishino, M., M. Takahashi, N. Okami, and S. Ichimura (1985), Estimation of the spectral absorption coefficients of phytoplankton in the sea, Bulletin of Marine Science, 37(2), 634-642.

Lohrenz, S. E. (2000), A novel theoretical approach to correct for pathlength amplification and variable sampling loading in measurements of particulate spectral absorption by the quantitative filter technique, Journal of Plankton Research, 22(4), 639-657.

Miller, R., M. Belz, C. Del Castillo, and R. Trzaska (2002), Determining CDOM absorption spectra in diverse coastal environments using a multiple pathlength, liquid core waveguide system, Continental Shelf Research, 22(9), 1301-1310.

Mitchell, B. (1990), Algorithms for determining the absorption coefficients for aquatic particulates using the quantitative filter technique, in Ocean Optics X, edited by R. W. Spinrad, pp. 137–148, SPIE, Orlando, FL, USA

Mitchell, B., and D. Kiefer (1988), Chlorophyll-alpha specific absorption and fluorescence excitation-spectra for light-limited phytoplankton, Deep Sea Research Part I-Oceanographic Research Papers, 35(5), 639-663.

Mitchell, B. G., M. Kahru, J. Wieland, and M. Stramska (2003), Determination of spectral absorption coefficients of particles, dissolved materials and phytoplankton for discrete water samples, in Ocean Optics Protocols For Satellite Ocean Color Sensor Validation, Revision 4, Volume 4: Inherent optical properties: instruments, characterization, field measurements and data analysis protocols, edited, NASA Tech. Rep., Greenbelt, Maryland.

Moore, L., R. Goericke, and S. Chisholm (1995), Comparative physiology of Synechococcus and Prochlorococcus: influence of light and temperature on growth, pigments, fluorescence and absorptive properties, Marine Ecology Progress Series, 116, 259-275.

Morel, A. (1987), Chlorophyll-specific scattering coefficient of phytoplankton. A simplified theoretical approach, Deep Sea Research Part I-Oceanographic Research Papers, 34(7), 1093-1105.

Morel, A., and A. Bricaud (1981), Theoretical results concerning light-absorption in a discrete medium, and application to specific absorption of phytoplankton, Deep Sea Research Part I-Oceanographic Research Papers, 28(11), 1375-1393.

Nelson, J., and C. Robertson (1993), Detrital spectral absorption - laboratory studies of visible-light effects on phytodetritus absorption, bacterial spectral signal, and comparison to field-measurements, Journal of Marine Research, 51(1), 181-207.

Nelson, N., and B. Prezelin (1993), Calibration of an integrating sphere for determining the absorption-coefficient of scattering suspensions, Applied Optics, 32(33), 6710-6717.

Nelson, N., B. Prezelin, and R. Bidigare (1993), Phytoplankton light-absorption and the package effect in California coastal waters, Marine Ecology Progress Series, 94(3), 217-227.

Peacock, T., K. Carder, P. Coble, Z. Lee, and S. Hawes (1994), Long-path spectrometer for measuring gelbstoff absorption in clear waters, Eos Transactions American Geophysical Union 75, 22.

Petzold, T. (1972), Volume Scattering Functions for Selected Ocean Waters.

Reynolds, R., D. Stramski, V. Wright, and S. Wozniak (2010), Measurements and characterization of particle size distributions in coastal waters, Journal of Geophysical Research-Oceans, 115, C08024.

Roesler, C. (1998), Theoretical and experimental approaches to improve the accuracy of particulate absorption coefficients derived from the quantitative filter technique, Limnology and Oceanography, 43(7), 1649-1660.

Sathyendranath, S., A. Longhurst, C. Caverhill, and T. Platt (1995), Regionally and seasonally differentiated primary production in the North Atlantic, Deep Sea Research Part I-Oceanographic Research Papers, 42(10), 1773-1802.

Sosik, H. M., and B. G. Mitchell (1991), Absorption, fluorescence, and quantum yield for growth in nitrogen-limited Dunaliella tertiolecta, Limnology and Oceanography, 910-921.

Stramski, D., and J. Piskozub (2003), Estimation of scattering error in spectrophotometric measurements of light absorption by aquatic particles from three-dimensional radiative transfer simulations, Applied Optics, 42(18), 3634-3646.

Tassan, S., and G. Ferrari (1995), An alternative approach to absorption measurements of aquatic particles retained on filters, Limnology and Oceanography, 40(8), 1358-1368.

Truper, H., and C. Yentsch (1967), Use of glass fiber filters for rapid preparation of in vivo absorption spectra of photosynthetic bacteria, Journal of Bacteriology, 94(4), 1255-1256.

van de Hulst, H. (1958), Light scattering by small particles, 198-199 pp., John Wiley & Sons, Ltd.

Yentsch, C. (1962), Measurement of visible light absorption by particulate matter in the ocean, Limnology and Oceanography, 7(2), 207-217.

Yentsch, C., and D. Phinney (1989), A bridge between ocean optics and microbial ecology, Limnology and Oceanography, 34(8), 1694-1705.

Zaneveld, J., R. Bartz, and J. Kitchen (1990), A reflective-tube absorption meter, in Ocean Optics X, edited by R. W. Spinrad, pp. 124-136, SPIE Orlando, FL, USA.

Zaneveld, J., J. Kitchen, and C. Moore (1994), Scattering error correction of reflecting-tube absorption meters, in Ocean Optics XII, edited by S. Ackleson, pp. 44-55, SPIE, Bergen, Norway.

CHAPTER 3: ABSORPTION PROPERTIES OF SHOAL DOMINATED WATERS IN THE ATCHAFALAYA SHELF, LOUISIANA, USA[1]

Introduction

Variations in distributions and concentration of organic and inorganic, dissolved and particulate matter are important for monitoring of water quality and their ecological implications in coastal ecosystems. Along the Louisiana coast influenced by two major rivers, the Mississippi and Atchafalaya Rivers, year-to-year increase in nutrient loading have resulted in increasing extent of hypoxic zone and algal blooms [*Rabalais and Turner*, 2001]. Recently the shoal dominated region of the Atchafalaya shelf in southern Louisiana has been identified as an important resource for sand mining in Louisiana, USA [*Stone et al.*, 2004], a major spawning ground for commercially important blue crab, and a biodiversity hotspot for macro infauna [*Dubois et al.*, 2009]. Little is known about the long-term effects of sand mining on the water column properties or water quality. On the short term likely effects of mining on the water column are the release of nutrients due to more mixing, an increase in the suspended sediment load in the water column, increasing turbidity affecting the light availability in the water column and also the release of contaminants to the water column from bottom sediments [*ICES*, 1992].

The concentration and composition of some of these in-water constituents have an influence on the optical properties used to study biological and biogeochemical processes [*Bissett et al.*, 2001; *Coble et al.*, 2004; *D'Sa et al.*, 2007; *Gould and Arnone*, 1997; *Hu et al.*, 2004; *IOCCG*, 2006]. The in-situ measurements of absorption can be used for monitoring and assessing water quality and harmful algal blooms. The ability of remote retrieval (Ocean Color Sensors e.g. Sea-viewing Wide Field-of-view Sensor (SeaWiFS)) of these optical properties in addition to

[1] Chapter 3 is reprinted with permission from the 'International Journal of Remote Sensing.'

chlorophyll-a by using bio-optical algorithms (Ocean Color Algorithms (OCA)) can be used for synoptic monitoring of the blooms occurring in coastal regions [*Hu et al.*, 2004; *Kahru and Mitchell*, 1998; *Stumpf et al.*, 2003]. These bio-optical algorithms require an understanding of the optical properties in these waters as they are affected by high levels of CDOM and suspended sediments [*Carder et al.*, 1989]. However, only a limited number of studies have been done on optically complex shoals dominated coastal areas [*D'Sa*, 2008; *D'Sa and Ko*, 2008; *Walker*, 1996].

The optical properties of absorption and scattering by in water constituents and by the water molecules themselves determine the so called color of natural waters. Absorption is an inherent optical property and is the sum of individual components within the water column, namely colored dissolved organic matter (CDOM), phytoplankton and non-algal particulate matter (NAP) and can be expressed as:

$$a_T(\lambda) = a_W(\lambda) + a_{CDOM}(\lambda) + a_{PHY}(\lambda) + a_{NAP}(\lambda) \quad \text{(Eq. 1)}$$

where $a_W(\lambda)$, $a_{CDOM}(\lambda)$, $a_{PHY}(\lambda)$ and $a_{NAP}(\lambda)$ are absorption coefficients due to pure water, CDOM, phytoplankton and non-algal particulate matter, respectively. Variation of any of these are clear indicators of changes in water constituents, which in turn would reveal some water characteristics (e.g., quality). Many parameters are derived from these constituents, such as dissolved organic carbon (DOC), particulate organic carbon (POC) and productivity [*IOCCG*, 2006].

The optical properties of 'case 1' waters (mostly open ocean waters) are well understood unlike the 'case 2' waters (mostly coastal waters). In case 1 waters the total non-water absorption is dominated by phytoplankton which covaries with other water constituents, whereas in case 2 waters phytoplankton do not dominate and phytoplankton may not co-vary with other water

constituents [*Morel and Prieur*, 1977]. In coastal waters, absorption is mostly influenced by riverine material and CDOM. In such waters, absorption properties are inadequately documented to illustrate their variability. However the reasons for variability of $a_{PHY}(\lambda)$ are known to a certain extent in these waters [*Bricaud et al.*, 1998; *Hoepffner and Sathyendranath*, 1991; *Sosik and Mitchell*, 1995]. $a_{CDOM}(\lambda)$ changes with respect to its compositions and origin (Carder *et al.* 1989). $a_{CDOM}(\lambda)$ in coastal areas has been found to be strongly influenced by river discharge [*Blough et al.*, 1993; *Chen and Gardner*, 2004; *D'Sa et al.*, 2006] and impacts the estimation of chlorophyll-a from OCA's [*Hochman et al.*, 1994]. $a_{NAP}(\lambda)$ is not as well understood as $a_{PHY}(\lambda)$ and $a_{CDOM}(\lambda)$ [*Babin et al.*, 2003; *Bowers and Binding*, 2006] and is known to depend on the size and composition of particles [*Ferrari et al.*, 2003]. The changes in water column characteristics caused by cold fronts are known to influence these bio-optical properties to a large extent; however few studies have examined these linkages [*D'Sa and Ko*, 2008; *D'Sa et al.*, 2006; *Vantrepotte et al.*, 2007].

The shoals that dominate the Atchafalaya shelf are affected biogeochemically by the shallow depths, wetlands in the vicinity, river influence and cold fronts. These factors make this region optically complex and difficult for the use of remote sensing techniques to determine water quality. The objectives of this study are thus to (i) examine and quantify the three main absorbing constituents of seawater (ii) address the spectral characteristics and contribution of $a_{CDOM}(\lambda)$, $a_{PHY}(\lambda)$ and $a_{NAP}(\lambda)$ to $a_T(\lambda)$ and (iii) assess the implications of the dominant constituent/s to OCA's through match up of in-situ and satellite data.

Materials and Methods

Study Region

In-situ observations were made onboard the *RV Pelican* in April, August and October 2007, in the shoal dominated region of Northern Gulf of Mexico spanning the area from latitude 28.66 N to 29.32 N and longitudes 90.46 W to 92.46 W (Figure 3.1, Table 3.1). Stations were located on and around 3 major shoals; Ship Shoal, Tiger Shoal and Trinity Shoal off the Atchafalaya River (AR) shelf (Figure 3.1).

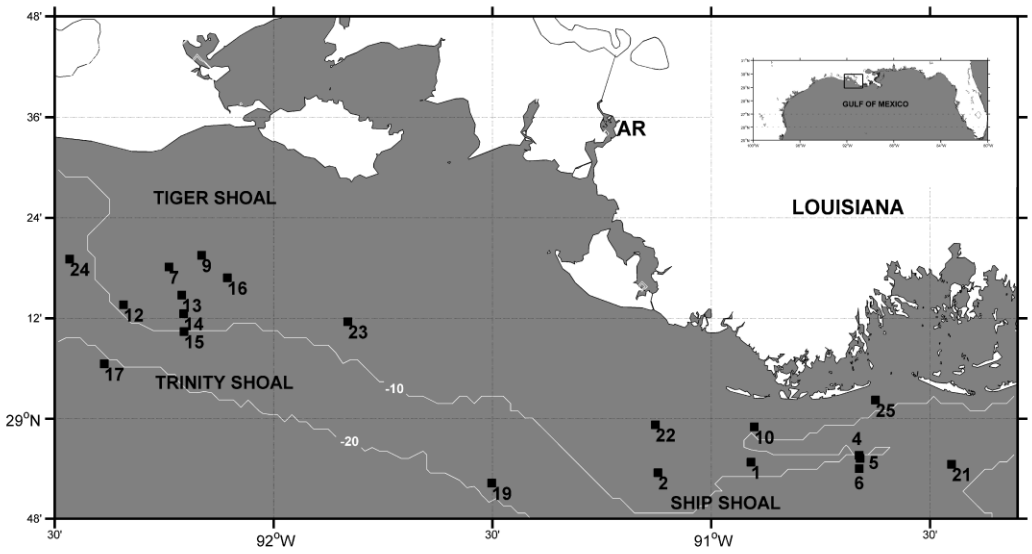

Figure 3.1. Location of stations sampled during the three cruises.

Table 3.1. Cruises and periods of sampling with station numbers.

Cruise	Period	Stations
April 2007	**1–5**	**25**
August 2007	**16–19**	**22**
October 2007	**5–7**	**11**

Due to the passage of a cold front and the subsequent bad weather fewer number of stations were covered in October 2007. At every station, salinity, temperature and density profiles were recorded with a conductivity temperature depth (CTD) (SeaBird-25) sensor equipped with a fluorometer (WETLabs-Wetstar), a transmissometer (WETLabs), a dissolved oxygen sensor (SBE 23) and a photosynthetically active radiation (PAR) sensor (Biospherical instruments, QSP-200L). Water samples were collected for optical analyses at 3 depths the surface, middle, and near-bottom of the water column using Niskin bottles attached to the CTD. Particulate absorption spectra were determined only for the August 2007 and October 2007 samples.

CDOM Absorption

Samples were filtered immediately after collection through a 0.22 μm nylon membrane filters under low vacuum. Filtered samples were stored in acid cleaned, pre-combusted amber colored glass bottles and stored at 4 ^{o}C before laboratory analysis. Prior to laboratory analysis the filtered samples were allowed to reach ambient room temperature to minimize temperature bias between samples and blank (Barnstead Nanopure Milli-Q water). CDOM absorbance ($A_{CDOM}(\lambda)$) was measured in a 1 cm quartz cell from 190 to 750 nm every 2 nm on a double beam Perkin Elmer Lambda 850 spectrophotometer equipped with a 150 mm spectralon coated integrating sphere. The absorbance spectra of Barnstead Nanopure Milli-Q water ($A_{MQ}(\lambda)$) were also recorded before and after the sample measurement to check the stability of the lamp. The absorbance data were corrected for scattering and baseline fluctuations by subtraction of the mean value of the measured absorbance from 700 - 750 nm [*Babin et al.*, 2003; *Bricaud et al.*, 1981] from each wavelength. The $a_{CDOM}(\lambda)$ for a cuvette of pathlength 'l' was calculated according to:

$$a_{CDOM}(\lambda) = 2.303[A_{CDOM}(\lambda) - A_{MQ}(\lambda)]/l \qquad \text{(Eq. 2)}$$

A non-linear exponential function was fitted to all CDOM spectra to obtain the absorption spectral slope coefficients of CDOM (S_{CDOM}) that describes the exponential decrease of absorption with increasing wavelength (Bricaud *et al.* 1981).

$$a_{CDOM}(\lambda) = a_{CDOM}(\lambda_0)e^{-S_{CDOM}(\lambda_0-\lambda)} \quad \text{(Eq. 3)}$$

where, $a_{CDOM}(\lambda)$ is the absorption coefficient at wavelength λ, λ_0 is a reference wavelength.

Phytoplankton and NAP Absorption

Seawater samples were filtered under low vacuum on 0.7 µm Whatman GF/F and immediately frozen in liquid nitrogen and stored in dark until laboratory analysis for chlorophyll-a, $a_{PHY}(\lambda)$ and $a_{NAP}(\lambda)$. The absorbance of total particulate matter ($A_P(\lambda)$) was measured using a Perkin Elmer Lambda 850 spectrophotometer equipped with a 150 mm spectralon coated integrating sphere at every 2nm intervals from 190 nm to 750 nm. The absorbance was converted to absorption coefficient by using equation (4):

$$a_P(\lambda) = (2.303[A_P(\lambda)])\ A/V \quad \text{(Eq. 4)}$$

where $a_P(\lambda)$ is the total particulate absorption, V is the volume filtered and A the area of the filter paper. The absorption spectra were corrected for pathlength amplification [*Mitchell*, 1990; *Tassan and Ferrari*, 1995] and baseline offset by subtracting the mean value from 700 - 750 nm [*Mitchell et al.*, 2003].

Phytoplankton pigments within the particulate matter were then separated from NAP using methanol extraction [*Kishino et al.*, 1985] and the absorbance of NAP ($A_{NAP}(\lambda)$) obtained in the same manner as $A_P(\lambda)$. $A_{NAP}(\lambda)$ was converted to $a_{NAP}(\lambda)$ using the same logic implied in equation (4). The $a_{PHY}(\lambda)$ was obtained by subtracting the $a_{NAP}(\lambda)$ from $a_P(\lambda)$.

$$a_{PHY}(\lambda) = a_P(\lambda) - a_{NAP}(\lambda) \quad \text{(Eq. 5)}$$

A non-linear exponential function was fitted to all NAP spectra to obtain the absorption spectral slope coefficients of NAP (S_{NAP}) that describes the exponential decrease of absorption with increasing wavelength [*Bricaud et al.*, 1981].

$$a_{NAP}(\lambda) = a_{NAP}(\lambda_0)e^{-S(\lambda_0 - \lambda)} \quad \text{(Eq. 6)}$$

where, $a_{NAP}(\lambda)$ is the absorption coefficient at wavelength λ, λ_0 is a reference wavelength. Chlorophyll-a specific phytoplankton absorption ($a^*_{PHY}(\lambda)$) was obtained by dividing $a_{PHY}(\lambda)$ by chlorophyll-a. Chlorophyll-a was determined by high performance liquid chromatography (HPLC) method. HPLC analysis was performed using a 201 Hewlett Packard 1100 liquid chromatograph coupled to a diode array spectrophotometer 202 and a Hewlett Packard 1046A fluorescence detector.

Satellite Data

SeaWiFS ocean color satellite Level 1 data of the study area were obtained for clear sky days from the Ocean Biology Processing Group (OBPG) NASA website (http://oceancolor.gsfc.nasa.gov/cgi/browse.pl? sen=am). The Level 1 data files were processed to Level 2 using SeaWiFS Data Analysis System (SEADAS) 5.3 to obtain chlorophyll-a and $a_{CDOM}(412)$. The standard OCA, OC4.v4, which utilizes the reflectance ratio of blue and green channels and the Gordon and Wang (1994) atmospheric correction, was used for chlorophyll-a retrieval. A detail description of the OCA and atmospheric corrections can be found at NASA OBPG website (oceancolor.gsfc.nasa.gov). For $a_{CDOM}(412)$ retrieval, regional OCA developed by D'Sa *et al.* (2006) was used with the same atmospheric correction.

The Medium Resolution Imaging Spectrometer (MERIS) Level 2 data were obtained from the European Space Agency (ESA) and processed using BEAM 4.5.3 software. The OCA, ALGAL2 which is tuned for coastal water applications was used for chlorophyll-a retrieval and

the D'Sa *et al.* (2006) algorithm, was used for $a_{CDOM}(412)$ retrieval. The documentation for MERIS products and atmospheric correction algorithms used for processing of data from Level 1 to Level 2 can be found at the ESA website (http://earth.esa.int/pcs/envisat/meris/documentation/). A 3 x 3 pixel box size with a time difference of ±12 hours between the in-situ sampling and satellite overpass was chosen for in-situ and satellite data match up.

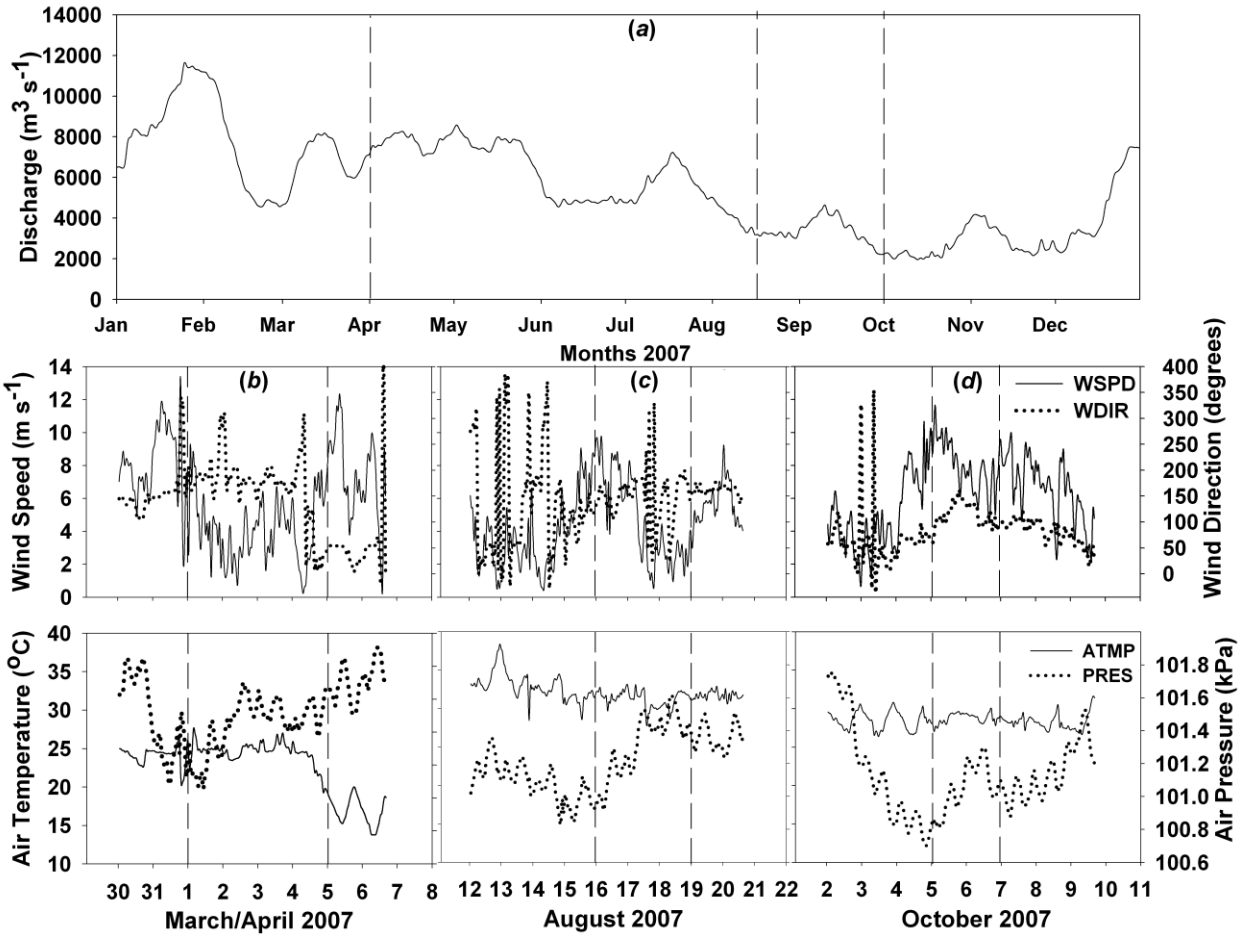

Figure 3.2. (a) AR discharge at Simmersport during the year 2007. Buoy data (CSI-3) near the study area showing the atmospheric conditions in the study area. Vertical dashed lines indicate cruise days for: (b) April 2007, (c) August 2007 and (d) October 2007.

Results

River Discharge and Cold Fronts

The study area (Tiger, Trinity and Ship Shoal) is mainly influenced by the Atchafalaya River (AR), though the Mississippi River plume also joins the AR flow [*Walker and Rabalais*, 2006]. Freshwater inputs to this region mainly fluctuate according to AR discharge. The magnitude of AR flow (Figure 3.2a) was highest in April (7447 $m^3 s^{-1}$), decreasing in August (3263 $m^3 s^{-1}$), and lowest in October (2146 $m^3 s^{-1}$). Each year about 30–40 cold fronts pass through the Louisiana coast between the months of October and April [*Roberts et al.*, 1987]. These cold fronts disturb the mainly westward coastal currents [*D'Sa and Ko*, 2008; *Walker and Hammack*, 2000] with potentially similar hydrodynamic effects during the three cruises of this study (Figure 3.2b, c and d). In the April 2007 cruise, sampling was done during the prefrontal and frontal passage of the cold front. In the prefrontal stage the dominant wind direction was southerly with wind speeds ~4 m s^{-1} which changed during the frontal passage to northerly winds (~12 m s^{-1}) and accompanied by increased pressure and decreased air temperature (Figure 3.2b). There were no cold front effects in the August 2007 in the study area (Figure 3.2c). Before the October 2007 cruise a cold front had passed through the study area on September 29, 2007 and another cold front occurred on the October 9, 2007 after the cruise (not shown, National Oceanic and Atmospheric Administration (NOAA), Hydrometeorological Prediction Center (HPC) cold front archives weather charts, http://www.hpc.ncep.noaa.gov/html). So the October 2007 cruise sampling was done in between the post frontal stage of a cold front that had occurred and pre-frontal stage of the next cold front (Figure 3.2d). Higher wind speeds (>8 m s^{-1}) were observed for most part of the sampling period during this cruise. This would have an effect on the

absorption properties due to water column mixing and resuspension of benthic micro algae which is dominant on these shoals [*Grippo et al.,* 2009].

In the April 2007 cruise the average surface salinity was 28.11 ± 4.22 and the average bottom water salinity was 30.48 ± 3.43. Salinity generally increased with depth, due to intrusion of higher density oceanic waters and AR discharge affecting the surface waters. The average of surface water salinity in the August 2007 cruise was 27.63 ± 2.58 and average of bottom water salinity was 29.86 ± 3.84. Whereas during October 2007 cruise the average surface and bottom water salinity was 30.72 ± 1.26 and 30.81 ± 1.25 respectively. The almost uniform water column salinity at the study sites were due to the mixing associated with relatively higher wind speeds associated with the cold fronts coupled with low AR flow in October 2007 (Figure 3.2a and 2(*d*)).

CDOM Absorption ($a_{CDOM}(\lambda)$)

The general $a_{CDOM}(\lambda)$ spectral curve of increasing $a_{CDOM}(\lambda)$ with decreasing wavelength was observed in the study area for all stations and their mean (black lines) and standard deviation (sd) (grey lines) for April 2007, August 2007 and October 2007 are shown in Figure 3.3a. The highest values of $a_{CDOM}(\lambda)$ were observed at stations located near Ship Shoal (e.g. Stn. 25, Stn. 22, Stn. 1, Stn. 10) during all the cruises. These stations are located closest to the wetlands in the vicinity of the study area; hence the high $a_{CDOM}(\lambda)$ could be due to exchange processes or local production within these wetlands [*Chen and Gardner,* 2004; *D'Sa*, 2008]. The average $a_{CDOM}(\lambda)$ at 412 nm ($a_{CDOM}(412)$) for surface water samples was highest for April 2007 cruise (0.539 ± 0.187 m^{-1}) followed by August 2007 cruise (0.485 ± 0.186 m^{-1}) and lowest for October 2007 cruise (0.314 ± 0.115 m^{-1}) (Figure 3.3a), suggesting a trend of $a_{CDOM}(\lambda)$ relating to the AR flow. Although the AR flow was variable for the three cruises, a significant relationship (p-

value<0.001) was observed between $a_{CDOM}(412)$ and salinity indicating a near-conservative linear mixing trend (Figure 3.3b) [*D'Sa and Miller*, 2003; *D'Sa et al.*, 2006]. However April 2007 samples showed a larger scatter, because the salinity was more variable during the cruise, whereas the October 2007 cruise showed the least scatter due to uniform mixing of the water column. Overall the surface water samples had higher $a_{CDOM}(\lambda)$ as compared to bottom water samples. However at some stations bottom water sample showed higher $a_{CDOM}(412)$ than surface water samples, suggesting effects of exchange processes between surrounding wetlands near the Atchafalaya bay and mixing processes in the shallow shoal waters.

Changes in spectral slope of CDOM absorption indicate changes in CDOM composition. The spectral slope of CDOM absorption at 412 nm (S_{CDOM}) calculated between 350 nm to 500 nm varied from 0.016–0.043 nm^{-1}. The average value of S_{CDOM} decreased from the April 2007 cruise to the October 2007 cruise. The average S_{CDOM} for April 2007, August 2007 and October 2007 cruise was 0.020 ± 0.003 nm^{-1}, 0.019 ± 0.002 nm^{-1} and 0.014 ± 0.001 nm^{-1}, respectively. Although the $a_{CDOM}(\lambda)$ showed a inverse relationship with salinity, the spectral slope showed a complex relationship (Figure 3.3c) as shown further by the $a_{CDOM}(412)$ versus S_{CDOM} (Figure 3.3d). The different relationship for the spectral slopes versus salinity and CDOM absorption observed during October 2007 is not clear. However the influence of bottom effects due to strong mixing could have played a role.

Phytoplankton Absorption ($a_{PHY}(\lambda)$)

The $a_{PHY}(\lambda)$ spectra obtained for the two cruises, August and October 2007 were highly variable and their mean and standard deviation (sd) are shown in Figure 3.4a (black lines). During August $a_{PHY}(\lambda)$ at 443 nm and 676 nm ranged from 0.025–0.144 m^{-1} and 0.010–0.123 m^{-1}, while in October it ranged from 0.046–0.137 m^{-1} and 0.025–0.081 m^{-1}, respectively.

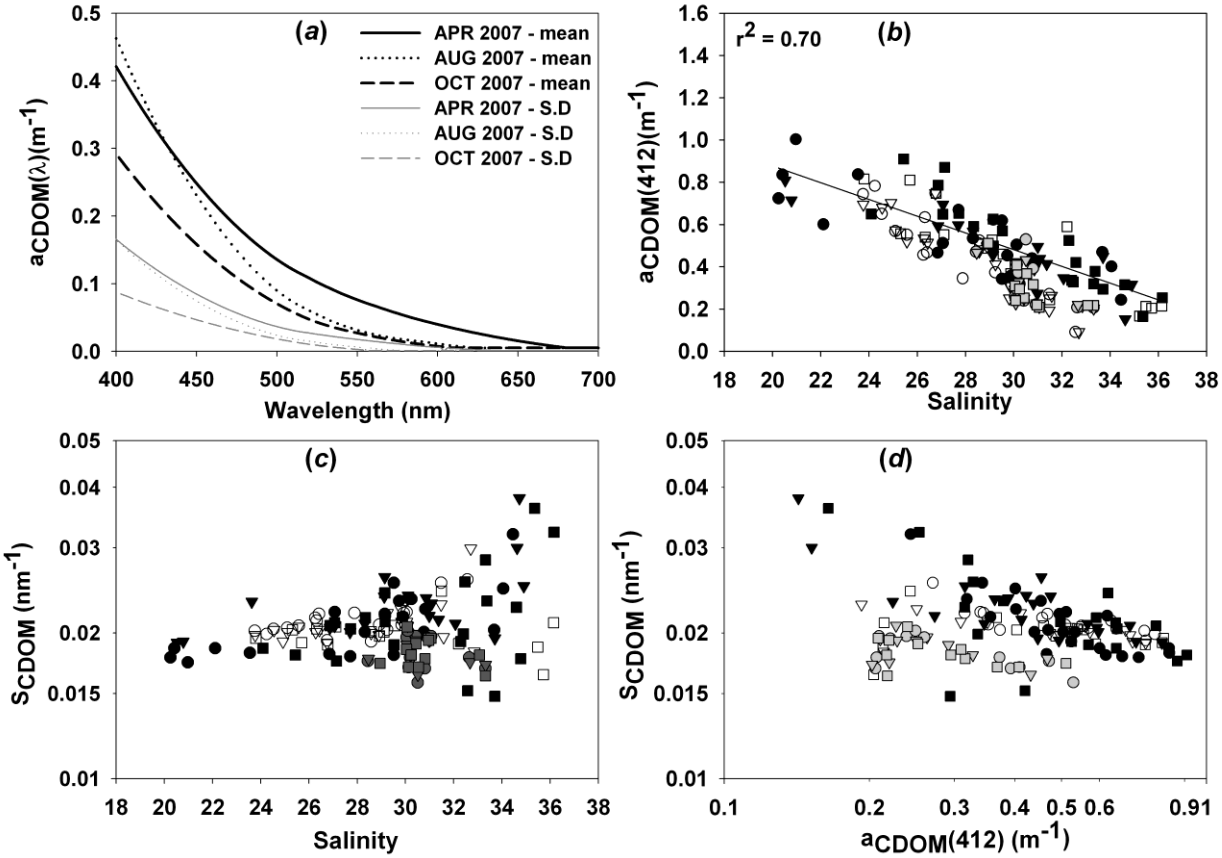

Figure 3.3. (a) Mean and standard deviation (sd) of CDOM absorption ($a_{CDOM}(\lambda)$) spectra for all samples collected during April 2007, August 2007 and October 2007. (b) $a_{CDOM}(\lambda)$ at 412 nm ($a_{CDOM}(412)$) versus salinity. CDOM spectral slopes (S_{CDOM}) at 412 nm versus (c) salinity and (d) $a_{CDOM}(412)$. Black filled symbols indicate April 2007 cruise, white filled symbols indicate August 2007 cruise and grey filled symbols indicate October 2007 cruise.

The off-shoal stations north of the shoals (e.g. Stns.23, 22, and 10) showed higher $a_{PHY}(\lambda)$ (0.101 ± 0.041 m^{-1}) as compared to off-shoal stations to the south of the shoals (e.g. Stns.17, 19, and 21) (0.018 ± 0.007 m^{-1}). The surface $a_{PHY}(\lambda)$ on an average were higher as compared to the bottom $a_{PHY}(\lambda)$ (0.0121 ± 0.006 m^{-1} and 0.009 ± 0.001 m^{-1}, respectively). However for both the cruises at some stations $a_{PHY}(\lambda)$ of bottom samples was almost equal to or higher than the surface samples. This could probably be attributed to the bottom sediments on these shoals, having a

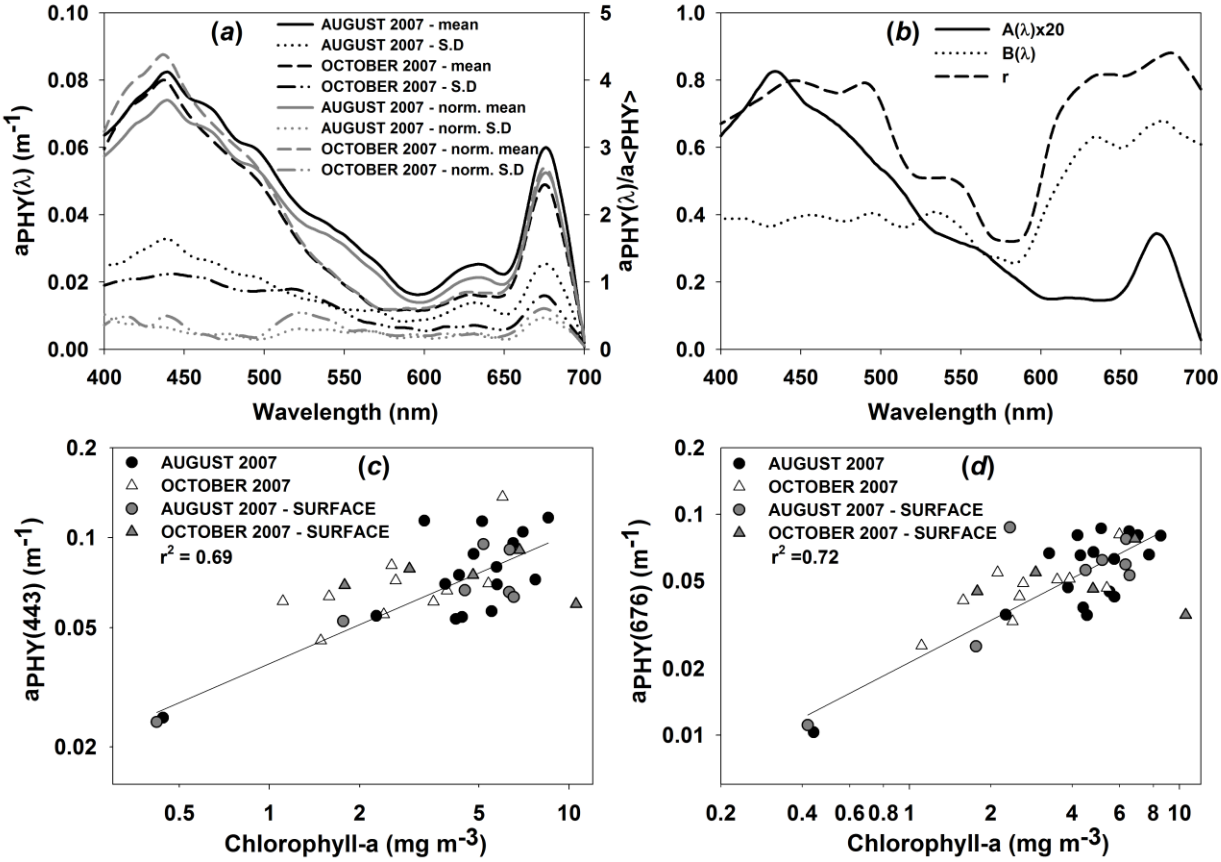

Figure 3.4. (a) Mean and standard deviation (sd) of phytoplankton absorption spectra ($a_{PHY}(\lambda)$) and normalized (norm.) phytoplankton absorption spectra ($a_{PHY}(\lambda)/a_{<PHY>}$) for all samples collected during August 2007 and October 2007. $a_{<PHY>}$ is the average $a_{PHY}(\lambda)$ between 400 and 700 nm. (b) Values of coefficients ($A(\lambda)$ and $B(\lambda)$) and correlation coefficient (r) of power fit applied to chlorophyll-a concentration and phytoplankton absorption at every 5 nm ($[aphy(\lambda)] = A(\lambda)\times[\text{chlorophyll-a}]^{B(\lambda)}$). The coefficient $A(\lambda)$ has been multiplied by 20 for visualization purpose. Log-linear relationship between $a_{PHY}(\lambda)$ and chlorophyll-a at (c) 443 nm and (d) 676 nm for all depths. Surface water samples are shown in grey symbols.

higher algal biomass primarily composed of benthic microalgae [*Grippo et al.*, 2009] which were likely resuspended in the shallow waters (~6 m) by the elevated wind speeds (>8 m s^{-1}). This was further substantiated by chlorophyll-a values of bottom water samples being higher than the surface samples. The $a_{PHY}(\lambda)$ spectra were normalized by the spectral mean of $a_{PHY}(\lambda)$ from 400 – 700 nm ($a_{<PHY>}$), so that variability only due to change in spectral shape could be examined

without influence of particle concentration and major packaging effects [*Roesler et al.*, 1989]. The mean and standard deviation (sd) of normalized $a_{PHY}(\lambda)$ is shown in Figure 3.4a (grey lines). The mean normalized $a_{PHY}(\lambda)$ (grey solid and dashed line) unlike the mean $a_{PHY}(\lambda)$ (black solid and dashed line) in the blue region was higher in October 2007 as compared to August 2007. Further, the standard deviation (sd) of the normalized $a_{PHY}(\lambda)$ (grey dotted lines) did not resemble the mean of normalized $a_{PHY}(\lambda)$ for both August and October 2007 data, being more variable in October 2007 and in blue part of the spectrum. The variation of $a_{PHY}(\lambda)$ with chlorophyll-a can be described by a power function representing a non-linear increase of $a_{PHY}(\lambda)$ with increasing chlorophyll-a [*Bricaud et al.*, 1998].

$$[\text{aphy}(\lambda)] = A(\lambda) \times [\text{chlorophyll-a}]^{B(\lambda)} \qquad \text{(Eq. 7)}$$

The power function and a least square fit are applied at every 5 nm and the coefficients and correlation coefficient 'r' determined (Figure 3.4b). The power function fits well in the red and blue region of the spectrum as seen from the 'r' value. However the correlation in the green region of the spectrum is not as good, probably due to the absorption in this region being dominated by accessory pigments rather than by chlorophyll-a [*Bricaud et al.*, 1995].

We found significant ($p<0.001$) log-linear correlation between chlorophyll-a and $a_{PHY}(\lambda)$ at 443nm and 676nm (Figure 3.4c and d). This agrees well with previous studies done in different environments [*D'Sa et al.*, 2006; *Lohrenz et al.*, 2003]. The chlorophyll-a specific phytoplankton absorption ($a^*_{PHY}(\lambda)$) indicates the efficiency with which phytoplankton absorbs light per unit chlorophyll. It can be broadly related to pigment composition, cell size, nutrient availability and photoadaptation [*Bricaud et al.*, 1995; *Carder et al.*, 1989]. The mean spectra of $a^*_{PHY}(\lambda)$ for surface water samples shows that the August 2007 samples had higher $a^*_{PHY}(\lambda)$ compared to October 2007 (Figure 3.5b). The $a^*_{PHY}(\lambda)$ at 443 nm ranged from 0.006–0.0612 $m^{-2}(\text{mg chla})^{-1}$

for August 2007 cruise and 0.006–0.0553 $m^{-2}(mg\ chla)^{-1}$ for October 2007. At 676 nm the $a^*_{PHY}(\lambda)$ for August 2007 ranged from 0.007–0.0370 $m^{-2}(mg\ chla)^{-1}$ and for October 2007 from 0.003–0.0257 $m^{-2}(mg\ chla)^{-1}$. The variability in $a^*_{PHY}(\lambda)$ could be due to pigment packaging effect (intracellular shading) or variation in pigment composition and cell size distribution [*Babin et al.*, 1993; *Harding et al.*, 2005]. From Figure 3.5a and b we see that the largest $a^*_{PHY}(\lambda)$ is between 400–500 nm with a lesser variation in the 650–700 nm waveband range.

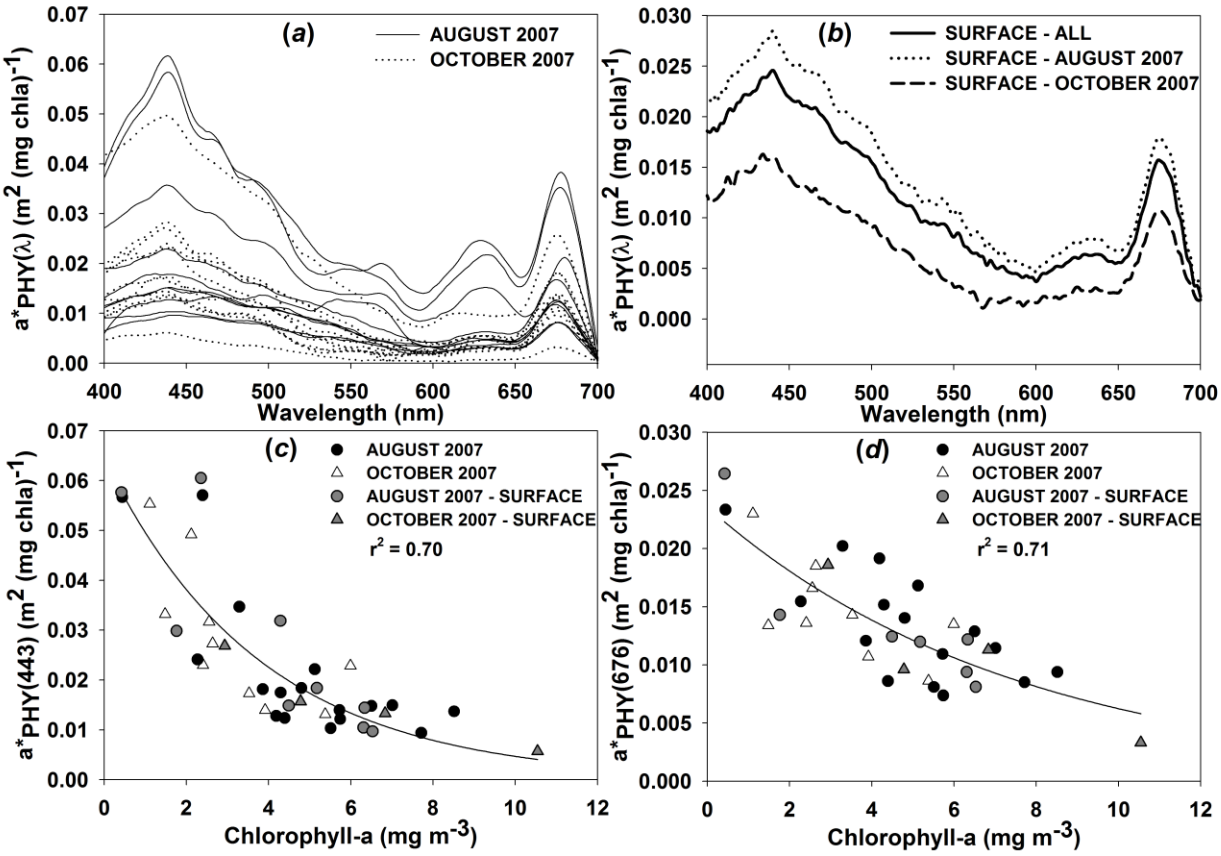

Figure 3.5. Specific phytoplankton absorption ($a^*_{PHY}(\lambda)$) of (a) all samples showing variability, (b) mean spectra of surface samples. Variation of $a^*_{PHY}(\lambda)$ at (c) 445 nm and (d) 676 nm with chlorophyll-a for all depths. Surface water samples are shown in grey symbols.

The relation of $a^*_{PHY}(\lambda)$ at 443 nm and 676 nm with chlorophyll-a would give a better picture of this variability. Similar to previous studies we saw that $a^*_{PHY}(\lambda)$ at 443 nm and 676 nm decreased with increasing chlorophyll-a ($p<0.001$) [*Bricaud et al.*, 1995] and there is more variability in $a^*_{PHY}(443)$ than in $a^*_{PHY}(676)$ (Figure 3.5c and d). This correlation has been explained before as being an indication of package effect [*Bricaud et al.*, 1995; *Ciotti et al.*, 1999]. The $a^*_{PHY}(676)$ variability can be ascribed to package effect, but variations in $a^*_{PHY}(443)$ may result from the combined contribution of package effect and changes in pigment composition as the absorbance peaks of accessory pigments are closer to 443 nm than to 676 nm [*Fujiki and Taguchi*, 2002]. As we observed more variability at 443 nm than at 676 nm (Figure 3.5c and d) which indicated that pigment composition may be the key source of variability of $a^*_{PHY}(\lambda)$. Further the bottom samples showed more variability in these plots suggesting that the accessory pigments are influenced during low light conditions. This variability in $a^*_{PHY}(\lambda)$ if not corrected could possible lead to errors in the estimation of chlorophyll concentration. To correct for the variability seen in $a^*_{PHY}(\lambda)$ spectra, it is important to quantify the differences in the $a^*_{PHY}(\lambda)$ due to package effect or pigment composition. This would require the distinction of different algal groups and information on pigment composition.

Non-Algal Particles Absorption ($a_{NAP}(\lambda)$)

The spatial variation of $a_{NAP}(\lambda)$ was large ranging between 0.022–1.313 m^{-1} at 400 nm (Figure 3.6a). For the August 2007 and October 2007 cruises $a_{NAP}(443)$ ranged from 0.017–0.910 m^{-1} and 0.063–0.624 m^{-1}, respectively. However some absorption by pigments due to incomplete extractions is seen in chlorophyll-a absorption band at 620-710 nm absorption range [*Babin et al.*, 2003].

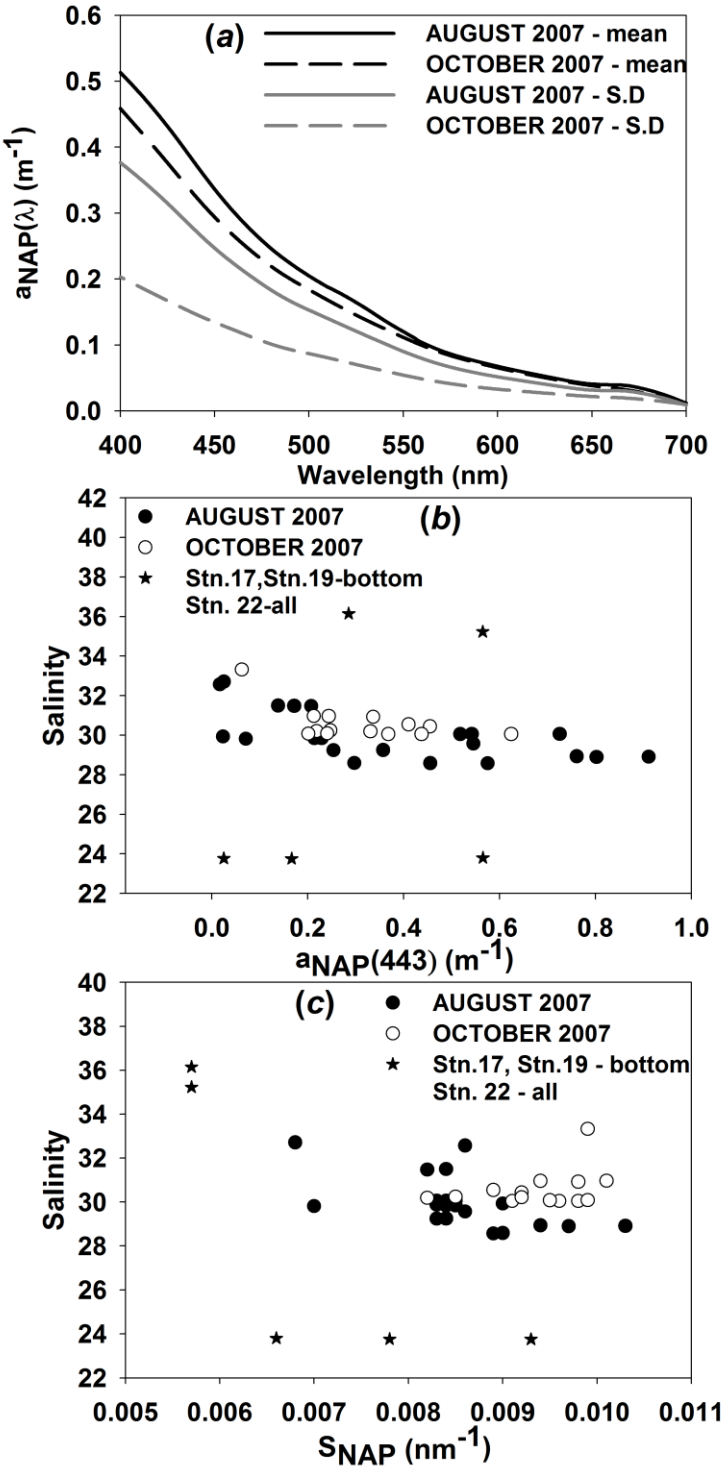

Figure 3.6. (a) Mean and standard deviation (sd) of non-algal particulate absorption, ($a_{NAP}(\lambda)$) for all samples collected in August 2007 and October 2007 cruises. Relation between Salinity and (b) $a_{NAP}(443)$ and (c) S_{NAP} for all depths.

The highest value of $a_{NAP}(\lambda)$ were found near to the coast, where the AR has larger influence (Stns. 16, 7) and the lowest values were seen at stations away from the coast (Stns. 17, 19). Further the $a_{NAP}(\lambda)$ increased with decreasing salinity, except at very low salinities (Stn. 22 - surface, middle and bottom) and at deeper stations (Stn.17- bottom, Stn.19 - bottom ~17 m), where mixing processes have a lesser influence (Figure 3.6b). The high $a_{NAP}(\lambda)$ values at low salinities suggest that adsorption of CDOM onto fine particulate material may be occurring. The regional variations in S_{NAP} are related to the particle composition and size structure. The spectral slope of NAP absorption was calculated between 300 nm to 700 nm. We observed very large variation of the spectral slope of NAP absorption (S_{NAP}) in the study area corresponding to large variation of $a_{NAP}(\lambda)$. The S_{NAP} varied from 0.006–0.010 nm^{-1} with a mean of 0.009 ± 0.001 nm^{-1}. These values are associated with inorganic or mineral dominated sediments [*Babin et al.*, 2003; *Bowers et al.*, 1996; *Ferrari et al.*, 2003]. The same tendency of increasing S_{NAP} with decreasing salinity was seen as with $a_{NAP}(\lambda)$ (Figure 3.6c). The S_{NAP} in August 2007 ranged from 0.006–0.010 nm^{-1} corresponding to salinity range 28.57–32.71 while in October 2007 S_{NAP} ranged from 0.008–0.010 nm^{-1} corresponding to salinity range of 30.05–33.32.

Discussion

The light absorption properties obtained in this study compared well with previous studies conducted in waters influenced mainly by the Mississippi River [*D'Sa et al.*, 2006; *Green et al.*, 2008]. Table 3.2 summarizes the absorption coefficients in different environments. As seen from table 3.2 in most case 2 waters $a_{CDOM}(\lambda)$ or $a_{NAP}(\lambda)$ or $a_{CDOM}(\lambda)$ and $a_{NAP}(\lambda)$ together contribute largely to the total non-water absorption. However indications of localized sources probably

Table 3. 2. Absorption by CDOM, phytoplankton and NAP particles in diverse regions.

Area	λ nm	a_{CDOM} (m^{-1})	a^*_{PHY} (m^{-1})	a_{NAP} (m^{-1})	Reference
Baltic Sea	443	0.3 – 0.7	-	0.1 – 0.4	Babin *et al.* 2003
English Channel	443	0.05 – 0.2	-	0.007 – 0.1	Babin *et al.* 2003
English Channel	440	0.2 – 1.1	0.018 – 0.048	0.03 – 0.08	Vantrepotte *et al.* 2007
North Sea	443	0.4	-	0.01 – 1	Babin *et al.* 2003
North Atlantic	443	0.01– 0.1	-	0.001 – 0.04	Babin *et al.* 2003
Irish Sea	442	0.01 – 0.35	0.003 – 0.067	0.02 – 0.14	Tilstone *et al.* 2005
Adriatic Sea	443	0.04 – 0.4	-	0.01 – 0.4	Babin *et al.* 2003
Black Sea	443	-	0.043 – 0.07	0.03 – 0.1	Chami *et al.* 2005
Huon Estuary, southeast Tasmania	440	† ~ 0.16 – 14	~ 0.02 – 0.06	0.17 – 0.623	Clementson *et al.* 2003
Tamar estuary, UK	440	0.04 – 3.63	0.013 – 0.059 (675 nm)	-	Doxaran *et al.* 2006
Gironde estuary, France	440	0.05 – 0.26	0.004 – 0.024 (675 nm)	-	Doxaran *et al.* 2006
Rhode River, Chesapeake Bay, USA	400	~1.12 - 2.8	0.01 - 0.045 (440 nm)	0.25 - 4.2	Gallegos,1990
Orinoco River plume, Venezuela	440	0.23 - 3.29	0.017 - 0.16	0.002 - 0.754	Odriozola *et al.* 2007
Mississippi River, Northern Gulf of Mexico, USA	443	0.04 - 1.2 (412 nm)	0.02 - 0.1	0.019 - 0.892	D' Sa *et al.* 2006
Coastal waters, Northern Gulf of Mexico, USA	443	0.046 - 1.4	~ 0.037 - 1.39 (a_{PHY})	0.0067 - 3.6	Green *et al.* 2008
Atchafalaya shelf, Northern Gulf of Mexico, USA	443	0.027 - 0.54	0.006 - 0.061	0.017 - 0.910	Present study

from the exchange/runoff from surrounding wetlands [*Chen and Gardner*, 2004; *Clementson et al.*, 2004; *D'Sa*, 2008] are seen from the higher $a_{CDOM}(\lambda)$ at some stations on or near the Ship shoal. The S_{CDOM} variation was large in the study area, but the mean of spectral slope from April to October 2007 (0.0183 ± 0.0038 nm^{-1}) was comparable to studies done in other regions; Bricaud *et al.* (1981) reported a mean S_{CDOM} of 0.014 ± 0.0032 for diverse water bodies, Babin *et al.* (2003) reported values of S_{CDOM} for coastal waters around Europe with a mean of 0.0176 ± 0.0020 nm^{-1} and Vantrepotte *et al.* (2007) found for the English Channel that S_{CDOM} varied from

0.013–0.018 nm^{-1}. The variability in $a^*_{PHY}(\lambda)$ observed, indicates a change in pigment composition or package effect. In particular the blue to red ratio for e.g. $a_{PHY}^*(443)/a_{PHY}^*(676)$ in this study varied from 2.5 to 1.1 demonstrating approximately a 2 fold decrease as chlorophyll-a increased from 0.41–10.54 mg m^{-3}. This ratio is strongly correlated with the ratio of accessory pigments to chlorophyll-a, as the accessory pigments are known to absorb significantly higher amount of light in the blue region than in the red region of the spectrum [*Lohrenz et al.*, 2003]. The inverse correlation of $a_{PHY}^*(443)/a_{PHY}^*(676)$ with chlorophyll-a is consistent with Bricaud *et al.* (1995), the high value of this ratio indicates dominance of smaller size phytoplankton and vice versa. Previous studies done on small sized phytoplankton like marine prochlorophytes [*Moore et al.*, 1995] and cyanobacteria [*Stramski and Morel*, 1990] have shown that the blue to red ratios of these small sized cells are typically greater than 2.5. Compared to other regions the blue to red ratio of $a^*_{PHY}(\lambda)$ in this study is relatively small. For instance in the California current system, Sosik and Mitchell (1995) found that this ratio varies between 2–4.5, Chami *et al.* (2005) found this ratio to be between 2.4–3.3 in the Black Sea., Babin *et al.* (2003) found it to be between 2–3.2 for the Atlantic. The smaller values of the blue to red ratio in this study (mean = 1.5 ± 0.4) show that large size phytoplankton may be dominant which in turn indicates probably a larger package effect. The package effect can be quantified at 676 nm, as we can assume that the main absorbing pigment at 676 nm is chlorophyll-a with minimal influence form accessory pigments. Using the approach used by Duysen (1956) and Morel and Bricaud (1981) the package effect can be quantified ($Qa^*(\lambda)$) as the ratio $a^*_{PHY}(\lambda)$ and specific phytoplankton absorption of the same pigmented material in suspension ($a^*_{PHY\_SOL}(\lambda)$). With $a^*_{PHY\_SOL}(676)$ taken equal to 0.0206 m^2mg^{-1} [*Bricaud et al.*, 1983], $Qa^*(676)$ was calculated. The $Qa^*(676)$ values decreased

from 0.97 to 0.16 with increasing chlorophyll-a concentration ($r^2 = 0.65$, $p<0.001$). There was no significant difference between August 2007 and October 2007 Qa*(676) values.

The variation in $a_{NAP}(443)$ was large, being about an order of magnitude with stations close to the coast having higher value of $a_{NAP}(443)$ than stations away from the coast consistent with other studies [*D'Sa et al.*, 2006; *Dupont et al.*, 1993]. The relative contribution of $a_{NAP}(443)$ to $a_P(443)$ ranged from ~31% at outermost station (Stn. 19) to ~93% (Stn. 16) with higher contribution during October (62–93%) than August cruise (31–89%). This could be explained to an extent by the river runoff or resuspension of bottom sediments [*Chami et al.*, 2005]. The higher values of $a_{NAP}(443)/a_P(443)$ seen in October 2007 cruise may be due to the resuspension of bottom sediments at muddy off shoal stations as seen from the higher wind speeds and almost uniform salinity profiles discussed earlier. The S_{NAP} varied between 0.006–0.010 nm^{-1}, these small values are associated with mineral or inorganic particles. Though S_{NAP} values are small they are consistent with studies done previously, in particular, D' Sa *et al.* (2006) found S_{NAP} values between 0.0085 – 0.0121 nm^{-1} with a mean of 0.011 nm^{-1}, Tilstone *et al.* (2005) [*Tilstone et al.*, 2005] found in the Irish Sea that S_{NAP} values ranged between 0.006 – 0.018 nm^{-1}. For coastal waters around Europe, Babin *et al.* (2003) found that the mean value of S_{NAP} was 0.0123 ± 0.0013 nm^{-1}. The high values of $a_{CDOM}(\lambda)$ and $a_{NAP}(\lambda)$ are indicative of typical case 2 waters [*Morel and Prieur*, 1977]. To address this further the covariabilty of $a_{CDOM}(\lambda)$ and $a_{NAP}(\lambda)$ with chlorophyll-a is examined below. An absorption budget for the study area is presented to analyze the dominating constituent/s in the total light absorption across the visible spectrum and its implications on OCA's are analyzed.

Relation of $a_{CDOM}(\lambda)$ and $a_{NAP}(\lambda)$ to Chlorophyll-a – Case 2 Waters

The relation of $a_{CDOM}(412)$ and $a_{NAP}(443)$ with chlorophyll-a is studied in an attempt to explain the variations in the magnitude of $a_{CDOM}(412)/ a_{NAP}(443)$ and to enable optical classification of waters as case 1 or case 2. In open ocean waters mostly this relation is positive i.e. increase in $a_{CDOM}(\lambda)$ with increasing chlorophyll, but in coastal waters this is not so (Figure 3.7).

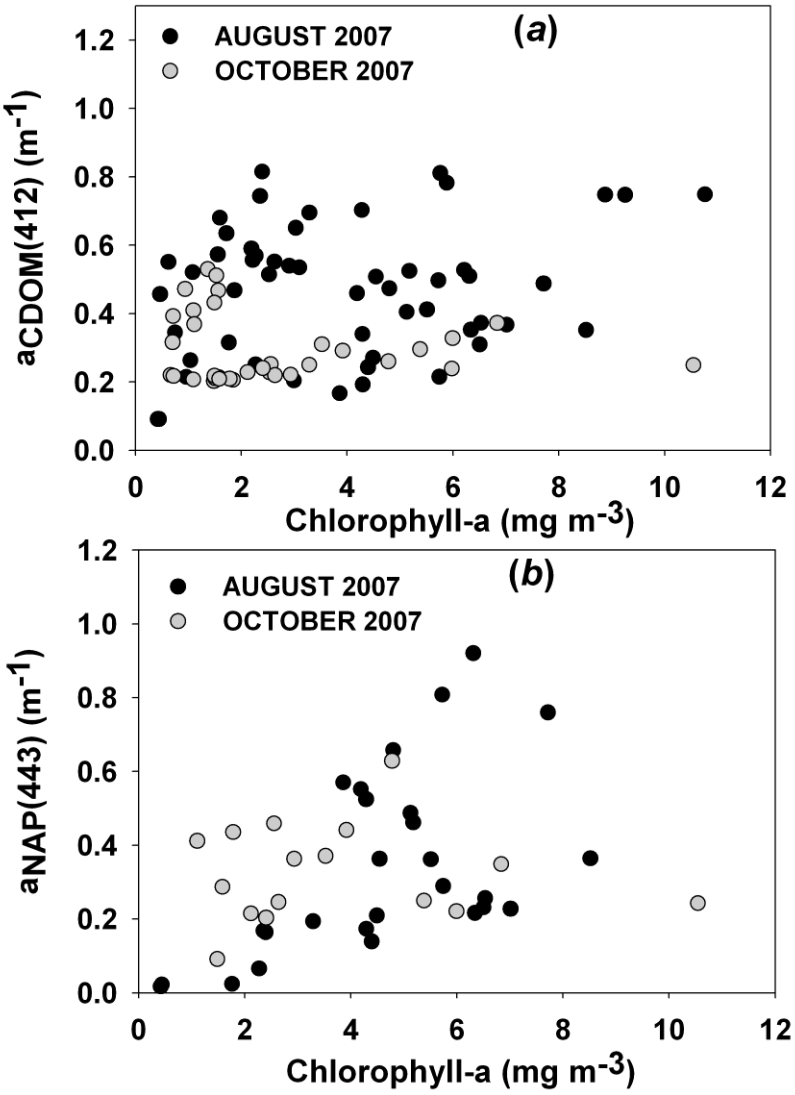

Figure 3.7. Relation of (a) $a_{CDOM}(\lambda)$ and (b) $a_{NAP}(\lambda)$ with chlorophyll-a for all depths.

Babin et al. (2003) found that over a range of coastal water types there is covariation of $a_{CDOM}(\lambda)$ with chlorophyll-a , but there is large unexplained variation in this relation as does in our study region (Figure 3.7a). Figure 3.7a also shows that data could be broadly separated into two groups. Group1 showing considerably lesser $a_{CDOM}(\lambda)$ between 0.5–6.0 mg m^{-3} of chlorophyll-a compared to Group 2 in the same chlorophyll-a range. All the stations in the Group 2 were near or on the ship shoal. The higher $a_{CDOM}(\lambda)$ may be due to the higher local production and exchange within the coastal wetlands present at the proximity of the ship shoal stations [*Chen and Gardner*, 2004; *D'Sa*, 2008].

Figure 3.7b clearly showed there is very little covariation between $a_{NAP}(443)$ and chlorophyll-a. The trend of increasing $a_{NAP}(443)$ with chlorophyll-a is somewhat present, but there is large scatter. Further, the correlation between $a_{CDOM}(443)$, $a_{NAP}(443)$ and $a_{PHY}(443)$ was less than 0.2. These results suggested that these shoal areas are typical of case 2 waters [*Morel and Prieur*, 1977] where phytoplankton was neither the dominant component affecting absorption properties nor did it co-vary with CDOM or NAP. Similar results were seen for regressions of $a_{CDOM}(443)$, $a_{NAP}(443)$ and $a_{PHY}(443)$, indicating non-covarying $a_{CDOM}(\lambda)$ and $a_{NAP}(\lambda)$ specifically at blue wavelengths could impede the retrievals of remotely sensed chlorophyll-a [*Tzortziou et al.*, 2007].

Dominant Constituent in the Total Light Absorption Coefficient

The optical classification of natural waters into three components i.e. absorption by CDOM, phytoplankton and NAP was first proposed by Prieur and Sathyendranath (1981). This partitioning of natural waters plotted on triangular plots provides information on the dominant absorbing constituents in natural waters (Figure 3.8). The combined contribution of $a_{CDOM}(\lambda)$ and $a_{NAP}(\lambda)$ decreased with increasing wavelength, being greater than 80% at lower wavelengths and

greater than 20% at higher wavelengths for both the cruises (Figure 3.8a and b). This is because of the exponential increase of $a_{CDOM}(\lambda)$ and $a_{NAP}(\lambda)$ with decreasing wavelength. At higher wavelengths (555 and 676 nm) this absorption was greater in August (> 50%) than in October 2007 (Figure 3.8c and d). While $a_{CDOM}(\lambda)$ is more dominant than $a_{NAP}(\lambda)$ in August 2007, the opposite is the case in October 2007 at all wavelengths. This

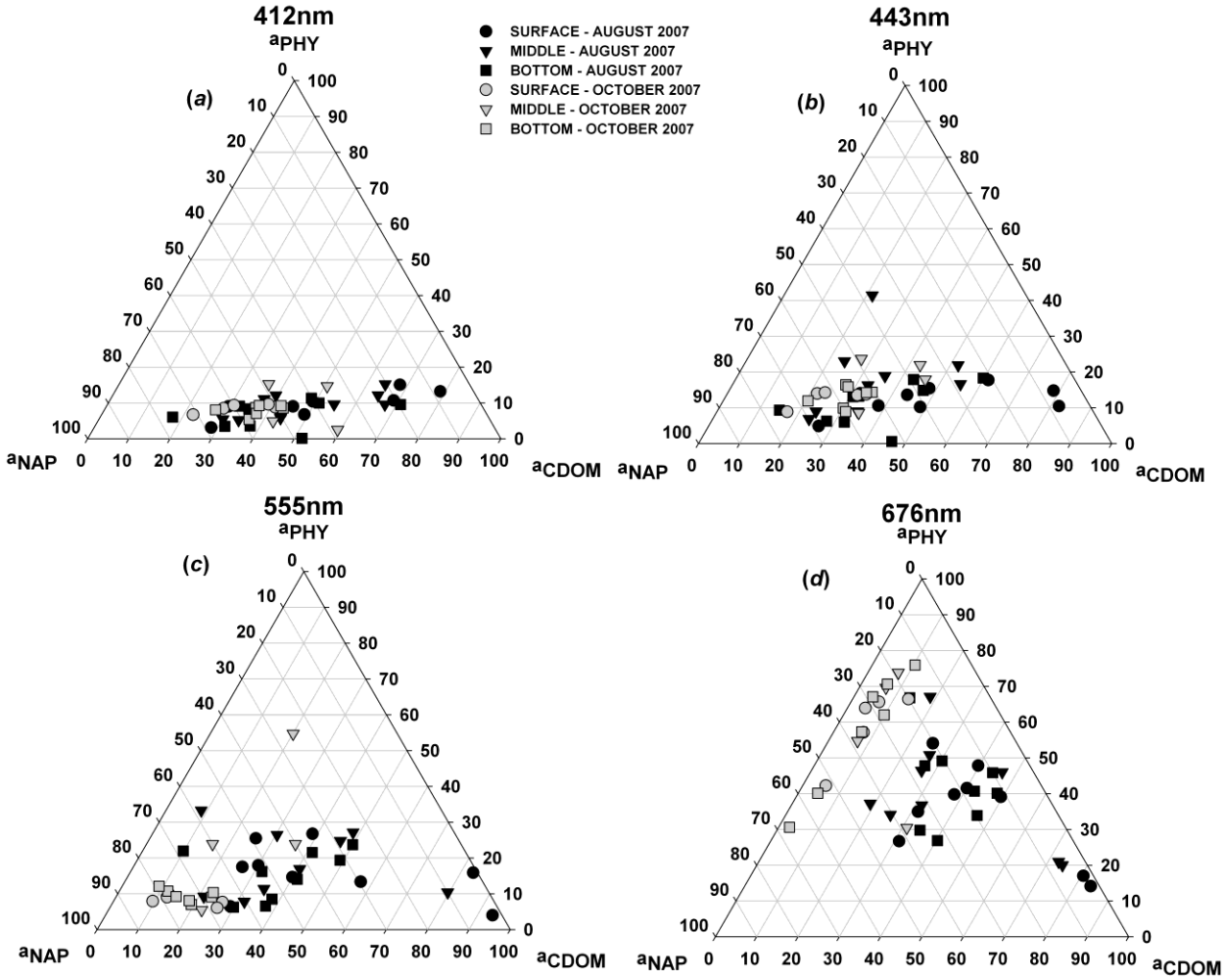

Figure 3.8. Ternary plots showing relative contribution of absorption by CDOM ($a_{CDOM}(\lambda)$), phytoplankton ($a_{PHY}(\lambda)$) and NAP ($a_{NAP}(\lambda)$) to total absorption for (a) 412 nm (b) 443 nm (c) 555 nm and (d) 676 nm. Filled black symbols indicate August 2007 cruise samples and filled grey symbols indicate October 2007 cruise samples.

hints that when the AR flow is high CDOM dominates and when the AR flow is low NAP dominates the total light absorption. The cold front passage may also have contributed to the relative increase in NAP absorption (Figure 3.8c). However a long-term dataset that contains monthly observations would give a more accurate picture.

It was interesting to see that at higher wavelengths (555 nm and 676 nm) most of the October samples fell into a different group as compared to the August 2007 cruise samples (Figure 3.8c and d). At 555 nm the higher $a_{NAP}(\lambda)$ relative to $a_{PHY}(\lambda)$ and $a_{CDOM}(\lambda)$ were observed for both August and October with being highest for October period. $a_{PHY}(\lambda)$ is generally dominant at 676 nm compared to $a_{CDOM}(\lambda)$ and $a_{NAP}(\lambda)$; this is shown by most samples in October 2007 cruise (greater than at least 30%) but the August 2007 cruise samples this dominance is not clearly seen due to the relatively large $a_{CDOM}(\lambda)$ and $a_{NAP}(\lambda)$. This clearly shows that $a_{CDOM}(\lambda)$ and $a_{NAP}(\lambda)$ are the major constituent in these shoal dominated waters having an effect on total absorption even at higher wavelengths where their influence is the least. This contrasts with case 1 waters where at the blue portion of the visible spectrum phytoplankton absorption dominates the total non-water light absorption [*Bricaud et al.*, 1998].However similar to results from coastal waters; Odriozola *et al.* 2007 found that in the Gulf of Paria and southeastern Caribbean Sea, $a_{CDOM}(\lambda)$ at 440nm was ~90%, Babin *et al.* (2003) found for European coastal waters at 443 nm that $a_{CDOM}(\lambda)$ dominates the light absorption (28–56%) followed closely by $a_{PHY}(\lambda)$ (28–52%) and least contribution is from $a_{NAP}(\lambda)$ (11–27%). The high values of $a_{CDOM}(\lambda)$ and $a_{NAP}(\lambda)$ obtained in this study seen at the lower wavelengths (blue end of the visible spectrum) significantly affect the underwater light field which would then affect the phytoplankton community within the water column. At stations where combined $a_{CDOM}(\lambda)$ and $a_{NAP}(\lambda)$ was high the $a^*_{PHY}(\lambda)$ increased with depth, indicating that smaller-size phytoplankton

which are more efficient in absorbing light may be dominant at higher depths. Recent studies done on these shoals have shown that greater than 5% of surface light reaches the bottom [*Grippo et al.*, 2009]. Results thus indicate that the shoal areas are typical case 2 waters where chlorophyll was neither the dominant component affecting absorption properties nor did it co-vary with $a_{CDOM}(\lambda)$ or $a_{NAP}(\lambda)$. Thus the variability in these waters was primarily due to $a_{CDOM}(\lambda)$ and $a_{NAP}(\lambda)$ rather than chlorophyll-a. The variability between $a_{PHY}(443)$ $a_{NAP}(443)$ and $a_{CDOM}(443)$ can be examined using the coefficient of variation (standard deviation/mean). The $a_{CDOM}(\lambda)$ and $a_{NAP}(\lambda)$ vary approximately 1.2 and 1.8 times respectively as much as phytoplankton absorption at 443 nm. This means that $a_{CDOM}(\lambda)$ and $a_{NAP}(\lambda)$ vary to a greater extent while phytoplankton absorption is relatively constant.

In-Situ and Satellite Data Match-up

SeaWiFS imagery for chlorophyll-a in the study region for 6 October, 2007 processed using standard OCA and atmospheric corrections described is shown in Figure 3.9a. The satellite images clearly show the gradients from high to low constituent concentration between the coast and the offshore waters as well as the Atchafalaya River outflow impact along the coast. The in-situ and satellite match-up results show an overestimation at lower chlorophyll-a concentrations (Figure 3.9c). The relative difference between in-situ and satellite derived chlorophyll-a retrievals was ~ ±3 times which is consistent with studies done near the Atchafalaya Bay [*Walker and Rabalais*, 2006]. Apart from the strong $a_{CDOM}(\lambda)$ and $a_{NAP}(\lambda)$, the variable $a^*_{PHY}(\lambda)$ spectra obtained in the study region described above, which is dependent on pigment composition and phytoplankton species further hamper accurate retrievals of chlorophyll-a. The regional $a_{CDOM}(\lambda)$ algorithm developed by D' Sa *et al.* (2006) is applied to SeaWiFS imagery (Figure 3.9b). The

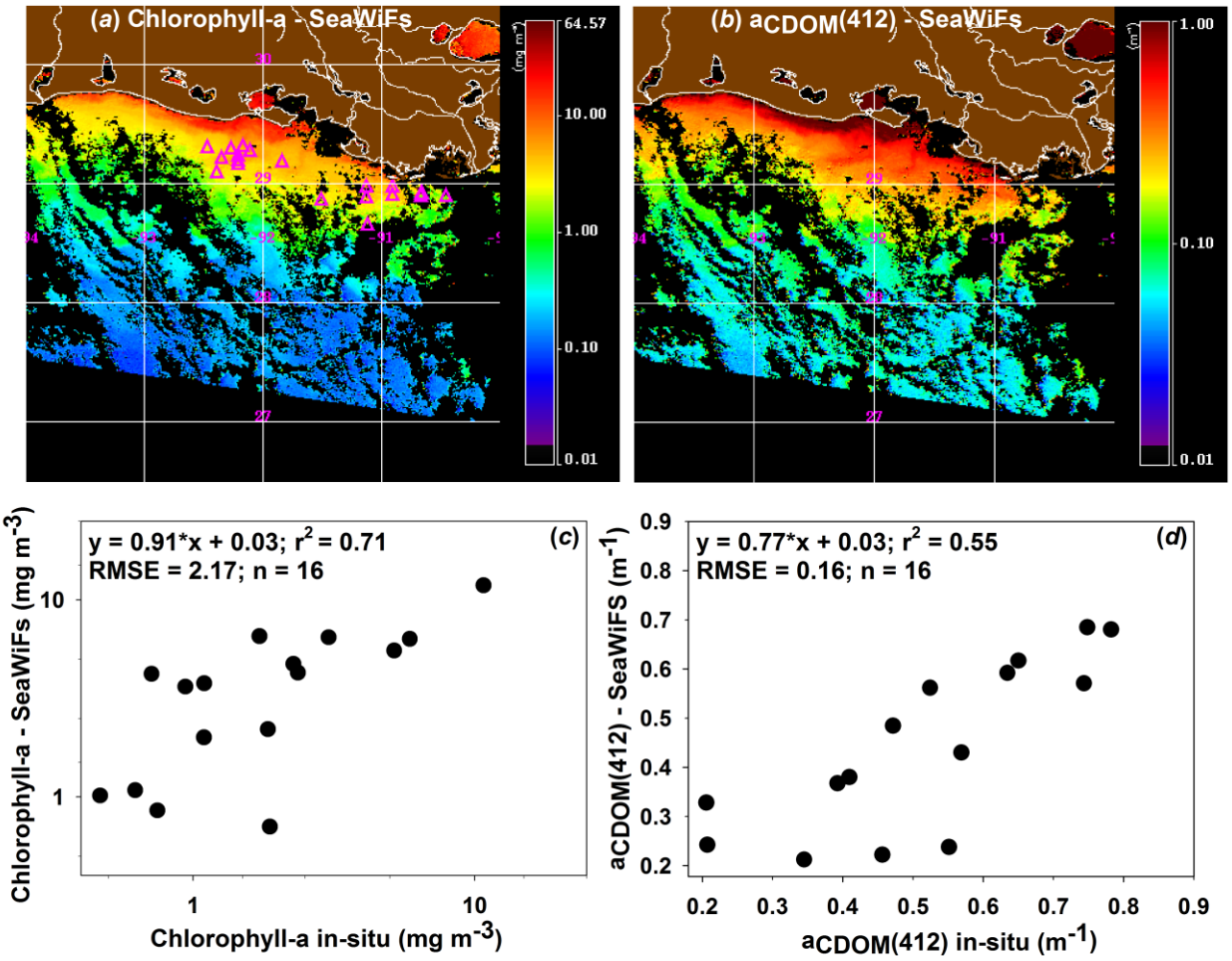

Figure 3.9. (a) Chlorophyll-a obtained using OC4.v4 algorithm (b) $a_{CDOM}(\lambda)$ at 412 nm obtained using D' Sa et al. 2006 algorithm for October, 6, 2007 SeaWiFS image. The triangles indicate sampling stations. Match up of (c) in-situ chlorophyll-a and SeaWiFS chlorophyll-a and (d) in-situ $a_{CDOM}(\lambda)$ at 412 nm and SeaWiFS $a_{CDOM}(\lambda)$ at 412 nm using D' Sa et al. 2006 algorithm. 'n' is the number of match-up points.

algorithm performed very well in the study region as seen from the relatively high 'r^2' value and low RMSE (Figure 3.9d).

The ALGAL2 algorithm used to retrieve chlorophyll-a from MERIS is optimized for coastal water applications. Figure 3.10a shows MERIS retrieved chlorophyll-a concentration for October, 6, 2007 which appears much clearer than the SeaWiFS retrieved chlorophyll-a for the same day shown in Figure 3.9a. Chlorophyll-a concentration retrieved from MERIS performs well in the study region as seen from the 'r^2', slope and RMSE values (Figure 3.10c). This result

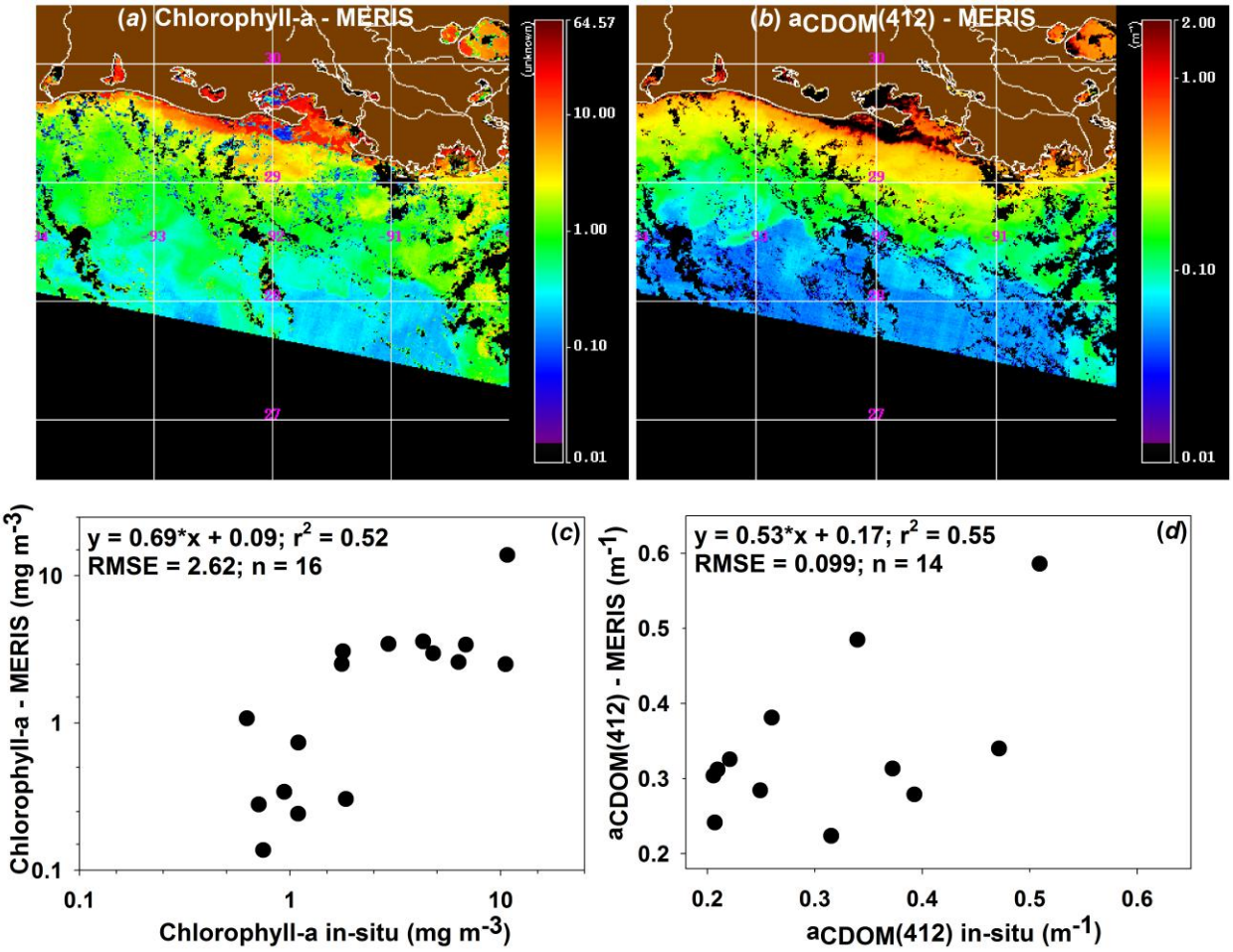

Figure 3.10. (a) Chlorophyll-a obtained using ALGAL2 algorithm (b) $a_{CDOM}(\lambda)$ at 412 nm obtained using D' Sa et al. 2006 algorithm for October, 6, 2007 MERIS image. Match up of (c) in-situ chlorophyll-a and MERIS chlorophyll-a and (d) in-situ $a_{CDOM}(\lambda)$ at 412 nm and MERIS $a_{CDOM}(\lambda)$ at 412 nm using D' Sa et al. 2006 algorithm.

is comparable to SeaWiFS retrieved chlorophyll-a, however the slope obtained from SeaWiFS is closer to one compared to slope obtained from MERIS.

The $a_{CDOM}(412)$ retrieved using D' Sa, *et al.* (2006) regional algorithm from MERIS for October, 6, 2007 is shown in Figure 3.10b and is comparable to the SeaWiFS retrieved $a_{CDOM}(412)$ shown in Figure 3.9b. The MERIS retrieved $a_{CDOM}(412)$ compared well to the in-situ $a_{CDOM}(412)$ (Figure 3.10d). We saw that the large contribution of non-covarying $a_{CDOM}(\lambda)$ and $a_{NAP}(\lambda)$ to total light absorption at blue wavelengths greatly affects the retrieval of chlorophyll-a from satellite data by using OCA's based on the blue-green reflectance ratio, this is because the

OCA do not account for such high $a_{CDOM}(\lambda)$ and $a_{NAP}(\lambda)$ [*Harding et al.*, 2005]. Most OCA's waters combine these two absorption components into one because of their similar spectral shape, although at times they do not covary. Also the lack of adequate knowledge of backscattering coefficients, as well as the higher uncertainty of remote sensing reflectance at shorter wavelengths (e.g., 412 and 443 nm) from satellite measurements further accentuates the difficulty of accurate retrieval [*IOCCG*, 2006]. The similar spectral shape of $a_{CDOM}(\lambda)$ and $a_{NAP}(\lambda)$ hampers attempts made to separate their individual involvement. But from the values of spectral slope of NAP we found that the mineral particles that are highly refractive likely dominate. These $a_{NAP}(\lambda)$ are found to correlate well with backscattering coefficient and ratio of remote sensing reflectance's at 670 nm and 555 nm in these types of waters [*D'Sa et al.*, 2007]. Hence this relationship can be used to obtain the contribution of NAP to total light absorption and also can be used for retrieval of $a_{NAP}(\lambda)$ from satellite measured remote sensing reflectance. To quantify the impact of the high $a_{CDOM}(\lambda)$ and $a_{NAP}(\lambda)$ on OCA's that use blue-green reflectance ratios for retrieval of chlorophyll-a is difficult without modelling techniques (e.g. Hydrolight). However due to the strong signal from CDOM and NAP absorption in the blue-green region, regionally specific algorithms that are based on the chlorophyll-a absorption feature at 675 nm can be used for retrieval of chlorophyll in waters with high CDOM and NAP absorption [*Dall'Olmo et al.*, 2005; *Ruddick et al.*, 2001].

Conclusions

CDOM and NAP absorption together dominate the total absorption of light in these shoal dominated waters. While the phytoplankton absorption was relatively constant, larger variations were observed in CDOM and NAP absorption. The CDOM absorption showed a near conservative relationship with salinity and responded to the AR flow. Spectral slope of CDOM

was consistent with those observed in other coastal regions. The NAP absorption showed similar trends as CDOM absorption. While CDOM absorption was dominant in August 2007 cruise, NAP absorption was dominant in October 2007. The average NAP spectral slope indicated predominantly mineral inorganic particulate matter. The phytoplankton absorption contributed the least to the total absorption during the study period. The specific phytoplankton absorption was found to be variable indicating package effect or changes in pigment composition. This would lead to lower values of phytoplankton absorption coefficient. The implications of this are important for water quality and monitoring of harmful blooms. Hydrodynamic features (AR flow, cold fronts) influenced absorption properties to a certain extent. However the most important feature in these waters was the large dominance of non-covarying CDOM and NAP absorption. We saw that the large contribution of non-covarying $a_{CDOM}(\lambda)$ and $a_{NAP}(\lambda)$ to total light absorption at blue wavelengths greatly affects the retrieval of chlorophyll-a from satellite data by using OCA's. This would greatly affect the inference of qualitative biological and geochemical information (in-situ as well by remote sensing) on CDOM, phytoplankton and non-algal particles from their optical characteristics (e.g. absorption and spectral slope). Further, for effective use of ocean color data to monitor blooms an algorithm that can determine contributions of CDOM and NAP and based on absorption in the red portion of the spectrum where their contribution is minimal will work better.

Long-term comprehensive datasets collected monthly of inherent optical properties along with pigment data in such complex coastal regions will play an important role in the monitoring of blooms, water quality and also in the development of regional OCA's.

References

Babin, M., J. Therriault, L. Legendre, and A. Condal (1993), Variations in the specific absorption-coefficient for natural phytoplankton assemblages - impact on estimates of primary production, Limnology and Oceanography, 38(1), 154-177.

Babin, M., D. Stramski, G. Ferrari, H. Claustre, A. Bricaud, G. Obolensky, and N. Hoepffner (2003), Variations in the light absorption coefficients of phytoplankton, nonalgal particles, and dissolved organic matter in coastal waters around Europe, Journal of Geophysical Research-Oceans, 108(C7).

Bissett, W. P., O. Schofield, S. Glenn, J. J. Cullen, W. L. Miller, A. J. Plueddemann, and C. D. Mobley (2001), Resolving the impacts and feedbacks of ocean optics on upper ocean ecology, Oceanography, 14, 30–49.

Blough, N., O. Zafiriou, and J. Bonilla (1993), Optical-absorption spectra of waters from the Orinoco River outflow - terrestrial input of colored organic-matter to the Caribbean, Journal of Geophysical Research-Oceans, 98(C2), 2271-2278.

Bowers, D., and C. Binding (2006), The optical properties of mineral suspended particles: A review and synthesis, Estuarine Coastal and Shelf Science, 67(1-2), 219-230.

Bowers, D., G. Harker, and B. Stephan (1996), Absorption spectra of inorganic particles in the Irish Sea and their relevance to remote sensing of chlorophyll, International Journal of Remote Sensing, 17(12), 2449-2460.

Bricaud, A., A. Morel, and L. Prieur (1981), Absorption by dissolved organic-matter of the sea (Yellow Substance) in the UV and visible domains, Limnology and Oceanography, 26(1), 43-53.

Bricaud, A., A. Morel, and L. Prieur (1983), Optical-efficiency factors of some phytoplankters, Limnology and Oceanography, 28(5), 816-832.

Bricaud, A., M. Babin, A. Morel, and H. Claustre (1995), Variability in the chlorophyll-specific absorption-coefficients of natural phytoplankton - analysis and parameterization, Journal of Geophysical Research-Oceans, 100(C7), 13321-13332.

Bricaud, A., A. Morel, M. Babin, K. Allali, and H. Claustre (1998), Variations of light absorption by suspended particles with chlorophyll a concentration in oceanic (case 1) waters: Analysis and implications for bio-optical models, Journal of Geophysical Research-Oceans, 103(C13), 31033-31044.

Carder, K., R. Steward, G. Harvey, and P. Ortner (1989), Marine humic and fulvic-acids - their effects on remote-sensing of ocean chlorophyll, Limnology and Oceanography, 34(1), 68-81.

Chami, M., E. Shybanov, T. Churilova, G. Khomenko, M. Lee, O. Martynov, G. Berseneva, and G. Korotaev (2005), Optical properties of the particles in the Crimea coastal waters (Black Sea), Journal of Geophysical Research-Oceans, 110(C11).

Chen, R., and G. Gardner (2004), High-resolution measurements of chromophoric dissolved organic matter in the Mississippi and Atchafalaya River plume regions, Marine Chemistry, 89(1-4), 103-125.

Ciotti, A., J. Cullen, and M. Lewis (1999), A semi-analytical model of the influence of phytoplankton community structure on the relationship between light attenuation and ocean color, Journal of Geophysical Research-Oceans, 104(C1), 1559-1578.

Clementson, L., J. Parslow, A. Turnbull, and P. Bonham (2004), Properties of light absorption in a highly coloured estuarine system in south-east Australia which is prone to blooms of the toxic dinoflagellate Gymnodinium catenatum, Estuarine Coastal and Shelf Science, 60(1), 101-112.

Coble, P., C. Hu, R. Gould, G. Chang, and W. A.M. (2004), Colored dissolved organic matter in the coastal ocean: An optical tool for coastal environmental assessment and management, Oceanography, 17, 50-59.

D'Sa, E. (2008), Colored dissolved organic matter in coastal waters influenced by the Atchafalaya River, USA: effects of an algal bloom, Journal of Applied Remote Sensing, 2.

D'Sa, E., and R. Miller (2003), Bio-optical properties in waters influenced by the Mississippi River during low flow conditions, Remote Sensing of Environment, 84(4), 538-549.

D'Sa, E., and D. Ko (2008), Short-term influences on suspended particulate matter distribution in the northern Gulf of Mexico: Satellite and model observations, Sensors, 8(7), 4249-4264.

D'Sa, E., R. Miller, and C. Del Castillo (2006), Bio-optical properties and ocean color algorithms for coastal waters influenced by the Mississippi River during a cold front, Applied Optics, 45(28), 7410-7428.

D'Sa, E., R. Miller, and B. Mckee (2007), Suspended particulate matter dynamics in coastal waters from ocean color: Application to the northern Gulf of Mexico, Geophysical Research Letters, 34(23).

Dall'Olmo, G., A. Gitelson, D. Rundquist, B. Leavitt, T. Barrow, and J. Holz (2005), Assessing the potential of SeaWiFS and MODIS for estimating chlorophyll concentration in turbid productive waters using red and near-infrared bands, Remote Sensing of Environment, 96(2), 176-187.

Dubois, S., C. Gelpi, R. Condrey, M. Grippo, and J. Fleeger (2009), Diversity and composition of macrobenthic community associated with sandy shoals of the Louisiana continental shelf, Biodiversity and Conservation, 18(14), 3759-3784.

Dupont, J. P., M. B. Collins, R. Lafite, L. Nash, M. F. Huault, S. J. Shimwell, S. Chaddock, C. Brunet, M. Wartel, and M. Lamboy (1993), Annual variations in suspended particulate matter within the Dover Strait, Oceanologica acta. Paris, 16(5), 507-516.

Duysens, L. (1956), The flattening of the absorption spectrum of suspensions, as compared to that of solutions, Biochimica Et Biophysica Acta, 19(1), 1-12.

Ferrari, G., F. Bo, and M. Babin (2003), Geo-chemical and optical characterizations of suspended matter in European coastal waters, Estuarine Coastal and Shelf Science, 57(1-2), 17-24.

Fujiki, T., and S. Taguchi (2002), Variability in chlorophyll alpha specific absorption coefficient in marine phytoplankton as a function of cell size and irradiance, Journal of Plankton Research, 24(9), 859-874.

Gould, R., and R. Arnone (1997), Remote sensing estimates of inherent optical properties in a coastal environment, Remote Sensing of Environment, 61(2), 290-301.

Green, R., R. Gould, and D. Ko (2008), Statistical models for sediment/detritus and dissolved absorption coefficients in coastal waters of the northern Gulf of Mexico, Continental Shelf Research, 28(10-11), 1273-1285.

Grippo, M., J. Fleeger, R. Condrey, and K. Carman (2009), High benthic microalgal biomass found on ship shoal, north-central Gulf of Mexico, Bulletin of Marine Science, 84(2), 237-256.

Harding, L., A. Magnuson, and M. Mallonee (2005), SeaWiFS retrievals of chlorophyll in Chesapeake Bay and the mid-Atlantic bight, Estuarine Coastal and Shelf Science, 62(1-2), 75-94.

Hochman, H., F. Mullerkarger, and J. Walsh (1994), Interpretation of the coastal zone color scanner signature of the Orinoco River plume, Journal of Geophysical Research-Oceans, 99(C4), 7443-7455.

Hoepffner, N., and S. Sathyendranath (1991), Effect of pigment composition on absorption properties of phytoplankton, Marine Ecology Progress Series, 73(1), 11-23.

Hu, C., Z. Chen, T. Clayton, P. Swarzenski, J. Brock, and F. Muller-Karger (2004), Assessment of estuarine water-quality indicators using MODIS medium-resolution bands: Initial results from Tampa Bay, FL, Remote Sensing of Environment, 93(3), 423-441.

ICES (1992), International Council for the Exploration of the Sea. Rep., Copenhagen Denmark.

IOCCG (2006), Remote Sensing of Inherent Optical Properties: Fundamentals, Tests of Algorithms, and ApplicationsRep., IOCCG, Dartmouth, Canada.

Kahru, M., and B. Mitchell (1998), Spectral reflectance and absorption of a massive red tide off southern California, Journal of Geophysical Research-Oceans, 103(C10), 21601-21609.

Kishino, M., M. Takahashi, N. Okami, and S. Ichimura (1985), Estimation of the spectral absorption-coefficients of phytoplankton in the sea, Bulletin of Marine Science, 37(2), 634-642.

Lohrenz, S., A. Weidemann, and M. Tuel (2003), Phytoplankton spectral absorption as influenced by community size structure and pigment composition, Journal of Plankton Research, 25(1), 35-61.

Mitchell, B. G. (1990), Algorithms for determining the absorption coefficients for aquatic particulates using the quantitative filter technique, paper presented at Ocean Optics X, SPIE.

Mitchell, B. G., M. Kahru, J. Wieland, and M. Stramska (2003), Determination of spectral absorption coefficients of particles, dissolved materials and phytoplankton for discrete water samples, in Ocean Optics Protocols For Satellite Ocean Color Sensor Validation, Revision 4, Volume 4: Inherent optical properties: instruments, characterization, field measurements and data analysis protocols, edited, NASA Tech. Rep., Greenbelt, Maryland.

Moore, L., R. Goericke, and S. Chisholm (1995), Comparative physiology of Synechococcus and Prochlorococcus - influence of light and temperature on growth, pigments, fluorescence and absorptive properties, Marine Ecology Progress Series, 116(1-3), 259-275.

Morel, A., and L. Prieur (1977), Analysis of variations in ocean color, Limnology and Oceanography, 22(4), 709-722.

Morel, A., and A. Bricaud (1981), Theoretical results concerning light-absorption in a discrete medium, and application to specific absorption of phytoplankton, Deep Sea Research Part I-Oceanographic Research Papers, 28(11), 1375-1393.

Odriozola, A., R. Varela, C. Hua, Y. Astor, L. Lorenzoni, and F. Muller-Karger (2007), On the absorption of light in the Orinoco River plume, Continental Shelf Research, 27(10-11), 1447-1464.

Prieur, L., and S. Sathyendranath (1981), An optical classification of coastal and oceanic waters based on the specific spectral absorption curves of phytoplankton pigments, dissolved organic-matter, and other particulate materials, Limnology and Oceanography, 26(4), 671-689.

Rabalais, N. N., and R. E. Turner (2001), Coastal Hypoxia: Consequences for Living Resources and Ecosystems, 464 pp., AGU, Washington, D. C.

Roberts, H. H., O. K. Huh, S. A. Hsu, L. J. Rouse Jr, and D. Rickman (1987), Impact of cold-front passages on geomorphic evolution and sediment dynamics of the complex Louisiana coast, paper presented at Coastal Sediments 1987, American Society of Civil Engineers, NewYork, New Orleans, Louisiana.

Roesler, C., M. Perry, and K. Carder (1989), Modeling insitu phytoplankton absorption from total absorption-spectra in productive inland marine waters, Limnology and Oceanography, 34(8), 1510-1523.

Ruddick, K., H. Gons, M. Rijkeboer, and G. Tilstone (2001), Optical remote sensing of chlorophyll a in case 2 waters by use of an adaptive two-band algorithm with optimal error properties, Applied Optics, 40(21), 3575-3585.

Sosik, H., and B. Mitchell (1995), Light absorption by phytoplankton, photosynthetic pigments and detritus in the California current system, Deep Sea Research Part I-Oceanographic Research Papers, 42(10), 1717-1748.

Stone, G., D. Pepper, J. Xu, and X. Zhang (2004), Ship shoal as a prospective borrow site for barrier island restoration, coastal south-central Louisiana, USA: Numerical wave modeling and field measurements of hydrodynamics and sediment transport, Journal of Coastal Research, 20(1), 70-88.

Stramski, D., and A. Morel (1990), Optical-properties of photosynthetic picoplankton in different physiological states as affected by growth irradiance, Deep Sea Research Part I-Oceanographic Research Papers, 37(2), 245-266.

Stumpf, R. P., M. E. Culver, P. A. Tester, M. Tomlinson, G. J. Kirkpatrick, B. A. Pederson, E. Truby, V. Ransibrahmanakul, and M. Soracco (2003), Monitoring Karenia brevis blooms in the Gulf of Mexico using satellite ocean color imagery and other data, Harmful Algae, 2(2), 147-160.

Tassan, S., and G. Ferrari (1995), An alternative approach to absorption measurements of aquatic particles retained on filters, Limnology and Oceanography, 40(8), 1358-1368.

Tilstone, G., T. Smyth, R. Gowen, V. Martinez-Vicente, and S. Groom (2005), Inherent optical properties of the Irish Sea and their effect on satellite primary production algorithms, Journal of Plankton Research, 27(11), 1127-1148.

Tzortziou, M., A. Subramaniam, J. Herman, C. Gallegos, P. Neale, and L. Harding (2007), Remote sensing reflectance and inherent optical properties in the mid Chesapeake Bay, Estuarine Coastal and Shelf Science, 72(1-2), 16-32.

Vantrepotte, V., C. Brunet, X. Meriaux, E. Lecuyer, V. Vellucci, and R. Santer (2007), Bio-optical properties of coastal waters in the Eastern English Channel, Estuarine Coastal and Shelf Science, 72(1-2), 201-212.

Walker, N. (1996), Satellite assessment of Mississippi River plume variability: Causes and predictability, Remote Sensing of Environment, 58(1), 21-35.

Walker, N., and A. Hammack (2000), Impacts of winter storms on circulation and sediment transport: Atchafalaya-Vermilion Bay region, Louisiana, USA, Journal of Coastal Research, 16(4), 996-1010.

Walker, N., and N. Rabalais (2006), Relationships among satellite chlorophyll a, river inputs, and hypoxia on the Louisiana continental shelf, gulf of Mexico, Estuaries and Coasts, 29(6B), 1081-1093.

CHAPTER 4: LIGHT ABSORPTION PROPERTIES IN SOUTHEASTERN BERING SEA DURING JULY 2008: ANALYSIS, PARAMETERIZATION AND ABSORPTION BUDGET

Introduction

The southeastern Bering Sea is one of the most productive marine ecosystems in the world and provides half of the commercial seafood caught in the United States [*Sigler et al.,* 2010]. As the Bering Sea ecosystem responds to variations in climate, its capability to supply the resources on which the national and local economy depends will possibly change [*Grebmeier et al.,* 2006]. Long-term monitoring is critical for understanding and predicting changes in this ecosystem [*Sigler et al.,* 2010]. Ocean color remote sensing is an important tool relative to in-situ observations in terms of spatial and temporal resolution to examine changes in the southeastern Bering Sea ecosystem. Apart from chlorophyll-a concentrations, ocean color sensors offer the potential to estimate other important variables, such as water column primary productivity (PP) and phytoplankton functional groups, which are essential for understanding long-term changes occurring in the Bering Sea ecosystem. Accurate estimates of these variables from space-based sensors require a thorough understanding of in-water optical properties. Despite the importance of the southeastern Bering Sea ecosystem as a biologically rich resource region, its optical properties have not been documented in detail. Patterns of phytoplankton distributions in relation to ice edges and polar frontal regions have been described for the Bering Sea [*Maynard and Clark*, 1987; *Müller-Karger et al.*, 1990]. Previous studies suggest that CZCS pigment concentrations derived for the Bering Sea using global ocean color algorithms are lower than in-situ estimates [*Maynard and Clark*, 1987]. More recently, Schallenberg et al., (2008), demonstrated that chlorophyll-a was overestimated by SeaWiFS OC2 algorithm in the Bering Sea. The explanation for such biases in the Bering Sea and polar regions have been attributed to

lower specific phytoplankton absorption and high CDOM and limited data for the development of ocean color algorithms [*Arrigo et al.*, 1998; *Cota et al.*, 2003; *Stramska et al.*, 2006; *Wang et al.*, 2005, *Matsuoka et al.*, 2007].

The light absorption coefficients of phytoplankton, non-algal particles (NAP), and colored dissolved organic matter (CDOM) are major parameters that determine the optical variability of oceanic waters and the understanding of their variations with ecological factors is one of the fundamentals to the fine-tuning of bio-optical models. The absorption of light by particulate and dissolved matter dominates the variance of both remote-sensing reflectance ($R_{rs}(\lambda)$) and diffuse attenuation coefficient ($K_d(\lambda)$). $R_{rs}(\lambda)$ is important for development of ocean color algorithms and $K_d(\lambda)$ is an important variable in estimating PP from standard PP models [*Behrenfeld and Falkowski*, 1997; *Westberry et al.*, 2008]. The total absorption coefficient of seawater is the sum of individual components within the water column, namely CDOM, phytoplankton and NAP and can be expressed as:

$$a_T(\lambda) = a_W(\lambda) + a_{CDOM}(\lambda) + a_{PHY}(\lambda) + a_{NAP}(\lambda) \quad \text{(Eq. 1)}$$

$$a_P(\lambda) = a_{PHY}(\lambda) + a_{NAP}(\lambda) \quad \text{(Eq. 2)}$$

$$a_{DG}(\lambda) = a_{CDOM}(\lambda) + a_{NAP}(\lambda) \quad \text{(Eq. 3)}$$

where $a_W(\lambda)$, $a_{CDOM}(\lambda)$, $a_{PHY}(\lambda)$, $a_{NAP}(\lambda)$, $a_P(\lambda)$ and $a_{DG}(\lambda)$ are absorption coefficients due to pure water, CDOM, phytoplankton, NAP, total particulate matter and dissolved plus detrital matter, respectively.

The absorption properties of high northern latitude regions [*Matsuoka et al.*, 2007; *Matsuoka et al.*, 2011; *Wang et al.*, 2005; *Stramska et al.*, 2006], particularly southeastern Bering Sea [*Naik et al.*, 2010], have only recently been studied in detail. Due to large biases observed in

retrievals of chlorophyll-a in the Arctic, region and season specific algorithms have been proposed with regional parameterization [*Stramska et al.*, 2006] involving in-situ inherent optical properties (IOPs e.g. absorption, backscattering), apparent optical properties (AOPs e.g. normalized water leaving radiance, $R_{rs}(\lambda)$) and chlorophyll-a. Even if regional or seasonal empirical algorithms developed specifically for the higher latitudes are used, biases would likely exist due to the diverse nature of absorbing coefficients in these regions. One such example is the Arctic OC4L developed by Cota et al., (2004) which performs less satisfactorily in the western Arctic when highly turbid waters are included [*Matsuoka et al.*, 2007]. A preferential approach would be to use semi-analytical algorithms that are based on the relationship between remote sensing reflectance ($R_{rs}(\lambda)$) and IOPs. Recently, Naik et al., (2010) have shown the potential of the Quasi Analytical Algorithm (QAA) to retrieve absorption coefficients [*Lee et al.*, 2002] in the southeastern Bering Sea. For the development/regional parameterization of empirical or semi-analytical ocean color algorithms and characterization of the bio-optical environment in the Bering Sea would require the knowledge of relationship between IOPs (absorption and scattering) and AOPs ($R_{rs}(\lambda)$ and $K_d(\lambda)$).

The objectives of this study are to (1) describe the spatial variation of phytoplankton, NAP, CDOM absorption coefficients, (2) examine relationships between absorption coefficients and their relative contributions to total absorption, over the entire chlorophyll-a range, (3) identify the dominant absorbing constituent in waters of southeastern Bering Sea during summer, and (4) describe the influence of the absorption coefficients on $R_{rs}(\lambda)$ and $K_d(\lambda)$. To achieve these goals we first describe the spatial variability of absorption coefficients in various across shelf and along shelf transects at different depths. We then discuss the influence of the absorption coefficients on chlorophyll-a, describe $a^*_{PHY}(\lambda)$ variability and parameterize the absorption

coefficients using simple regression models. Finally, we identify the dominant absorbing coefficients in total light absorption through normalized ternary plots and illustrate the influence of absorption on the $R_{rs}(\lambda)$ and $K_d(\lambda)$ from modeling and in-situ measurements.

Methods and Materials

Study Area

The Bering Sea is a semi-enclosed basin (Figure 4.1) with an extensive continental shelf in the east, a steep shelf break and deep basin waters towards the west. During summer the southeastern Bering Sea, shelf waters can be broadly classified into three domains, the coastal domain (<50 m depth) extending from the Alaskan coast to the inner front at ~50 m isobath, the middle domain (50 -100 m depth) extending from the inner front to the central front at ~100 m isobath, and the outer domain (100 - 200 m depth) extending from the central front to the shelf break and based on frontal structures associated with wind, bathymetry and tides [*Kachel et al.*, 2002]. During summer changes in water column density are driven by temperature rather than by salinity.

The general circulation in the Bering Sea is part of the North Pacific sub-arctic gyre with advection of Pacific water from the Aleutian Stream through the various passes along the Aleutian Islands with net outflow into the Arctic through the Bering Strait [*Schumacher and Stabeno*, 1998]. Most of the shelf circulation is characterized by diffuse flows to the north following the bathymetry with tidal energy dominating most of the shelf. The hydrographic structure of the northern shelf is driven by salinity whereas the southern shelf is driven by temperature. Sea ice melt is the primary source of freshwater that influences the central and outer domains [*Aguilar-Islas et al.*, 2008]. Apart from ice melt, the Bering shelf receives large volume of freshwater input from the Yukon and Kuskokwim rivers. The Yukon River has the fifth

largest drainage basin in North America and delivers an annual average discharge of ~200 km^3 freshwater to the northern Bering shelf [*Stabeno et al.*, 2006] while Kuskokwim has much smaller drainage basin delivering ~34 km^3 of freshwater to the southern and eastern parts of the Bering Sea [*Feely et al.*, 1981]. The maximum discharge occurs during the peak ice melt in May and June with a small pulse in August.

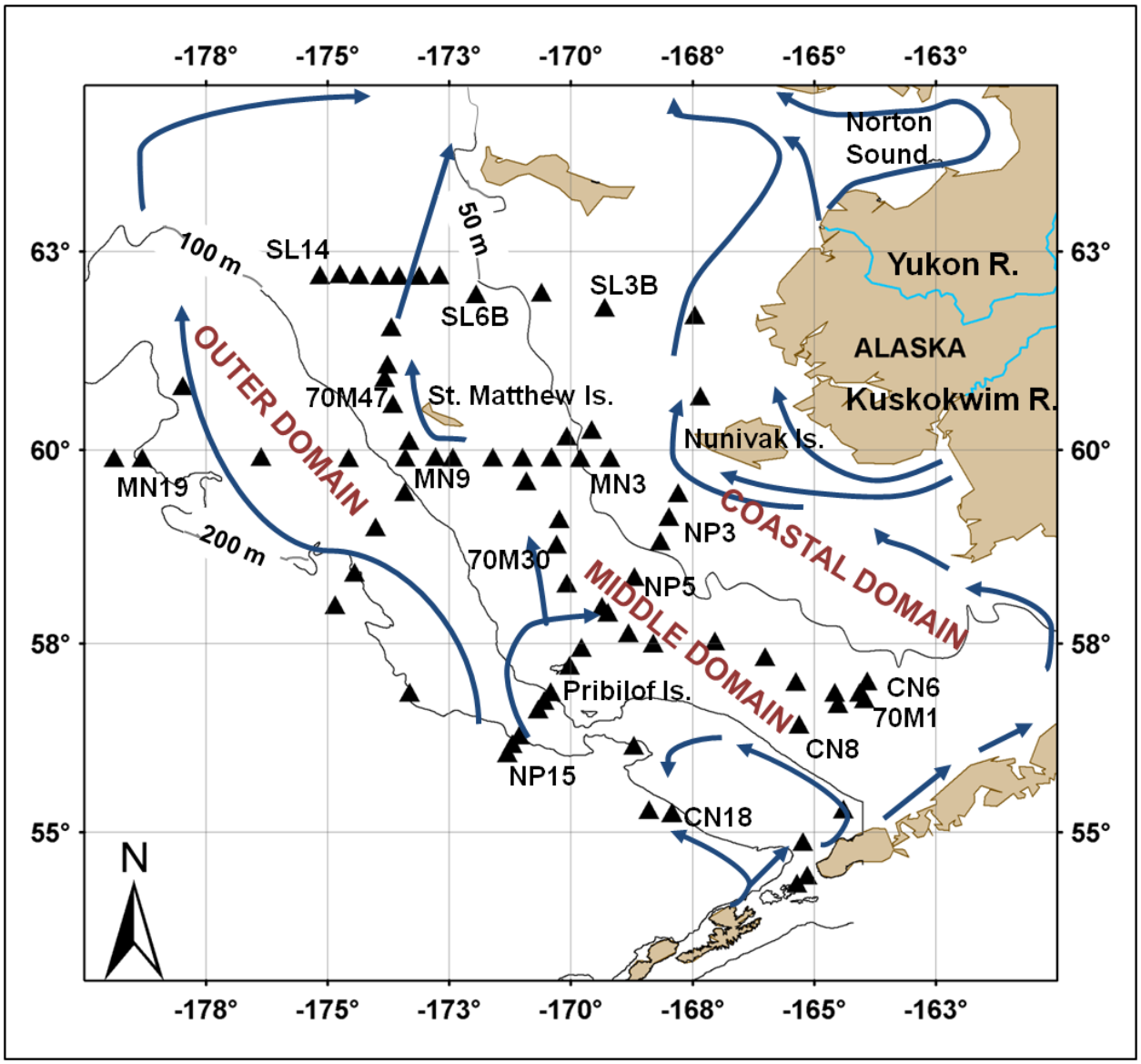

Figure 4.1. Station map showing station locations (black triangles) covered during a cruise in July 2008. The general circulation (blue arrows) is from Stabeno et al., (2006). The Coastal Domain, Middle Domain and Outer Domain are also shown.

Although the runoff from both the rivers is constrained to the coast by strong inner shore currents, the Kuskokwim River has a greater influence in our study region as the runoff flows along the coast with part of it diverging at the Nunivak islands along the shelf to north, driven mainly by winds and tidal currents (Figure 4.1). The Yukon River is less constrained to the coast but most of the runoff flows through the Norton Sound and a smaller part heads towards the Bering Strait. Although the maximum influence of river runoff is in the coastal domain, its influence is significant on the vertical structure of the coastal domain where it combines with shelf waters forming the low salinity water mass known as the Alaskan Coastal waters (ACW) [*Coachman,* 1986]. The signature of ACW is also found in the Arctic waters (Chukchi Sea) where it influences CDOM absorption [*Matsuoka et al.,* 2011].

In-situ Water Sampling

Station locations that were sampled are shown in Figure 4.1. Physical, biological measurements and water sampling was conducted along cross shelf and along shelf transect lines covering the coastal, middle and outer domains during a cruise on the USCGC Healy in July 2008. The southernmost transect was the CN line which is located at the inner front between the inner and middle hydrographic domains ending at Cape Newenham. The NP transect extended from the Nunivak Island to offshore of St Paul Island, while the MN transect extended from the Nunivak Island passing south of St. Matthews Island over the outer shelf into the deeper slope waters. The SL transect was the northernmost transect located south of St. Lawrence Island extending from near shore of the northern shelf to the end of the middle domain. A transect was also sampled along the 70 m isobath running north to south along the shelf starting from SL and ending at the northern part of CN, which captured the variability between northern shelf and southern shelf. The Bering Sea was ice-free during the entire cruise. At every station, salinity,

temperature and density profiles were recorded with a SeaBird SBE-911 plus CTD unit and water samples were collected for absorption analyses at 3 depths (or more) – surface, middle 1 and middle 2 using Niskin bottles attached to the CTD. The middle 1 depth corresponded to the chlorophyll fluorescence maximum depth if it was present at the station, while middle 2 depth was a few meters below the chlorophyll fluorescence maximum depth.

Particulate Absorption

Particulate absorption measurements were made following the standard quantitative filter technique (QFT) procedure [*Mitchell*, 1990]. The discrete water samples were filtered immediately after collection under low vacuum on 0.7μm Whatman GF/F glass fiber filters and stored in liquid nitrogen until analysis for particulate absorption and chlorophyll-a. Chlorophyll-a concentration was determined fluorometrically with 90% acetone [*Holm-Hansen et al.*, 1965] in a Turner Designs fluorometer. The volume of water filtered was adjusted between water types so that sufficient particles were loaded on the filter taking care not to overload the filter. Bulk of the particulate absorption measurements were carried out onboard and the remaining samples were brought back to the lab for analysis.

The samples were first thawed to room temperature after removing from liquid nitrogen by keeping them in the dark at room temperature for half an hour. Filter blanks were prepared by filtering 15 ml of filtered seawater corresponding to the station and depth under analysis. Absorbance measurements of total particulate matter ($A_P(\lambda)$) were done by scanning the sample filter paper using a shipboard WPI Ultrapath^{TM} hyperspectral waveguide capillary system (Ultrapath, WPI Inc., Sarasota, FL, USA) from 190 – 722 nm at 1 nm intervals. The Ultrapath is a spectrophotometer together with a waveguide and has a user-selectable pathlength (2, 10, 50 and 200 cm) through a fiber optic cable. A peristaltic pump is used to inject water samples into

the sample cell. The incident light is provided by Deuterium and Halogen light sources and is coupled to the sample cell via a fiber optic cable. The light travels by internal reflection within the waveguide and after exiting the waveguide is collected by a fiber optic cable connected to a photodiode array fiber optic spectrometer. The spectrophotometer is specified to have a dynamic range of 0.002 – 231 m^{-1}, with a maximum deviation in replicate spectra < 0.001 absorbance units [*Miller et al.,* 2002]. For measurements of particles on filters, the spectrophotometer had an attachment for mounting the filters which connected the light source and detector by fiber optic cables [*Belz et al.,* 2006]. To separate the phytoplankton pigments within the particulate matter from NAP, methanol extraction was done [*Kishino et al.,* 1985]. The sample filter paper was scanned again to obtain non-algal particulate (NAP) absorbance ($A_{NAP}(\lambda)$). To minimize the differences between sample and blank filters all the sample spectra were shifted to zero near infra-red by subtracting the average absorbance from 712 – 722 nm.

In laboratory studies the spectrophotometer used in this study showed good agreement with comparisons done on a dual beam Lambda 850 spectrophotometer equipped with an integrating sphere for both phytoplankton cell cultures as well as field samples (r^2=0.989, slope=0.976, n=75 for phytoplankton cultures; r^2=0.93 slope=0.956, n=50 for field samples averaged over the visible spectrum). The largest differences were found in the primary absorbance peaks of chlorophyll-a around 443 nm and 676 nm, which were underestimated by the Ultrapath relative to lambda 850 [*Belz et al.,* 2006]. A few samples (n=50) were run on both the lambda 850 and Ultrapath and the average difference between the two were less than 10% at 443 nm and 676 nm. The optical densities were corrected for pathlength amplification by developing a beta (β) correction algorithm. The β correction algorithm was determined by comparing absorbances of phytoplankton cells in suspension and on filters measured on Lambda 850 spectrophotometer

equipped with an integrating sphere, using 9 monospecific cultures (*Thalassiosira nordenskioeldii, Chaetoceros atlanticus, Coscinodiscus radiates, Skeletonema costatum, Phaeocystis Antarctica, Myrionecta rubra, Heterocapsa arctica, Pyramimonas parkeae, Emiliania huxleyi*), following procedures described in Mitchell (1990). The coefficients derived from the beta equation were: $Abs_{SUS} = 0.405*(Abs_{FILTER}) + 0.475*(Abs_{FILTER})^2$ ($r^2 = 0.97$), where Abs_{FILTER} and Abs_{SUS} correspond to absorbance due to material retained on filter and due to suspended material. The beta equation obtained in this study is similar to the equation obtained by Cleveland and Weidemann, (1993) and is between those obtained by Mitchell, (1990) and Bricaud and Stramski, (1990). The precision of $a_P(\lambda)$ values was tested using replicate samples and was less than 0.001 absorbance units and the accuracy of $a_P(\lambda)$ values taking into consideration the beta factor inconsistency and instrumental factors would be less than 20 %.

The absorbances were converted to absorption coefficients using the equation:

$$a_P(\lambda) = \frac{2.303\left[A_P(\lambda)\right]}{(V/A)} \qquad \text{(Eq. 4)}$$

where $a_P(\lambda)$ (m^{-1}) is the total particulate absorption. The coefficient 2.303 is a factor for converting from base e to base 10 logarithm, V (m^3) is the volume filtered, and A (m^2) the filter paper clearance area. $A_{NAP}(\lambda)$ was also converted to $a_{NAP}(\lambda)$ using eq. 4. The phytoplankton absorption ($a_{PHY}(\lambda)$ (m^{-1})) spectra were obtained by subtracting the $a_{NAP}(\lambda)$ (m^{-1}) from $a_P(\lambda)$ using the relation:

$$a_{PHY}(\lambda) = a_P(\lambda) - a_{NAP}(\lambda) \qquad \text{(Eq. 5)}$$

The $a_{NAP}(\lambda)$ spectra can be expressed by an exponential function:

$$a_{NAP}(\lambda) = a_{NAP}(\lambda_0)\, e^{\left(-S_{NAP}(\lambda-\lambda_0)\right)} \qquad \text{(Eq. 6)}$$

The wavelength λ_0 (443 nm) is the reference wavelength in this study and S_{NAP} represents the spectral slope for $a_{NAP}(\lambda)$. A non-linear least square fit was applied to calculate S_{NAP} from 350 to 700 nm. Although residual absorption from inefficient removal of pigments through methanol extraction was not evident in $a_{NAP}(\lambda)$ spectra, we excluded the 400-480 nm and 620-700 nm ranges to avoid any residual pigment absorption that might still have been present [*Babin et al.,* 2003].

Chlorophyll-a specific phytoplankton absorption ($a^*_{PHY}(\lambda)$ (m^2 (mg chl *a*)$^{-1}$)) was obtained by dividing $a_{PHY}(\lambda)$ by chlorophyll-a (mg m^{-3}). Regression analysis was conducted to determine the relationship between $a_{PHY}(\lambda)$ and chlorophyll-a from 400 to 700 nm at 2 nm intervals, as done in Bricaud et al., (1998):

$$a_{PHY}(\lambda) = \alpha_{CHL}(\lambda)[\text{chlorophyll-a}]^{(\beta_{CHL}(\lambda))} \quad \text{(Eq. 7)}$$

where $\alpha_{CHL}(\lambda)$ and $\beta_{CHL}(\lambda)$ are the coefficients of the fit derived from our dataset.

For parameterization of $a_{PHY}(\lambda)$ and total absorption minus water ($a_{T\text{-}W}(\lambda)$), the following relationships were used:

$$a_{PHY}(\lambda) = \alpha_{PHY}(\lambda)[a_{PHY}(443)]^{(\beta_{PHY}(\lambda))} \quad \text{(Eq. 8)}$$

$$a_{T\text{-}W}(\lambda) = \alpha_{T-W}(\lambda)[a_{T\text{-}W}(443)]^{(\beta_{T-W}(\lambda))} \quad \text{(Eq. 9)}$$

where $a_{PHY}(443)$ and $a_{T\text{-}W}(\lambda)$ are the phytoplankton absorption and total absorption minus water absorption at 443 nm respectively, $\alpha_{PHY}(\lambda)$, $\beta_{PHY}(\lambda)$ and $\alpha_{T\text{-}W}(\lambda)$, $\beta_{T\text{-}W}(\lambda)$ are the coefficients of regression derived for our dataset from 400-700 nm at 2 nm interval.

CDOM Absorption

For CDOM absorption ($a_{CDOM}(\lambda)$), discrete water samples were filtered immediately after collection through 0.2 μm nylon membrane filters under low vacuum. Most samples were

immediately analyzed onboard and the remaining filtered samples were stored in acid cleaned, pre-combusted amber colored glass bottles and stored at 4 ^{o}C. The filtered samples were allowed to reach ambient room temperature to minimize temperature bias between samples and blank. Absorbance measurements of CDOM ($A_{CDOM}(\lambda)$) were done on a shipboard WPI Ultrapath^{TM} hyperspectral waveguide capillary system from 190 – 722 nm at 1 nm intervals. The pathlength was variable (either 10 cm or 50 cm) depending on whether significant absorbance was observed between 400 – 500 nm. The sample cell was cleaned between measurements using successive rinses of Methanol, 10% HCL and Milli-Q water. For the reference, salt solutions with the refractive indices close to seawater samples was prepared using granular NaCl (Mallinckrodt) and Milli-Q water, to minimize the differences in refractive index between sample and reference, which can cause offsets in absorbance measurements [*D'Sa et al.*, 1999].

The absorbance data were corrected for baseline fluctuations by subtraction of the mean value over 5 nm interval of the measured absorbance at 700 nm from each wavelength [*Mitchell et al.*, 2003]. The $a_{CDOM}(\lambda)$ (m^{-1}) for pathlength, L (m^{-1}) was calculated according to:

$$a_{CDOM}(\lambda) = \frac{2.303\left[A_{CDOM}(\lambda)\right]}{(L)} \qquad \text{(Eq. 10)}$$

Spectra of $a_{CDOM}(\lambda)$ can be expressed as exponential functions as follows:

$$a_{CDOM}(\lambda) = a_{CDOM}(\lambda_0)\, e^{\left(-S_{CDOM}(\lambda-\lambda_0)\right)} \qquad \text{(Eq. 11)}$$

where λ_0 is the reference wavelength which was chosen as 443 nm, and S_{CDOM} denotes the spectral slope for CDOM absorption. For each $a_{CDOM}(\lambda)$ spectra, S_{CDOM} was calculated by fitting a non-linear least square to an exponential function from 350-500 nm [*Babin et al.*, 2003; *Twardowski et al.*, 2004]. Similarly, for CDOM plus NAP absorption ($a_{DG}(\lambda)$), the spectral slope

of CDOM plus NAP (S_{DG}) was calculated by applying a non-linear least square fit to every $a_{DG}(\lambda)$ spectra from 350-550 nm with the exclusion of the 400-480 nm range [*Babin et al.*, 2003].

$$a_{DG}(\lambda) = a_{DG}(\lambda_0)\, e^{(-S_{DG}(\lambda-\lambda_0))} \qquad \text{(Eq. 12)}$$

Modeling of Remote Sensing Reflectance ($R_{rs}(\lambda)$) and Diffuse Attenuation Coefficient for Downwelling Irradiance ($K_d(\lambda)$)

To comprehend the influence of absorption coefficients on $R_{rs}(\lambda)$ (sr^{-1}) and $K_d(\lambda)$ (m^{-1}) we modeled them using in-situ absorption coefficients (discrete and continuous profile) and backscattering coefficients ($b_b(\lambda)$ (m^{-1})) (modeled and continuous profile). We also modeled them with $a_{CDOM}(\lambda)$ excluded from $a_T(\lambda)$ to show the effect of $a_{CDOM}(\lambda)$. The validity of the modeled $R_{rs}(\lambda)$ and $K_d(\lambda)$ were tested by comparing them with in-situ derived $R_{rs}(\lambda)$ and $K_d(\lambda)$. The details on the modeling process are described below.

$R_{rs}(\lambda)$ at the surface was modeled through IOPs according to the equations shown below [*Gordon et al.*, 1988; *Mobley*, 1994]:

$$R_{rs}(\lambda) - \text{Discrete Model} = 0.54(f/Q)\left[\frac{b_{b(model)}(\lambda)}{a_T(\lambda) + b_{b(model)}(\lambda)}\right] \qquad \text{(Eq. 13)}$$

$$R_{rs}(\lambda) - \text{BOP Model} = 0.54(f/Q)\left[\frac{b_{b(ECO)}(\lambda)}{a_{T(ac-s)}(\lambda) + b_{b(ECO)}(\lambda)}\right] \qquad \text{(Eq. 14)}$$

$$R_{rs}(\lambda) - \text{Dicrete model - no CDOM} = 0.54(f/Q)\left[\frac{b_{b(model)}(\lambda)}{a_{T-CDOM}(\lambda) + b_{b(model)}(\lambda)}\right] \qquad \text{(Eq. 15)}$$

where the value of 0.54 accounts for the Fresnel reflectivity at the sea surface, f/Q ratio was set equal to 0.094 [*Gordon et al.*, 1988]. $R_{rs}(\lambda)$ – Discrete model is $R_{rs}(\lambda)$ modeled from discrete measurements of IOPs. $R_{rs}(\lambda)$ – Discrete Model- no CDOM is $R_{rs}(\lambda)$ modeled from discrete measurements of IOPs without contribution from CDOM. $R_{rs}(\lambda)$ – BOP model is $R_{rs}(\lambda)$ modeled

from measurements of IOPs from a continuous profiling bio-optical package (BOP). $a_T(\lambda)$ is total water absorption coefficient obtained from discrete water measurements and $a_{T(ac\text{-}s)}(\lambda)$ is total water absorption coefficient measurements from an hyperspectral absorption and attenuation meter (ac-s, WET Labs) on the BOP, which were corrected for temperature, salinity, and scattering [*Pegau et al.*, 1997; *Zaneveld et al.*, 1994] using optically clean Milli-Q water as a reference (obtained from the calibration of the ac-s multiple times during the cruise). $a_{T\text{-}CDOM}(\lambda)$ is total water absorption minus $a_{CDOM}(\lambda)$ from discrete measurements. $b_{b(ECO)}(\lambda)$ is the backscattering coefficient obtained from backscattering meter (ECO VSF3 or ECO BB9, WET Labs) on the BOP, corrected for salinity and light loss due to absorption over the path length at each angle and wavelength using the ac-s data [*Boss et al.*, 2004]. Time-stamped data from instruments on the BOP were aligned to the CTD (also on the BOP) data and vertical profiles were binned at 0.5 m depth intervals. $b_{b(model)}(\lambda)$ is backscattering modeled according Morel and Maritorena, (2001):

$$b_p(\lambda) = 0.416\left[\text{chlorophyll-a}^{0.766}\right](550/\lambda) \qquad \text{(Eq. 16)}$$

$$b_{b(model)}(\lambda) = 1/2 b_w(\lambda) + B b_p(\lambda) \qquad \text{(Eq. 17)}$$

where $b_p(\lambda)$ is the particulate scattering coefficient, $b_b(\lambda)$ is the backscattering coefficient, $b_w(\lambda)$ is scattering by pure water and B (=0.0183) is the backscattering ratio treated as constant [*Gould et al.*, 1999].

$K_d(\lambda)$ was modeled through IOPs according to the equations given below [*Kirk*, 1994]:

$$K_d(\lambda) \text{ - Discrete Model} = \frac{1}{\mu_0}\left[a_T(\lambda)^2 + (g_1\mu_0 - g_2)a_T(\lambda)b_b(\lambda)\right]^{1/2} \qquad \text{(Eq. 18)}$$

$$K_d(\lambda) \text{ - Discrete Model - no CDOM} = \frac{1}{\mu_0}\left[a_{T\text{-}CDOM}(\lambda)^2 + (g_1\mu_0 - g_2)a_{T\text{-}CDOM}(\lambda)b_b(\lambda)\right]^{1/2} \qquad \text{(Eq. 19)}$$

$$K_d(\lambda)\text{- BOP Model} = \frac{1}{\mu_0}\left[a_{T(ac-s)}(\lambda)^2 + (g_1\mu_0 - g_2)a_{T(ac-s)}(\lambda)b_{b(ECO)}(\lambda)\right]^{1/2} \qquad \text{(Eq. 20)}$$

μ_0 is the cosine of the solar zenith angle (calculated from date and time of station location), g_1 and g_2 are constants taken equal to 0.425 and 0.19 respectively [*Kirk*, 1994]. $K_d(\lambda)$ – Discrete model is $K_d(\lambda)$ modeled from discrete measurements of IOPs. $K_d(\lambda)$ – Discrete Model- no CDOM is $K_d(\lambda)$ modeled from discrete measurements of IOPs without contribution from CDOM. $K_d(\lambda)$ – BOP model is $K_d(\lambda)$ modeled from measurements of IOPs from a continuous profiling BOP.

Continuous measurement of in-situ radiation fields were conducted using either a SPMR (SeaWiFS Profiling Multichannel Radiometer, Satlantic) or a hyperspectral downwelling spectral irradiance and upwelling spectral radiance meter (HyperOCR, Satlantic). The irradiance ($E_d(\lambda)$) and radiance ($L_u(\lambda)$)) data were processed using the Prosoft 7.7.16 (Satlantic). A 5-point moving linear regression of ln $E_d(\lambda)$ versus depth was used to obtain $K_d(\lambda)$. Radiometer $R_{rs}(\lambda)$ was calculated as ratio of upwelling radiance and downwelling irradiance just above the sea surface. As the performance of Medium Resolution Imaging Spectrometer (MERIS) in the study area has been found to be reasonable [*Naik et al., 2010*], $R_{rs}(\lambda)$ was also obtained from MERIS Level 2 data (http://merci-srv.eo.esa.int/merci/) using a 3 x 3 pixel box size (1.2 km/pixel for MERIS) with a time difference of ±8 hours between the in-situ sampling and satellite overpass.

Results and Discussion

Spatial Distribution of Light Absorption Properties in Relation to Hydrographic and Biogeochemical Characteristics

The hydrographic structure, nutrients, and productivity in the Bering Sea during the in-situ sampling are described in detail in Mathis et al., (2010). The shelf could be divided into 6 distinct zones based on hydrographic and biogeochemical characteristics. Across the shelf in all

transects over the entire water column a front extended along the 50 m isobath (inner front) while a second front was identified at approximately 100 m isobath (central front) on the MN and NP transects (not clear on SL transect) by temperature. These fronts divided the shelf into 3 domains – Coastal Domain, Middle Domain and the Outer Domain. Along the 70 m isobath, a broad transitional zone was present at 60 N in hydrography (density and bottom water temperatures), nutrients and chlorophyll dividing the eastern shelf into northern shelf (60 N and above) and southern shelf (below 60 N). Over the northern shelf the ice melt influenced the SL and MN transects creating a fresh water lens ~20 m deep seaward from the inner front. The spatial distributions of nutrients and productivity generally coincided with the frontal transition zones [*Mathis et al.*, 2010]. Typical of the study region, the coastal domain was low in macronutrients but high in iron and the outer domain was high in macronutrients but low in iron. Production was high just below the pycnocline with intense subsurface chlorophyll fluorescence maxima and subsurface supersaturation of oxygen. The productivity was lowest in the coastal domain in both the northern and southern shelf due to limited macronutrients and highest over the central front due to the confluence of shelf (high in iron) and basin waters (high in nitrate) [*Mathis et al.*, 2010].The $a_{PHY}(\lambda)$, $a_{DG}(\lambda)$, and $a_{T\text{-}W}(\lambda)$, variability at representative stations along the 5 transects (CN, MN, NP, SL and 70M) are shown in Figure 4.2. Stations along transects were chosen to cover the innermost, middle and outermost sections of the transects at 3 depths (surface, middle 1, middle 2). The surface distribution of absorption properties in the study area has been covered in detail in Naik et al., (2010). The surface distribution of $a_{PHY}(443)$ revealed relatively higher values around the Pribilof Islands which is due to the enhanced production near the islands caused by interaction of tides and currents with bathymetry [*Kachel et al.*, 2002; *Stabeno et al.*, 2008]. Patterns of $a_{PHY}(443)$ were similar to productivity [*Mathis et al.*, 2010] with the highest

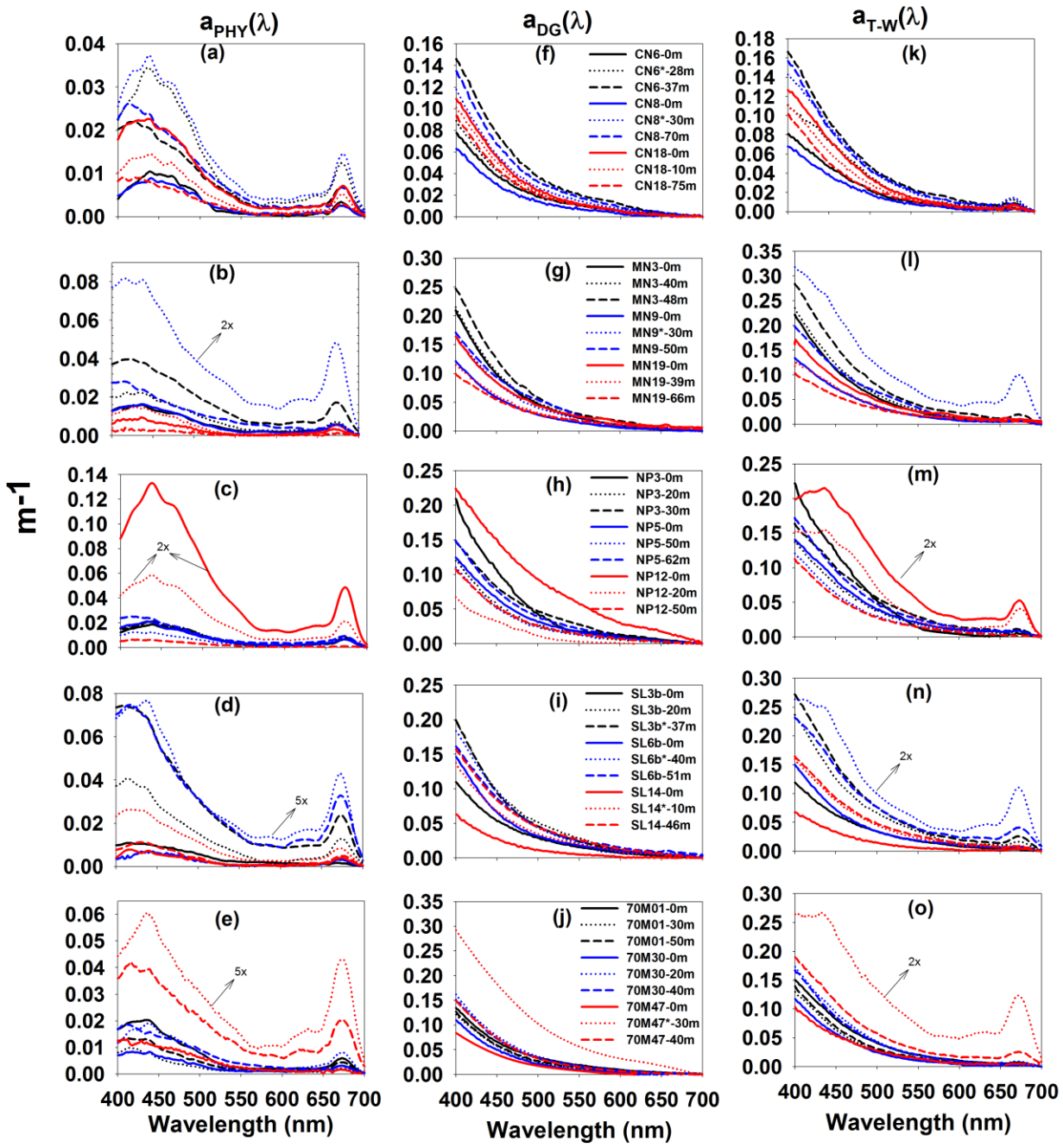

Figure 4.2. Absorption along CN transect, MN transect, NP transect, SL transect and 70M transect by (a-e) phytoplankton ($a_{PHY}(\lambda)$ (m^{-1})), (f-j) NAP plus CDOM ($a_{DG}(\lambda)$ (m^{-1})), and (k-o) total absorption minus water ($a_{T-W}(\lambda)$ (m^{-1})). The black lines are for the innermost, the blue lines are for the middle and the red lines for the outermost stations along the transects that were samples. The solid lines are for surface, the dotted lines are for the middle 1 and the dashed lines are for the middle 2 depths. Note that some spectra have been scaled (shown by an arrow), these spectral values should be multiplied by the factor indicated by the arrow.

values near the Pribilof Islands of the southern shelf and along the central front in the middle domain, and the lowest values throughout the coastal domain. . The $a_{PHY}(443)$ was higher in the middle depths relative to surface due to the influence of sub surface chlorophyll maximum (marked by an '*' next to sample name in Figure 4.2). The appearance of chlorophyll fluorescence maximum is common in the middle and outer domain (more intense in the northern shelf) of the study region during summer, where wind speeds are not efficient enough in mixing the water column resulting in a two layer system observed during the study period [*Mathis et al.*, 2010]. The highest values of $a_{PHY}(\lambda)$ were seen in the NP, SL, and 70M transects followed by MN and CN transects. A marked shoulder at ~ 475 nm was observed in most of the $a_{PHY}(\lambda)$ spectra, which is usually associated with alloxanthin and 19`-hexanoyloxyfucoxanthin pigments present in prymnesiophytes [*Cota et al.*, 2003]. The prymnesiophyte Phaeocystis was dominant at many stations during the cruise which explains the presence of the above feature in the $a_{PHY}(\lambda)$ spectra. The range of $a_{DG}(\lambda)$ was about one order of magnitude, but the variability in $a_{DG}(\lambda)$ was relatively less as compared to $a_{PHY}(\lambda)$, particularly between the surface and middle depths.

The $a_{DG}(\lambda)$ was higher than $a_{PHY}(\lambda)$ at blue wavelengths at most stations and depths along the transects with the exception of a few depths where the chlorophyll maximum was particularly strong ($a_{PHY}(\lambda) > 0.15\ m^{-1}$). Within $a_{DG}(\lambda)$, $a_{CDOM}(\lambda)$ was more dominant relative to $a_{NAP}(\lambda)$. Higher values of $a_{DG}(443)$ were observed in the coastal domain of northern shelf showing the influence of Kuskokwim river runoff which is carried to the north by prevailing northern currents and constrained to the coast by the inner front. The highest contribution of $a_{NAP}(\lambda)$ to $a_{DG}(\lambda)$ was at NP12-0m, SL-6b-40m and 70M47-30m, where the $a_{PHY}(\lambda)$ as well as chlorophyll-a were high, indicating that most of the contribution to detrital matter was due to the elevated biomass for these samples. The spectral shape of $a_{T\text{-}W}(\lambda)$ in blue region resembles the $a_{DG}(\lambda)$ spectra in most

of the stations except the stations where the $a_{PHY}(\lambda)$ was dominant. Although the blue absorption peaks of $a_{PHY}(\lambda)$ were masked by the high values of $a_{DG}(\lambda)$ at most stations, the red absorption peaks are visible at almost all stations. The highest values of $a_{T\text{-}W}(\lambda)$ were observed at the SL, northern part of 70M, and MN transects followed by the NP transect (ignoring the stations near Pribilof Islands) and least $a_{T\text{-}W}(\lambda)$ was observed in the CN transect. If the depths corresponding to the highest values of $a_{PHY}(\lambda)$ and chlorophyll-a are ignored in transects NP, SL and 70M, all the transects have similar ranges of $a_{T\text{-}W}(\lambda)$ values.

Relationship of Chlorophyll-a with Absorption

The $a_{PHY}(443)$, and $a_P(443)$ ranged two orders of magnitude from 0.002 – 0.370 m^{-1}, and 0.007 – 0.420 m^{-1} respectively, while $a_{DG}(443)$, and $a_{T\text{-}W}(443)$ ranged one order of magnitude, 0.032 – 0.207 m^{-1}, and 0.057 – 0.520 m^{-1} respectively, corresponding with a two order magnitude chlorophyll-a range of 0.04 – 32.30 mg m^{-3}. Non-linear relationship expressed as a power function was applied between $a_{PHY}(\lambda)$, $a_P(\lambda)$, $a_{DG}(\lambda)$ and $a_{T\text{-}W}(\lambda)$ at 443 nm and 676 nm along with chlorophyll-a (Figure 4.3). A significant correlation was obtained between $a_{PHY}(\lambda)$, $a_P(\lambda)$, $a_{T\text{-}W}(\lambda)$ and chlorophyll-a consistent with other studies (Table 4.1) [*Arrigo et al.*, 1998; *Bricaud et al.*, 2004; *Cota et al.*, 2003; *Matsuoka et al.*, 2007]. For the $a_{PHY}(443 \text{ or } 676)$ and chlorophyll-a relation there was no significant difference between surface and other depths (Figure 4.3a). The fit obtained for our data was remarkably similar to the Matsuoka et al. (2007) fit for the Chukchi Sea and western part of southern Beaufort Sea. Our $a_{PHY}(443)$ values are lower than the values estimated using middle and lower latitudes relationship of Bricaud et al., (1998) ($a_{PHY}(443) = 0.0378*\text{chlorophyll-a}^{0.627}$), north polar Atlantic relationship during summer of Stramska et al., (2006) ($a_{PHY}(443) = 0.058*\text{chlorophyll-a}^{0.575}$), Labrador Sea relationship of Cota et al., (2003) ($a_{PHY}(443) = 0.0402*\text{chlorophyll-a}^{0.578}$) and higher than the values estimated by Western Arctic

Table 4.1. Coefficients, r^2 and number of samples (n) for the power fit expressed as $a_x(443 \text{ or } 676) = A_x(443 \text{ or } 676)*[\text{chlorophyll-a}]^B x^{(443 \text{or } 676)}$. Where subscript x indicates PHY – phytoplankton absorption, P - particulate absorption, NAP – Non-algal particulate, CDOM- Colored dissolved organic matter, DG-CDOM + NAP or T-W – total absorption minus water. * indicates not statically significant.

	This study (ANOVA; p<0.001)			
	A	**B**	**r^2**	**n**
$a_{PHY}(443)$ vs chlorophyll-a	0.026	0.758	0.88	143
$a_P(443)$ vs chlorophyll-a	0.047	0.646	0.85	143
$a_{NAP}(443)$ vs chlorophyll-a	0.020	0.427	0.58	143
$a_{CDOM}(443)$ vs chlorophyll-a*	0.050	0.070	0.12	143
$a_{DG}(443)$ vs chlorophyll-a	0.085	0.152	0.30	143
$a_{T-W}(443)$ vs chlorophyll-a	0.120	0.360	0.66	143
$a_{PHY}(676)$ vs chlorophyll-a	0.010	0.934	0.87	143
$a_P(676)$ vs chlorophyll-a	0.012	0.853	0.77	143
$a_{T-W}(676)$ vs chlorophyll-a	0.014	0.781	0.75	143

relationship of Wang et al. (2005) ($a_{PHY}(443) = 0.0151*\text{chlorophyll-a}^{0.957}$, below chlorophyll-a range of 10 mg m^{-3}. This suggests a cautious approach towards generalization of bio-optical properties of polar and lower-latitude regions. In most samples (chlorophyll-a > 0.5 mg m^{-3}) investigated, phytoplankton cells were the dominant part of $a_P(443)$ with variable contribution from $a_{NAP}(443)$. The $a_{PHY}(443)/a_P(443)$ ratio values ranged between 0.25-0.91, while $a_{NAP}(443)/a_P(443)$ ranged between 0.12-0.70, and are within the ranges reported in literature from different regions [*Bricaud et al.*, 2004; *Bricaud et al.*, 1998; *Cleveland*, 1995]. Despite this variability for all samples analyzed $a_{PHY}(443)$ dominates $a_P(443)$; $a_{PHY}(443)$ and $a_{NAP}(443)$ contributed on an average 62% and 38 % respectively to $a_P(443)$ over all stations and depths. The difference

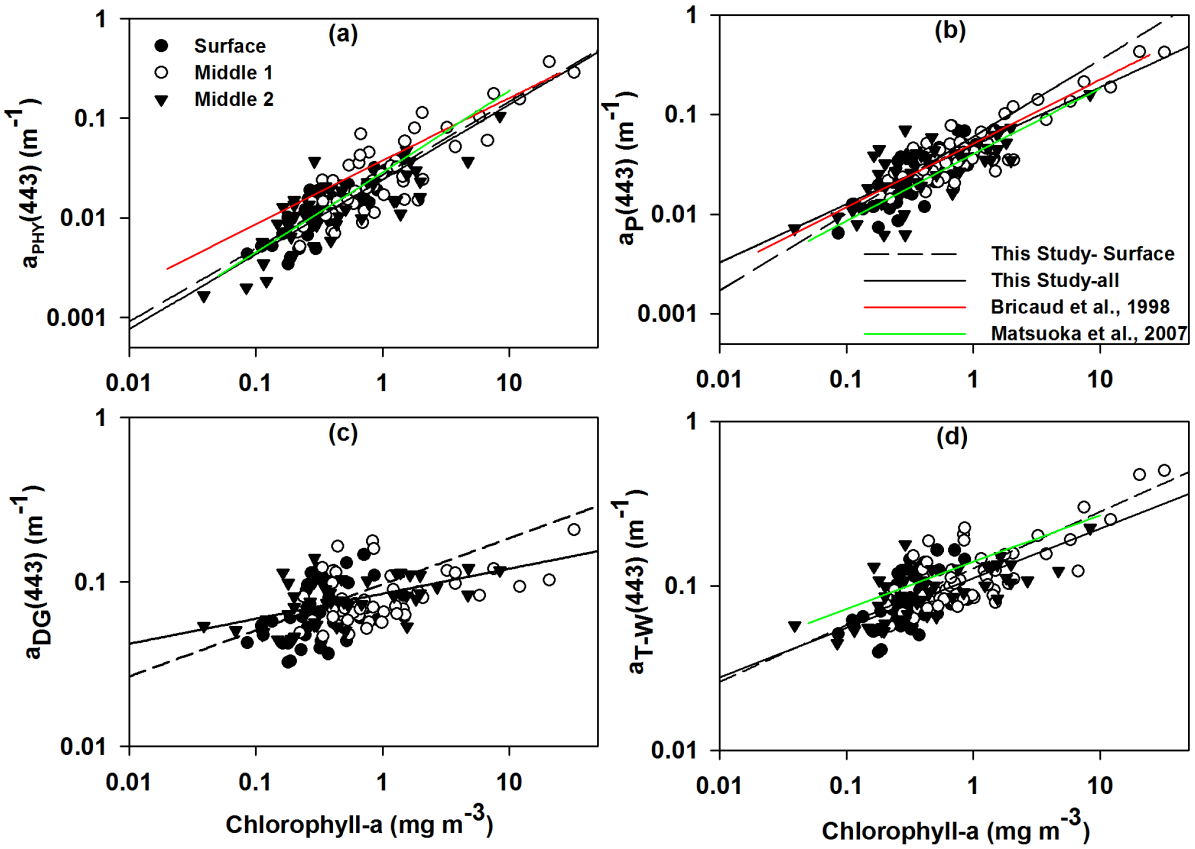

Figure 4.3. Relationship between chlorophyll-a and (a) phytoplankton absorption at 443 nm ($a_{PHY}(443)$) (b) particulate absorption at 443 nm ($a_P(443)$) (c) NAP plus CDOM absorption at 443 nm ($a_{DG}(443)$) (d) total absorption minus water at 443 nm ($a_{PHY}(443)$), for surface (filled circles), middle 1 (closed circles) and middle 2 (filled triangles) depths. Regression fits for surface only (dashed lines) and all depths (solid lines) are shown. The statistics of the fit are shown in Table 4.1. For comparison regression fits from literature are also shown (Bricaud et al., (1998) (red solid line) and Matsuoka et al., (2007) (green solid line)).

between the fit obtained in our study and the Bricaud et al., (1998) study for $a_P(443)$ vs. chlorophyll-a (RMSE = 0.001) was relatively less as compared to that of $a_{PHY}(443)$ vs. chlorophyll-a (RMSE = 0.005). The $a_{DG}(443)$ showed only a weak correlation with chlorophyll-a (Table 4.1, Figure 4.3c). This relation was influenced by combined contribution of $a_{NAP}(\lambda)$ and $a_{CDOM}(\lambda)$; although $a_{NAP}(\lambda)$ showed a significant positive relation with chlorophyll-a, $a_{CDOM}(\lambda)$ did not show a strong positive correlation with chlorophyll-a (Table 4.1). The weak correlation

between $a_{CDOM}(443)$ and chlorophyll-a was also seen in other high northern latitudes studies [*Matsuoka et al.*, 2007; *Wang et al.*, 2005], which could be due to CDOM processes being out of phase with phytoplankton biomass or production and that most CDOM in this region is of terrestrial origin. Even though $a_{DG}(443)$ was not strongly correlated to chlorophyll-a, the $a_{T-W}(443)$ was relatively strongly correlated to chlorophyll-a (Figure 4.3d, Table 4.1).

The relationships between ratios of $a_{PHY}(443)$, $a_{CDOM}(443)$ and $a_{DG}(443)$ to $a_{T-W}(443)$ and chlorophyll-a show the relative contribution of each of these components to total non-water absorption in relation to phytoplankton biomass (Figure 4.4). The $a_{PHY}(443)/a_{T-W}(443)$ ratio increased with increasing chlorophyll-a with large variability at chlorophyll-a < 1 mg m^{-3} (Figure 4.4a). The $a_{CDOM}(443)/a_{T-W}(443)$ ratio decreased with increasing chlorophyll-a, emphasizing that as phytoplankton biomass increases, $a_{CDOM}(443)$ becomes less important relative to the $a_P(443)$ in $a_{T-W}(443)$ (Figure 4.4b). The inverse relation between $a_{DG}(443)/a_{T-W}(443)$ and chlorophyll-a was not as strong as between $a_{CDOM}(443)/a_{T-W}(443)$ ratio and chlorophyll-a and was relatively constant up to chlorophyll-a value of 5 mg m^{-3} (Figure 4.4c). The most prominent outcome of this relation is the relatively strong contribution of $a_{DG}(443)$ to the $a_{T-W}(443)$; even at chlorophyll-a concentration of 8 mg m^{-3}, $a_{DG}(443)$ contributed to more than half of $a_{T-W}(443)$. The significance of this result is evident while evaluating the absorption budget in relation to modeling $R_{rs}(\lambda)$ and $K_d(\lambda)$ (see last section of results). An important conclusion drawn from these relatively high r^2 (except $a_{CDOM}(443)$ vs. chlorophyll-a and consequently $a_{DG}(443)$ vs. chlorophyll-a), is that the relationships between absorption and chlorophyll-a is strong in the study region. The contribution of $a_{DG}(\lambda)$ was large and did not correlate well with chlorophyll-a, and will thus pose a challenge for chlorophyll dependent global ocean color algorithms and bio-optical parameterizations. On a cautionary note, these relationships may not be applicable to

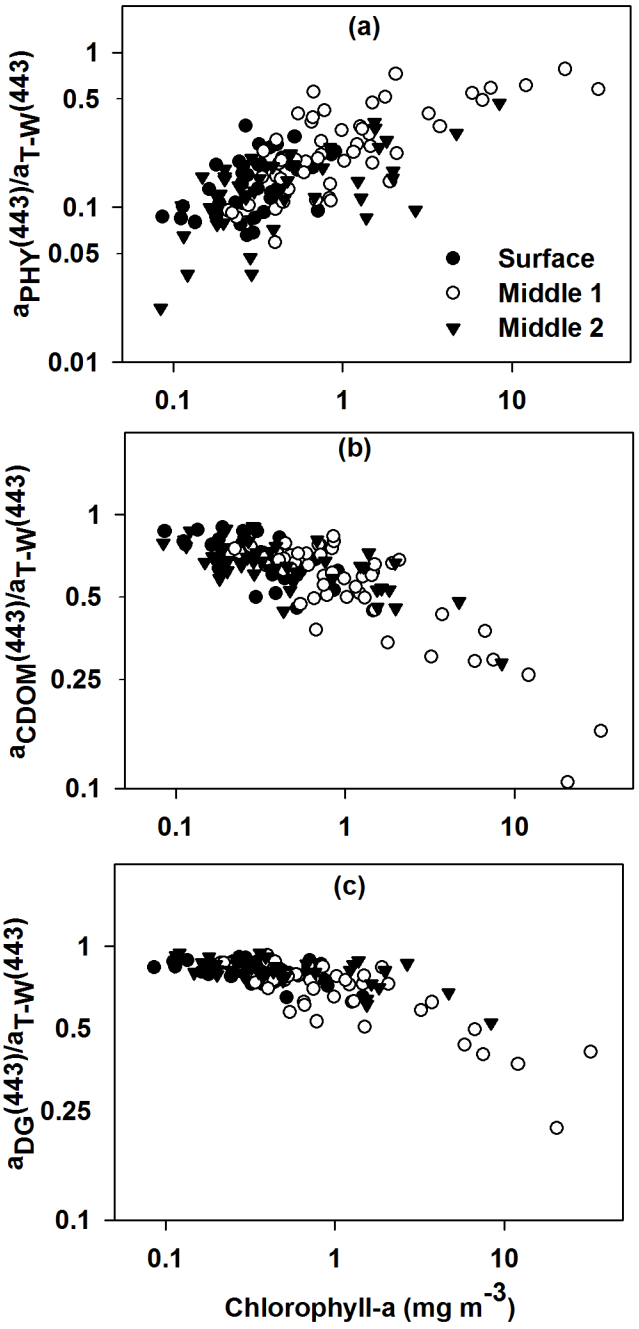

Figure 4.4. Relationship between chlorophyll-a and absorption ratios of (a) phytoplankton absorption and total absorption minus water at 443 nm ($a_{PHY}(443)$ / $a_{T-W}(443)$) (b) CDOM absorption and total absorption minus water ($a_{CDOM}(443)$ / $a_{T-W}(443)$), and (c) CDOM plus NAP absorption and total absorption minus water ($a_{DG}(443)$ / $a_{T-W}(443)$). Note that y-axis is in log scale. See Figure 4.3 for symbols.

other regions or the same regions in different seasons and are valid only over the chlorophyll-a range of this study.

Relationship of Chlorophyll-a with Specific Phytoplankton Absorption

The chlorophyll-a specific phytoplankton absorption ($a^*_{PHY}(\lambda)$) is defined as the $a_{PHY}(\lambda)$ per unit concentration of chlorophyll-a [*Morel and Bricaud*, 1981]. Phytoplankton pigments can be less efficient at absorbing light when they are within cell structures relative to when they are in solution resulting in reduction of the pigment absorption, known as pigment packaging [*Kirk*, 1994; *Morel and Bricaud*, 1981]. The $a^*_{PHY}(\lambda)$ showed large variability in the study region which poses problems when a^*_{PHY} is considered to be constant in many bio-optical models [*Bannister*, 1974; *Morel and Maritorena*, 2001] (Figure 4.5a). The $a^*_{PHY}(443)$ surface distribution showed large spatial variability and was far from being constant (Figure 4.5). The variability was greater in the blue region of the spectrum with values ranging from 0.003-0.120 m^2 (mg chl-a)$^{-1}$ at 443 nm than in the red with values ranging from 0.002-0.030 m^2 (mg chl-a)$^{-1}$ at 676 nm. At 443 nm, carotenoids, chlorophyll-b, chlorophyll-c and phycobilins can contribute to the absorption, so the variations in $a^*_{PHY}(443)$ may be due to the package effect and/or changes in pigment composition [*Bricaud et al.*, 1995]. The $a^*_{PHY}(\lambda)$ at chlorophyll-a absorbance peak of 676 nm can be used as a measure of pigment packaging effect, where the influence of accessory pigments is considered to be minimal [*Bricaud et al.*, 1995]. The mean value at 676 nm was 0.012±0.006 m^2 (mg chl-a)$^{-1}$ which was much smaller than the range 0.023-0.029 m^2 (mg chl-a)$^{-1}$ for unpackaged pigments [*Moisan and Mitchell*, 1999], indicating significant pigment packaging in the southeastern Bering Sea. Pigment packaging has been found to be significant at high latitudes as phytoplankton cells acclimate themselves to the low-light and nutrient-rich environment [*Cota et al.*, 2003; *Matsuoka et al.*, 2011]. Larger phytoplankton cells

tend to have higher pigment packaging [*Bricaud et al., 1995*; *Morel and Bricaud,* 1981]. Size fractionated data from our study region revealed that about 70% of chlorophyll-a in middle

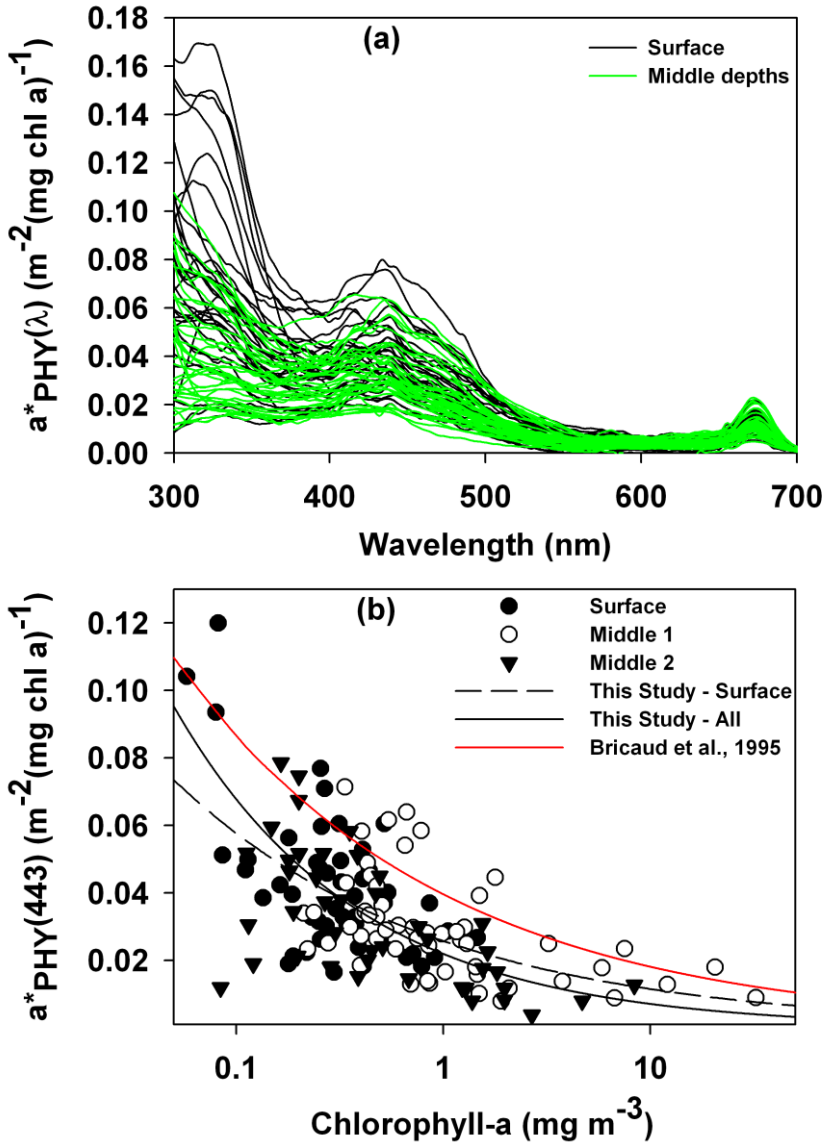

Figure 4.5. Specific phytoplankton absorption ($a^*_{PHY}(\lambda)$) (a) variability between 300 – 400 nm showing characteristic peaks at surface (black solid line) and middle depths (green solid line), and (b) at 443 nm relation with chlorophyll-a. Regression fit for surface only (dashed black line) and all depths (solid black line). For comparison regression fit from Bricaud et al., 1995 study (red solid line) is also shown. See Figure 4.3 for symbols.

depths and 47% of chlorophyll-a in surface samples was from greater than 5 μm sized phytoplankton cells (pers. comm. Dr. Michael Lomas). The phytoplankton cell abundance observations indicated that nanoplankton followed by microplankton were the dominant size fractions (pers. comm. Dr. Michael Lomas). The distribution of phytoplankton size classes showed relatively larger cells at most stations, but stations where small cells dominated were also observed. This is consistent with the predominantly lower $a^*_{PHY}(\lambda)$ in the study region and the large variability due to larger values of $a^*_{PHY}(\lambda)$ observed at some locations.

The variability in $a^*_{PHY}(\lambda)$ was not just restricted to the visible region, the UV (300-400 nm) region too showed large variability with high absorption (Figure 4.5a). Peaks around 320 nm were observed in some of the surface values which diminished in magnitude or were mostly absent in samples from middle depths. Peaks around these wavelengths have been attributed to mycosporine like amino acids (MAAs) [*Riegger and Robinson*, 1997], although these compounds were not measured directly during our study. MAAs are a group of UV absorbing compounds that act as sunscreens to reduce UV induced damage [*Riegger and Robinson*, 1997]. The higher amplitude of peaks in the surface samples relative to middle depths indicate that the concentration of MAAs decreased with depth in the study region. The higher presence of MAAs in the surface phytoplankton populations of the region could be due to change in species composition or indicate photoacclimation processes [*Helbling et al.*, 1996]. Photoacclimation processes may result in high relative levels of photo-protective carotenoids [*Laurion et al.*, 2002], the absorption bands of photoprotective caretenoids are in the 400-530 nm range [*Bricaud et al., 1995*] which could partially explain the relatively high values of $a^*_{PHY}(443)$ in some surface samples.

A decreasing trend of $a^*_{PHY}(443)$ from 0.120-0.003 m^2 (mg chl-a)$^{-1}$ was observed with increasing chlorophyll-a concentration from 0.04-32.30 mg m^{-3} (Figure 4.5b). Similar trends are seen for $a^*_{PHY}(\lambda)$ with chlorophyll-a concentration over the entire visible spectrum. The inverse relationship is considered to be caused by an increase in pigment package effect and a decrease in relative abundance of accessory pigments with increasing chlorophyll-a [*Cleveland*, 1995; *Duysens*, 1956; *Morel and Bricaud*, 1981; *Bricaud et al., 1995*]. The Bricaud et al., (1995) fit was clearly higher than the fit obtained for our study for the whole range of chlorophyll-a concentration. This demonstrates $a^*_{PHY}(443)$ was consistently lower for our study as compared to the Bricaud et al., (1995) study, indicating the change in pigment composition and/or change in pigment packaging that exists in our study region is consistent with other higher latitude studies [*Arrigo et al.*, 1998; *Cota et al.*, 2003; *Matsuoka et al.*, 2007]. The blue to red ratio of $a^*_{PHY}(\lambda)$ (e.g., $a^*_{PHY}(443)/a^*_{PHY}(676)$) in this study varied from 6.9 to 1.1 demonstrating approximately a 6 fold decrease as chlorophyll-a increased from 0.04 to 32.3 mg m^{-3} (Figure 4.6a). The $a^*_{PHY}(443)/a^*_{PHY}(676)$ inverse relation with chlorophyll-a was consistent with Bricaud et al. (1995). This ratio was found to be strongly correlated with the ratio of accessory pigments to chlorophyll-a, as the accessory pigments are known to absorb significantly higher amount of light in the blue region than in the red region of the spectrum [*Lohrenz et al.*, 2003]. Higher values of $a^*_{PHY}(443)/a^*_{PHY}(676)$ are associated with smaller cells. The $a^*_{PHY}(443)/a^*_{PHY}(676)$ values greater than 3 are generally associated with small phytoplankton cells [*Moore et al.*, 1995; *Stramski and Morel*, 1990]. Although the majority of $a^*_{PHY}(443)/a^*_{PHY}(676)$ values were less than 3 and lower $a^*_{PHY}(676)$ indicating relatively larger size phytoplankton to be dominant and hence larger package effect, several

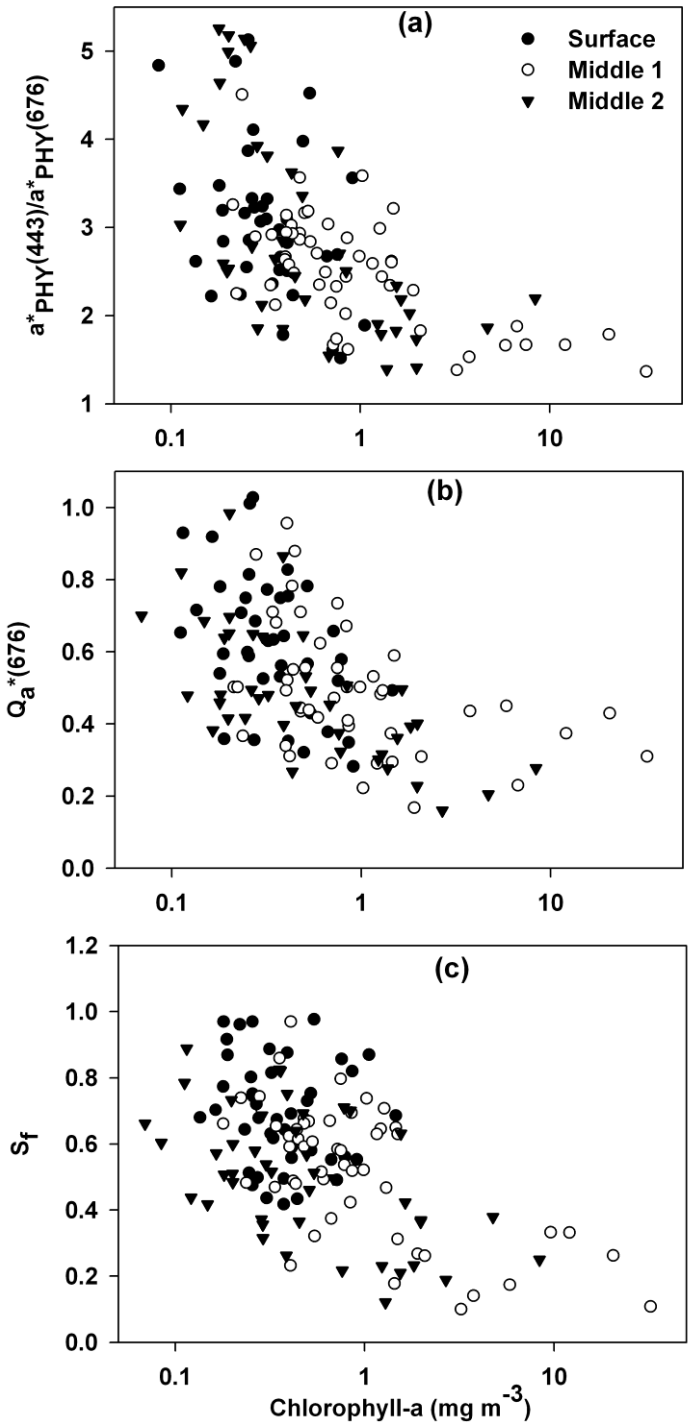

Figure 4.6. Relationship between chlorophyll-a and (a) ratio of specific phytoplankton absorption ($a^*_{PHY}(\lambda)$) at 443 nm and 676 nm (b) quantification of package effect by a dimensionless factor at 676 ($Q^*_a(676)$), and (c) spectral size parameter (S_f) calculated according to Ciotti et al., 2002. See Figure 4.3 for symbols.

$a^*_{PHY}(443)/a^*_{PHY}(676)$ values greater than 3 were observed, consistent with observed variability in the phytoplankton community size-structure.

Using the approach used by Duysen (1956) and Morel and Bricaud, (1981), the package effect can be quantified by calculating $Q_a^*(\lambda)$ as the ratio $a^*_{PHY}(\lambda)$ and specific phytoplankton absorption of the same pigmented material in suspension ($a^*_{PHY\_SOL}(\lambda)$). $Q_a^*(\lambda)$ varies from 1 (no package effect) to 0 (maximal package effect). With $a^*_{PHY\_SOL}(676)$ set equal to 0.0207 m^2mg^{-1} [*Bricaud et al.,* 1995], $Q_a^*(676)$ was calculated. The $Q_a^*(676)$ values decreased from 1.02 to 0.16 with increasing chlorophyll-a concentration (Figure 4.6b). However, a large scatter was observed in $Q_a^*(676)$. This scatter was the greatest at lower chlorophyll concentrations (and thus lower absorption values) and these two samples exceeded the theoretical upper limit of 1. The scatter in this relationship is attributed to uncertainty in the β factor [*Bricaud and Stramski*, 1990]. The spectral size parameter (S_f) was calculated according to Ciotti et al., (2002) using their pico ($a_{<pico>}(\lambda)$) and micro ($a_{<micro>}(\lambda)$) basis vectors which are absorption spectra normalized by their own average over the visible spectrum for samples dominated by picoplankton and samples dominated by microplankton-sized organisms. Every normalized spectrum was decomposed using the mixed spectral model:

$$a_{PHY}(\lambda) = a_{<PHY>}(\lambda)\left\{\left[S_f\, a_{<pico>}(\lambda)\right] + \left[\left(1-S_f\right) a_{<micro>}(\lambda)\right]\right\} \qquad \text{(Eq. 21)}$$

The $a_{<PHY>}(\lambda)$ is the scaling factor to be applied to the normalized absorption [*Ciotti et al.,* 2002]. The spectral mixing model constrains S_f between 0 and 1, where S_f values close to 0 indicate phytoplankton is dominated by large cells (> 20 μm) and S_f values close to 1 are dominated by small cells (< 2 μm) [*Ciotti et al.*, 2002]. Values between 0 and 1 represent the possible position between large and small size cells. The computation of S_f is included in this study as a method independent of chlorophyll-a concentration to support the results obtained

from $a^*_{PHY}(443)$, $a^*_{PHY}(443)/a^*_{PHY}(676)$ and $Q_a^*(676)$ analysis. The comparison of measured and reconstructed phytoplankton absorption spectra using computed S_f was in good agreement with r^2 greater than 0.9 averaged over the visible spectrum (400-700 nm) (data not shown). Figure 4.6c shows a plot of S_f against chlorophyll-a, where an inverse relationship can be seen. The S_f showed large variability and varied between 0.15 and 0.97, with higher values associated with small sized cells and lower chlorophyll-a, and smaller values are associated with larger sized cells and higher chlorophyll-a. While majority of S_f values were lower, several high values of S_f were also observed, similar to $a^*_{PHY}(443)/a^*_{PHY}(676)$ and $Q_a^*(676)$ results. These results are consistent with the chlorophyll-a fractionated and cell abundance data which revealed that although larger cells were dominant there were stations where smaller cells dominated (pers. comm. Dr. Michael Lomas). It must be noted that the $a^*_{PHY}(\lambda)$ values in this study would show some discrepancies from literature $a^*_{PHY}(\lambda)$ values due to the diversity of techniques used to correct for pathlength amplification for particles on filter paper and whether the $a_{PHY}(\lambda)$ was normalized with chlorophyll-a or chlorophyll-a plus phaeopigments from HPLC or fluorometric measurements. Also uncertainty on the variability of $a^*_{PHY}(\lambda)$ in the UV domain exists, path length amplification factor has not been well studied and the MAAs if present are known to leak out from intact cells during filtration process causing an artificial increase in absorption [*Laurion et al.*, 2003]. These different techniques are known to introduce large biases; we assume that these are not sufficiently large to bias our results. Moreover, if we had applied the β correction used in Bricaud et al, (1995) the average difference between our values of $a_{PHY}(\lambda)$ and Bricaud et al., (1995) values would have been less than 15% for the entire chlorophyll-a range.

Our relatively small regional data set showed the decrease of $a^*_{PHY}(443)$ with increasing chlorophyll-a concentration. The lower $a^*_{PHY}(\lambda)$ holds in other polar regions too compared with

low-latitude and mid-latitude waters, due to significant packaging effect [*Mitchell and Holm-Hansen*, 1991; *Sosik et al.*, 1992] and was identified as the cause of the underestimation of surface chlorophyll-a concentration by ocean color algorithms in the southeastern Bering Sea [*Müller-Karger et al.*, 1990]. However, recent studies show that chlorophyll-a is overestimated [*Schallenberg et al.*, 2008] owing to the influence of higher $a_{CDOM}(\lambda)$, though they did not make any measurement of absorption coefficients. The point here is which one of the two factors (lower $a^*_{PHY}(443)$ and higher $a_{CDOM}(\lambda)$) supersedes the other (or exist concomitantly) and has a significant effect on $R_{rs}(\lambda)$ and their ratios (hence pigment estimates) in the study region, we discuss the effect of these factors in the later section.

Parameterization of a_{PHY}, a_{DG} and a_{T-W}

Parameterization of absorption coefficients developed by using spectral slopes, absorption coefficients at a certain wavelength and/or chlorophyll-a, provides a means of extending absorption measurements at a specific wavelength to absorption for hyperspectral wavelengths [*Barnard et al.*, 1998; *Wang et al.*, 2005; *Matsuoka et al.*, 2011]. Ocean color sensors have a limited number of channels that are not sufficient to decipher spectral shape of absorption coefficients over the visible domain. Further, the $a_{PHY}(\lambda)$ at all wavelengths specifically the absorbance peak of $a_{PHY}(\lambda)$ at 676 nm cannot be retrieved as accurately from ocean color sensors as at this wavelength reflectance is significantly influenced by pure water absorption. So spectral relationships based on statistical analyses of in-situ data can be used to obtain absorption at hyperspectral wavelengths. For parameterization using absorption coefficient at a certain wavelength, the wavelength 443 nm was selected as it is located at one of the primary absorbance peaks of $a_{PHY}(\lambda)$ in the blue region of the spectrum and is a channel that is present in most ocean color satellite sensors (SeaWiFS, MODIS, MERIS, etc.). Naik et al., [2010] found

that $a_{PHY}(443)$ and $a_{DG}(443)$ can be retrieved more accurately than other wavelengths in southeastern Bering Sea from MERIS Rrs(λ) using the Lee et al., (2002) Quasi Analytical Algorithm (QAA).

Phytoplankton Absorption Parameterization through Chlorophyll-a and $a_{PHY}(443)$

Good correlation between $a_{PHY}(443)$ and chlorophyll-a (Figure 4.3a), suggested it would be appropriate to parameterize $a_{PHY}(\lambda)$ with chlorophyll-a. Despite the variability seen in the $a_{PHY}(\lambda)$ spectra good correlations were observed between $a_{PHY}(\lambda)$ and chlorophyll-a over the visible spectrum using eq. 7, with weakest correlations in the 450 nm to 500 nm range (Figure 4.7a, Table 4.2). The 450 to 500 nm is the range where pigments other than chlorophyll-a have a significant effect on the $a_{PHY}(\lambda)$ spectra, thus the lowest r^2. Using the above parameterization, the $a^*_{PHY}(\lambda)$ spectra can be modeled for various concentrations of chlorophyll-a. This technique helps us to evaluate $a^*_{PHY}(\lambda)$ variability in our study in comparison to other studies. Figure 4.7b shows the results of modeling $a^*_{PHY}(\lambda)$ and the apparent flattening of the spectra due to the package effect which was more pronounced with increasing chlorophyll-a, as the phytoplankton cell size increases as demonstrated in the previous section. We clearly see that $a^*_{PHY}(\lambda)$ is lower than the Bricaud et al., (1998) study for all wavelengths in the visible domain. It was also interesting to note that the modeled $a^*_{PHY}(\lambda)$ from Matsuoka et al., (2007) study done in the western Arctic was similar to the modeled $a^*_{PHY}(\lambda)$ from our study. The regression coefficients and r^2 for relationship between $a_{PHY}(\lambda)$ and $a_{PHY}(443)$ expressed as eq. 8 are shown in Figure 4.7c and Table 4.2. To test the strength of this parameterization we divided the data randomly into two halves, for one half we developed the parameterization and tested it with the other half. The results of this analysis at specific wavelengths shows a good linear relationship between the

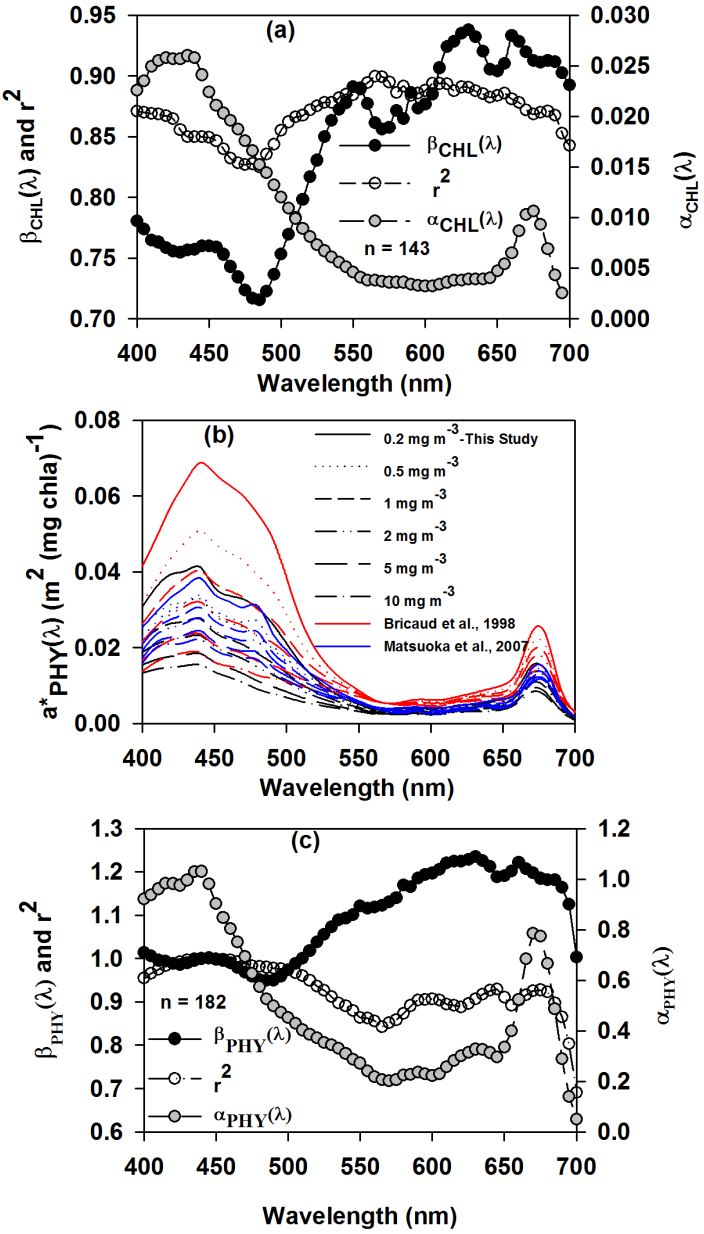

Figure 4.7. Parameterization of phytoplankton absorption ($a_{PHY}(\lambda)$). (a) Coefficients and r^2 of regression using chlorophyll-a through the eq: $a_{PHY}(\lambda) = \alpha_{CHL}(\lambda)[\text{chlorophyll-a}]^{(\beta_{CHL}(\lambda))}$ (b) modeled specific phytoplankton absorption ($a^*_{PHY}(\lambda)$) showing the flattening effect of absorption spectra with increasing chlorophyll-a. For comparison spectra from literature (Bricaud et al., 1995 (red) and Matsuoka et al., 2007 (blue)) are also shown, and (c) coefficients and r^2 of regression using $a_{PHY}(443)$ through eq: $a_{PHY}(\lambda) = \alpha_{PHY}(\lambda)[a_{PHY}(443)]^{(\beta_{PHY}(\lambda))}$. Note, that Figure 4.6c is for parameterization of $a_{PHY}(\lambda)$ with $a_{PHY}(443)$, while Figure 4.6a is for parameterization of $a_{PHY}(\lambda)$ with chlorophyll-a.

Table 4.2. Coefficients, and r^2 and number of samples (n) at specific wavelengths for the non-linear regression expressed as $a_Q(\lambda) = \alpha_X(\lambda)*[X]^{\beta}x^{(\lambda)}$ (see eqs. 7-9). Where $a_Q(\lambda)$ is either phytoplankton absorption or T-W – total absorption minus water from 400 -700 nm at 2 nm interval. X = chlorophyll-a, or PHY – phytoplankton absorption at 443 nm, or T-W – total absorption minus water at 443 nm, λ is the wavelength.

	Chlorophyll-a n = 143			**$a_{PHY}(443)$ n = 182**			**$a_{T-W}(443)$ n =182**		
λ (nm)	**$\alpha_{CHL}(\lambda)$**	**$\beta_{CHL}(\lambda)$**	**r^2**	**$\alpha_{PHY}(\lambda)$**	**$\beta_{PHY}(\lambda)$**	**r^2**	**$\alpha_{T-W}(\lambda)$**	**$\beta_{T-W}(\lambda)$**	**r^2**
400	0.023	0.780	0.871	0.920	1.013	0.954	0.927	0.762	0.940
412	0.025	0.764	0.869	0.971	0.994	0.979	0.958	0.827	0.972
443	0.026	0.758	0.882	-	-	-	-	-	-
490	0.014	0.725	0.835	0.498	0.953	0.978	0.537	1.004	0.978
510	0.010	0.784	0.845	0.406	1.002	0.958	0.430	1.034	0.962
560	0.004	0.876	0.855	0.221	1.119	0.853	0.218	1.033	0.916
665	0.009	0.927	0.877	0.664	1.208	0.915	0.730	1.764	0.956
676	0.009	0.912	0.870	0.642	1.182	0.915	0.681	1.742	0.957

measured and modeled $a_{PHY}(\lambda)$ (Table 4.3). Thus, the approach used here is helpful for describing $a_{PHY}(\lambda)$ spectra over the visible domain using $a_{PHY}(443)$ derived from ocean color.

$a_{DG}(\lambda)$ Parameterization through $a_{DG}(443)$ and $S_{DG}(443)$

The mean value of the spectral slope of CDOM and NAP (S_{DG}) was used to parameterize the $a_{DG}(\lambda)$ spectra using eq. 9. In most ocean color applications CDOM and NAP absorption are considered together, due to their similar spectral shapes. For all samples, the $a_{CDOM}(\lambda)$ and $a_{NAP}(\lambda)$ could be expressed well by exponential function given by eq. 6 and eq. 11, respectively. The standard error of both S_{CDOM} and S_{NAP} estimate was less than 0.1% and r^2 was greater than 0.95. The S_{NAP} values were found to vary between 0.007-0.016 nm^{-1} with an average value of 0.0110±0.0017 nm^{-1}. Variations in S_{NAP} are related to the relative concentrations of mineral and organic matter [*Babin et al.,* 2003]. The large variation in S_{NAP} observed in this study suggests that NAP matter consists of diverse organic matter. The S_{CDOM} values were found to vary between 0.008-0.022 nm^{-1} with an average value of 0.0151±0.0016 nm^{-1}. The S_{CDOM} showed a weak inverse relation with $a_{CDOM}(443)$ (r^2 = 0.29, n = 189) whereas S_{NAP} did not show any trend

Table 4. 3. Linear regression results at specific wavelengths from modeled and measured values of phytoplankton absorption, Colored dissolved organic matter (CDOM) plus non-algal matter (NAP) absorption and total absorption minus water. λ is the wavelength.

n = 91	**$a_{PHY}(\lambda)$**		**$a_{DG}(\lambda)$**		**$a_{T-W}(\lambda)$**	
λ (nm)	**Slope**	**r^2**	**Slope**	**r^2**	**Slope**	**r^2**
400	0.987	0.984	1.026	0.997	0.996	0.947
412	0.998	0.992	0.993	0.997	0.997	0.979
490	1.051	0.987	0.986	0.993	0.988	0.963
510	1.064	0.980	0.974	0.959	0.964	0.924
560	0.996	0.956	0.929	0.908	0.900	0.910
665	1.047	0.963	-	-	0.901	0.920
676	1.050	0.959	-	-	0.930	0.905

with $a_{NAP}(443)$. The S_{NAP} values were less variable as compared to S_{CDOM} consistent with several studies [*Babin et al.*, 2003; *Matsuoka et al.*, 2011]. The S_{DG} values varied between 0.009-0.020 nm^{-1} and did not show any clear inverse relationship with $a_{DG}(443)$ (Figure 4.8a). We did not observe any significant difference in S_{DG} between surface and middle depths. The utility of the parameterization of $a_{DG}(\lambda)$ with S_{DG} was tested by calculating the mean value of S_{DG} for one half of the data and applying the mean value S_{DG} to the remaining half for wavelengths between 400-560 nm. The linear regression results between the modeled and measured $a_{DG}(\lambda)$ are shown in Table 4.3; the r^2 was greater than 0.9 and slope close to 1 for the wavelengths analyzed.

Total Absorption Parameterization through $a_{T-W}(443)$

The procedure for parameterization of $a_{T-W}(\lambda)$ was similar to the parameterization of $a_{PHY}(\lambda)$. The coefficients and r^2 of the regression expressed by eq. 9 are shown in Figure 4.8b and Table 4.2. The parameter $\alpha_{T-W}(\lambda)$ has a spectral shape similar in appearance to $a_{PHY}(\lambda)$ which is interesting as the $a_{T-W}(\lambda)$ also includes absorption from CDOM and detrital matter. This also that indicated although $a_{DG}(\lambda)$ has a larger contribution to $a_{T-W}(\lambda)$ compared to $a_{PHY}(\lambda)$, the variation in $a_{PHY}(\lambda)$ was much larger compared to $a_{DG}(\lambda)$. A good linear relationship was seen between the

measured and modeled $a_{T\text{-}W}(\lambda)$ with slope close to 1 and r^2 greater than 0.9 (Table 4.3). The results obtained here are of significance to satellite remote sensing since bio-optical information is usually limited in most cases. To fully utilize such an approach it is essential that more

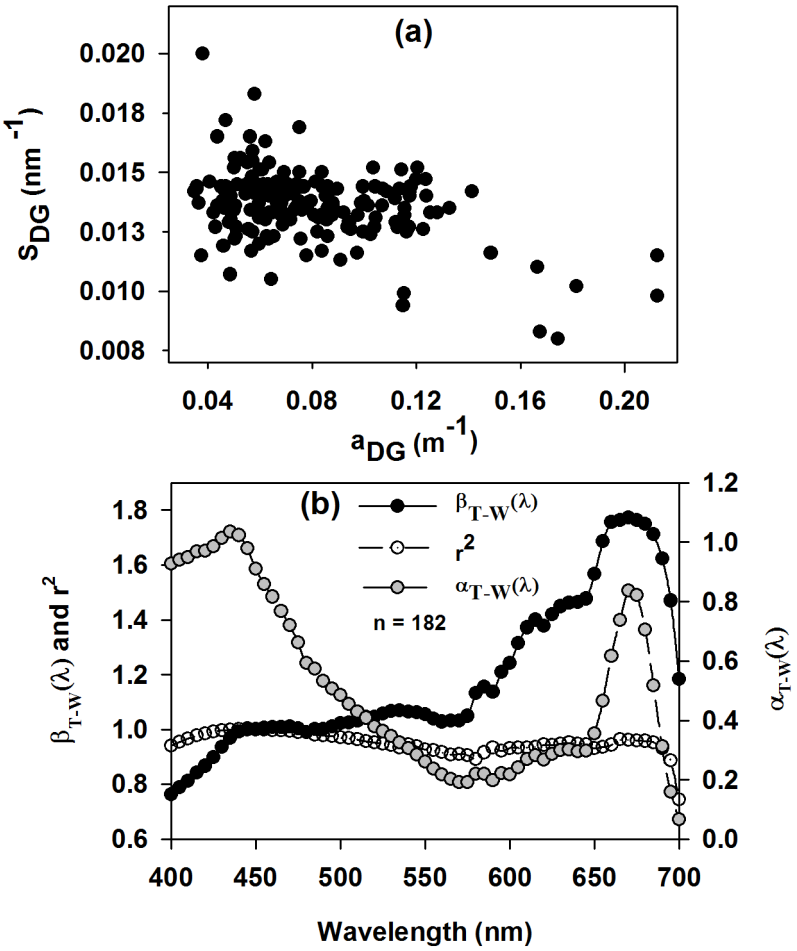

Figure 4.8. (a) Parameterization of NAP plus CDOM absorption through spectra slope parameter through eq: $a_{DG}(\lambda) = a_{DG}(\lambda_0)e^{(-S_{DG}(\lambda-\lambda_0))}$ and (b) parameterization of total minus water absorption ($a_{T\text{-}W}(\lambda)$) using ($a_{T\text{-}W}(443)$) through the eq: $a_{T\text{-}W}(\lambda) = \alpha_{T-W}(\lambda)[a_{T\text{-}W}(443)]^{(\beta_{T-W}(\lambda))}$.

intricate models be developed and tuned with absorption on seasonal scales given the wide range of variability associated with the absorption components [*Barnard et al.*, 1998; *Wang et al.*, 2005].

An Absorption Budget for Tte Southeastern Bering Sea: Relative Contributions of a_{PHY}, a_{NAP} and a_{CDOM} to a_{T-W}

An understanding of the relative contributions of phytoplankton, NAP and CDOM to total light absorption at specific wavelengths is helpful for predicting and interpreting the IOPs and AOPs of the oceans. To examine the relative contributions of each coefficient to total non-water absorption, the coefficients were displayed on a normalized ternary plot at wavebands that correspond to most ocean color sensors as well as wavebands at which the constituents show characteristic features (Figure 4.9). The normalized plots remove uncertainties due to errors associated with measurement of each component of total absorption (mentioned in methods section). At all wavelengths examined except 676 nm, $a_{CDOM}(\lambda)$ dominates the total non-water absorption coefficient followed by $a_{PHY}(\lambda)$ and $a_{NAP}(\lambda)$. Excluding a few samples, the contribution of $a_{CDOM}(\lambda)$ was greater than 50% at all depths and wavelengths except 676 nm. This result is consistent with previous findings (e.g.[*Belanger et al.*, 2006; *Brown et al.*, 2008; *Matsuoka et al.*, 2007]), where a high contribution of $a_{CDOM}(\lambda)$ at higher latitudes was observed. At 443nm, where the chlorophyll-a absorption is maximum, $a_{PHY}(\lambda)/ a_{T-W}(\lambda)$, $a_{NAP}(\lambda)/ a_{T-W}(\lambda)$, and $a_{CDOM}(\lambda)/ a_{T-W}(\lambda)$ was 20%, 14%, and 66%, respectively for surface samples, 28%, 15%, and 57%, respectively for middle1 depth, and 19%, 16%, and 65%, respectively for middle 2 depth. The relative contribution of each component remains similar from the surface to below the chlorophyll-a maximum with the only noticeable change being the increase in $a_{PHY}(443)/ a_{T-W}(443)$ and corresponding decrease in $a_{CDOM}(443)/ a_{T-W}(443)$ at middle 1 depths. The CDOM contribution to total non-water absorption was generally dominant in the near ultraviolet region of the spectrum (380 nm – data not shown) and nearly null in the red region (676 nm) while the

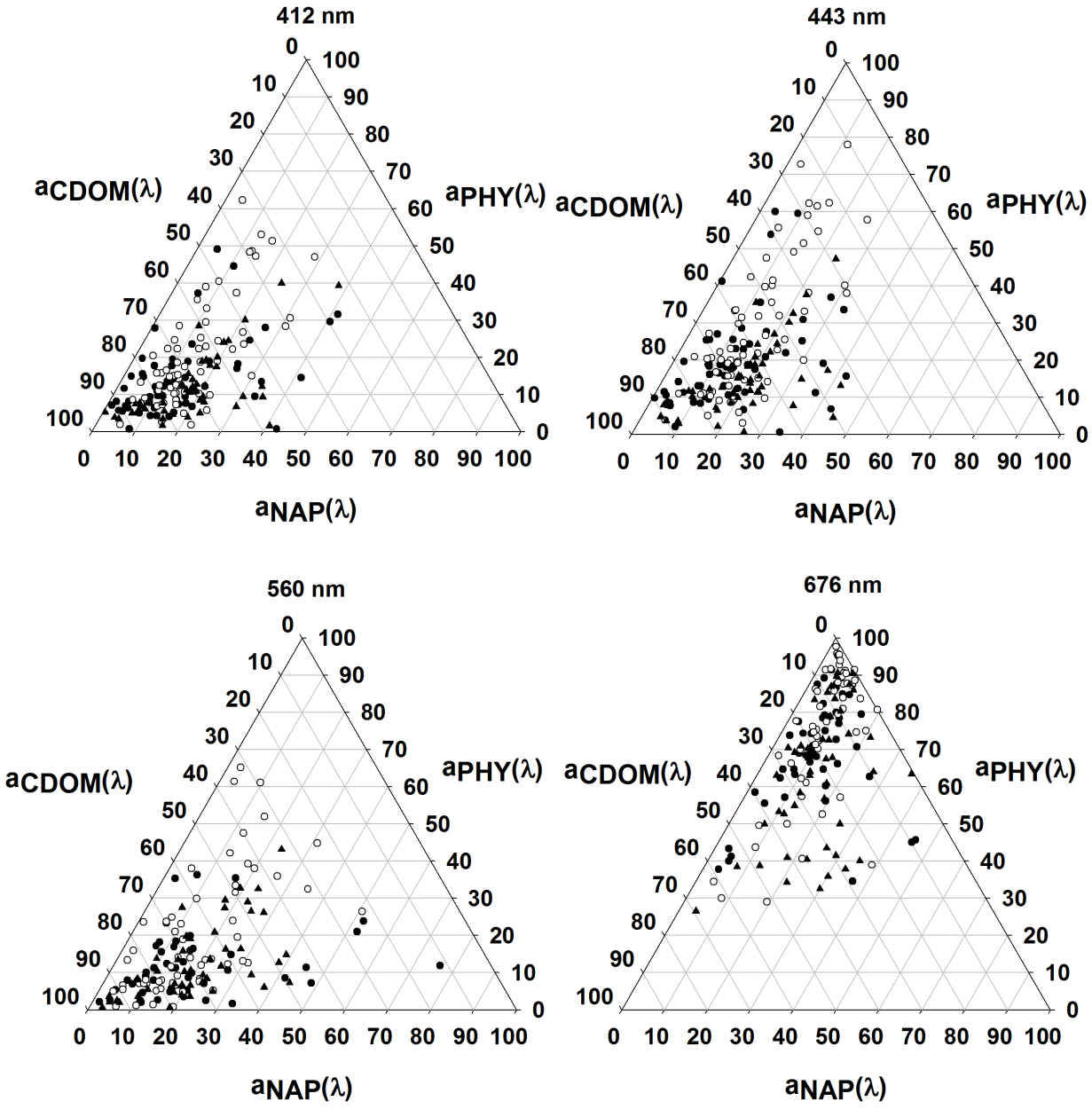

Figure 4.9. Absorption budget for the southeastern Bering Sea through ternary plots of phytoplankton absorption ($a_{PHY}(\lambda)$), NAP absorption (($a_{PHY}(\lambda)$)) and CDOM absorption ($a_{CDOM}(\lambda)$) at 412 nm, 443 nm, 560 nm and 676 nm. See Figure 4.3 for symbols.

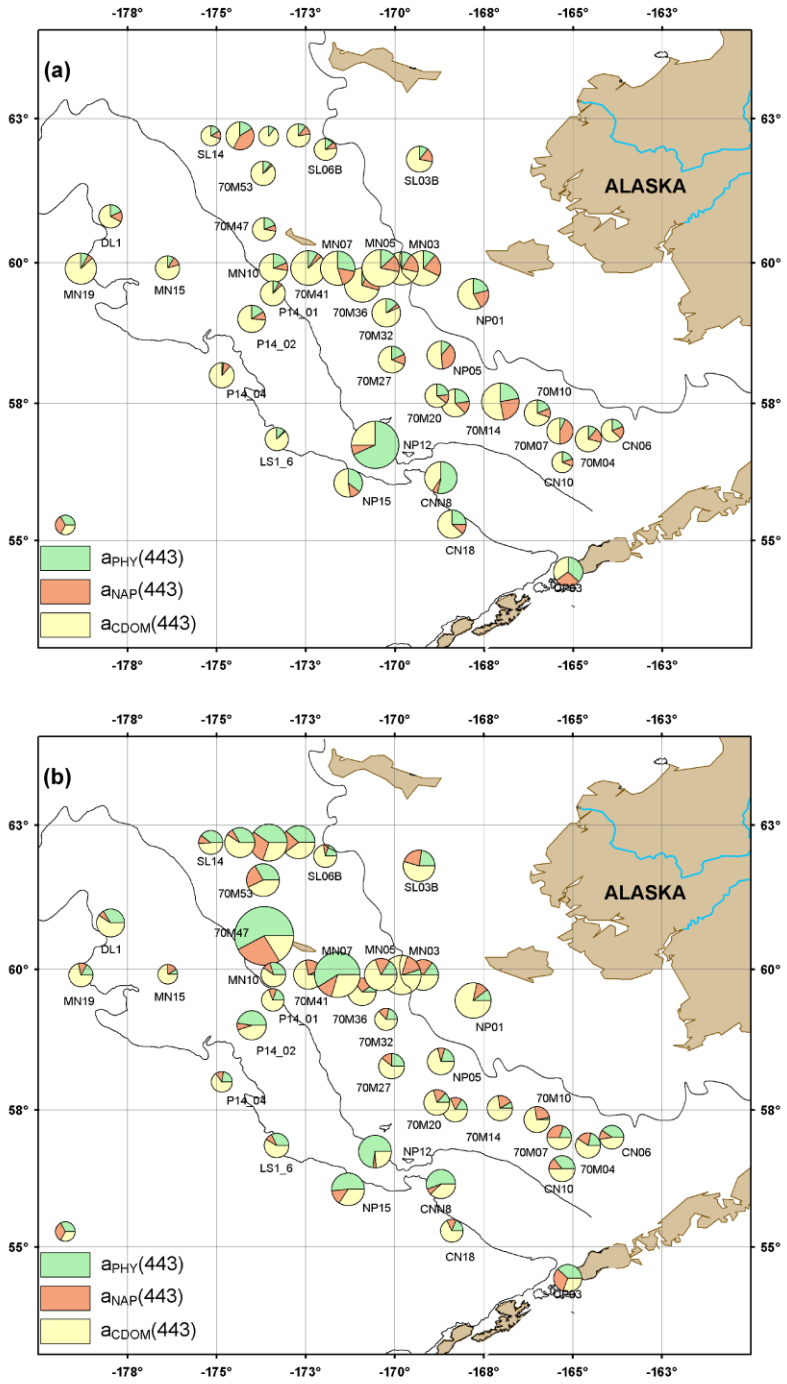

Figure 4.10. Spatial distribution of the absorption budget at 443 nm for (a) surface and (b) middle 1 depth. Green represents phytoplankton contribution, orange represents NAP absorption, and yellow represents CDOM contribution to total non-water absorption in the pie symbols. The size of pie symbols is proportional to the total non-water absorption at the station locations shown in Figure 4.1.

relative contribution of NAP to total non-water absorption was highest at 560 nm and highest relative contribution of phytoplankton to total non-water absorption was at 676 nm. The relative contribution of NAP plus CDOM at 443 nm was around 80% near the surface, which is slightly higher than the range (70% at 443 nm) of satellite estimates provided by Siegel et al. (2005) for the study region.

The spatial distribution of the absorption budget follows closely the spatial distributions along the transects described earlier (Figure 4.10). The distribution of the absorption budget in the surface and middle depth clearly shows the dominance of $a_{CDOM}(443)$ except at stations located near the Pribilof Islands where $a_{PHY}(443)$ was dominant. The northern shelf (60 N and above) showed a higher relative contribution from CDOM as compared to the southern shelf (below 60N). The increase in contribution of $a_{PHY}(443)$ to total absorption was apparent going from surface samples to middle 1 depths, but contribution of $a_{CDOM}(443)$ was still dominant at most stations (Figure 4.10). Some studies have shown the importance of relative contribution of pure water absorption to total water absorption [*Bricaud et al.*, 2010; *Sasaki et al.*, 2001]. It was not the case in this study as on average, the relative contribution of pure water absorption was 8% at surface, 5% at middle 1 depths and 7% at middle 2 depths at 443 nm.

Influence of Absorption On Remote Sensing Reflectance ($R_{rs}(\lambda)$) and Diffuse Attenuation Coefficient of Downwelling Irradiance ($K_d(\lambda)$)

The primary purpose of this section is to describe the effect of absorption on the above water and underwater light field, while the blue to green reflectance ratios are described briefly for completeness. Higher than normal CDOM concentrations are known to clearly produce an overestimate of chlorophyll, since they absorb strongly at 443 nm and less so at 550 nm and 560 nm. Brown et al., (2008) showed that the second order variability of chlorophyll-a concentration could be explained by CDOM and particulate backscattering. So, at high latitudes CDOM and

backscattering may be erroneously contributing to chlorophyll-a estimates from ocean color sensors. To investigate the effect of absorption on $R_{rs}(\lambda)$ and $K_d(\lambda)$, we modeled them using IOPs (absorption and backscattering). The IOPs that were used in modeling were from both discrete measurements as well as continuous vertical profile measurements. A comparison was made between modeled and radiometer measured $R_{rs}(\lambda)$ and $K_d(\lambda)$. To evaluate the influence of CDOM absorption, we modeled $R_{rs}(\lambda)$ and $K_d(\lambda)$ using total absorption as well as total absorption minus the absorption from CDOM (see Methods section). Optical closure between $R_{rs}(\lambda)$ (and $K_d(\lambda)$) and IOPs (both discrete as well as continuous) is achieved at all wavelengths between 400 nm to 700 nm at 1 nm interval, providing confidence to the accuracy of individual measurements (Figure 4.11 and Figure 4.12). The average percent difference (a.p.d) between discrete and continuous IOPs based model was less than 10% for $R_{rs}(\lambda)$ and $K_d(\lambda)$ at all wavelengths, with the largest differences in the red wavelengths. For the IOP modeled and radiometer measured $R_{rs}(\lambda)$ and $K_d(\lambda)$ the a.p.d was 15% (except red wavelengths a.p.d was less than 30%) and 10% (except red wavelengths a.p.d was less than 15%) respectively. The modeled and measured $R_{rs}(\lambda)$ showed fairly good agreement with MERIS retrieved $R_{rs}(\lambda)$, with a.p.d less than 25% except at red wavelengths (a.p.d less than 35%). The results from the closure between $R_{rs}(\lambda)$ and IOPs is significant for empirical formulations linking $R_{rs}(\lambda)$ to IOPs and accurate modeling of $R_{rs}(\lambda)$ or IOPs.

The effect of $a_{CDOM}(\lambda)$ on the blue wavelengths and to a lesser extent on the green wavelengths was apparent on the $R_{rs}(\lambda)$ spectra for most of the samples analyzed (Figure 4.11). Based on the closure analysis we found that the blue to green $R_{rs}(\lambda)$ were lower in the study region causing chlorophyll-a in the range of 0.05 to 0.9 mg m^{-3} to be overestimated by a factor of

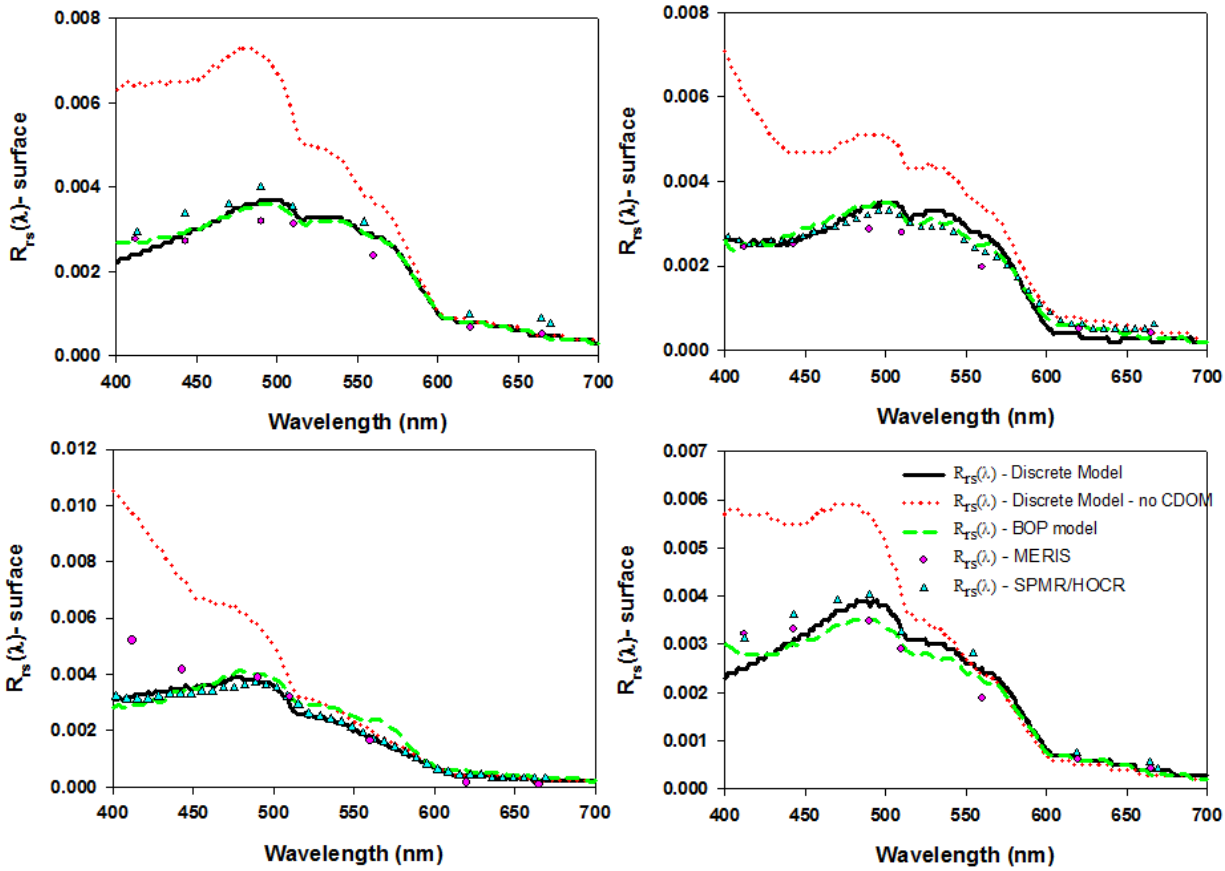

Figure 4. 11. Remote sensing reflectance spectra ($R_{rs}(\lambda)$) modeled at hyperspectral wavelengths from IOPs (absorption and scattering (model - see eqs. 16-17 or in-situ)) for discrete measurement ($R_{rs}(\lambda)$ – Discrete Model (solid black line)), discrete measurements minus the contribution from CDOM ($R_{rs}(\lambda)$ – Discrete Model – no CDOM (dotted red line)) and continuous measurements using a bio-optical package (BOP) ($R_{rs}(\lambda)$ – BOP Model (dashed green line)) using eqs. 13-15. Also shown for comparison are the $R_{rs}(\lambda)$ spectra determined from in-water radiometric measurements using either an SPMR or HyperOCR ($R_{rs}(\lambda)$ – SPMR/HOCR – solid cyan triangles) and MERIS derived $R_{rs}(\lambda)$ ($R_{rs}(\lambda)$ – MERIS – solid pink circles). The top panels are representative of stations with better closure while bottom panels represent stations where the closure wasn't as good.

~2 using the OC4.v4 algorithm. The lower blue to green $R_{rs}(\lambda)$ can be ascribed to the high $a_{CDOM}(\lambda)$ and the high backscattering (>0.004 at 443 nm; n = 20). As the $R_{rs}(\lambda)$ – Discrete Model in which the backscattering was modeled using a global relationship [*Morel and Maritorena, 2001*] and $R_{rs}(\lambda)$ – BOP Model in which backscattering was from in-situ measurements showed good agreement, also from differences between $R_{rs}(\lambda)$ – Discrete Model and $R_{rs}(\lambda)$ – Discrete

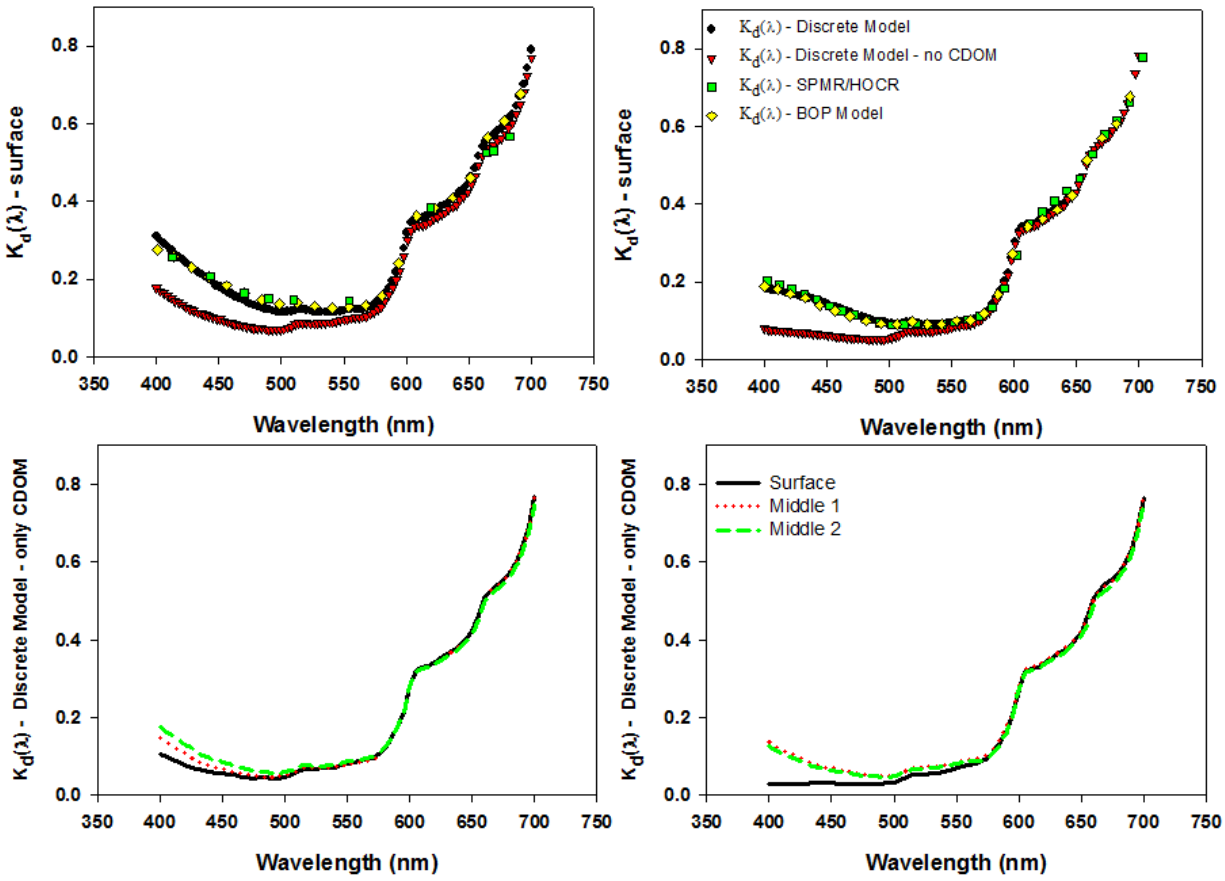

Figure 4.12. Diffuse attenuation coefficient of downwelling irradiance ($K_d(\lambda)$) modeled at hyperspectral wavelengths from IOPs (absorption and scattering(model - see eqs. 16-17 or in-situ)) (a,b) for discrete measurement ($K_d(\lambda)$ – Discrete Model (black filled circles)), discrete measurements minus the contribution from CDOM ($K_d(\lambda)$ – Discrete Model – no CDOM (red filled triangles)) and continuous measurements using a bio-optical package (BOP) ($K_d(\lambda)$ – BOP Model (yellow filled diamonds)) using eqs. 13-15. Also shown for comparison is the $K_d(\lambda)$ spectra determined from in-water radiometric measurements using either an SPMR or HyperOCR ($K_d(\lambda)$ – SPMR/HOCR (green filled squares)).(c,d) represent the vertically variability of $K_d(\lambda)$ only due to CDOM ($K_d(\lambda)$ - Discrete Model – only CDOM), at 3 depths Surface (solid black line), Middle 1(dotted red line) and Middle 2 (green dashed line).

Model – no CDOM, we believe that backscattering had a relatively lesser influence on $R_{rs}(\lambda)$ as compared to $a_{CDOM}(\lambda)$. From comparisons between $R_{rs}(\lambda)$ – Discrete Model and R_{rs} (λ) – Discrete Model – no CDOM we found that the blue to green $R_{rs}(\lambda)$ ratios decreased by a factor of ~2 due to the influence of $a_{CDOM}(\lambda)$. As observed in the earlier sections $a_{CDOM}(\lambda)$ dominates the light absorption relative to $a_{PHY}(\lambda)$ especially at lower chlorophyll-a concentration, hence higher

CDOM overrides the lower $a^*_{PHY}(\lambda)$ influencing the green to blue reflectance ratios in our study region during summer. Similar results can be expected for other biogeochemical variables retrieved from global ocean color algorithms based on a blue to green $R_{rs}(\lambda)$ ratio.

From modeled $K_d(\lambda)$, we see that there is significant influence of $a_{CDOM}(\lambda)$ on $K_d(\lambda)$ accounting for >50% of $K_d(\lambda)$ at blue wavelengths (Figure 4.12). Moreover, the influence of $a_{CDOM}(\lambda)$ on $K_d(\lambda)$ is not uniform through the water column (Figure 4.12c-d). PP models usually utilize phytoplankton biomass, a photoadaptive variable and some function of sub-surface light field in their formulation [*Behrenfeld and Falkowski*, 1997]. In vertically integrated PP models, $K_d(\lambda)$ is assumed to be constant above the mixed layer depth (MLD) and a function of chlorophyll-a below MLD with some models including a constant contribution from CDOM throughout the water column [*Westberry et al.*, 2008]. Chlorophyll-a is the principal model variable that influences calculation of PP from PP models [*Behrenfeld and Falkowski*, 1997]. The vertical variability in $K_d(\lambda)$ (only from CDOM) taken together with the error in estimates of chlorophyll-a will result in large errors in the estimation of PP in the study region. The precise influence of the bio-optical properties on estimation of PP would require more involved analysis of model variables which is beyond the scope of this paper. However, it can be concluded unequivocally that the higher CDOM absorption supersedes the lower $a^*_{PHY}(\lambda)$ at low chlorophyll-a concentration and if unaccounted for, would greatly influence the estimation of biogeochemical variables from ocean color and underwater light field in the study region.

Conclusions

The absorption coefficients showed large variability on the shelf across the coastal, middle and outer domains and were closely tied to distinctive hydrographic and biogeochemical characteristics in each domain. Higher values of $a_{PHY}(443)$ were observed at the central front and

low values in the coastal domain in agreement with the productivity patterns from Mathis et al., [2010] study. The range of $a_{DG}(443)$ was about one order of magnitude while its variability was relatively less as compared to $a_{PHY}(443)$. The surface distribution of $a_{DG}(443)$ with the larger contribution from $a_{CDOM}(443)$, showed higher values in the coastal domain of the northern shelf due to the Kuskokwim River runoff.

We found strong correlations between $a_{PHY}(\lambda)$, $a_P(\lambda)$ and $a_{T\text{-}W}(\lambda)$ at 443 nm and 676 nm and chlorophyll-a. Over the chlorophyll-a range observed we found that most of $a_{PHY}(443)$ values were smaller than those measured in waters at middle and lower latitudes. The contribution of $a_{NAP}(443)$ to $a_P(443)$ was variable at low chlorophyll-a concentration, despite this variability $a_{PHY}(443)$ dominated $a_P(443)$ (on an average 62% at all stations and depth). $a_{DG}(443)$ was weakly correlated with chlorophyll-a even though $a_{NAP}(\lambda)$ showed a significant positive relation with chlorophyll-a but $a_{CDOM}(\lambda)$ did not show a strong positive correlation with chlorophyll-a. $a^*_{PHY}(\lambda)$ at 443 nm was highly variable and was inversely related to chlorophyll-a with $a^*_{PHY}(443)$ values being consistently lower than those obtained from middle and lower latitudes, which suggested that a change in pigment composition and/or package effect is prevalent in the study region. The $Q_a^*(676)$, which gives a quantification of the package effect, decreased from 1.02 to 0.16 with increasing chlorophyll-a concentration and the spectral size parameter (S_f) obtained according to Ciotti et al., [2002] varied between 0.15 and 0.97, with higher values associated with small sized cells and lower chlorophyll-a, and lower values are associated with larger sized cells and higher chlorophyll-a. While the $a^*_{PHY}(443)/a^*_{PHY}(676)$ (< 3), lower values of $a^*_{PHY}(676)$ (mean - 0.012±0.006 m^2 (mg chl-a)$^{-1}$), $Q_a^*(676)$, and S_f suggested generally larger size phytoplankton to be dominant in our study region higher values of $a^*_{PHY}(443)/a^*_{PHY}(676)$ (> 3)., $Q_a^*(676)$ and S_f were also observed at some locations indicating large variability in

$a^*_{PHY}(\lambda)$ consistent with the phytoplankton community size-structure which revealed that although larger cells were dominant there were stations where smaller cells dominated.

The parameterizations of absorbing coefficients through statistical relationships are strong at all wavelengths examined. Such an approach makes it possible to predict absorption coefficients across the visible domain from a single wavelength and is of great significance in ocean color remote sensing since bio-optical information is usually limited to few wavelengths. One remarkable conclusion of the present study was that the relative contribution of $a_{CDOM}(\lambda)$ to total non-water absorption was greater than 50% at all depths and wavelengths (except red wavelengths). The relative contribution of $a_{CDOM}(443)$ to $a_{T\text{-}W}(443)$ decreased with increasing chlorophyll-a with relatively less scatter, emphasizing that as chlorophyll-a increases $a_P(443)$ takes up more of the absorption budget. The surface distribution of the absorption budget clearly showed the dominance of $a_{CDOM}(443)$ except at stations located near the Pribilof Islands where $a_{PHY}(443)$ was dominant. The implications of this are huge to ocean color algorithms where higher than normal CDOM may be incorrectly contributing to chlorophyll-a estimates. To assess the influence of high $a_{CDOM}(\lambda)$ and lower $a^*_{PHY}(\lambda)$ on AOPs we modeled $R_{rs}(\lambda)$ and $K_d(\lambda)$ using IOPs (absorption (total and total minus $a_{CDOM}(\lambda)$) and backscattering). Good optical closure was observed between modeled and radiometer measured values of $R_{rs}(\lambda)$ and $K_d(\lambda)$. The influence of $a_{CDOM}(\lambda)$ superseded the lower $a^*_{PHY}(\lambda)$, which was evident on modeled $R_{rs}(\lambda)$ and $K_d(\lambda)$ especially at blue wavelengths. The $a_{CDOM}(\lambda)$ caused the blue to green $R_{rs}(\lambda)$ ratios to decrease by a factor of ~2. The $a_{CDOM}(\lambda)$ had a significant influence on $K_d(\lambda)$ accounting for >50% of $K_d(\lambda)$ at blue wavelengths which was variable with depth. The error in estimation of chlorophyll-a along with vertical variability of $K_d(\lambda)$ would introduce large biases in estimates of PP, which is essential for understanding changes occurring in the Bering Sea ecosystem in the long term. The

present study provides important insight for improvement of ocean color algorithms and bio-optical models as well as accurate retrieval of absorbing coefficients in the southeastern Bering Sea.

References

Aguilar-Islas, A. M., R. D. Rember, C. W. Mordy, and J. Wu (2008), Sea ice derived dissolved iron and its potential influence on the spring algal bloom in the Bering Sea, Geophysical Research Letters, 35(24).

Arrigo, K. R., D. H. Robinson, D. L. Worthen, B. Schieber, and M. P. Lizotte (1998), Bio-optical properties of the southwestern Ross Sea, Journal of Geophysical Research-Oceans, 103(C10), 21683-21695.

Babin, M., D. Stramski, G. M. Ferrari, H. Claustre, A. Bricaud, G. Obolensky, and N. Hoepffner (2003), Variations in the light absorption coefficients of phytoplankton, nonalgal particles, and dissolved organic matter in coastal waters around Europe, Journal of Geophysical Research, 108(C7), 3211.

Bannister, T. (1974), Production equations in terms of chlorophyll concentration, quantum yield, and upper limit to production, Limnology and Oceanography, 19(1), 1-12.

Barnard, A. H., W. S. Pegau, and J. R. V. Zaneveld (1998), Global relationships of the inherent optical properties of the oceans, Journal of Geophysical Research-Oceans, 103(C11), 24955-24968.

Behrenfeld, M. J., and P. G. Falkowski (1997), A consumer's guide to phytoplankton primary productivity models, Limnology Oceanography, 42(7), 1479-1491.

Belanger, S., H. X. Xie, N. Krotkov, P. Larouche, W. F. Vincent, and M. Babin (2006), Photomineralization of terrigenous dissolved organic matter in Arctic coastal waters from 1979 to 2003: Interannual variability and implications of climate change, Global Biogeochemical Cycles, 20(4).

Belz, M., K. Larsen, and K.-F. Klein (2006), Fiber optic sample cells for polychromatic detection of dissolved and particulate matter in natural waters, paper presented at Advanced Environmental, Chemical, and Biological Sensing Technologies IV, SPIE, Boston, MA, USA

Boss, E., W. S. Pegau, M. Lee, M. Twardowski, E. Shybanov, G. Korotaev, and F. Baratange (2004), Particulate backscattering ratio at LEO 15 and its use to study particle composition and distribution, Journal of Geophysical Research-Oceans, 109(C1).

Bricaud, A., and D. Stramski (1990), Spectral absorption coefficients of living phytoplankton and nonalgal biogenous matter - a comparison between the Peru upwelling area and the Sargasso Sea, Limnology and Oceanography, 35(3), 562-582.

Bricaud, A., M. Babin, A. Morel, and H. Claustre (1995), Variability in the chlorophyll-specific absorption-coefficients of natural phytoplankton - analysis and parameterization, Journal of Geophysical Research-Oceans, 100(C7), 13321-13332.

Bricaud, A., H. Claustre, J. Ras, and K. Oubelkheir (2004), Natural variability of phytoplanktonic absorption in oceanic waters: Influence of the size structure of algal populations, Journal of Geophysical Research-Oceans, 109(C11).

Bricaud, A., A. Morel, M. Babin, K. Allali, and H. Claustre (1998), Variations of light absorption by suspended particles with chlorophyll a concentration in oceanic (case 1) waters: Analysis and implications for bio-optical models, Journal of Geophysical Research-Oceans, 103(C13), 31033-31044.

Bricaud, A., M. Babin, H. Claustre, J. Ras, and F. Tieche (2010), Light absorption properties and absorption budget of Southeast Pacific waters, Journal of Geophysical Research-Oceans, 115.

Brown, C. A., Y. Huot, P. J. Werdell, B. Gentili, and H. Claustre (2008), The origin and global distribution of second order variability in satellite ocean color and its potential applications to algorithm development, Remote Sensing of Environment, 112(12), 4186-4203.

Ciotti, A. M., M. R. Lewis, and J. J. Cullen (2002), Assessment of the relationships between dominant cell size in natural phytoplankton communities and the spectral shape of the absorption coefficient, Limnology and Oceanography, 47(2), 404-417.

Cleveland, J. S. (1995), Regional models for phytoplankton absorption as a function of chlorophyll-a concentration, Journal of Geophysical Research-Oceans, 100(C7), 13333-13344.

Cleveland, J. S., and A. D. Weidemann (1993), Quantifying absorption by aquatic particles - a multiple-scattering correction for glass-fiber filters, Limnology and Oceanography, 38(6), 1321-1327.

Coachman, L. K. (1986), Circulation, water masses, and fluxes on the southeastern Bering Sea shelf, Continental Shelf Research, 5(1-2), 23-108.

Cota, G. F., H. Wang, and J. C. Comiso (2004), Transformation of global satellite chlorophyll retrievals with a regionally tuned algorithm, Remote Sensing of Environment, 90(3), 373-377.

Cota, G. F., W. G. Harrison, T. Platt, S. Sathyendranath, and V. Stuart (2003), Bio-optical properties of the Labrador Sea, Journal of Geophysical Research-Oceans, 108(C7).

D'Sa, E. J., R. G. Steward, A. Vodacek, N. V. Blough, and D. Phinney (1999), Determining optical absorption of colored dissolved organic matter in seawater with a liquid capillary waveguide, Limnology and Oceanography, 44(4), 1142-1148.

Duysens, L. N. M. (1956), The flattening of the absorption spectrum of suspensions, as compared to that of solutions, Biochimica et Biophysica Acta, 19(1), 1-12.

Feely, R. A., G. J. Massoth., and A. J. Paulson. (1981), The distribution and elemental composition of suspended particulate matter in Norton Sound and the northeastern Bering Sea shelf: Implications for Mn and Zn recycling in coastal waters, U. S. Dep. of Comm., Washington, D. C.

Gordon, H. R., O. B. Brown, R. H. Evans, J. W. Brown, R. C. Smith, K. S. Baker, and D. K. Clark (1988), A semianalytic radiance model of ocean color, Journal of Geophysical Research-Atmospheres, 93(D9), 10909-10924.

Gould, R. W., R. A. Arnone, and P. M. Martinolich (1999), Spectral dependence of the scattering coefficient in case 1 and case 2 waters, Applied Optics, 38(12), 2377-2383.

Grebmeier, J. M., J. E. Overland, S. E. Moore, E. V. Farley, E. C. Carmack, L. W. Cooper, K. E. Frey, J. H. Helle, F. A. McLaughlin, and S. L. McNutt (2006), A Major Ecosystem Shift in the Northern Bering Sea, Science, 311(5766), 1461-1464.

Helbling, E. W., B. E. Chalker, W. C. Dunlap, O. HolmHansen, and V. E. Villafane (1996), Photoacclimation of Antarctic marine diatoms to solar ultraviolet radiation, Journal of Experimental Marine Biology and Ecology, 204(1-2), 85-101.

Holm-Hansen, O., C. J. Lorenzen, R. W. Holmes, and J. D. H. Strickland (1965), Fluorometric determination of Chlorophyll, Journal du Conseil. Conseil permanent international pour l'exploration de la mer 30(1), 3-15.

Kachel, N. B., G. L. Hunt, S. A. Salo, J. D. Schumacher, P. J. Stabeno, and T. E. Whitledge (2002), Characteristics and variability of the inner front of the southeastern Bering Sea, Deep Sea Research Part II-Topical Studies in Oceanography, 49(26), 5889-5909.

Kirk, J. T. O. (1994), Light and Photosynthesis in Aquatic Ecosystems, 2 ed., Cambridge University Press, New York.

Kishino, M., M. Takahashi, N. Okami, and S. Ichimura (1985), Estimation of the spectral absorption-coefficients of phytoplankton in the sea, Bulletin of Marine Science, 37(2), 634-642.

Laurion, I., A. Lami, and R. Sommaruga (2002), Distribution of mycosporine-like amino acids and photoprotective carotenoids among freshwater phytoplankton assemblages, Aquatic Microbial Ecology, 26(3), 283-294.

Laurion, I., F. Blouin, and S. Roy (2003), The quantitative filter technique for measuring phytoplankton absorption: Interference by MAAs in the UV waveband, Limnology and Oceanography-Methods, 1, 1-9.

Lee, Z. P., K. L. Carder, and R. A. Arnone (2002), Deriving inherent optical properties from water color: a multiband quasi-analytical algorithm for optically deep waters, Applied Optics, 41(27), 5755-5772.

Lohrenz, S. E., A. D. Weidemann, and M. Tuel (2003), Phytoplankton spectral absorption as influenced by community size structure and pigment composition, Journal of Plankton Research, 25(1), 35-61.

Mathis, J. T., J. N. Cross, N. R. Bates, S. B. Moran, M. W. Lomas, C. W. Mordy, and P. J. Stabeno (2010), Seasonal distribution of dissolved inorganic carbon and net community production on the Bering Sea shelf, Biogeosciences, 7(5), 1769-1787.

Matsuoka, A., Y. Huot, K. Shimada, S. I. Saitoh, and M. Babin (2007), Bio-optical characteristics of the western Arctic Ocean: implications for ocean color algorithms, Canadian Journal of Remote Sensing, 33(6), 503-518.

Matsuoka, A., V. Hill, Y. Huot, M. Babin, and A. Bricaud (2011), Seasonal variability in the light absorption properties of western Arctic waters: Parameterization of the individual components of absorption for ocean color applications, Journal of Geophysical Research, 116(C2), C02007.

Maynard, N. G., and D. K. Clark (1987), Satellite color observations of spring blooming in Bering Sea shelf waters during the ice edge retreat in 1980, Journal of Geophysical Research, 92(C7), 7127-7139.

Miller, R. L., M. Belz, C. Del Castillo, and R. Trzaska (2002), Determining CDOM absorption spectra in diverse coastal environments using a multiple pathlength, liquid core waveguide system, Continental Shelf Research, 22(9), 1301-1310.

Mitchell, B. G. (1990), Algorithms for determining the absorption coefficients for aquatic particulates using the quantitative filter technique, paper presented at Ocean Optics X, SPIE.

Mitchell, B. G. (1992), Predictive biooptical relationships for polar oceans and marginal ice zones, Journal of Marine Systems, 3(1-2), 91-105.

Mitchell, B. G., and O. Holm-Hansen (1991), Bio-optical properties of Antarctic Peninsula waters - differentiation from temperate ocean models, Deep Sea Research Part I-Oceanographic Research Papers, 38(8-9), 1009-1028.

Mitchell, B. G., M. Kahru, J. Wieland, and M. Stramska (2003), Determination of spectral absorption coefficients of particles, dissolved materials and phytoplankton for discrete water samples, in Ocean Optics Protocols For Satellite Ocean Color Sensor Validation, Revision 4, Volume 4: Inherent optical properties: instruments, characterization, field measurements and data analysis protocols, edited, NASA Tech. Rep., Greenbelt, Maryland.

Mobley, C. D. (1994), Light and Water: Radiative Transfer in Natural Waters, Academic Press.

Moisan, T. A., and B. G. Mitchell (1999), Photophysiological acclimation of Phaeocystis antarctica Karsten under light limitation, Limnology and Oceanography, 44(2), 247-258.

Moore, L., R. Goericke, and S. Chisholm (1995), Comparative physiology of Synechococcus and Prochlorococcus: influence of light and temperature on growth, pigments, fluorescence and absorptive properties, Marine Ecology Progress Series, 116, 259-275.

Morel, A., and A. Bricaud (1981), Theoretical results concerning light absorption in a discrete medium, and application to specific absorption of phytoplankton, Deep Sea Research Part 1-Oceanographic Research Papers, 28(11), 1375-1393.

Morel, A., and S. Maritorena (2001), Bio-optical properties of oceanic waters: A reappraisal, Journal of Geophysical Research-Oceans, 106(C4), 7163-7180.

Müller-Karger, F. E., C. R. McClain, R. N. Sambrotto, and G. C. Ray (1990), A comparison of ship and coastal zone color scanner mapped distribution of phytoplankton in the southeastern Bering Sea, Journal of Geophysical Research, 95(C7), 11483-11499.

Naik, P., E. J. D'Sa, J. I. Goes, and H. R. Gomes (2010), Assessment of particulate absorption properties in the southeastern Bering Sea from in-situ and remote sensing data, Journal of Applied Remote Sensing, 4(1), 043561.

Pegau, W. S., D. Gray, and J. R. V. Zaneveld (1997), Absorption and attenuation of visible and near-infrared light in water: dependence on temperature and salinity, Applied Optics, 36(24), 6035-6046.

Riegger, L., and D. Robinson (1997), Photoinduction of UV-absorbing compounds in Antarctic diatoms and Phaeocystis antarctica, Marine Ecology Progress Series, 160, 13-25.

Sasaki, H., S.-I. Saitoh, and M. Kishino (2001), Bio-optical properties of seawater in the western Subarctic Gyre and Alaskan Gyre in the subarctic North Pacific and the southern Bering Sea during the Summer of 1997, Journal of Oceanography, 57(3), 275-284.

Schallenberg, C., M. R. Lewis, D. E. Kelley, and J. J. Cullen (2008), Inferred influence of nutrient availability on the relationship between Sun-induced chlorophyll fluorescence and incident irradiance in the Bering Sea, Journal of Geophysical Research-Oceans, 113(C7), C07046.

Schumacher, J. D., and P. J. Stabeno (1998), The continental shelf of the Bering Sea, John Wiley and Sons, Inc., New York, NY.

Siegel, D. A., S. Maritorena, N. B. Nelson, and M. J. Behrenfeld (2005), Independence and interdependencies among global ocean color properties: Reassessing the bio-optical assumption, Journal of Geophysical Research-Oceans, 110(C7).

Sigler, M. F., H. R. Harvey, C. J. Ashjian, M. W. Lomas, J. M. Napp, P. J. Stabeno, and T. I. V. Pelt (2010), How Does Climate Change Affect the Bering Sea Ecosystem?, EOS, Transactions American Geophysical Union, 91(48), 457.

Sosik, H. M., M. Vernet, and A. D. Mitchell (1992), A comparison of particulate absorption properties between high- and mid-latitude surface waters, Antarctic Journal of the United States, 27, 162-164.

Stabeno, P. J., J. Hunt, G. L.,, J. M. Napp, and J. D. Schumacher (2006), Physical forcing of ecosystem dynamics on the Bering Sea shelf, Harvard University Press, Cambridge, MA.

Stabeno, P. J., N. Kachel, C. Mordy, D. Righi, and S. Salo (2008), An examination of the physical variability around the Pribilof Islands in 2004, Deep Sea Research Part II-Topical Studies in Oceanography, 55(16-17), 1701-1716.

Stramska, M., D. Stramski, S. Kaczmarek, D. B. Allison, and J. Schwarz (2006), Seasonal and regional differentiation of bio-optical properties within the north polar Atlantic, Journal of Geophysical Research-Oceans, 111(C8).

Stramski, D., and A. Morel (1990), Optical properties of photosynthetic picoplankton in different physiological states as affected by growth irradiance, Deep Sea Research Part a-Oceanographic Research Papers, 37(2), 245-266.

Twardowski, M. S., E. Boss, J. M. Sullivan, and P. L. Donaghay (2004), Modeling the spectral shape of absorption by chromophoric dissolved organic matter, Marine Chemistry, 89(1-4), 69-88.

Wang, J., G. F. Cota, and D. A. Ruble (2005), Absorption and backscattering in the Beaufort and Chukchi Seas, Journal of Geophysical Research-Oceans, 110(C4).

Westberry, T., M. J. Behrenfeld, D. A. Siegel, and E. Boss (2008), Carbon-based primary productivity modeling with vertically resolved photoacclimation, Global Biogeochemical Cycles, 22(2).

Zaneveld, J. R. V., J. C. Kitchen, and C. C. Moore (1994), Scattering error correction of reflecting-tube absorption meters, paper presented at Ocean Optics XII, SPIE, Bergen, Norway.

CHAPTER 5: ASSESSMENT OF PARTICULATE ABSORPTION PROPERTIES IN THE SOUTHEASTERN BERING SEA FROM IN-SITU AND REMOTE SENSING DATA[2]

Introduction

In recent decades satellites have offered synoptic views across large spatial and temporal scales in the global oceans. Ocean color sensors such as MODIS and SeaWiFS have shown the utility of using ocean color data for understanding the oceans role in global biogeochemical cycles. Although ocean color imagery has shown that high-latitude oceans are among the most productive in the world, but very few in-situ observations are present to validate and quantify the satellite observations. Also frequent cloud and ice cover reduce good imagery and contaminate retrieval of biogeochemical variables from ocean reflectance observations. The combinations of the above problems along with difficulties in atmospheric corrections at high latitudes have limited the usefulness of ocean color imagery. Recently the ocean color community has directed its attention towards such high latitude regions as the sensitivity of these regions under climate changing scenarios needs to be understood [*Cota et al.*, 2004; *Dierssen and Smith*, 2000].

Absorption coefficients are very important bio-optical properties in the study of primary production, carbon flux [*Behrenfeld et al.*, 2005], water quality [*Mueller*, 2000] and even physical processes in the ocean [*Rochelle-Newall and Fisher*, 2002]. The total absorption coefficient of seawater is the sum of individual components within the water column, namely colored dissolved organic matter (CDOM), phytoplankton and non-algal particulate matter (NAP) and can be expressed as:

$$a_T(\lambda) = a_W(\lambda) + a_{CDOM}(\lambda) + a_{PHY}(\lambda) + a_{NAP}(\lambda) \quad \text{(Eq. 1)}$$

[2] Chapter 5 is reprinted with permission from the 'Journal of Applied Remote Sensing.'

$$a_P(\lambda) = a_{PHY}(\lambda) + a_{NAP}(\lambda) \quad \text{(Eq. 2)}$$

where $a_W(\lambda)$, $a_{CDOM}(\lambda)$, $a_{PHY}(\lambda)$, $a_{NAP}(\lambda)$ and $a_P(\lambda)$ are absorption coefficients due to pure water, CDOM, phytoplankton, non-algal particulate matter and particulate matter, respectively.

Chlorophyll distributions and primary productivity studies illustrate that the Bering Sea is a highly productive region, with primary productivity ranging from 175–275 g C m^{-2} yr^{-1} near the shelf break also known as the 'greenbelt' [*Springer et al.*, 1996]. The absorption of light by particulate and dissolved matter transforms the sub-surface light field and is important for estimation of primary productivity from remote sensing over large spatial and temporal scales. Such data on a decadal scale provides a synoptic view which can be used to study variability due to climate shifts. The Bering Sea has been subjected to such large scale climatic variations that have lead to large variations in biology of the region [*Hare and Mantua*, 2000]. Bio-optical data in the Bering Sea have very limited spatial and temporal coverage. Recently conducted studies have shown seasonal and inter-annual variability of chlorophyll-a from monthly SeaWiFS climatologies (http://seawifs.gsfc.nasa.gov) for 1998–2002 [*Iida and Saitoh*, 2007].

The southeastern Bering Sea shelf waters during summer can be characterized by their hydrographic structure and currents into three domains coastal (<50 m depth), middle (50 - 100 m depth) and outer (100 - 200 m depth) domain [*Kachel et al.*, 2002] (Figure 5.1). The shelf is broad and shallow with a steep shelf break and during summer changes in water column density are driven by temperature rather than by salinity. The coastal domain under the influence of tidal and wind mixing is well mixed, the middle domain is characterized by a tidally mixed lower layer and a well mixed surface layer as warm surface waters together with low wind energy cause inefficient wind mixing of the water column. The outer shelf domain is similar to the

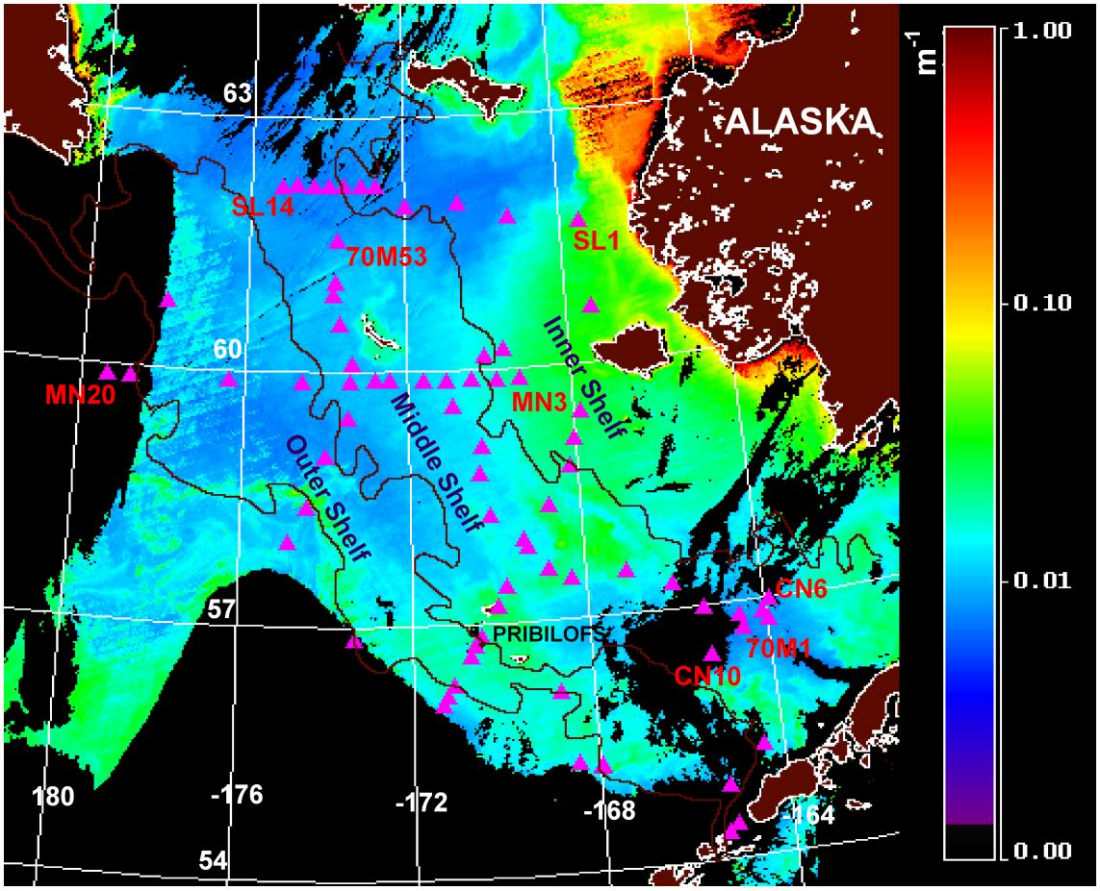

Figure 5.1. Locations of stations sampled during the cruise in July 2008 overlaid on a MODIS Aqua QAA - $a_{PHY}(443)$ image collected on July, 7, 2008.

middle domain except that the wind-mixed surface layer and a tidally mixed bottom layer are separated by a transition layer. Previous studies on bio-optical properties in high latitudes focused on the impact of the absorption properties on the retrieval of chlorophyll-a primarily from in-situ remote sensing reflectance ($R_{rs}(\lambda)$) data, with little or no utilization of $R_{rs}(\lambda)$ from satellite data [*Cota et al.*, 2004; *Dierssen and Smith*, 2000]. Further, these studies did not attempt to match-up in-situ and satellite retrieved absorption products. The main goal of this study is to test the potential of Lee et al., (2002) [*Lee et al.*, 2002] Quasi Analytical Algorithm (QAA) for retrieval of absorption (phytoplankton and non-algal particulate plus CDOM absorption) using MERIS and MODIS ocean color satellites. The main objectives of this study

are (1) describe the variability of particulate absorption in the study region which control the variability in $R_{rs}(\lambda)$, (2) describe particulate ($a_P(\lambda)$), phytoplankton ($a_{PHY}(\lambda)$) and specific phytoplankton ($a^*_{PHY}(\lambda)$) absorption in relation to chlorophyll-a, (3) conduct match-up of in-situ and QAA retrieved absorption coefficients, and (4) relate simple two band $R_{rs}(\lambda)$ ratio to the in-situ absorption coefficients in the study area.

Methods

In-situ Water Sampling

Station locations that were sampled are shown in Figure 5.1. Sampling was conducted along cross shelf as well as along shelf transects covering the coastal, middle and outer domain during a cruise in July 2008. At every station, salinity, temperature and density profiles were recorded with a SeaBird SBE-911 plus CTD unit and water samples were collected for absorption analyses at the surface using Niskin bottles attached to the CTD.

Absorption – Phytoplankton, NAP and CDOM

Particulate absorption was determined using the standard QFT procedure [*Mitchell et al.*, 2002]. The discrete water samples were filtered under low vacuum on 0.7μm Whatman GF/F glass fiber filters and stored in liquid nitrogen until analysis for particulate absorption and chlorophyll-a. The volume to be filtered ranged from 100 – 2000 ml and care was taken not to overload the filter.

For particulate absorption, samples were first thawed to room temperature after removing from liquid nitrogen by keeping them in the dark at room temperature for half an hour. Filter paper blanks were prepared by filtering 15 ml of filtered seawater corresponding to the station under analysis. Absorbance measurements of total particulate matter ($A_P(\lambda)$) were done by scanning the sample filter paper using a shipboard WPI Ultrapath^{TM} hyperspectral waveguide

capillary system from 190 – 722 nm at 1 nm intervals. The absorbance was converted to absorption coefficient by using the equation given below:

$$a_P(\lambda) = \frac{2.303[A_P(\lambda)]}{(V/A)} \quad \text{(Eq. 3)}$$

where $a_P(\lambda)$ (m^{-1}) is the total particulate absorption, V (m^3) is the volume filtered, and A (m^2) the area of the filter paper.

To separate the phytoplankton pigments within the particulate matter from NAP, methanol extraction was done [*Kishino et al.*, 1985]. The sample filter paper was scanned again following the procedure described above to obtain non-algal particulate (NAP) absorbance ($A_{NAP}(\lambda)$). $A_{NAP}(\lambda)$ was converted to $a_{NAP}(\lambda)$ using the equation shown above. The phytoplankton absorption ($a_{PHY}(\lambda)$ (m^{-1})) spectra were obtained by subtracting the $a_{NAP}(\lambda)$ (m^{-1}) from $a_P(\lambda)$ using the relation:

$$a_{PHY}(\lambda) = a_P(\lambda) - a_{NAP}(\lambda) \quad \text{(Eq. 4)}$$

To correct for residual and scattering offsets in the absorption measurements the mean value from 700 – 722 nm was subtracted from the entire spectra [*Mitchell et al.*, 2002] and the Cleveland and Weidemann (1993) [*Cleveland and Weidemann*, 1993] procedure was utilized to correct for pathlength amplification. Chlorophyll-a specific phytoplankton absorption ($a^*_{PHY}(\lambda)$ (m^2 (mg chl *a*)$^{-1}$)) was obtained by dividing $a_{PHY}(\lambda)$ by chlorophyll-a (mg m^{-3}). Chlorophyll-a concentrations were determined fluorometrically with 90% acetone [*Holm-Hansen et al.*, 1965] in a Turner Designs fluorometer.

For CDOM absorption ($a_{CDOM}(\lambda)$), discrete water samples were filtered immediately after collection through 0.2 μm nucleopore membrane filters under low vacuum. Filtered samples were stored in acid cleaned, pre-combusted amber colored glass bottles and stored at 4 ^oC. The filtered samples were allowed to reach ambient room temperature to minimize temperature bias

between samples and blank (Milli-Q water). Absorbance measurements of CDOM ($A_{CDOM}(\lambda)$) were done on a shipboard hyperspectral waveguide capillary system from 190 – 722 nm at 1 nm intervals using Milli-Q water as blank. The absorbance data were corrected for baseline fluctuations by subtraction of the mean value over 5 nm interval of the measured absorbance at 700 nm from each wavelength [*Mitchell et al.*, 2002]. The $a_{CDOM}(\lambda)$ (m^{-1}) for pathlength, L (m^{-1}) was calculated according to:

$$a_{CDOM}(\lambda) = \frac{2.303[A_{CDOM}(\lambda)]}{(L)} \qquad \text{(Eq. 5)}$$

Remote Sensing Data – MERIS and MODIS Aqua Imagery

Level 1 MODIS Aqua imagery from July 3 - July 31, 2008 was obtained from the OBPG NASA Ocean Color website (http://oceancolor.gsfc.nasa.gov/) and was processed to Level 2 using the SeaDAS 5.3 software package. The standard atmospheric correction algorithm was used which is based on the Gordon and Voss (1999) approach [*Gordon and Voss*, 1999]. The pixels were masked out after atmospheric correction by the following flags: land, cloud or ice, high top-of-atmosphere radiance, low normalized water-leaving radiance at 551 nm, stray light, sun-glint, or atmospheric correction failure. The MERIS Level 2 data was obtained from the ESA website (http://merci-srv.eo.esa.int/merci/) and processed using BEAM 4.5.3 software. The documentation for MERIS products and atmospheric correction algorithms used for processing of data from Level 1 to Level 2 can be found at the ESA website (http://earth.esa.int/pcs/ envisat/meris/ documentation/). The Lee et al., (2002) QAA (version 5) [*Lee et al.*, 2002], http://www.ioccg.org/groups/Software_OCA/ QAA_v5.pdf] was used to derive absorption products from satellite $R_{rs}(\lambda)$ (sr^{-1}). The QAA was selected amongst other semi-analytical models (e.g. GSM, Carder) as it output greater positive values of absorption and least number of pixels

with algorithm fail. The QAA retrieves $a_{PHY}(\lambda)$ but does not retrieve $a_{NAP}(\lambda)$, however it retrieves a combination of NAP and CDOM absorption ($a_{DG}(\lambda)$). Hence for analyses of in-situ and remote sensing of $a_{DG}(\lambda)$, the in-situ $a_{CDOM}(\lambda)$ was added to in-situ $a_{NAP}(\lambda)$ to obtain in-situ $a_{DG}(\lambda)$. A 3 x 3 pixel box size (1.2 km/pixel for MERIS and 1 km/pixel for MODIS) with a time difference of ±8 hours between the in-situ sampling and satellite overpass was chosen for in-situ and satellite data match-up analyses.

Results and Discussion

Spatial Distribution of In-situ $a_{PHY}(443)$, $a_{NAP}(443)$ and $a_P(443)$

The $a_{PHY}(443)$, $a_{NAP}(443)$, and $a_P(443)$ reveal a range from 0.004 – 0.097 m^{-1}, 0.002 – 0.048 m^{-1}, and 0.007 – 0.112 m^{-1} in the study area, respectively. The surface distribution of $a_{PHY}(443)$ revealed relatively higher $a_{PHY}(443)$ around the Pribilof Islands which is mostly due to the enhanced production near the islands caused by interaction of tides and currents with bathymetry [*Kachel et al.*, 2002; *Stabeno et al.*, 2008](Figure 5.2). The highest values were seen near the Pribilof Islands and the lowest values were seen on the northern part of the outer-shelf in the study region (Figure 5.2a). The $a_{NAP}(443)$ surface distribution generally showed higher values closer to the coast and lower values were seen on the outer-shelf except near the Pribilofs where there seems to be some influence of elevated biomass on $a_{NAP}(443)$ (Figure 5.2b). The relative contribution of $a_{PHY}(443)$ and $a_{NAP}(443)$ to $a_P(443)$ was highly variable and ranged from 15% - 90% and 10% - 85% respectively, suggesting that different parts of the study region have variable contributions from $a_{PHY}(443)$ and $a_{NAP}(443)$. Figure 5.2c shows this variability in terms of $a_{PHY}(443)$ by $a_P(443)$ ratio; the inner-shelf shows the least and the middle-shelf the highest contribution of $a_{PHY}(443)$ to $a_P(443)$. The northern part of the outer-shelf shows lower contribution of $a_{PHY}(443)$ to $a_P(443)$ as compared to the southern part. On average the

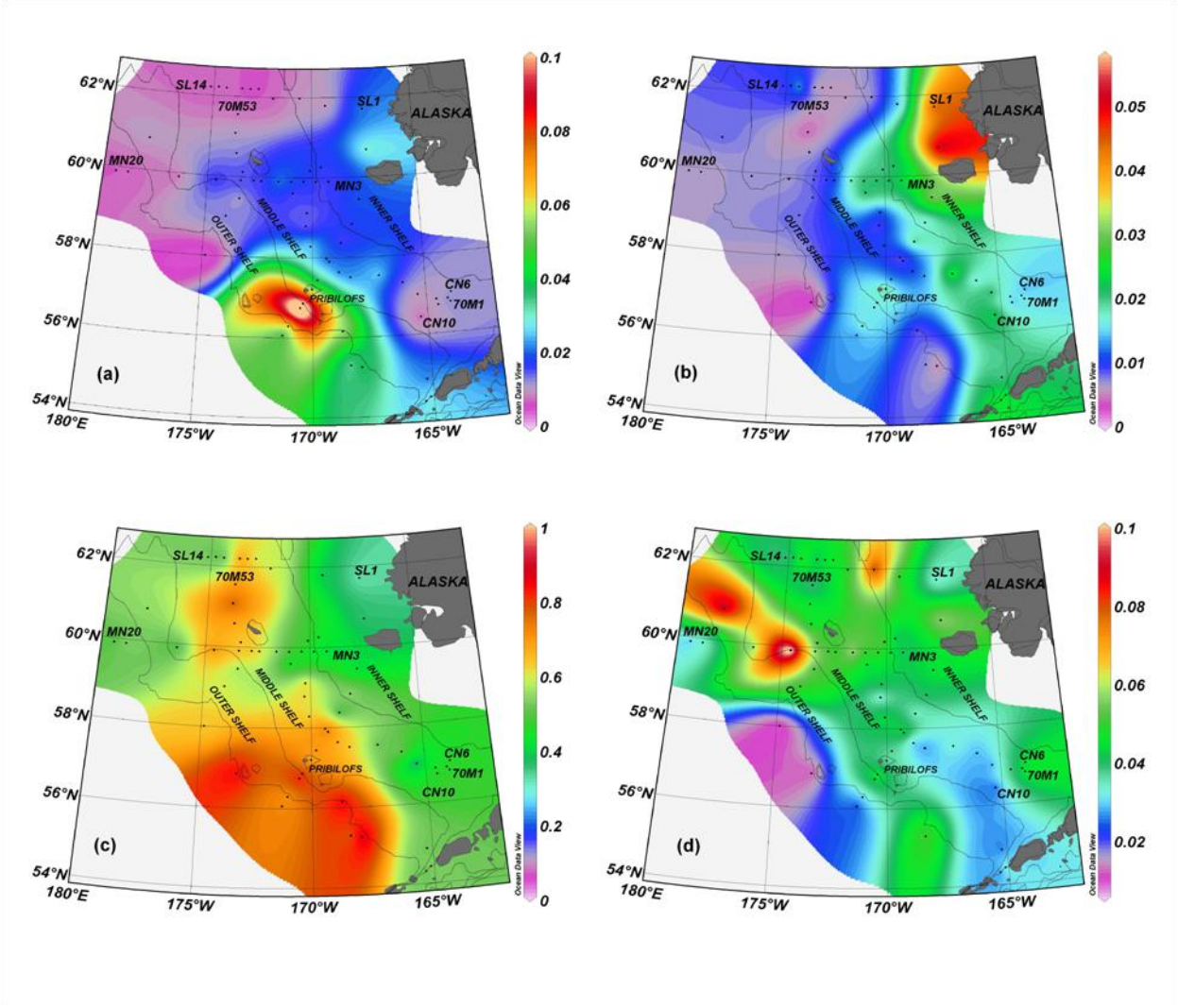

Figure 5.2. Surface distribution of (a) phytoplankton absorption, $a_{PHY}(443)$ (m^{-1}) (b) Non-algal/detrital absorption, $a_{NAP}(443)$ (m^{-1}), (c) ratio of phytoplankton and total particulate absorption, $a_{PHY}(443)/a_P(443)$ and (d) chlorophyll-a specific phytoplankton absorption, $a^*_{PHY}(443)$ (m^2 (mg chl *a*)$^{-1}$) at 443 nm.

contribution from $a_{PHY}(443)$ was higher (~ 65%) as compared to $a_{NAP}(443)$ (~ 35%) to $a_P(443)$. A relatively higher correlation between $a_{PHY}(443)$ and $a_P(443)$ ($R^2 = 0.80$, n = 45, $p<0.001$), and lower correlation between $a_{NAP}(443)$ and $a_P(443)$ ($R^2 = 0.65$, n = 45, $p<0.001$) was observed in the study area. The $a^*_{PHY}(443)$ surface distribution shows large variability and is far from being constant (Figure 5.2d).. In general the southern part of the study region showed lower values as compared to the northern part of the study region. High values (> 0.06 m^2 (mg chl *a*)$^{-1}$) are

observed where the chlorophyll-a concentration is < 0.2 mg m^{-3} and low values (< 0.06 m^2 (mg chl $_a$)$^{-1}$) are observed where the chlorophyll-a concentration is > 0.2 mg m^{-3}. The high values indicate a low packaging effect and/or change in pigment composition. A detailed description on the spatial distribution of absorption coefficients across and along the shelf is covered in Naik et al. (2009a) [*Naik et al.*, 2009b] and Naik et al., (2009b) [*Naik et al.*, 2009a], respectively.

In-situ $a_{PHY}(443)$, $a_P(443)$ Relation with Chlorophyll-a

A power function is applied to $a_{PHY}(443)$, $a_P(443)$ and chlorophyll-a relationship in accordance with Bricaud et al., (1998) [*Bricaud et al.*, 1998] to investigate $a_{PHY}(443)$ and $a_P(443)$ in the southeastern Bering Sea in comparison to other regions (Figure 5.3). We found a good correlation between $a_{PHY}(443)$, $a_P(443)$, and chlorophyll-a consistent with studies done both in the higher latitudes [*Cota et al.*, 2004; *Matsuoka et al.*, 2007] as well as lower latitudes [*Bricaud et al.*, 1998](Table 5.1). The Bricaud et al., (1998) exponents for $a_{PHY}(443)$ and $a_P(443)$ are lower whereas the amplitude is higher for $a_{PHY}(443)$ and lower for $a_P(443)$ compared to our study. The power fit applied to $a_{PHY}(443)$ and chlorophyll-a for our data is significantly different (t-test, $p < 0.001$) from the Bricaud et al., (1998) fit.

Table 5.1. Coefficients, R2 and number of samples (n) for the power fit expressed as ax(443) = Ax(443)*[chlorophyll-a]Bx(443). Where x = P - particulate absorption or PHY – phytoplankton absorption.

	This study (ANOVA; p<0.0001)				**Bricaud et al., 1998**			**Matsuoka et al., 2007**		
	A	**B**	**R^2**	**n**	**A**	**B**	**R^2**	**A**	**B**	**R^2**
$a_{PHY}(443)$ vs chlorophyll-a	0.0275	0.741	0.75	45	0.0378	0.627	0.90	0.0288	0.820	0.80
$a_P(443)$ vs chlorophyll-a	0.060	0.772	0.70	45	0.0520	0.635	0.91	0.0403	0.659	0.75

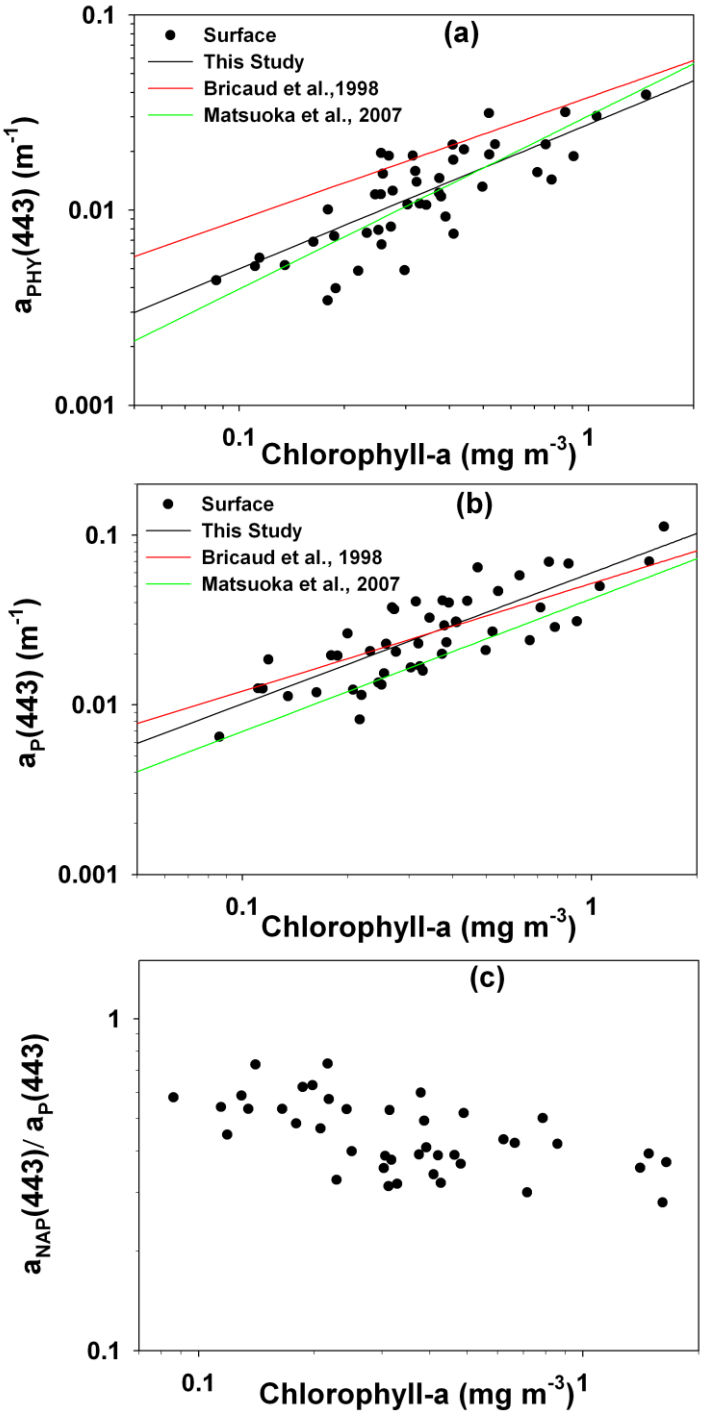

Figure 5.3. Power fit applied to (a) phytoplankton absorption, $a_{PHY}(443)$, and (b) particulate absorption, $a_P(443)$, and chlorophyll-a relation, (c) ratio of $a_{NAP}(443)$ to $a_P(443)$ versus chlorophyll-a. The red and blue solid lines are power fits derived from Refs. 19 and 20 are shown for comparison. The statistics are shown in Table 5.1.

The coefficients of the fit for $a_{PHY}(443)$ and chlorophyll-a obtained for our study are remarkably close to those found by Matsuoka et al., (2007) [*Matsuoka et al.,* 2007] in western Arctic Ocean. This suggests that methodological differences involved in obtaining $a_{PHY}(443)$ through the QFT method are not an issue and the trends seen are characteristic of these high latitude oceans. One reason attributed for the difference between higher and lower latitudes is due to change in pigment composition and/or pigment packaging; the separation of these effects is difficult in natural water samples [*Bricaud et al.,* 1998; *Matsuoka et al.,* 2007]. These effects are explored through the $a^*_{PHY}(\lambda)$ and chlorophyll-a in the next section. This emphasizes a need for a regional/seasonal approach to ocean color algorithm development and applications. Although high correlation and tendency of increasing $a_{PHY}(\lambda)$ with chlorophyll-a is comparable with Bricaud et al., 1998, a systematic departure is seen over the entire range of chlorophyll-a between our fit and Bricaud et al., 1998 fit.

In order to investigate these difference further, we observed the variability in $a_{PHY}(\lambda)$ at the blue and red part of the spectrum. The $a_{PHY}(\lambda)$ was highly variable in the blue part of the spectrum (e.g., 0.004 - 0.097 m^{-1} at 443 nm) as compared to the red part of the spectrum (e.g., 0.001 - 0.016 m^{-1} at 667 nm); an additional indication of change in pigment composition or pigment package effect [*Bricaud et al.,* 1998; *Matsuoka et al.,* 2007; *Wang et al.,* 2005]. The trends for $a_P(443)$ versus chlorophyll-a for the above mentioned studies are not significantly different from each other. The non-linearity in the trend is mainly at lower chlorophyll-a values where the contribution from $a_{PHY}(443)$ and $a_{NAP}(443)$ is almost equal at some stations (Figure 5.2c). The contribution of $a_{PHY}(443)$ and $a_{NAP}(443)$ to $a_P(443)$ is highly variable at lower chlorophyll-a concentrations (< 0.5 mg m^{-3}). From the difference in coefficients of the power fit applied for $a_{PHY}(443)$ and $a_P(443)$ we saw that the $a_{NAP}(443)$ made a considerable contribution to

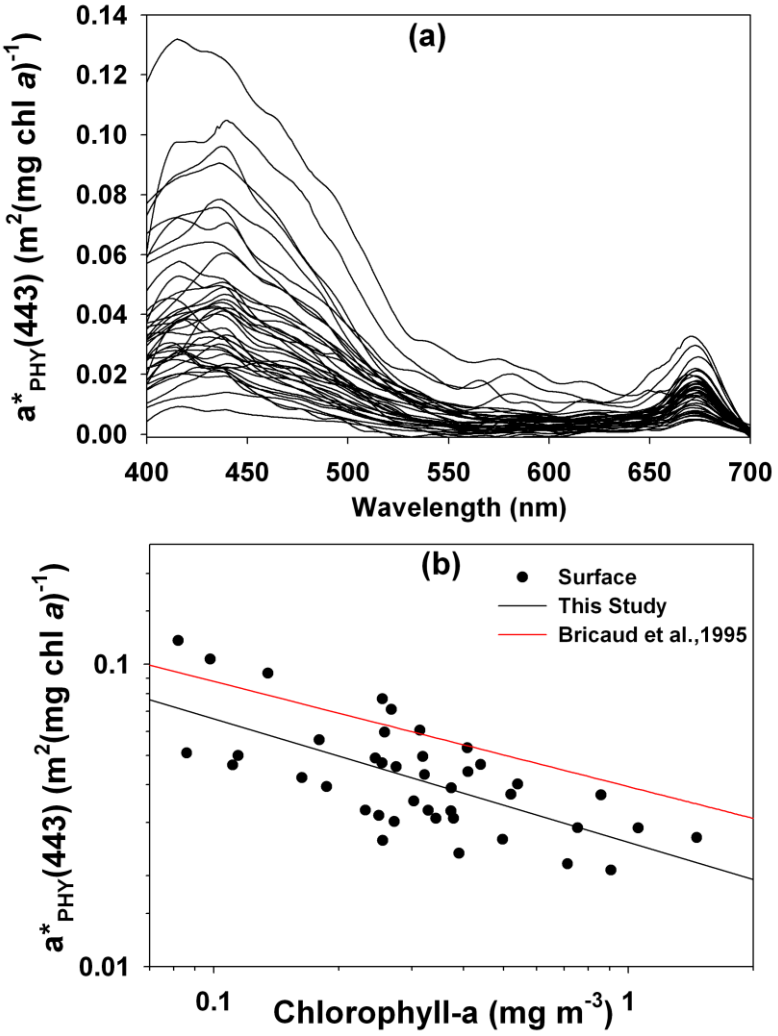

Figure 5.4. Variability in (a) in-situ $a^*_{PHY}(\lambda)$ spectra for all stations, and (b) $a^*_{PHY}(443)$ with chlorophyll-a ($R^2 = 0.52$; N = 45, ANOVA; $p < 0.0001$). The red solid line is the fit obtained from Ref. 19 is shown for comparison.

the observed relation. Further, the ratio of $a_{NAP}(\lambda)$ to $a_P(\lambda)$ at 443 nm showed an inverse relation with chlorophyll-a (Figure 5.3c) arguing that an increase in $a_{NAP}(443)$ relative to $a_{PHY}(443)$ in low chlorophyll-a regions is responsible for the observed trend between $a_P(443)$ and chlorophyll-a. In general, the $a_{PHY}(443)$ and $a_P(443)$ as a function of chlorophyll-a are lower in the study region as compared to other mainly lower latitude regions, consistent with studies done at higher latitudes .

In-situ $a^*_{PHY}(443)$ Relation with Chlorophyll-a

Variations in light level, nutrients and phytoplankton species composition cause seasonal and regional variation of $a^*_{PHY}(\lambda)$ [*Sathyendranath et al.,* 1999]. For our study region we found a large variation in $a^*_{PHY}(\lambda)$ spectra with variability greater in the blue (0.005 – 0.120 m^2 (mg chl $_a$)$^{-1}$ at 443 nm) than the red region of the spectrum (0.003 – 0.0302 m^2 (mg chl a)$^{-1}$ at 676 nm) (Figure 5.4a) [*Naik et al.*, 2009a; *Naik et al.*, 2009b].

The $a^*_{PHY}(676)$ variability can be mainly attributed to package effect, but variations in $a^*_{PHY}(443)$ may be due to package effect and/or changes in pigment composition [*Fujiki and Taguchi*, 2002]. As we observed more variability at 443 nm than at 676 nm, change in pigment composition may be the key source of variability of $a^*_{PHY}(\lambda)$. A decreasing trend of $a^*_{PHY}(443)$ from 0.120 - 0.005 m^2 (mg chl $_a$)$^{-1}$ is observed with increasing chlorophyll-a concentration from 0.05 – 2 mg m^{-3} (Figure 5.4b). The Bricaud et al., (1995) fit is higher than the fit obtained for our study for almost the whole range of chlorophyll-a concentration. This indicates that $a^*_{PHY}(443)$ is consistently lower for our study as compared to Bricaud et al., (1995) study, further indicating that change in pigment composition and/or change in pigment packaging exist in our study region consistent with studies done at higher latitudes [*Matsuoka et al.*, 2007; *Wang et al.*, 2005]. In particular the blue to red ratio of $a^*_{PHY}(\lambda)$ for e.g., $a_{PHY}^*(443)/a_{PHY}^*(676)$ in this study varied from 6.9 to 1.1 demonstrating approximately a 6 fold decrease as chlorophyll-a increased from 0.08 to 1.46 mg m^{-3}. The $a_{PHY}^*(443)/a_{PHY}^*(676)$ inverse relation with chlorophyll-a is consistent with Bricaud et al. (1995). This ratio is found to be strongly correlated with the ratio of accessory pigments to chlorophyll-a, as the accessory pigments are known to absorb significantly higher amount of light in the blue region than in the red region of the spectrum [*Lohrenz et al.*, 2003]. Similar trends are seen for $a^*_{PHY}(\lambda)$ with chlorophyll-a concentration over the whole visible spectrum. These results have a large effect when parameterization of $a_{PHY}(\lambda)$ is done based

solely on the concentration of the main pigment. For remote sensing applications involving empirical algorithms, the change in pigment composition and/or packaging effect influenced $R_{rs}(\lambda)$ ratios, however this effect would be subtle as compared to the effect of the bulk absorption properties. Empirical algorithms that utilize blue (412 nm or 443 nm or 490 nm) to green (555 nm or 560 nm) $R_{rs}(\lambda)$ ratios to estimate chlorophyll-a concentration, are overestimated when $a^*_{PHY}(\lambda)$ is lower which results in chlorophyll-a concentrations to be underestimated in the study region [*Muller-Karger et al.*, 1990]. Further, even the semi-analytical algorithms like Carder, GSM01 and QAA algorithm are affected by $a^*_{PHY}(\lambda)$ variability as they use $R_{rs}(\lambda)$ ratios for estimation of absorption.

Comparison of Satellite Retrieved and In-situ Absorption

Use of satellite data in the study region, like other high latitude regions, are often hampered by frequent ice and cloud cover. The Bering Sea is essentially ice free during summers (our study period) but thick cloud cover limited the number of clear sky images. The MODIS and MERIS overpass and in-situ sampling time window was fixed at ± 8 hours for this analysis. Very few collocated stations were obtained for MODIS and are included in this analysis for qualitative and comparison purpose. The total absorption ($a_T(\lambda)$) and backscattering coefficients ($b_b(\lambda)$) control the spectral variability of $R_{rs}(\lambda)$ and can be expressed as:

$$R_{rs}(\lambda) \approx \frac{b_b(\lambda)}{a_T(\lambda) + b_b(\lambda)} \qquad \text{(Eq. 6)}$$

The satellite retrieved $R_{rs}(\lambda)$ from MODIS and MERIS are shown in Figure 5.5a and Figure 5.5b, respectively. About half of the match-up stations showed blue and green reflectance's high and low, respectively, similar to other high latitude regions [*Dierssen and Smith*, 2000]. The Rrs(λ) spectra and total absorption minus absorption by pure water ($a_{T\text{-}W}(\lambda)$) spectra were

separated into groups based on geographical locations (Figure 5.1) along the transects CN, MN, SL and 70M (Figure 5.5(c-j)). One way ANOVA and *post hoc* Tukey tests were conducted in MATLAB statistics toolbox 7.3 to find significance between groups. There were significant differences in magnitudes and spectral shapes of $R_{rs}(\lambda)$ in the blue region of the spectra along the transects (ANOVA; CN transect – p = 0.002, CN6 significantly different from CN8 and CN10, MN transect - p = 0.01, MN5 significantly different from MN20, SL transect - p = 0.004, SL8 significantly different from SL13, and 70M transect - p = 0.003, 70M4 significantly different from 70M7 and 70M10, 70M7 significantly different from 70M4 and 70M14) as well as across transects (ANOVA, p = 0.002, CN transect is significantly different from MN and SL transect), which show that different types of water masses exist in the study region. This is supported by the corresponding varied $a_{T\text{-}W}(\lambda)$ obtained in the study area. The lowest values of $a_{T\text{-}W}(\lambda)$ and corresponding highest values of $R_{rs}(\lambda)$ were obtained for the most offshore stations where the clearest waters were found containing lowest biomass levels and in-situ particulate absorption. At these stations the $R_{rs}(\lambda)$ are known to be most influenced by $a_{NAP}(\lambda)$ and $a_{CDOM}(\lambda)$ rather than $a_{PHY}(443)$. So, the total absorption coefficient of surface waters often dominates the variability of $R_{rs}(\lambda)$ in our study. Hence absorption properties can be retrieved using simple reflectance ratios or semi-analytical algorithms. We will focus on comparing in-situ and satellite derived $a_{PHY}(\lambda)$ and $a_{DG}(\lambda)$.

Variation of $a_{PHY}(\lambda)$ and $a_{DG}(\lambda)$ with MERIS retrieved $R_{rs}(\lambda)$ Band Ratios

Empirical methods in which band ratios of ocean $R_{rs}(\lambda)$ are related to surface water properties such as chlorophyll-a concentration, absorption, suspended matter are common in ocean color remote sensing [*D' Sa et al.*, 2007; *O' Reilly et al.*, 1998]. The basic thought behind

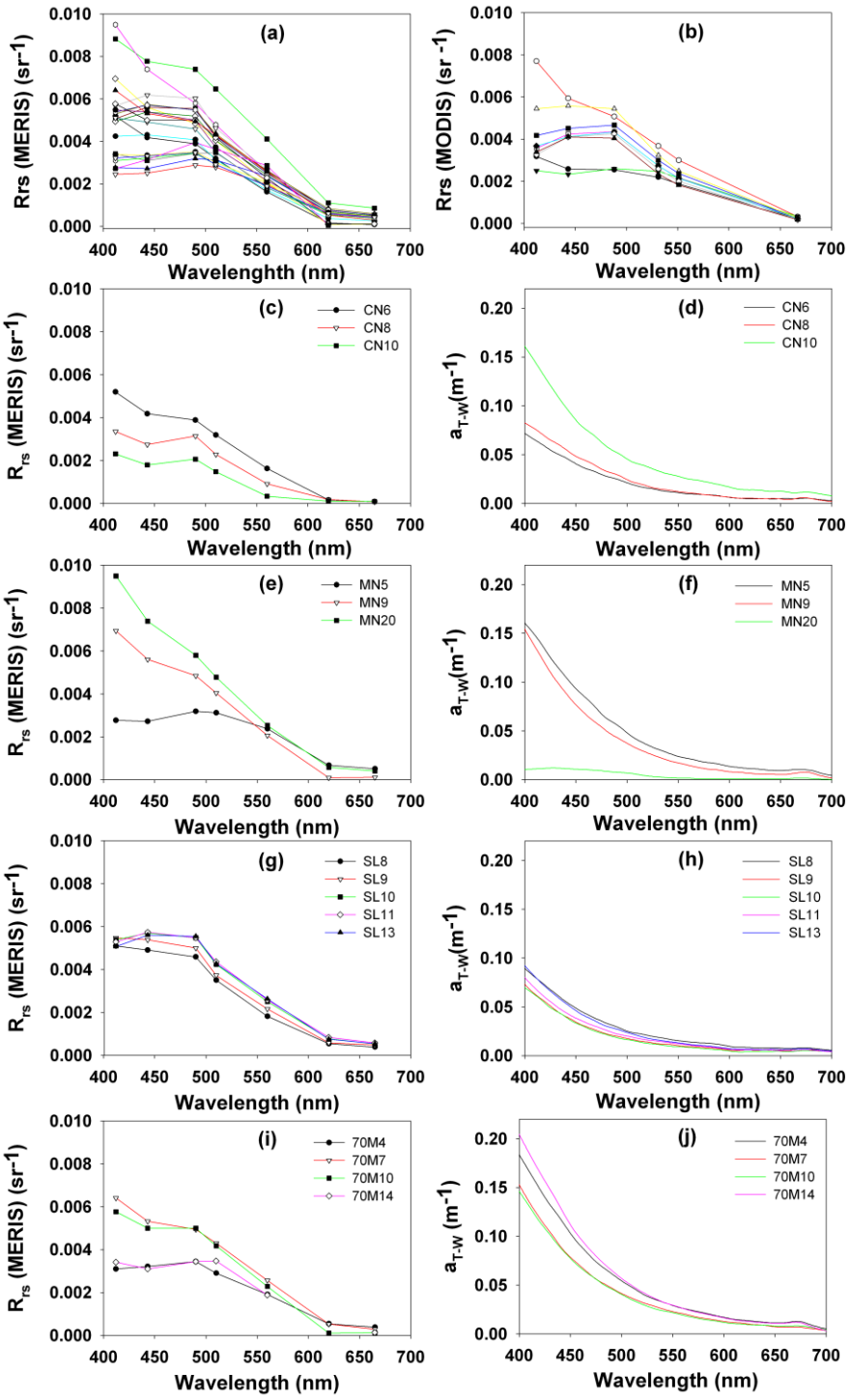

Figure 5.5. Remote Sensing reflectance spectra ($R_{rs}(\lambda)$) from (a) MERIS, and (b) MODIS ocean color sensors. Comparison of MERIS $R_{rs}(\lambda)$ and in-situ $a_{T\text{-}W}(\lambda)$ for (c-d) CN transect, (e-f) MN transect, (g-h) SL transect, and (i-j) 70M transect. Transect and station locations are shown in Figure 5.1.

selecting and examining these band combinations and ratios is that variations in $R_{rs}(\lambda)$ at the blue wavelengths are strongly affected by absorption and variations in $R_{rs}(\lambda)$ at the green wavelengths are the most affected by light scattering by particles. The ratio of two bands reduces the effect of factors such as measurement geometry and atmosphere on the retrieval [*O' Reilly et al.*, 1998]. From a different perspective, the $R_{rs}(\lambda)$ band ratio is approximately equal to the product of backscattering ratio and absorption ratio [*Gordon et al.*, 1988] and can be expressed as:

$$\frac{R_{rs}(\lambda_1)}{R_{rs}(\lambda_2)} \approx \left[\frac{b_b(\lambda_1)}{b_b(\lambda_2)}\right]\left[\frac{a_T(\lambda_2)}{a_T(\lambda_1)}\right] \qquad \text{(Eq. 7)}$$

So variations in $R_{rs}(\lambda)$ band ratios are driven primarily by the variability in backscattering and absorption. We didn't look at the backscattering properties and its influence on $R_{rs}(\lambda)$ in this study, however from Figure 5.5(c-j) it appears that the $R_{rs}(\lambda)$ spectra are mostly influenced by absorption. Hence, we can examine this variability by relating $R_{rs}(\lambda)$ ratios and absorption. We used simple $R_{rs}(\lambda)$ band ratios on MERIS satellite data for deriving $a_{PHY}(\lambda)$ at 443 nm and 676 nm; which are the main absorption peaks in $a_{PHY}(\lambda)$ spectra (Figure 5.6). Further, the in-situ $a_{PHY}(443)$ can be correlated to in-situ $a_{PHY}(\lambda)$ at other wavelengths using empirical relationships in the study region. For example the following relationship was obtained between in-situ $a_{PHY}(443)$ and in-situ $a_{PHY}(490)$:

$$a_{PHY}(490) = 0.38[a_{PHY}(443)] + 0.55[a_{PHY}(443)]^2$$
$$(R^2 = 0.98;\ n = 65)$$

Different combinations of band ratios were tested; the band ratios that gave highest R^2 were selected i.e. $R_{rs}(443)/R_{rs}(510)$ (R_1) and $R_{rs}(490)/R_{rs}(510)$ (R_2). A simple 1st order inverse power fit was applied to $a_{PHY}(\lambda)$ at 443 nm and 676 nm and the reflectance ratios. The R_2 reflectance band ratio yielded the best results showing good correlations with $a_{PHY}(\lambda)$ at 443 nm and 676 nm

(Figure 5.6b and Figure 5.6d). Irrespective of the band ratio used the relationship between $a_{PHY}(443)$ and the band ratio was similar; in general as the band ratios increased the $a_{PHY}(443)$ decreased. In most analytical or semi-analytical models, the NAP/detrital and CDOM components are considered together as they have similar spectral shape [*Carder et al.*, 1999; *Lee et al.*, 2002]. Various band ratios were related to $a_{DG}(443)$ through a 1st order inverse power fit (Figure 5.7). The $a_{DG}(443)$ was selected as it correlated well with $a_{DG}(\lambda)$ at other wavelengths using the spectral slope parameter (S_{DG}).

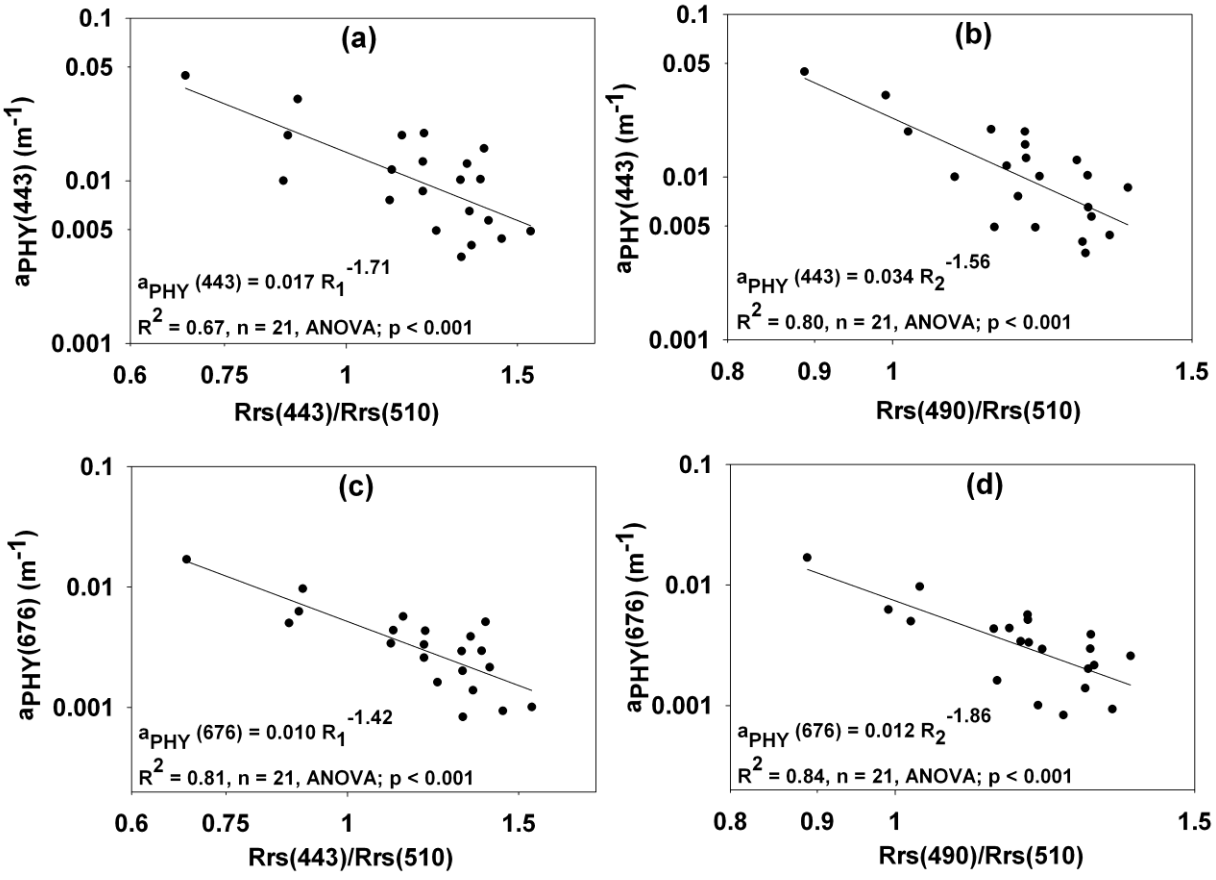

Figure 5. 6. Relationships between $a_{PHY}(\lambda)$ at 443 nm and the blue-to-green ratio of $R_{rs}(\lambda)$. (a) $a_{PHY}(443)$ versus $R_{rs}(443)/R_{rs}(510)$ (R_1), (b) $a_{PHY}(443)$ versus $R_{rs}(490)/R_{rs}(510)$ (R_2), (c) $a_{PHY}(676)$ versus $R_{rs}(443)/R_{rs}(510)$ (R_1), and (d) $a_{PHY}(676)$ versus $R_{rs}(490)/R_{rs}(510)$ (R_2). The least squares fit (solid lines and equations), the R^2 for log-transformed data, and the number of observations (n) are shown.

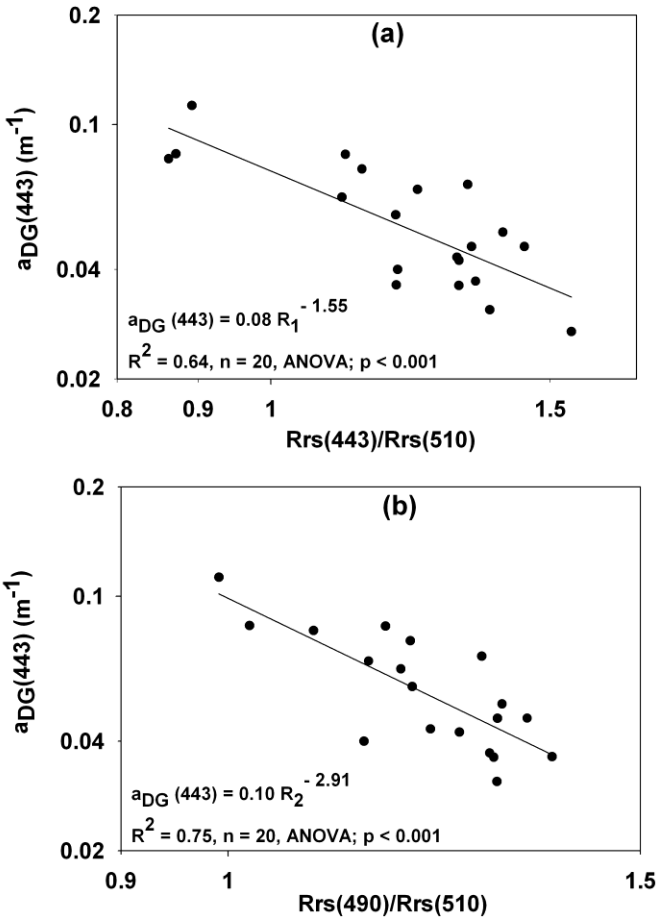

Figure 5.7. Relationships between $a_{DG}(\lambda)$ at 443 nm and the blue-to-green ratio of $R_{rs}(\lambda)$. (a) $a_{DG}(443)$ versus $R_{rs}(443)/R_{rs}(510)$ (R_1), and (b) $a_{DG}(443)$ versus $R_{rs}(490)/R_{rs}(510)$ (R_2). The least squares fit (solid lines and equations), the R^2 for log-transformed data, and the number of observations (n) are shown.

For example in-situ $a_{DG}(412)$ can be calculated from in-situ $a_{DG}(443)$ using the mean value of in-situ $S_{DG} = 0.015 \pm 0.003$ as shown below:

$$a_{DG}(412) = a_{DG}(443)e^{(-0.015(\lambda-443))}$$
$$(R^2 = 0.95;\ n = 65)$$

The highest R^2 were obtained for $R_{rs}(443)/R_{rs}(510)$ (R_1) and $R_{rs}(490)/R_{rs}(510)$ (R_2). The R_2 ratio performed the best as compared to the other band ratios (Figure 5.7b). Comparing the

contribution of $a_{PHY}(443)$ and $a_{DG}(443)$ to R_2, the contribution of the non-pigmented (exponent = -2.91, Figure 5.7) component was on an average higher than phytoplankton absorption (exponent = -1.55, Figure 5.6). These results suggested that the variations between two band reflectance ratios could be used to retrieve $a_{PHY}(443)$, $a_{PHY}(676)$ and $a_{DG}(443)$ in the study region. The number of data points (21) is statistically insufficient to establish robust algorithms; however it points out the future potential of this approach.

$a_{PHY}(\lambda)$ and $a_{DG}(\lambda)$ Derived Using QAA from MERIS and MODIS retrieved $R_{rs}(\lambda)$

Stations for which the QAA algorithm did not retrieve positive values of absorption at all wavelengths less than 580 nm were excluded from the comparison analysis. Absorption at wavelengths greater than 580 nm will not be analyzed as the QAA algorithm returns negative values at these wavelengths. The reason for the negative values is described in Lee and Carder., (2004). In brief, at wavelengths greater than 580 nm the total absorption coefficient is mostly dominated by pure water absorption with very little contribution of $a_{PHY}(\lambda)$, hence $a_{PHY}(\lambda)$ cannot be determined accurately from $R_{rs}(\lambda)$ at these wavelengths. The match-ups of in-situ and MERIS retrieved $a_{PHY}(\lambda)$ using QAA after log-transformation showed reasonable agreement with R^2 ranging from 0.50 – 0.71 and slope ranging from 0.77 to 0.87 at all wavelengths (Figure 5.8, Table 5.2). More importantly $a_{PHY}(443)$ which corresponds to the maximum of $a_{PHY}(\lambda)$ spectra and is correlated to chlorophyll-a (Figure 5.3a) was retrieved relatively more accurately (RMSE = 0.316) as compared to other wavelengths. The retrievals in the blue wavelengths were better than the green wavelength as $a_{PHY}(\lambda)$ usually shows a maximum in the blue region and a minimum in the green region of the spectra. In general, the QAA derived $a_{PHY}(\lambda)$ from MERIS overestimated $a_{PHY}(\lambda)$ at all wavelengths analyzed. The possible reason for this could be pigment packaging or change in pigment composition leads to

Table 5. 2. Slope, R^2 and RMSE for the linear fit (ANOVA; $p < 0.001$) expressed as $a_{PHY}(\lambda)$ (in-situ) = $A_{PHY}(\lambda)$*[$a_{PHY}(\lambda)$ (satellite retrieved – MERIS/MODIS)].

Wavelength	A_{PHY}(slope)	R^2	RMSE	n
MERIS				
413 nm	0.83	0.70	0.242	18
443 nm	0.78	0.71	0.316	18
490 nm	0.77	0.50	0.431	18
510 nm	0.87	0.50	0.542	18
560 nm	0.82	0.50	0.674	18
All	0.82	0.74	0.503	90
MODIS				
410 nm	0.84	0.89	0.255	5
443 nm	0.77	0.75	0.382	5
490 nm	0.73	0.62	0.489	5
530 nm	0.79	0.86	0.378	4
550 nm	0.86	0.90	0.476	4
All	0.83	0.80	0.525	23

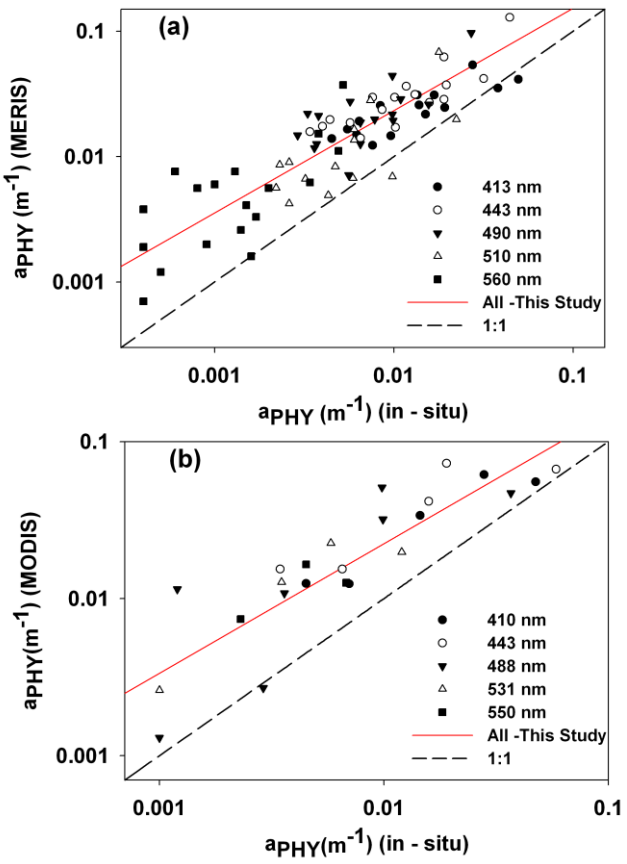

Figure 5.8. Relationship between log-transformed in-situ $a_{PHY}(\lambda)$ versus QAA retrieved (a) MERIS $a_{PHY}(\lambda)$, and (b) MODIS $a_{PHY}(\lambda)$. Statistics of the linear fit for each wavelength are shown in Table 5.2.

lower phytoplankton absorption and thus results in higher $R_{rs(}\lambda)$ [*Carder et al.*, 2004](discussed later). The retrievals in the blue wavelengths were better than the green wavelength as $a_{PHY}(\lambda)$ usually shows a maximum in the blue region and a minimum in the green region of the spectra. In general, the QAA derived $a_{PHY}(\lambda)$ from MERIS overestimated $a_{PHY}(\lambda)$ at all wavelengths analyzed. The possible reason for this could be pigment packaging or change in pigment composition leads to lower phytoplankton absorption and thus results in higher Rrs(λ) [*Carder et al.*, 2004] (discussed later).

The match-ups of in-situ and MODIS retrieved $a_{PHY}(\lambda)$ using QAA after log-transformation showed much better agreement, but was not statistically reliable due to small sample size (n = 5). However, at all wavelengths except 490 nm, R^2 ranged from 0.75 – 0.90 and slope ranged from 0.77 – 0.86. The relationship of in-situ $a_{PHY}(\lambda)$ and QAA derived $a_{PHY}(\lambda)$ from MERIS as well as MODIS at all wavelengths showed reasonable agreement (Table 5.2).

The QAA does not retrieve NAP/detrital absorption but retrieves NAP/detrital plus CDOM ($a_{DG}(\lambda)$) absorption. For the purpose of match-up analysis the CDOM absorption was added to the NAP/detrital absorption. Figure 5.9 shows the match-up of in-situ and QAA derived satellite $a_{DG}(\lambda)$ for MERIS and MODIS. Wavelengths greater than 580 nm were not included in the analysis as beyond 600 nm $a_{DG}(\lambda)$ values are very low due to the typical exponential decrease with increasing wavelength of $a_{DG}(\lambda)$ spectra. The satellite retrieved $a_{DG}(\lambda)$ is consistent with in-situ data in terms of lower wavelengths showing higher absorption and higher wavelengths showing lower absorption after log-transformation. However $a_{DG}(\lambda)$ retrieved from MODIS did not statistically fit into a linear relationship with in-situ $a_{DG}(\lambda)$ at every wavelength, but over the entire waveband a good linear fit was obtained with $R^2 = 0.80$, slope = 1.01 and RMSE = 0.362 (Table 5.3). The $a_{DG}(\lambda)$ retrieved from MERIS shows better agreement with in-situ data at lower

Table 5. 3. Slope, R^2 and RMSE for the linear fit (ANOVA; $p < 0.001$) expressed as $a_{DG}(\lambda)$ (in-situ) = $A_{DG}(\lambda)$*[$a_{DG}(\lambda)$ (satellite retrieved – MERIS/MODIS)].

Wavelength	A_{DG}(slope)	R^2	RMSE	n
MERIS				
413 nm	1.11	0.60	0.401	18
443 nm	1.15	0.61	0.391	18
490 nm	1.16	0.61	0.381	18
510 nm	1.16	0.58	0.388	18
560 nm	1.18	0.44	0.433	18
All	1.16	0.84	0.416	90
MODIS				
All	1.01	0.80	0.362	27

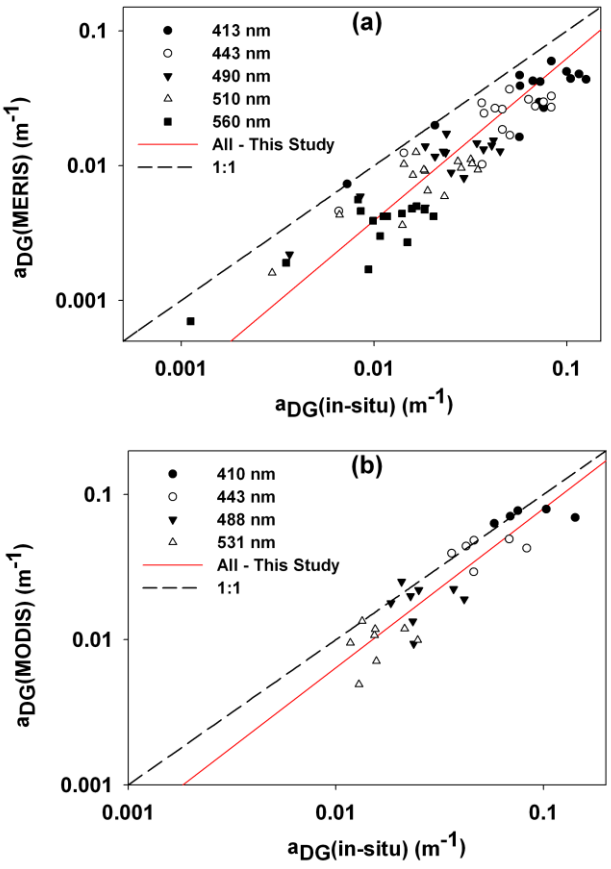

Figure 5. 9. Relationship between log-transformed in-situ $a_{DG}(\lambda)$ versus QAA retrieved (a) MERIS $a_{DG}(\lambda)$, and (b) MODIS $a_{DG}(\lambda)$. Statistics of the linear fit for each wavelength are shown in Table 5.3.

wavelengths than at higher wavelengths as seen from the decrease in R^2 and increase in RMSE values with increasing wavelength (Table 5.3). The QAA retrieved $a_{DG}(\lambda)$ from MERIS underestimated in-situ $a_{DG}(\lambda)$ at all wavelengths. The relationship of in-situ $a_{DG}(\lambda)$ and QAA derived $a_{DG}(\lambda)$ from MERIS at all wavelengths showed good agreement (Table 5.3). However at higher wavelengths few outliers along the 1:1 line could have influenced the relationship (Figure 5.9). The inconsistencies in match-up of both $a_{PHY}(\lambda)$ and $a_{DG}(\lambda)$ could be explained through few limitations in the derivation of $a_{PHY}(\lambda)$ and $a_{DG}(\lambda)$ using QAA. One of the limitations is the choice of spectral slope of CDOM and NAP/detrial absorption (S_{DG}). The QAA was run using the standard input for S_{DG} which was calculated from $R_{rs}(\lambda)$ for all collocated points. S_{DG} is known to be variable in natural systems ranging from 0.01 – 0.02 nm^{-1} [*Kirk*, 1994]. Ideally S_{DG} values corresponding to the stations should be used which cannot be accurately determined using just $R_{rs}(\lambda)$ values [*Lee and Carder*, 2004]. To evaluate the effect of S_{DG} we calculated in-situ S_{DG} values from in-situ $a_{DG}(\lambda)$ by applying an exponential fit. The QAA was run with the in-situ S_{DG} to obtain $a_{PHY}(\lambda)$ and $a_{DG}(\lambda)$, however there was not much change in the retrieval of $a_{PHY}(\lambda)$ and $a_{DG}(\lambda)$. The average percent difference between QAA retrieved $a_{PHY}(\lambda)$ or $a_{DG}(\lambda)$ with fixed S_{DG} and QAA retrieved $a_{PHY}(\lambda)$ or $a_{DG}(\lambda)$ in-situ S_{DG} was ~7% at all wavelengths.

The other major factor that likely influenced the QAA outputs is the pigment packaging or change in pigment composition seen in our study. The low $a^*_{PHY}(\lambda)$ especially at stations where $a_{PHY}(\lambda)$ dominates the total absorption could result in increased $R_{rs}(\lambda)$ in the blue region leading to higher blue to green reflectance ratios. The blue to green reflectance ratios ($R_{rs}(443)/R_{rs}(560)$ for our study) are used in QAA to get $a_{PHY}(411)/a_{PHY}(443)$ and $a_{DG}(411)/a_{DG}(443)$, that are finally used to decompose $a_{PHY}(\lambda)$ and $a_{DG}(\lambda)$ from total water absorption [*Lee et al.*, 2002], http://www.ioccg.org/groups/ Software_OCA/QAA_v5.pdf]. Higher blue to green ratios would

result in lower $a_{PHY}(411)/a_{PHY}(443)$ and $a_{DG}(411)/a_{DG}(443)$ [*Lee et al.*, 2002]. The mean value of $a_{PHY}(411)/a_{PHY}(443)$ and $a_{DG}(411)/a_{DG}(443)$ from in-situ data was 0.90±0.21 and 1.60±0.18 while the QAA gave a mean value of 0.81±0.02 and 1.55±0.17. In the QAA the difference between $a_{PHY}(411)/a_{PHY}(443)$ and $a_{DG}(411)/a_{DG}(443)$ is inversely related to $a_{DG}(\lambda)$ [*Lee et al.*, 2002]. This difference as estimated by QAA is larger than in-situ resulting in underestimation of $a_{DG}(\lambda)$, and hence overestimation of $a_{PHY}(\lambda)$ by QAA relative to in-situ values.

In determination of $a_{PHY}(\lambda)$ values using the QFT method there is uncertainty in the 'Beta factor (β)' which can cause errors of about 10 – 20% [*Carder et al.*, 1999]. Lee and Carder, (2004) found that even when in-situ $R_{rs}(\lambda)$ used as input to QAA an average percent difference of 21.4% existed between derived $a_{PHY}(\lambda)$ and in-situ $a_{PHY}(\lambda)$. Also in-situ $a_{PHY}(\lambda)$ and $a_{DG}(\lambda)$ are from discrete water samples whereas the QAA derived $a_{PHY}(\lambda)$ and $a_{DG}(\lambda)$ are integrated over the near surface upper water column [*Gordon and Clark*, 1980]. Considering these uncertainties the match-up results obtained in this study are encouraging and can be used to determine $a_{PHY}(\lambda)$ and $a_{DG}(\lambda)$ from $R_{rs}(\lambda)$ at wavelengths ranging from 400 – 500 nm.

Conclusions

The total particulate and phytoplankton absorption coefficient in southeastern Bering Sea are well correlated with chlorophyll-a and are lower as a function of chlorophyll-a compared to low latitude regions. Variable specific phytoplankton absorption spectra with more variability in the blue than in the red part of the spectrum indicated change in pigment composition or package effect. There were significant differences in the magnitudes and spectral shapes of $R_{rs}(\lambda)$ spectra, which indicate that different types of waters exist in the study region. This was supported by the varied $a_{T\text{-}W}(\lambda)$ spectra obtained in study area. About half of our $R_{rs}(\lambda)$ spectra showed blue and green reflectances that were high and low, respectively. Simple two band ratios involving $R_{rs}(\lambda)$

ratios can be used to examine variability and retrieve $a_{PHY}(\lambda)$ from MERIS at 443 nm and 676 nm in the study region with $R_{rs}(490)/R_{rs}(510)$ giving best results. Similarly for $a_{DG}(\lambda)$ reflectance band ratio of $R_{rs}(490)/R_{rs}(510)$ could be used in the study region. The match-ups of in-situ and MERIS retrieved $a_{PHY}(\lambda)$ using QAA after log-transformation showed reasonable agreement. In general the QAA derived $a_{PHY}(\lambda)$ from MERIS overestimated in-situ $a_{PHY}(\lambda)$ at all wavelengths analyzed. The satellite retrieved $a_{DG}(\lambda)$ is consistent with in-situ data in terms of lower wavelengths showing higher absorption and higher wavelengths showing lower absorption. The QAA retrieved $a_{DG}(\lambda)$ from MERIS underestimated in-situ $a_{DG}(\lambda)$ at all wavelengths. The inconsistencies seen in the match-up analysis could be ascribed to uncertainties in the QFT method, discrete (in-situ) versus integrated (satellite) absorption coefficients comparison and change in pigment composition or package effect. Taking into account these errors the results obtained from the match-up analysis are encouraging and can be used for identification of major pigments and modeling purposes.

The results in this paper are obtained using a seasonally-limited in situ data set collected in July, 2008. The effects on the results during other seasons where relative contributions to absorption by phytoplankton and NAP/detrital matter varies from the conditions captured during the July 2008 sampling needs to be determined. Future applications would require optimization of the input parameters to the QAA. Also the satellite overpass and in-situ sampling time window could be increased so as to get more collocated data points.

References

Behrenfeld, M., E. Boss, D. Siegel, and D. Shea (2005), Carbon-based ocean productivity and phytoplankton physiology from space, Global Biogeochemical Cycles, 19(1).

Bricaud, A., M. Babin, A. Morel, and H. Claustre (1995), Variability in the chlorophyll-specific absorption-coefficients of natural phytoplankton - analysis and parameterization, Journal of Geophysical Research-Oceans, 100(C7), 13321-13332.

Bricaud, A., A. Morel, M. Babin, K. Allali, and H. Claustre (1998), Variations of light absorption by suspended particles with chlorophyll a concentration in oceanic (case 1) waters: Analysis and implications for bio-optical models, Journal of Geophysical Research-Oceans, 103(C13), 31033-31044.

Carder, K. L., F. Chen, Z. Lee, S. Hawes, and D. Kamykowski (1999), Semianalytic Moderate-Resolution Imaging Spectrometer algorithms for chlorophyll a and absorption with bio-optical domains based on nitrate-depletion temperatures, Journal of Geophysical Research-Oceans, 104(C3).

Carder, K. L., F. R. Chen, Z. Lee, S. K. Hawes, and J. P. Cannizzaro (2004), MODIS Ocean Science Team Algorithm Theoretical Basis Document, College of Marine Sciences, University of Florida, St. Petersburg, 84.

Cleveland, J., and A. Weidemann (1993), Quantifying absorption by aquatic particles - a multiple-scattering correction for glass-fiber filters, Limnology and Oceanography, 38(6), 1321-1327.

Cota, G., H. Wang, and J. Comiso (2004), Transformation of global satellite chlorophyll retrievals with a regionally tuned algorithm, Remote Sensing of Environment, 90(3), 373-377.

D' Sa, E., R. Miller, and B. Mckee (2007), Suspended particulate matter dynamics in coastal waters from ocean color: Application to the northern Gulf of Mexico, Geophysical Research Letters, 34(23), L23611.

Dierssen, H., and R. Smith (2000), Bio-optical properties and remote sensing ocean color algorithms for Antarctic Peninsula waters, Journal of Geophysical Research-Oceans, 105(C11), 26301-26312.

Fujiki, T., and S. Taguchi (2002), Variability in chlorophyll alpha specific absorption coefficient in marine phytoplankton as a function of cell size and irradiance, Journal of Plankton Research, 24(9), 859-874.

Gordon, H. R., and D. K. Clark (1980), Remote-sensing optical-properties of a stratified ocean - an improved interpretation, Applied Optics, 19(20), 3428-3430.

Gordon, H. R., and K. J. Voss (1999), MODIS Normalized Water-leaving Radiance Algorithm Theoretical Basis Document (MOD 18) Version 4Rep.

Gordon, H. R., O. B. Brown, R. H. Evans, J. W. Brown, R. C. Smith, K. S. Baker, and D. K. Clark (1988), A semianalytic radiance model of ocean color, Journal of Geophysical Research-Atmospheres, 93(D9), 10909-10924.

Hare, S., and N. Mantua (2000), Empirical evidence for North Pacific regime shifts in 1977 and 1989, Progress in Oceanography, 47(2-4), 103-145.

Holm-Hansen, O., C. J. Lorenzen, R. W. Holmes, and J. D. H. Strickland (1965), Fluorometric determination of chlorophyll, Journal du Conseil, 30(1), 3.

Iida, T., and S. Saitoh (2007), Temporal and spatial variability of chlorophyll concentrations in the Bering Sea using empirical orthogonal function (EOF) analysis of remote sensing data, Deep Sea Research Part II-Topical Studies in Oceanography, 54(23-26), 2657-2671.

Kachel, N., G. Hunt, S. Salo, J. Schumacher, P. Stabeno, and T. Whitledge (2002), Characteristics and variability of the inner front of the southeastern Bering Sea, Deep Sea Research Part II-Topical Studies in Oceanography, 49(26), 5889-5909.

Kirk, J. T. O. (1994), Light and Photosynthesis in Aquatic Ecosystems, 2 ed., Cambridge University Press, New York.

Kishino, M., M. Takahashi, N. Okami, and S. Ichimura (1985), Estimation of the spectral absorption-coefficients of phytoplankton in the sea, Bulletin of Marine Science, 37(2), 634-642.

Lee, Z., and K. Carder (2004), Absorption spectrum of phytoplankton pigments derived from hyperspectral remote-sensing reflectance, Remote Sensing of Environment, 89(3), 361-368.

Lee, Z., K. Carder, and R. Arnone (2002), Deriving inherent optical properties from water color: a multiband quasi-analytical algorithm for optically deep waters, Applied Optics, 41(27), 5755-5772.

Lohrenz, S., A. Weidemann, and M. Tuel (2003), Phytoplankton spectral absorption as influenced by community size structure and pigment composition, Journal of Plankton Research, 25(1), 35-61.

Matsuoka, A., Y. Huot, K. Shimada, S. Saitoh, and M. Babin (2007), Bio-optical characteristics of the western Arctic Ocean: implications for ocean color algorithms, Canadian Journal of Remote Sensing, 33(6), 503-518.

Mitchell, B. G., M. Kahru, J. Wieland, and M. Stramska (2002), Determination of spectral absorption coefficients of particles, dissolved material and phytoplankton for discrete water samples, Ocean Optics Protocols For Satellite Ocean Color Sensor Validation, Revision 3, Part II, 231.

Mueller, J. L. (2000), SeaWiFS algorithm for the diffuse attenuation coefficient, K (490), using water-leaving radiances at 490 and 555 nmRep., 24–27 pp, NASA Goddard Space Flight Center, Greenbelt, MD.

Muller-Karger, F., C. McClain, R. Sambrotto, and G. Ray (1990), A comparison of ship and coastal zone color scanner mapped distribution of phytoplankton in the southeastern Bering Sea, Journal of Geophysical Research-Oceans, 95(C7), 11483-11499.

Naik, P., E. J. D'Sa, and J. I. Goés (2009a), Absorption properties along the 70-m isobath in the southeastern Bering Sea during July 2008, paper presented at OCEANS 2009, IEEE, Biloxi, MS.

Naik, P., E. J. D'Sa, J. I. Goés, and H. R. Gomes (2009b), Particulate absorption properties from MODIS ocean color and four in-situ transects in the southeastern Bering Sea shelf during July 2008.

O' Reilly, J., S. Maritorena, B. Mitchell, D. Siegel, K. Carder, S. Garver, M. Kahru, and C. McClain (1998), Ocean color chlorophyll algorithms for SeaWiFS, Journal of Geophysical Research-Oceans, 103(C11), 24937-24953.

Rochelle-Newall, E., and T. Fisher (2002), Production of chromophoric dissolved organic matter fluorescence in marine and estuarine environments: an investigation into the role of phytoplankton, Marine Chemistry, 77(1), 7-21.

Sathyendranath, S., V. Stuart, B. Irwin, H. Maass, G. Savidge, L. Gilpin, and T. Platt (1999), Seasonal variations in bio-optical properties of phytoplankton in the Arabian Sea, Deep Sea Research Part II-Topical Studies in Oceanography, 46(3-4), 633-653.

Springer, A., C. McRoy, and M. Flint (1996), The Bering Sea Green Belt: Shelf-edge processes and ecosystem production, Fisheries Oceanography, 5(3-4), 205-223.

Stabeno, P., N. Kachel, C. Mordy, D. Righi, and S. Salo (2008), An examination of the physical variability around the Pribilof Islands in 2004, Deep Sea Research Part II-Topical Studies in Oceanography, 55(16-17), 1701-1716.

Wang, J., G. Cota, and D. Ruble (2005), Absorption and backscattering in the Beaufort and Chukchi Seas, Journal of Geophysical Research-Oceans, 110(C4).

CHAPTER 6: SUMMARY

Sub-arctic regions like the Bering Sea are among the most biologically productive and vulnerable areas of the world's oceans and as such they are some of the most intensely studied areas for environmental scientific research. However, due to the complexity of the interactions between physical, chemical and biological phenomena in these regions, these waters are among the most challenging for methodical scientific research. A main impediment to obtain concentrations of optically active components (such as CDOM, NAP, and phytoplankton) from remote sensors in these waters has been the lack of data on the optical characteristics of southeastern Bering Sea. A central focus of this dissertation was to obtain a suite of in-water measurements for characterization of light absorption properties in the southeastern Bering Sea which would help to address the above issue.

The approach to reach the goals set for this dissertation consisted of two parts: the first was to improve the accuracy of the absorption measurements (through development of pathlength amplification factor for the spectrophotometers used in the study) (chapter 2) and development and application of methodology to the Atchafalaya shelf regions which is optically complex owing to high CDOM and NAP absorption (chapter 3). The second part was the application of these methods to understand the optical variability in the southeastern Bering Sea (chapter 4 and chapter 5).

Chapter 2 showed that the two spectrophotometers for absorption of particles on filter paper performed similarly and the pathlength amplification factor developed gave improved estimations of particulate absorption. Chapter 3 demonstrated that the methods developed can be used to decipher the large contribution of non-covarying CDOM and NAP absorption to total light absorption at blue wavelengths and its effects on the retrieval of chlorophyll-a and CDOM

absorption from satellite data in the Atchafalaya shelf region. This showed the potential utility of these methods for applications in case 2 waters (e.g. Bering Sea).

The methods similar to chapter 3 were applied to the southeastern Bering Sea (chapters 4 and 5). The light absorption coefficients under different oceanographic domains with unique biogeochemical characteristics were studied in order to examine the spatial variability in light absorption properties in the study region. The absorption coefficients were well structured with respect to hydrographic and biogeochemical characteristics of the shelf. The highest values of phytoplankton absorption at 443 nm were observed along the central front, a region of high productivity due to mixing of shelf (high in iron) and basin waters (high in macronutrients). The lowest values of phytoplankton absorption at 443 nm were found in the coastal domain, a low productivity region associated with limited macronutrients. Values of NAP plus CDOM absorption revealed an east-west gradient pattern with higher values in the coastal domain due to influence of river runoff, and lower values in the outer domain. With the exception of CDOM and NAP absorption coefficients all of the absorbing coefficients correlated well with chlorophyll-a ($r^2 > 0.6$). Lower specific phytoplankton absorption observed relative to middle and lower latitude waters indicated changes in pigment composition and/or package effect. These two effects are intermingled and cannot be separated out. While the ratio of specific phytoplankton absorption at 443 nm and 676 nm (< 3), lower values of specific phytoplankton absorption at 443 nm at 676 nm (mean - 0.012±0.006 m^2 (mg chl-a)$^{-1}$), index of package effect at 676 nm, and spectral size parameter suggested generally larger size phytoplankton to be dominant in our study region, values of these quantities at some locations indicated large variability in specific phytoplankton absorption consistent with the phytoplankton community size-structure which revealed that although larger cells were dominant at most stations there

were stations where smaller cells dominated. The parameterizations of absorbing coefficients through statistical relationships are strong at all wavelengths examined. Such an approach makes it possible to predict absorption coefficients across the visible domain from a single wavelength and is of great significance in ocean color remote sensing since bio-optical information is usually limited to few wavelengths.

The absorption budget revealed that CDOM was the dominant light absorbing constituent at all wavelengths examined except at 676 nm. The average contribution by CDOM to total minus water absorption was greater than 50% at all depths and wavelengths except 676 nm, and was larger at the shorter wavelengths 412 and 443 nm, due to the exponential increase of CDOM absorption with decreasing wavelength. At 443 nm, where the chlorophyll-a absorption is maximum, contribution of phytoplankton, NAP and CDOM absorption to total minus water absorption was 20%, 14%, and 66%, respectively for surface samples, 28%, 15%, and 57%, respectively for middle1 depth, and 19%, 16%, and 65%, respectively for middle 2 depth. The relative contribution of each component remains similar from the surface to below the chlorophyll-a maximum with the only noticeable change being the increase in contribution from phytoplankton absorption and corresponding decrease in contribution of CDOM absorption at middle 1 depths. The relative contribution of CDOM absorption to total minus water absorption at 443 nm decreased with increasing chlorophyll-a with relatively less scatter, emphasizing that as chlorophyll-a increases, particulate absorption at 443 nm takes up more of the absorption budget. As noted, there was no strong covariation found between chlorophyll-a and absorption by NAP or CDOM. Therefore, total absorption of light at wavelengths examined in the southeastern Bering Sea waters, is largely affected by constituents other than phytoplankton, that do not covary with chlorophyll-a. The implications of this are huge to ocean color algorithms

where higher than normal CDOM may be incorrectly contributing to ocean color estimates. To assess the influence of two conflicting factors i.e. high CDOM absorption (would cause lower $R_{rs}(\lambda)$) and lower specific phytoplankton absorption (would cause higher $R_{rs}(\lambda)$) on AOPs, we modeled remote sensing reflectance ($R_{rs}(\lambda)$) and diffuse light attenuation coefficient ($K_d(\lambda)$) of downward light using IOPs (absorption (total and total minus CDOM absorption) and backscattering).

The measurements of synchronized IOPs and AOPs in the southeastern Bering Sea waters allowed for "optical closure" studies, where the AOPs could be modeled using in-situ measured IOPs which can then be compared to the in-situ measured AOPs. Good agreement was obtained between measured and model estimated AOPs. The average percent difference (a.p.d) between discrete (specific depths and measured in laboratory) and continuous (profiles and measured in-situ) IOPs based model was less than 10% for $R_{rs}(\lambda)$ and $K_d(\lambda)$ at all wavelengths, with the largest differences in the red wavelengths. For the IOP modeled and radiometer measured $R_{rs}(\lambda)$ and $K_d(\lambda)$, the a.p.d was 15% (except red wavelengths a.p.d was less than 30%) and 10% (except red wavelengths a.p.d was less than 15%) respectively. The modeled and measured $R_{rs}(\lambda)$ showed fairly good agreement with satellite (MERIS) retrieved $R_{rs}(\lambda)$, with a.p.d less than 25% except at red wavelengths (a.p.d less than 35%). Taking into account the errors associated in measurements of individual IOPs and AOPs, the above results are very good. These results gave credence to the accuracy of individual measurements of AOPs and IOPs and suggested that the modeled AOPs can be used in the study region in absence of in-situ measured AOPs at least in the blue region of the visible spectrum. The overall results of the closure analysis helped to understand the influence of individual absorbing constituent on the underwater light field and remote-sensing signal.

The accuracy of all satellite derived ocean color products (e.g. absorption coefficients, chlorophyll concentration and PP) depends on the quality and accuracy of the principal parameters (normalized water leaving radiances or $R_{rs}(\lambda)$) measured by the satellite sensor. Modeling of $R_{rs}(\lambda)$ and $K_d(\lambda)$ from IOPs revealed the strong influence of CDOM absorption on $R_{rs}(\lambda)$ and $K_d(\lambda)$. The CDOM absorption caused the blue to green $R_{rs}(\lambda)$ ratios to decrease by a factor of 2 and accounted for >50% of $K_d(\lambda)$ which was vertically variable. The effect of CDOM absorption on the blue wavelengths and to a lesser extent on the green wavelengths was apparent on the $R_{rs}(\lambda)$ spectra. Based on the closure analysis, the blue to green $R_{rs}(\lambda)$ ratios were lower in the study region causing chlorophyll-a in the range of 0.05 to 0.9 mg m^{-3} to be overestimated by a factor of ~2 using the OC4.v4 algorithm (standard global empirical algorithm). The main reason for this disagreement in the southeastern Bering Sea waters is that CDOM absorption that does not necessarily covary with chlorophyll-a concentration, significantly affects the total absorption, and therefore $R_{rs}(\lambda)$, at the blue-green wavelengths used in the empirical chlorophyll algorithms. As observed in the earlier sections, CDOM absorption dominates the light absorption relative to phytoplankton absorption especially at lower chlorophyll-a concentration, hence higher CDOM overrides the lower specific phytoplankton absorption influencing the green to blue reflectance ratios in our study region for chlorophyll-a range of 0.05 to 0.9 mg m^{-3}. Chlorophyll-a is the principal model variable that influences calculation of PP from PP models. The vertical variability in $K_d(\lambda)$ (only from CDOM) taken together with the error in estimates of chlorophyll-a will result in large errors in the estimation of PP in the study region. Empirical algorithms were developed for retrieval of absorption coefficients from satellite data, while satellite retrieved absorption coefficients were validated by using a semi-analytical algorithm, QAA, which is based on global parameterization. The empirical algorithms were developed

where simple satellite retrieved $R_{rs}(\lambda)$ ratios were related to in-situ phytoplankton and CDOM plus NAP absorption by applying an inverse power fit; $R_{rs}(490)/R_{rs}(510)$ gave the best results for phytoplankton and CDOM plus NAP absorption at 443 nm (R^2 - 0.80 and 0.75), respectively. The semi-analytical approach was tested by application of QAA to the study region. The match-ups of in-situ and MERIS retrieved phytoplankton and CDOM plus NAP absorption using QAA after log-transformation showed reasonable agreement with R^2 of 0.71 and 0.61 and RMSE of 0.316 and 0.391 at 443 nm, respectively. The QAA derived phytoplankton and CDOM plus NAP absorption from MERIS was overestimated and underestimated, respectively to the in-situ measurements, at all wavelengths. This systematic bias suggested the requirement for regional parameterization of QAA which is based on global parameterizations. For retrieval of absorption coefficients from satellite data in the study region either the empirical algorithms developed in this study can be used or retrievals from QAA after appropriate regional parameterization can be used. However semi-analytical algorithms are relatively more robust over different trophic status as compared to purely empirical algorithms.

With overall results from the dissertation, the questions addressed in the framework of this dissertation can be answered:

(i) How are the absorption coefficients of phytoplankton, CDOM and NAP in the southeastern Bering Sea waters distributed with respect to hydrographic and biogeochemical characteristics of the shelf and can these be parameterized using spectral relationships?

The absorption coefficients were well structured with respect to hydrographic and biogeochemical characteristics of the shelf, with largest variability seen in phytoplankton absorption. The absorption coefficients could be parameterized by applying simple spectral relationships.

(ii) How does the specific phytoplankton absorption in the southeastern Bering Sea compare relative to lower and middle latitudes waters?

The specific phytoplankton absorption was lower relative to lower and middle latitudes waters over the entire chlorophyll-a range examined, which indicated significant pigment packaging and/or change in pigment composition. The variability in the specific phytoplankton absorption was consistent with variability in phytoplankton community structure.

(iii) What is the contribution of phytoplankton, CDOM and NAP to the total light absorption in Bering Sea waters (optical classification through absorption budget) and how do they affect the light field?

CDOM absorption showed the largest contribution to total minus water absorption followed by phytoplankton absorption. The CDOM absorption accounted for greater than 50% of $K_d(\lambda)$ and caused the $R_{rs}(\lambda)$ to be lower more in blue than green region of the visible spectrum causing the blue to green reflectance ratios to be decreased by a factor of ~2.

(iv) How is the "optical closure" between measured IOPs and modeled AOPs based on simplified radiative transfer modeling?

Good optical closure can be obtained between measured IOPs and modeled AOPs with a.p.d of 15% (except red wavelengths a.p.d was less than 30%) and 10% (except red wavelengths a.p.d was less than 15%) for $R_{rs}(\lambda)$ and $K_d(\lambda)$, respectively. This suggested that the model estimations of $R_{rs}(\lambda)$ and $K_d(\lambda)$ can be used (cautiously at the red wavelengths) when underwater radiances are not measured.

(v) How well do satellite estimations of remote sensing reflectance and surface absorption coefficients in the southeastern Bering Sea waters compare to in-situ measurements and are the

bio-optical models or empirical relationships currently used in satellite algorithms applicable to the southeastern Bering Sea waters?

The satellite estimates of $R_{rs}(\lambda)$ showed fairly good agreement to in-situ $R_{rs}(\lambda)$, with a.p.d less than 25% except at red wavelengths (a.p.d less than 35%). The satellite estimates of absorption coefficients using the QAA showed systematic bias relative to in-situ measurements which suggested a regional parameterization of the QAA. The bio-optical models and empirical algorithms used presently in satellite algorithms are not applicable to the southeastern Bering Sea waters due to the higher contribution of CDOM absorption to the total minus water absorption. This suggested development of regional algorithms; regional empirical algorithms were developed for absorption coefficients using $R_{rs}(\lambda)$ ratios for the study region.

This dissertation is a contribution towards attaining an improved understanding of the optical characteristics of phytoplankton, NAP and CDOM, in the southeastern Bering Sea waters, and the manner in which they influence the underwater light filed as well as the amount of light leaving the water surface that can be measured in-situ or remotely from satellites. This information is essential when in-situ or satellite measurements of $R_{rs}(\lambda)$ are used to acquire information on chlorophyll concentrations and IOPs (e.g. absorption coefficients). The results from this dissertation will contribute, to a better understanding of the bio-optical variability and to obtain more accurate measurements of optically active constituents from remote sensing sensors of sub-arctic regions.

Future steps would involve: i) Regional parameterization of QAA through detailed radiative transfer modeling using the Hydrolight software (Sequoia) to account for the optical variability in study region.

ii) More research on water's optical properties in southeastern Bering Sea waters for different seasons (spring bloom, summer, fall bloom) to identify seasonal trends. For e.g. what is the seasonal trend of specific phytoplankton absorption as the phytoplankton community structure changes?

iii) Reprocessing of ocean color satellite data of absorption coefficients with the regionally developed models for different ocean color satellites.

iv) Long-term trends of absorption coefficients (especially CDOM absorption) in relation to climatic variability.

APPENDIX A: LIST OF SYMBOLS AND ABBREVIATIONS

ε	Fraction of the scattering coefficient, $b(\lambda)$ (dimensionless)
$\beta(\theta)$	$\beta(\theta)$ is the normalized VSF at angle (θ) (sr^{-1})
$a_{PHY}(\lambda)$	Phytoplankton absorption coefficient (m^{-1})
$a_{P}(\lambda)$	Particulate absorption coefficient ($a_{PHY}(\lambda) + a_{NAP}(\lambda)$) ($m^{-1}$)
A	Clearance area of filter (m^2)
$a^*_{PHY}(\lambda)$	Phytoplankton absorption per unit concentration of chlorophyll-a (m^2 mg^{-1})
$A_{CDOM}(\lambda)$	Absorbance of CDOM (dimensionless)
$a_{CDOM}(\lambda)$	CDOM absorption coefficient (m^{-1})
$a_{cm}(\lambda)$	Absorption coefficient of the cell material (m^{-1})
$a_{DG}(\lambda)$	Spectral absorption coefficient for non-phytoplankton particles + dissolved material (m^{-1})
$a_i^*(\lambda)$	HPLC volume based concentration of pigment i (mg m^{-3})
$A_{NAP}(\lambda)$	Absorbance of non-algal particulate matter (dimensionless)
$a_{NAP}(\lambda)$	Non-algal particulate matter (NAP) absorption coefficient (m^{-1})
AOPs	Apparent Optical Properties
$A_P(\lambda)$	Absorbance of particulate matter (dimensionless)
$a_{T\text{-}CDOM}(\lambda)$	Total water absorption minus $a_{CDOM}(\lambda)$ (m^{-1})
$a_{T\text{-}W}(\lambda)$	Total absorption coefficient minus absorption by pure sea-water (m^{-1})
$a_T(\lambda)$	Total absorption coefficient (m^{-1})
$a_W(\lambda)$	Absorption coefficient of pure water (m^{-1})
B	Backscattering ratio treated as constant (dimensionless)
$b_b(\lambda)$	Total backscattering coefficient (m^{-1})
$b_W(\lambda)$	Scattering coefficient of pure sea water (m^{-1})
$b(\lambda)$	Total scattering coefficient (m^{-1})
CDOM	Chromophoric Dissolved Organic Matter
C_i	Intracellular chlorophyll-a concentration per unit cell volume (mg m^{-3})
c_i	Concentration of pigment i in cell suspension(mg m^{-3})
$c(\lambda)$	Total beam attenuation coefficient (m^{-1})
d	Cell diameter (μm)
$E_d(\lambda)$	In-water downwelling irradiance (W m^{-2} nm^{-1})
$E_u(\lambda)$	In-water upwelling irradiance (W m^{-2} nm^{-1})
IOPs	Inherent Optical Properties
$K_d(\lambda)$	Diffuse attenuation coefficient of downwelling irradiance (m^{-1})
$L_u(\lambda)$	In-water upwelling radiance (W m^{-2} nm^{-1} sr^{-1})
$L_W(\lambda)$	Water leaving radiance
MAAs	Mycosporine-like Amino Acids
MERIS	Medium Resolution Imaging Spectrometer
MODIS	Moderate Resolution Imaging Spectroradiometer
$nL_W(\lambda)$	Normalized water leaving radiance
$OD(\lambda)$ or $Abs(\lambda)$	Optical density or absorbance (dimensionless)
$OD(\lambda)$	Optical density or absorbance (dimensionless)
$OD_f(\lambda)$	Optical density or absorbance of particles concentrated on filter paper (dimensionless)

$OD_f(\lambda)$ or $Abs_{FILTER}(\lambda)$	Optical density or absorbance of particles on concentrated on filter paper (dimensionless)
$OD_s(\lambda)$ or $Abs_{SUS}(\lambda)$	Optical density or absorbance of particles in suspension (dimensionless)
$OD_s(\lambda)$	Optical density or absorbance of particles in suspension (dimensionless)
$Q_a(\lambda)$	Cell absorption efficiency factor (dimensionless)
$Q_a^*(\lambda)$	Specific absorption efficiency (= package effect), dimensionless
QAA	Quasi Analytical Algorithm
QFT	Quantitative filter technique
$R_{rs}(\lambda)$	Remote sensing reflectance (sr^{-1})
S_{CDOM}	Spectral slope of CDOM absorption coefficient (nm^{-1})
S_{DG}	Spectral slope of CDOM plus NAP absorption coefficient (nm^{-1})
S_f	Size fraction of small and large phytoplankton cells (0 to 1) (dimensionless)
S_{NAP}	Spectral slope non-algal matter coefficient (nm^{-1})
V	Volume filtered (ml)
VSF	Volume scattering function (m^{-1} sr^{-1})
β	Pathlength amplification factor (dimensionless)
λ	Wavelength (nm)
λ_0	Reference wavelength (nm)
μ_0	Cosine of the solar zenith angle
$\rho'(\lambda)$	Dimensionless product of the absorption coefficient of the cell material ($a_{cm}(\lambda)$) and the cell diameter (d)

APPENDIX B: EMPIRICAL ORTHOGONAL FUNCTION (EOF) ANALYSIS OF SEA-SURFACE TEMPERATURE AND CHLOROPHYLL IN THE EASTERN BERING SEA[3]

Introduction

A large number of studies on synoptic climatology and effects on sea ice have been carried out in the Bering Sea [*Niebauer*, 1981; *Overland*, 1981]. Recently remotely sensed ocean color satellite data have been used for studying the synoptic spatial relationship between chlorophyll biomass and physical variables [*Brickley and Thomas*, 2004; *Thomas et al.*, 2003; *Yoder et al.*, 1993]. These studies have provided a link between physical processes and biological variability. The Bering Sea is semi-enclosed Sea with a broad continental shelf in the east and is one of the most productive ecosystems in the world [*Tsyban*, 1999] and supports a large commercial fishing industry [*Loughlin et al.*, 1999]. It is connected with the Arctic Ocean through the Bering Strait, and with the North Pacific through the Aleutian Islands (Figure B1). Sea ice develops in winter in the northern and eastern regions, affecting not only the physical conditions but also the biological conditions [*Hunt et al.*, 2002]. Recent reports indicate that climate change is affecting the abundance of phytoplankton, zooplankton, and fish in the Bering Sea [*Hunt et al.*, 2002].

With increasing availability of remotely sensed ocean-color data from satellite sensors, it is now possible to study the synoptic spatial relationship between chlorophyll and physical conditions (sea surface temperature (SST), wind, sea level pressure (SLP), photosynthetic available radiation (PAR), etc.). Long term synoptic climatology studies at very fine resolution can be conducted which is not possible by traditional shipboard measurements. To handle such large multivariate dataset, Empirical Orthogonal Functions (EOF) has been particularly useful tool [*Brickley and Thomas*, 2004].

[3] This appendix is reprinted with permission from proceedings of SPIE.

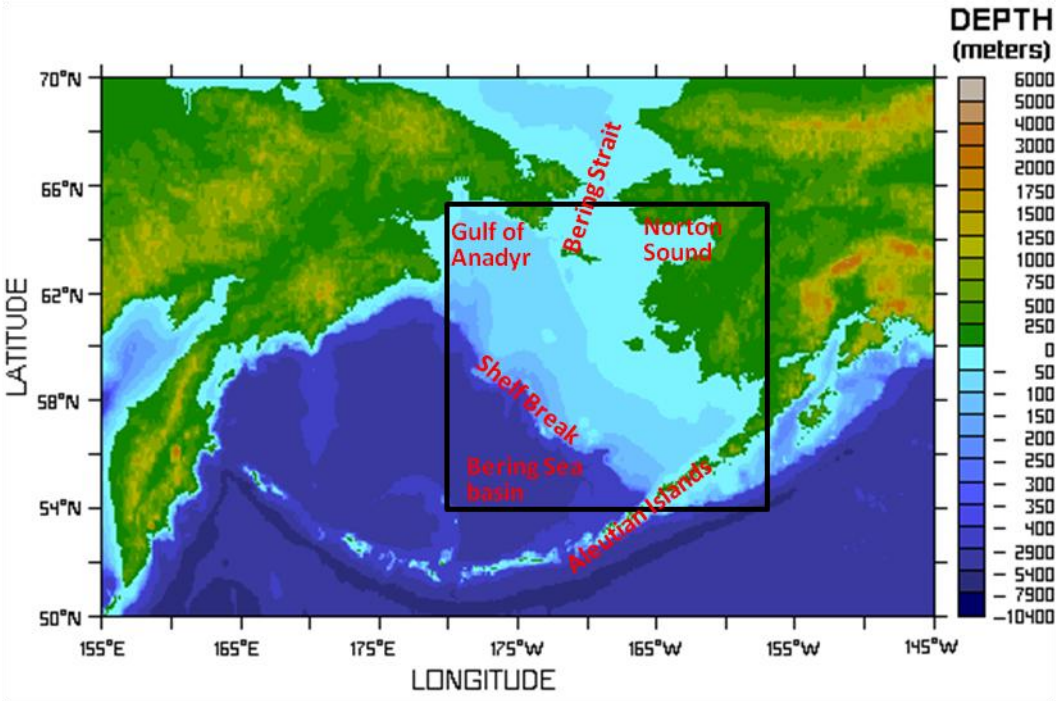

Figure B1. Bering Sea bathymetry map showing the broad continental shelf and the steep shelf break. The study region is indicated by the black box. (disc.sci.gsfc.nasa.gov)

EOF analysis partitions covariance of the data among locations into a series of orthogonal modes each having a spatial pattern that is associated with a time series of variability in that mode. Each mode explains a decreasing percentage of the total variance present in the space - time series. In the coastal Gulf of Alaska region, Brickley and Thomas (2004) [*Brickley and Thomas*, 2004] showed that the dominant mode (27% of total variance) of the inter-annual variation in spring bloom patterns is associated with the coast of the Gulf of Alaska. They then evaluated the dominant mode with wind and surface temperatures which indicated that the spring bloom was related to wintertime wind mixing during the previous winter rather than temperature anomalies. In this study, the SST and chlorophyll variability will be examined over the eastern Bering Sea using EOF analysis of remotely sensed data from Moderate Resolution Imaging Spectroradiometer (MODIS) sensor. The main objectives (1) to examine remotely sensed SST

and chlorophyll variability using EOF analysis, and (2) to study the EOF modes of SST and chlorophyll in relation to the Bering Sea climate indices.

Methods

MODIS Aqua SST and ocean color data have an advantage that both SST and chlorophyll measurements are made synchronously by the same sensor. MODIS Level 3 monthly composite Standard Mapped Image (SMI) of SST and chlorophyll for May, June, July, August, and September (MJJAS) from 2003 – 2009 for the eastern Bering Sea (54 N, 157 W, 65 N, 180 W) were obtained from the NASA Goddard Space Flight Center (GSFC) Distributed Active Archive Center (DAAC). These months were chosen as they had the least number of missing pixels and as EOF does not allow missing values, these pixels need to be interpolated. MODIS data have spatial resolutions of about 9 km. All images were processed using the SeaWiFS Data Analysis System (SeaDAS) version 5.3 software package developed by NASA. The data were systematically calibrated by NASA to meet mission specifications [*McClain et al.*, 1998], which called for less than 35% uncertainties in the chlorophyll concentration retrievals.

EOF analysis was done on monthly anomaly images (‘time centered’, ‘space centered’, removing semi-annual means) using Singular Value Decomposition (SVD) in MATLAB. Prior to the EOF analysis data were smoothed by using nearest neighbor interpolation to account for missing pixel data in the MODIS monthly SST and chlorophyll images. Land pixels were removed from the data by applying a land mask.

Results

The time series of monthly SST and chlorophyll averaged over the study area for the seven year study period is shown in Figure B2. There was lag between the SST and chlorophyll data, the minimum/maximum chlorophyll concentration did not occur at same time of

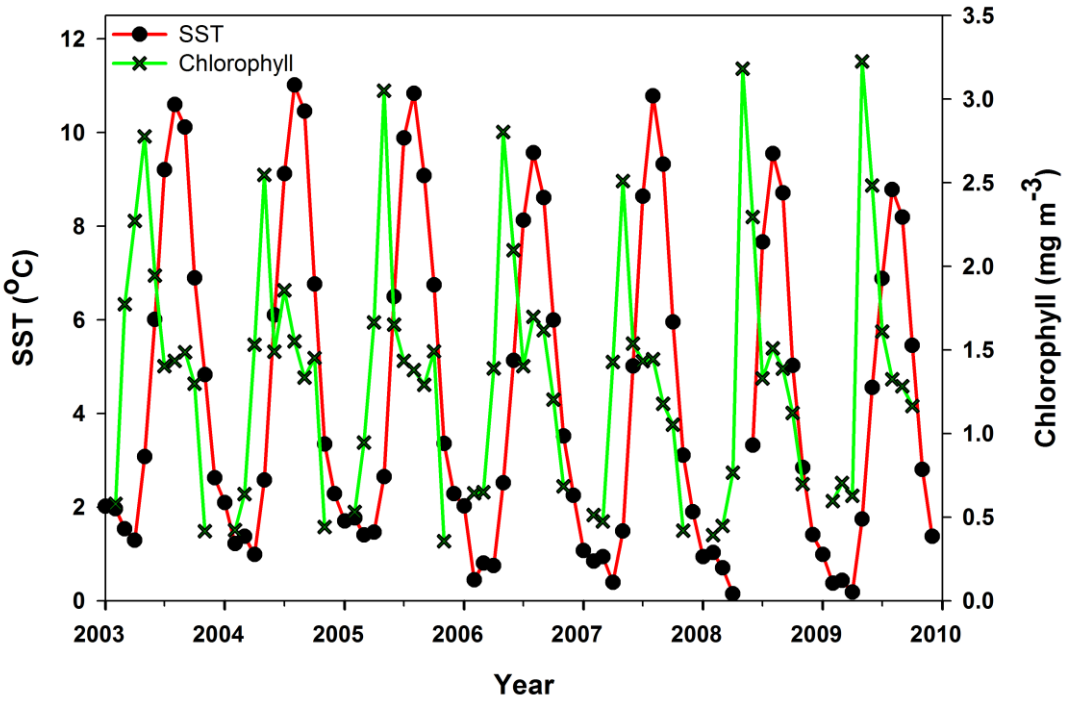

Figure B2. Area averaged time series of MODIS SST and Chlorophyll for the study period. Data points not connected indicate missing data for the particular month.

minimum/maximum SST. The lowest SST values occurred every spring (March-April) and coincided with high chlorophyll concentration. From May, the SST began to rise, reaching a maximum (~10 ^{o}C) during summer (June–September). The correlation between SST and chlorophyll was strong (r^2 =0.78) for these months (MJJAS) and was weak (r^2=0.1) for all months of the year taken together. SST decreased during fall to winter (October–February), reaching a minimum (~0.2 ^{o}C) in spring (March). The chlorophyll was highest during the spring bloom in April-May every year from 2003 to 2009, with the highest concentration (~3.25 mg m^{-3}) occurring in May 2008 and 2009 and the lowest (~2 mg m^{-3}) in May 2004 and 2007. The small peaks after the spring blooms peaks corresponded to the fall bloom occurring in September-October every year. During the winter, chlorophyll concentrations were low (< 0.5 mg m^{-3}).

EOF Analysis - SST Spatial and Temporal Variability

The "scree" plot after performing SVD was used to determine the number of modes to be retained. The first 3 EOF modes were retained as they explained greater than 70% variability in the data and EOF's higher than 3 remained relatively constant probably indicating noise in the data. The first 3 EOF modes explained 59.5%, 12.7% and 4.5% variation in the data, respectively and together explained 76.7% variability in the data. The change in variance between the first and second modes was very large indicating that the SST in the study region was dominated by unique spatial and temporal patterns. The spatial variations of the first 3 EOF modes revealed 3 distinct spatial patterns (Figure B3). The spatial pattern of the first SST EOF is more restricted in the shallow shelf region, suggesting that the deep basin and shallow shelf region exhibit qualitatively similar changes with the larger amplitudes in the shelf region (Figure B3a). This mode illustrated the dominant summer temperature patterns in the SST variance. The strongest (positive) loadings were seen on the shelf and the weakest (negative) loadings near the Norton Sound. The time series of the amplitude associated with the spatial pattern of this mode showed a gradually decreasing trend since 2005 (Figure B3a). The amplitudes were positive prior to August 2005 and negative afterwards, except May 2006 and August 2007 where they were slightly positive.

The strongest amplitude was seen during 2004, and the weakest occurred in May-June 2008 and July 2009. This indicates that after 2005 a rapid decrease in SST occurred with a minimum SST occurring in summer of 2008 and 2009. This dominant cooling in SST during the warm months despite the continued Arctic warming could be possibly due to the La Nina and positive Arctic oscillation [*Overland et al.*, 2008]. The second SST EOF spatial pattern contains 12.7% of the total variance. Its spatial pattern showed clear demarcation between the northern and southern parts of the study region (Figure B3b). The strongest positive loadings occurred at the

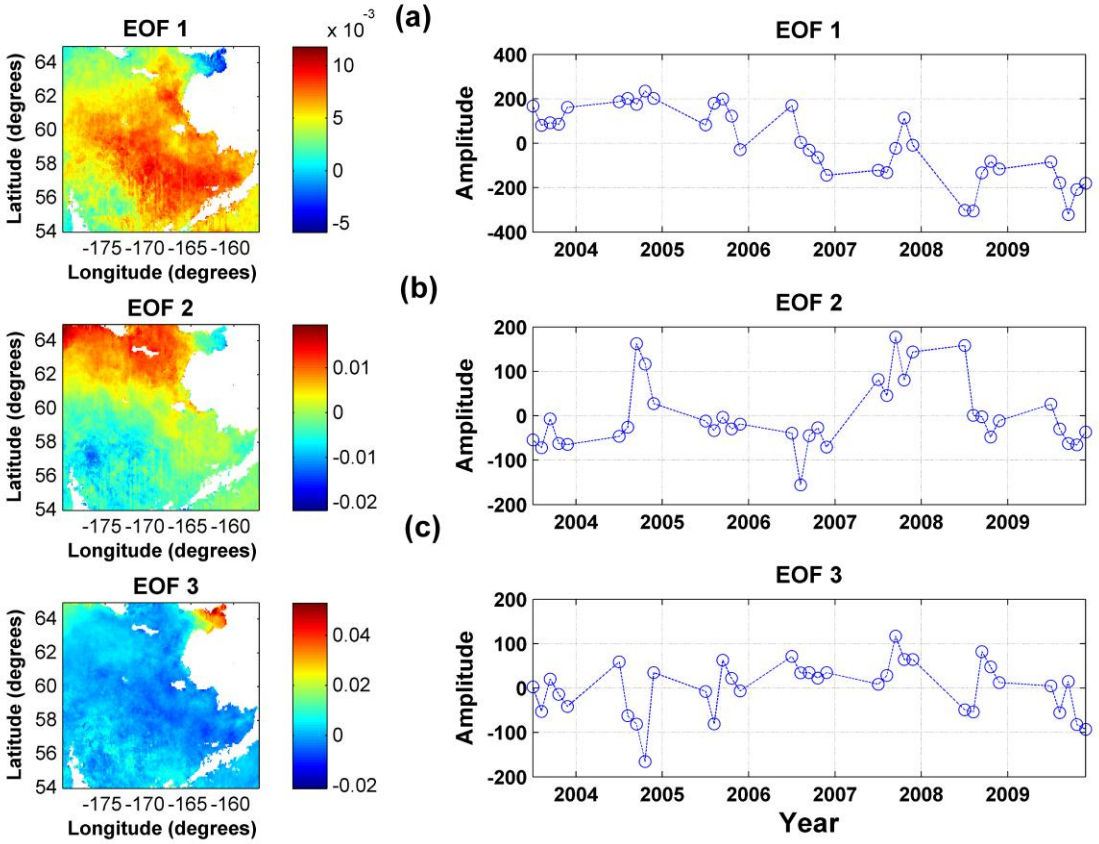

Figure B3. Spatial patterns and temporal amplitudes of first 3 EOF modes (a) first EOF, (b) second EOF, and (c) third EOF of MODIS SST for MJJAS time series (^{o}C).

northern portion of the study area near to the Bering Strait and Gulf of Anadyr, while the weakest loadings which were negative occurred near the Bering Sea basin off the eastern Bering Sea shelf break. The amplitude function of this mode was mostly negative or near zero for most years (Figure B3b). The May amplitude is negative from 2003-2006 and positive from 2007-2009. The highest amplitude is seen in July 2004 and lowest in June 2006.

The third mode of EOF explained 4.5% of the total variance. Its spatial pattern showed varying magnitude in the study region, with the strongest (positive) loadings seen near the Norton Sound, while the weakest (negative) loadings occurred in parts of the shelf region of the study area (Figure B3c). In terms of spatial pattern this mode is shows a pattern opposite to the

spatial pattern of the first SST EOF. The amplitude function of this mode peaked during July of every year except 2004 and 2006 (Figure B3c). The relatively strong negative amplitude was seen in August 2004, while the most positive amplitudes were in July 2007 and 2008. It was interesting to note that the May amplitude fluctuated alternatively from being near zero in 2003, 2005 and 2007 and positive in 2004 and 2006; however in 2008 it became negative by almost the same magnitude as the positive peaks and returned to near zero in 2009. This small scale transition was also seen earlier in earlier SST EOF's.

EOF Analysis - Chlorophyll Spatial and Temporal Variability

The percent variation explained by the EOF analysis of MODIS chlorophyll data for MJJAS months for a time period from 2003 to 2009 is shown in Figure B4. The first 3 EOF modes were retained although the 4th EOF mode (10.4%) explained only slightly less variance than 3rd EOF mode (14.6%), however it didn't reveal any distinct spatial pattern. The first 3 EOF modes explain 58.5% of the total variance in the chlorophyll data. The first EOF mode explained 28.14% of the spatial and temporal variability in the study area (Figure B4a). The spatial pattern showed that the eastern Bering Sea shelf break mostly covaries inversely with the eastern Bering Sea shelf and basin. The temporal amplitude showed the seasonal variability of chlorophyll in the Bering Sea which was characterized by a spring bloom (May–June) increase, a summer decrease (July–August) and start of a fall bloom (September) (Figure B4a). The temporal pattern has strong negative amplitude in May 2006 indicating that during May 2006 a spring bloom possibly occurred in the eastern Bering Sea shelf break, while very low chlorophyll values were seen on the eastern Bering Sea basin compared with other years.

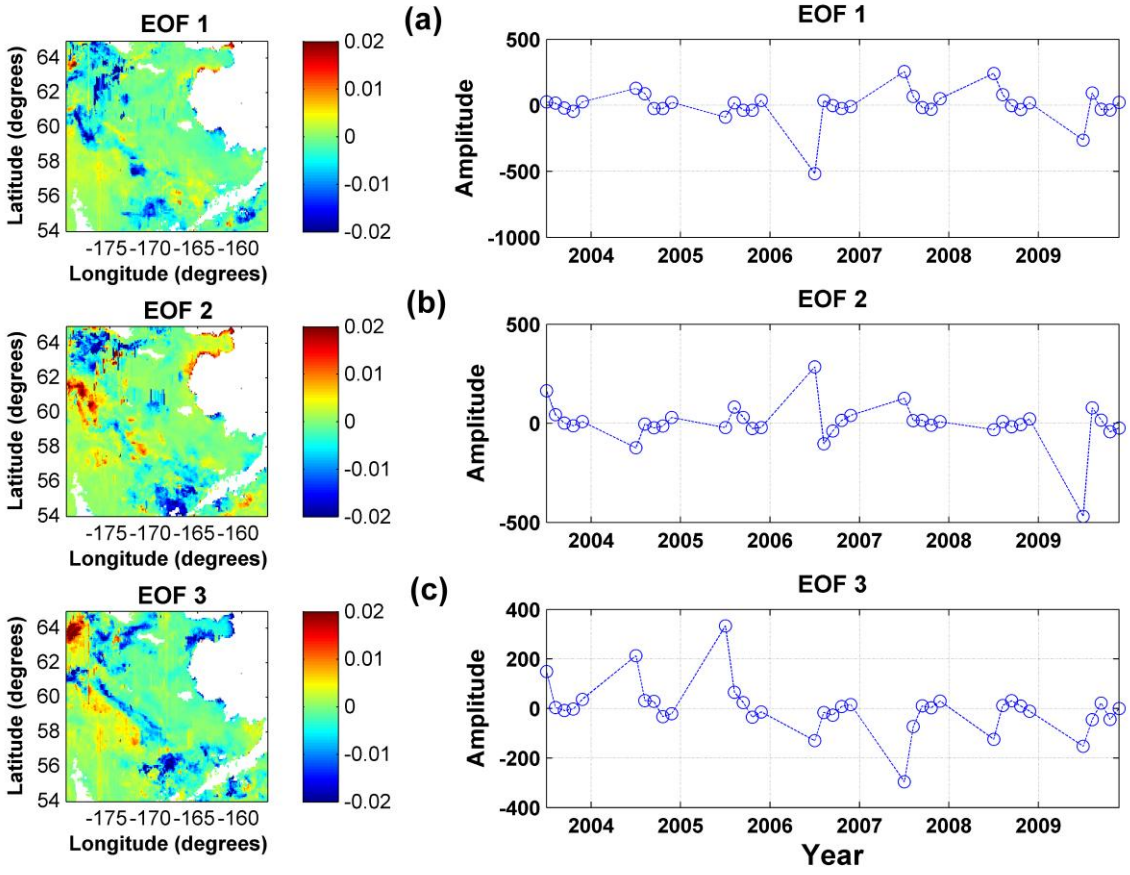

Figure B4. Spatial patterns and temporal amplitudes of first 3 EOF modes (a) first EOF, (b) second EOF, and (c) third EOF of MODIS chlorophyll for MJJAS time series (mg m^{-3}).

Relatively strong positive amplitudes were seen in May 2007 and May 2008 indicating a bloom occurred in the eastern Bering Sea shelf. The second EOF mode contains 17.8% of the total variance and its spatial pattern reveals the high chlorophyll concentration usually seen at the shelf break (Figure B4b). The higher chlorophyll concentration at the shelf break is direct effect of the eddy mixing which sustain the supply of nutrients throughout the summer season [*Mizobata and Saitoh*, 2004]. The temporal variation indicates relatively strong positive amplitudes in May 2006 and May 2007 (Figure B4b), possibly indicates that a spring bloom occurred in eastern Bering Sea shelf break. In contrast relatively strong negative amplitude seen in May 2009 indicates that there is low chlorophyll concentration in the eastern Bering Sea shelf

break and that early spring bloom might have occurred in the eastern Bering Sea shelf which caused nutrient depletion.

The third EOF mode explained 14.57% of the spatial and temporal variability and its spatial pattern showed that the eastern Bering Sea shelf (low loadings) and deep Bering Sea basin (high loadings) covary inversely and are separated by a distinct transition zone which marks the shelf break (lowest loadings) (Figure B4c). The time series pattern showed that the amplitude was mostly positive from 2003-2005 after which there amplitude switched to mostly negative (Figure B4c). Such a transition in 2006 was also observed from the amplitude of SST EOF's. The positive values (2003-2005) of the amplitude would indicate that the late spring bloom occurred in the eastern Bering Sea shelf resulting in chlorophyll values relatively lower on shelf and higher in the Bering Sea basin, while negative values (2006-2009) indicate an early spring bloom occurred with chlorophyll values relatively higher on shelf and lower in the basin.

EOF Modes and Bering Sea Climate Indices

The indices data are taken from the NOAA website on Bering Climate (http://www.beringclimate.noaa.gov/ data/index.php). The description for each of the indices studied below can be found on the same website.

SST's in summer, after ice has retreated from the eastern Bering Sea are largely dependent on the processes that occurred during the previous winter [*Overland and Stabeno*, 2004]. The ice cover index (ICI) is the average ice concentration for Jan 1-May 31. The SST EOF 1 mode for the study region shows an inverse relation with the ICI, as the ICI increases the SST EOF 1 mode decreases (Figure B5a). In 2006 as the ICI became positive at the same time the SST EOF 1 amplitudes became negative. This shows that the ICI is inversely related to the spring-summer time SST's in the study region [*Overland and Stabeno*, 2004]. Figure B5d also show the

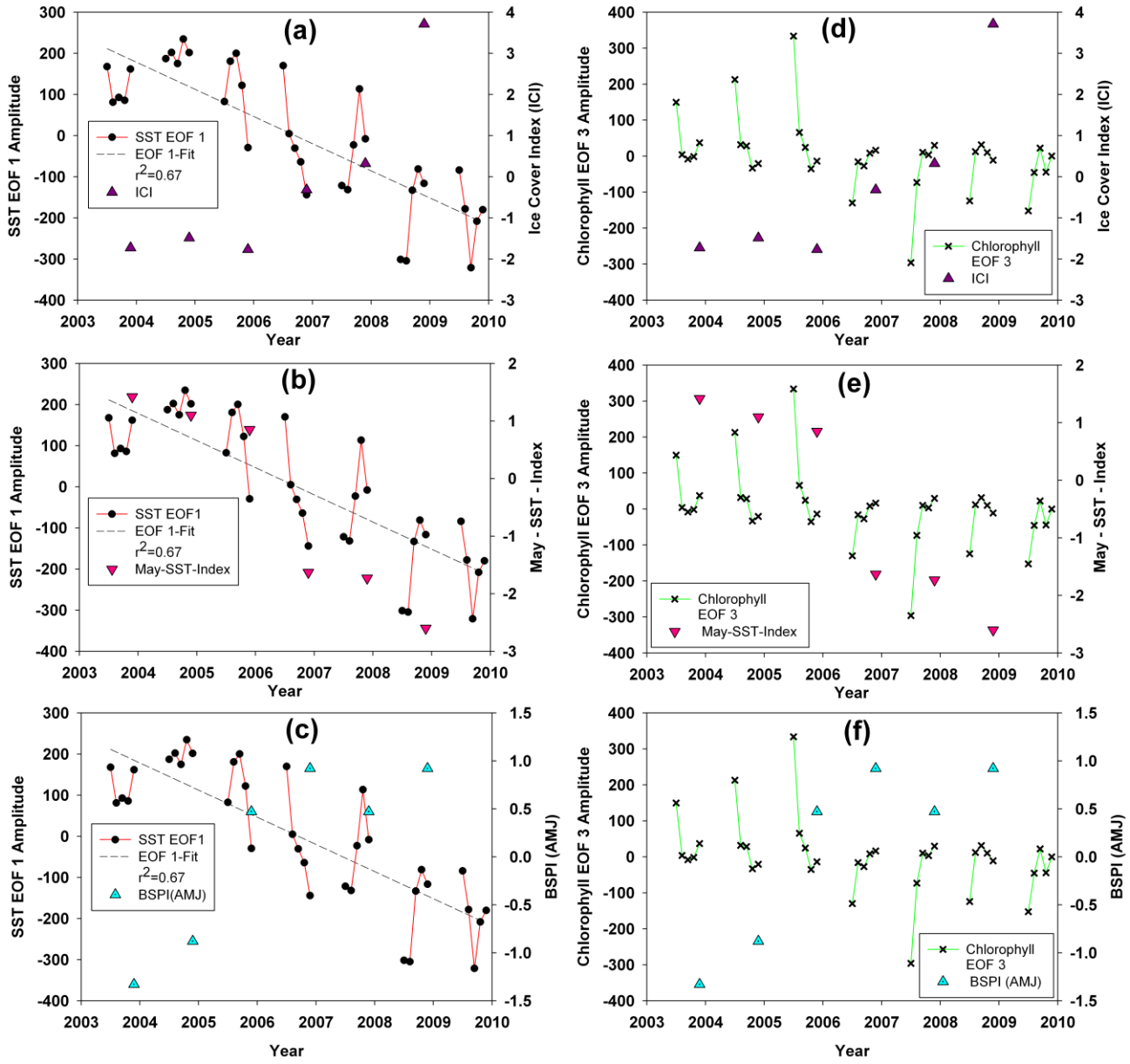

Figure B5. Variation of Ice Cover Index (ICI), May-SST Index, and Bering Sea Pressure Index (BSPI) with (a-c) SST EOF 1, and (d-f) chlorophyll EOF 3 respectively.

chlorophyll EOF 3 variation with ICI. In general as the ICI increases and becomes more positive, the chlorophyll EOF 3 amplitude is mostly positive. After 2006 as ICI shifts from negative to positive, the chlorophyll EOF 3 amplitude becomes mostly negative. This hints that chlorophyll concentration and ICI are directly linked through a certain extent by the decreasing SST's. An increase in ICI favors the formation of an edge spring bloom in the eastern Bering Sea, however

in addition to SST, other physical forcing effect the distribution of chlorophyll in the Bering Sea, like the position of the Aleutian low which affects the storms in the Bering Sea [*Hunt et al.*, 2002], light conditions, stratification and upwelling [*Sambrotto et al.*, 1986]. The May-SST index characterizes SST during May in the eastern Bering Sea. The May SST index is strongly correlated to the ICI and also portrays the wind mixing processes during spring. The amplitude of the first mode of SST data in this study period compares well to the trend of decreasing May-SST index (Figure B5b). The transition time of the May-SST index (2006) is the same as that for the ICI; this is expected as the extent of ice cover determines the summer-spring time temperatures. The comparison further validates that the SST EOF 1 mode describes appropriate variability of SST on the shelf during MJJAS months in the study region. The May SST index and the chlorophyll EOF 3 amplitude are positive prior to 2006 and become negative after 2006 (Figure B5e).

The importance of sea ice cover and the response in the study region is evident from the analysis of the indices mentioned above. Variability in ice cover in the Bering Sea depends on both temperature and atmospheric circulation [*Overland and Stabeno*, 2004]. The main climate feature influencing the eastern Bering Sea is the Aleutian Low [*Rodionov et al.*, 2005]. Cold winter climatic regimes in the eastern Bering Sea tend to be associated with the periods of anomalous high sea level pressure (SLP). The Bering Sea pressure index (BSPI) for spring, defined as the area-weighted averages of SLP for April through June in the east Bering Sea. Positive values of the BSPI in 2006 indicate predominance of high pressure with less storms and cooler temperatures; this is associated with the Aleutian low pressure region having higher than normal SLP. The first EOF mode of SST responds to the BSPI shift (Figure B5c). The chlorophyll also responded to the change of BSPI to positive values (Figure B5f).

Conclusions

In this study, satellite ocean color time series data collected by MODIS were used to determine the synoptic quantifications of spatial and temporal variability of SST and chlorophyll by using EOF analysis. The first 3 EOF modes of MODIS SST and chlorophyll explained about 76.7% and 58.5% of the total variance respectively. The first EOF SST mode indicated dominant cooling of SST's in the study area. The second mode of chlorophyll was found to be associated with the high chlorophyll concentrations at the shelf break. A comparison was made between various Bering Sea climate indices and EOF modes of MODIS SST and chlorophyll. The decreasing trend in the time series of the amplitude of first EOF of SST and the switching from mostly positive to mostly negative in the time series of the amplitude of third EOF of chlorophyll was supported by comparisons with these indices. The indices revealed that the decrease of SST's during the warm months and corresponding shifts in chlorophyll in the study area was related to increase in sea ice cover during winter, the positive values of BSPI associated with the higher than normal SLP in the Aleutian low pressure region in 2006. This study illustrates that ocean color satellite data from MODIS can be used for long term synoptic study of Bering Sea. Further studies should focus on inclusion of more physical forcing variables including SST to see the response on chlorophyll employing decadal multi-sensor satellite data.

References

Brickley, P., and A. Thomas (2004), Satellite-measured seasonal and inter-annual chlorophyll variability in the Northeast Pacific and Coastal Gulf of Alaska, Deep Sea Research Part II-Topical Studies in Oceanography, 51(1-3), 229-245.

Hunt, G., P. Stabeno, G. Walters, E. Sinclair, R. Brodeur, J. Napp, and N. Bond (2002), Climate change and control of the southeastern Bering Sea pelagic ecosystem, Deep Sea Research Part Ii-Topical Studies in Oceanography, 49(26), 5821-5853.

Loughlin, T. R., I. N. Sukhanova, E. H. Sinclair, and R. C. Ferrero (1999), Summary of biology and ecosystem dynamics in the Bering Sea, 387-407 pp., University of Alaska Sea Grant, Fairbanks, AK.

McClain, C., M. Cleave, G. Feldman, W. Gregg, S. Hooker, and N. Kuring (1998), Science quality SeaWiFS data for global biosphere research, Sea Technology, 39(9), 10-16.

Mizobata, K., and S. Saitoh (2004), Variability of Bering Sea eddies and primary productivity along the shelf edge during 1998-2000 using satellite multisensor remote sensing, Journal of Marine Systems, 50(1-2), 101-111.

Niebauer, H. J. (1981), Recent fluctuations in sea ice distribution in the eastern Bering Sea, 133-140 pp., NOAA, Distributed by University of Washington Press, Seattle.

Overland, J., M. Wang, L. C., S. P., B. N., and S. S. (2008), FOCI Report 2008.

Overland, J. E. (1981), Marine climatology of the Bering Sea, NOAA, University of Washington Press, Seattle,WA.

Overland, J. E., and P. J. Stabeno (2004), Is the climate of the Bering Sea warming and affecting the ecosystem, EOS, 85(33), 309-316.

Rodionov, S., J. Overland, and N. Bond (2005), The Aleutian low and winter climatic conditions in the Bering Sea. Part I: Classification, Journal of Climate, 18(1), 160-177.

Sambrotto, R., H. Niebauer, J. Goering, and R. Iverson (1986), Relationships among vertical mixing, nitrate uptake, and phytoplankton growth during the spring bloom in the southeast Bering Sea middle shelf, Continental Shelf Research, 5(1-2), 161-198.

Thomas, A., P. Strub, and P. Brickley (2003), Anomalous satellite-measured chlorophyll concentrations in the northern California Current in 2001-2002, Geophysical Research Letters, 30(15), -.

Tsyban, A. (1999), The BERPAC Project: development and overview of ecological investigations in the Bering and Chukchi Seas, 713-729 pp., University of Alaska Sea Grant, , Fairbanks, AK.

Yoder, J., C. Mcclain, G. Feldman, and W. Esaias (1993), Annual cycles of phytoplankton chlorophyll concentrations in the global ocean - a satellite view, Global Biogeochemical Cycles, 7(1), 181-193.

APPENDIX C: PERMISSION

Puneeta Naik <puneeta123@gmail.com>

Reprint papers

2 messages

Scott McNeill <scottm@spie.org> **Wed, Aug 10, 2011 at 1:16 PM**
To: Puneeta Naik <pnaik2@lsu.edu>

Dear Ms. Puneeta Naik,

Thank you for seeking permission from SPIE to reprint material from our publications. As an author of the cited works, you retain co-owner rights to the original content therein. Publisher's permission is hereby granted under the following conditions: (1) the material to be used has appeared in our publication without credit or acknowledgment to another source; and (2) you credit the original SPIE publication. Include the authors' names, title of paper, volume title, SPIE volume number, and year of publication in your credit statement.

Sincerely,

Scott McNeill for

Eric Pepper, Director of Publications

SPIE

P.O. Box 10, Bellingham WA 98227-0010 USA

360/676-3290 (Pacific Time)

VITA

Puneeta Naik is a citizen of India. She obtained her basic education from various schools in different parts of India. She graduated from high school from Mary Immaculate Girls High School, Goa, and completed her undergraduate and graduate degrees in physics from the Goa University, India. During her Bachelor of Science degree she obtained a certificate course in Remote Sensing and GIS. During her Master of Science degree from Goa University, she was among 20 students selected for the Department of Atomic Energy Scholarship under Young Scientist Research Programme-2004, held at Center for Advanced Technology (CAT), Indore, India. She was awarded the IV SERC School in Physics gold medal and certificate of merit for having stood first at the Master of Science (physics) examination held by Goa University, Goa, India. Soon after graduating she worked as a lecturer in physics for undergraduate colleges in Goa and as a research assistant at the National Institute of Oceanography (NIO), Goa, India. She will be receiving her Doctor of Philosophy degree from the Department of Oceanography and Coastal Sciences at LSU in December, 2011.